A study of the actin-like MamK from *Magnetospirillum gryphiswaldense* MSR-1 and its role in magnetosome organisation

Jennifer Mary Louise Bell

School of Biological Sciences PhD Scholarship
The University of Edinburgh
2008

Declaration

I declare that this thesis was composed by me and the research presented is my own, except where otherwise stated.

Jennifer Mary Louise Bell
2008

I have a spelling checker,
It came with my pea sea.
It plane lee marks four my revue
Miss steaks aye can knot sea.

- Mark Eckman and Jerrold H. Zar

To all the members of the Darwin, Swann and Hugh Robson buildings at the University of Edinburgh, Scotland

Prologue

Motivation

There is multidisciplinary interest in magnetic bacteria, approaches of which include biological, ecological, behavioural, geological, physical, chemical, cosmological, industrial, and more. Furthermore, the bacterial cytoskeleton was not believed to exist until relatively recently. It was generally accepted that Eukaryotes had evolved cytoskeletons to order components of their "highly complex" cells whilst bacterial cell components floated in the cytosol or were supported by the lipids of the cell wall. At the outset of this work *mamK* was a nucleotide sequence likely to code a novel bacterial cytoskeletal protein with amino acid sequence homology to actin and other relatively recently discovered bacterial actin-like proteins. Studies of actin and bacterial-actin-like proteins can have a "top-down-bottom-up" effect on our understanding of their biochemistry and evolution. The study of magnetic bacteria and MamK are of broad scientific interest and provide a number of opportunities to achieve novel results contributing to awareness in related research.

Aim

The aims of this thesis are 1) to give a comprehensive background to an understanding of magnetic bacteria and bacterial actin-like proteins, and 2) to present novel results of *in vitro* behaviour of recombinant MamK to inspire further collaboration from experienced members and newcomers to the subject.

Philosophy

The philosophy of this thesis is to outline the importance of magnetic bacteria and MamK discernable from a broad perspective and to critically present and discuss novel results pertaining to the *in vitro* characterisation of recombinant MamK.

Scope

The introduction chapter is divided into a three part reduction from a broad perspective of interest in magnetic bacteria to their cellular processes to outlining the background of MamK at a molecular level as a bacterial actin-like protein. The methods and materials chapter is written to enable the reader to reproduce the results without having to refer to outside sources. The results can be attributed to general

methods and techniques practiced by the molecular biology community and some to methods that are more specific and well established in the study of actin. Four results chapters are presented with subsections including background information, results, and discussion pertaining to the immediacy of each situation and in relation to the work of other researchers. A recap of the results is described and directions for further work based on the findings are highlighted in the conclusions and further work chapter. The references are presented in the final section in alphabetical order.

Acknowledgements

I would like to extend warm thanks to:

Dr. Chris French and Dr. Bruce Ward for allowing me to be independent yet giving me technical and moral support to the completion of my PhD.

Dr. Sutherland Maciver and Dr. Paul McLaughlin for imparting their specialist knowledge of actin and giving me support and bench space to carry out comparative studies on MamK.

Thanks to the many people that made coming into work a great pleasure and to the tireless ears of my family and friends.

Abstract

Magnetospirillum gryphiswaldense MSR-1 is one of a number of species to have a genetic system enabling the biomineralisation of iron in c. 40 linearly arranged organelles within its cell. These organelles are popularly known as magnetosomes and are believed to be selectively advantageous to cells as a biological compass that helps to minimise the search for nutrients from a three dimensional environment to a one dimensional environment. In nature the bacterium follows the magnetic field of the Earth up and down between aerobic and anaerobic conditions to find its ideal growth conditions. The magnetosomes are linearly arranged to capitalise on the net magnetic force.

The gene, *mamK*, is part of the genetic system involved in the production of magnetosomes and encodes an amino acid sequence with homology to actin and bacterial cell cycle proteins, such as MreB, ParM and FtsA. Prior to the outset of this work MamK was hypothesised to have an integral structural role in the linear arrangement of magnetosomes within bacterial cells.

Results discussed in this thesis outline *in vitro* characterisation of recombinant *Magnetospirillum gryphiswaldense* MSR-1 MamK. MamK was expressed in *Escherichia coli* with and without an N-terminal His-tag and/or a C-terminal GFP domain or a C-terminal cysteine mutation. In all cases, inclusion bodies were formed. MamK was purified from inclusion bodies and resolubilised. Purified MamK was found to self-associate, as indicated by light-scattering assays, in the presence of divalent cations. In contrast to actin and some other bacterial actin-like proteins polymerisation did not appear to require the presence of NTP; however, ATP or GTP was required for purification by ion exchange column chromatography. Polymerisation did not result in a detectable change in tryptophan fluorescence. Depolymerisation was not readily induced by dilution, but slow depolymerisation occurred in the presence of EGTA, as judged by a decrease in light scattering. Microscopy showed the formation of large two-dimensional sheets. These results are consistent with *in vivo* microscopic studies of MamK where polymerisation has been observed.

Abbreviations

DNA	deoxyribonucleic acid
DSMZ	Deutsche Sammlung von Mikroorganismen und Zellkulturen
nT	nano Teslas
OATZ	oxic-anoxic transition zone
OD	optical density
PCR	polymerase chain reaction
RNA	ribonucleic acid

Abbreviations of chemicals and reagents used

APS	ammonium persulfate
CnBr	cyanogen bromide
dH_2O	distilled water
DMSO	dimethyl sulphoxide
EB	elution buffer
EDTA	ethylenedinitrilotetraacetic acid
EGTA	ethylene glycol-bis(beta-aminoethyl ether)-N,N,N',N'-tetra acetic acid
EtOH	ethanol
LB	Luria Bertani broth
MetOH	methanol
Na_2EDTA	disodium ethylenedinitrilotetraacetic acid
PBS	phosphate-buffered saline
PEG	polyethylene glycol
SDS	sodium dodecyl sulphate
TAE	tris-acetate- ethylenedinitrilotetraacetic acid
TEMED	tetramethylethylenediamine
TSS	transformation and storage solution

List of tables

List of figures

Table of contents

1 INTRODUCTION

1.1 THE DISCOVERY OF MAGNETIC BACTERIA AND MAGNETOSOMES

Richard Blakemore first reported the discovery of a magnetic bacterium, *Magnetospirillum* MS-1 (Figure 1.1), in the 1970s as an undergraduate student (Blakemore, 1975). He was examining water sediment samples under a microscope when he noticed some of the organisms were swimming in parallel lines. He held a magnet close to the platform of the microscope and saw that the bacteria responded to its positioning. It was later found that the bacterium harboured intracellular magnetic iron mineral crystals enclosed in a lipid membrane similar to that of the cytoplasmic membrane constituting what has in the past been described as a magnetic organelle (Blakemore *et al.*, 1980). Today this organelle is referred to as the "magnetosome" a term coined by Balkwill *et al.* (1980). It is most popularly believed that magnetic bacteria require biological bar magnets in order to navigate and lessen the distances covered in their search for nutrients.

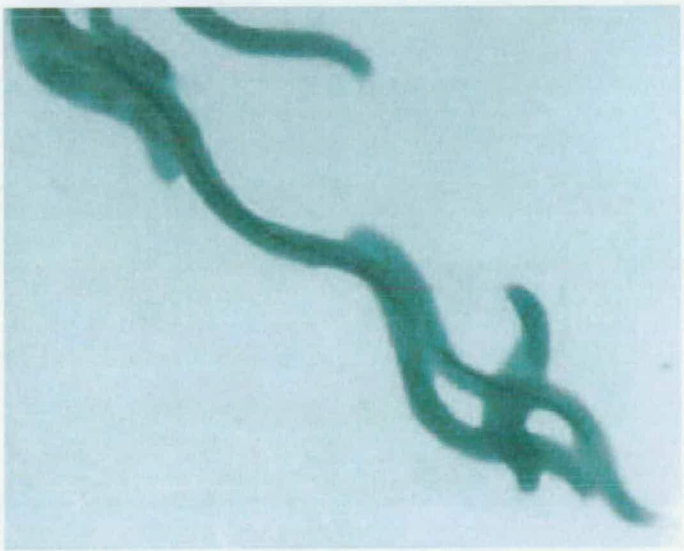

Figure 1.1 *Magnetospirillum magnetotacticum* MS-1. (http://genome.jgi-psf.org/ draft_ microbes/ magma/ magma.home.html)

Since Blakemore's first paper on the subject was published in 1975 it has been cited frequently in reports (Figure 1.2) concerning magnetic responses in complex organisms as well as manuscripts in more distant fields of research. Objectively speaking, short of 30 citations in one year for a land mark paper does not seem worth

much merit (Figure 1.2). Regardless, the diversity of interest that the paper has attracted is impressive. Over the years the interest has moved from one trend of research to another such as animal behaviour, neuroanatomy, biomineralisation, the geological history of Earth, planetary theories of Mars, the origin of life, bioremediation, electronics, materials science and more. The maxim is that the study of bacterial magnetosomes is of widespread importance as the following information will outline.

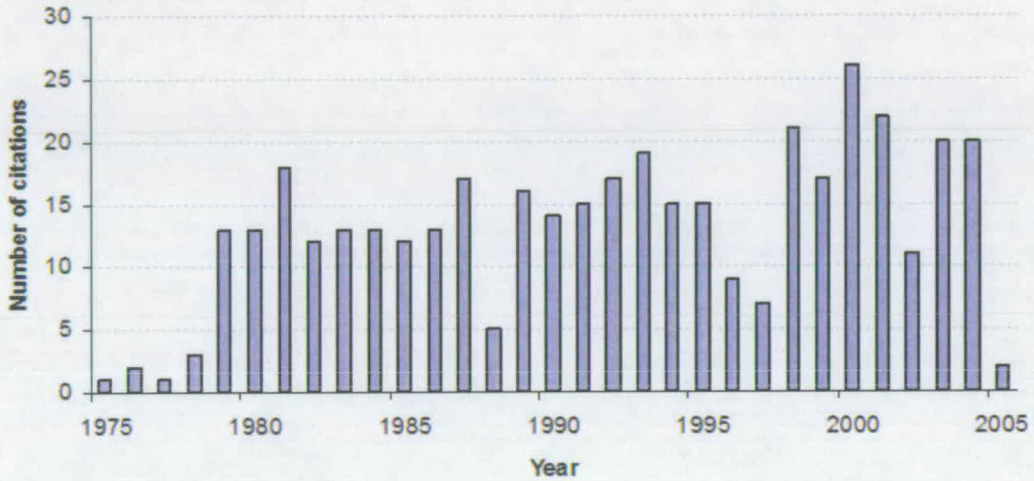

Figure 1.2 The number of hits scored for the citation of Blakemore, Richard P. (1975) Magnetotactic bacteria, Science, 190, 377-385, at the ISI Web of Knowledge website (http://wok.mimas.ac.uk) over thirty years.

1.1.1 Ecology of magnetic bacteria

Magnetotactic bacteria distribute themselves in stratified populations within the oxic-anoxic transition zone (OATZ) (Bazylinski *et al.,* 2000). The oxic-anoxic transition zone is an interface environment of sharp chemical, redox and pH gradients between oxygen-rich and oxygen-starved water and sediment. This zone contains a succession of organisms with various nutrient requirements thus inhabiting various niches in this environment (Bazylinski *et al.,* 2000; Simmons *et al.,* 2004). It is a harsh environment where each organism requires a survival strategy of its own. Magnetotactic bacteria have the ability to bio-accumulate iron oxides and iron sulphides and for this reason are likely to play an important role in sulphur and iron cycling in their environment (Bazylinski *et al.,* 2000; Posfai *et al.,* 1998; Simmons *et al.,* 2004).

1.1.2 Diversity of magnetic bacteria

Magnetotactic bacteria display a variety of cell morphologies (Figure 1.1 and 1.3) spanning unicellular coccoids, multicellular coccoids, rods, vibrios and spirilla propelled by polar, bipolar or tufted flagella. They can be divided into categories depending on magnetosome biosynthesis of magnetite (Fe_3O_4) from iron oxides, or greigite (Fe_3S_4) from iron sulphides (De Long *et al.*, 1993). There are bacteria that biomineralise both magnetite and greigite within the same cell (Stolz, 1993). Magnetic bacteria can be categorised further into obligate microaerophilic magnetite producers, facultative microaerophilic magnetite and iron sulphide producers, and strictly anaerobic iron sulphide producers (Stoltz, 1993).

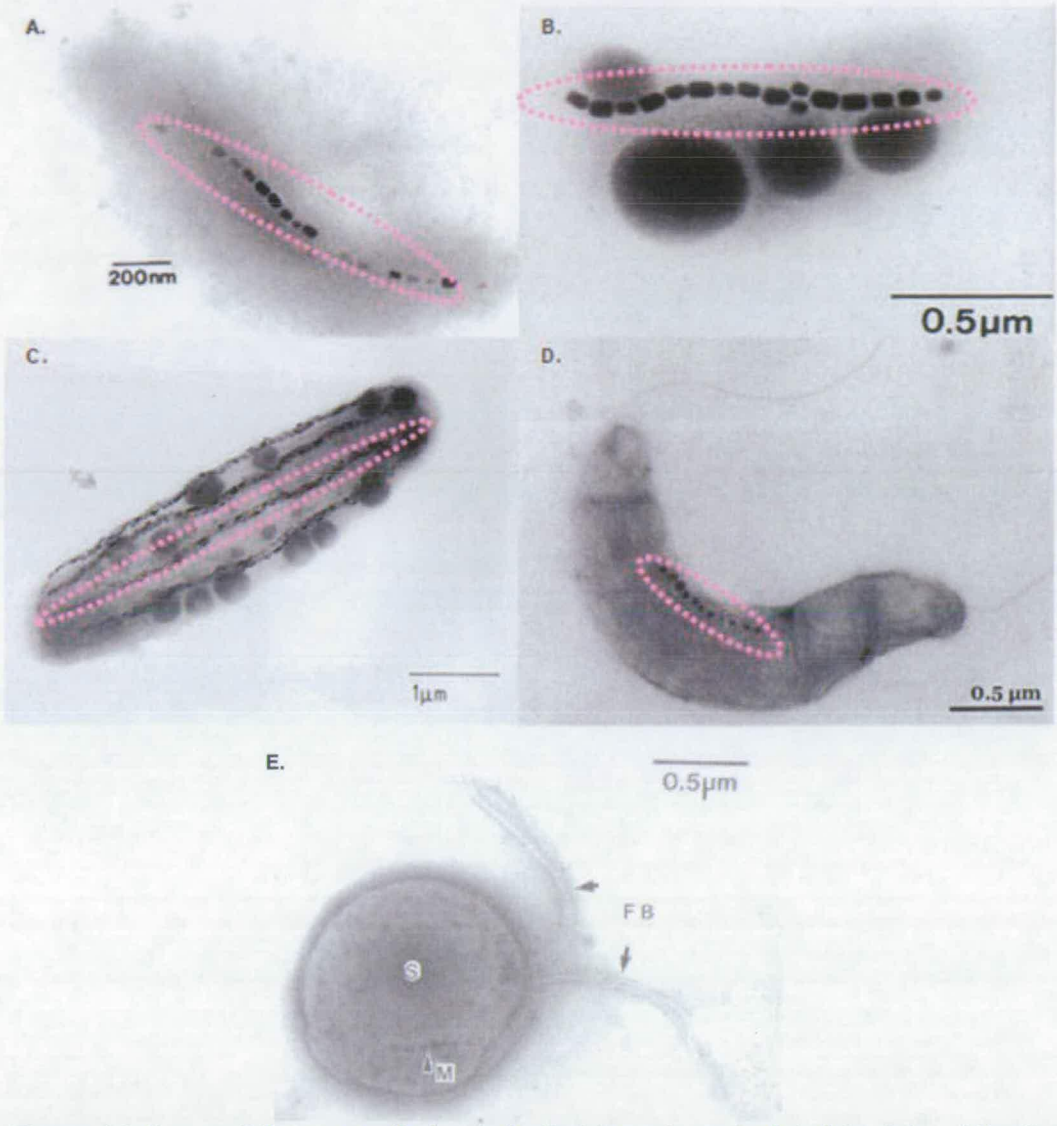

Figure 1.3 Some of the magnetic bacteria that have been isolated to date. Attention has been drawn to their magnetosomes using dotted circles not to be confused with the larger sulphur granules. (A) Magnetic vibroid MV-1 cells; (B) magnetic vibroid MV-4; (C) *Magnetobacterium bavaricum*; (D) *Magnetospirillum gryphiswaldense.* (Plates courtesy of Dirk Schüler and Dennis Bazylinski) and (e) *Magnetococcus* MC-1 ((M) Magnetosomes; (S) Sulphur granule; (FB) Flagellar bundles) (Plate courtesy of Richard Frankel).

All magnetite-producing bacteria are closely associated with the α-subgroup of the Proteobacteria, whereas greigite-producing bacteria are more closely associated with the δ-subdivision of the Proteobacteria (De Long *et al.,* 1993). Some magnetotactic bacteria from the α-subgroup are closely related to the nonmagnetotactic,

photosynthetic, non-sulphur purple bacteria with which they share the feature of intracytoplasmic membrane formations (Schüler, 1999). There is an instance of a magnetotactic rod, *Magnetobacterium bavaricum* (Figure 1.3 c), being assigned to the *Nitrospira* phylum (Schüler, 1999). Table 1.1 outlines some of the characteristics of a number of magnetic bacteria that have been isolated over the years.

The majority of magnetic bacteria observed in the environment have not been grown in pure culture in the laboratory (Simmons *et al.*, 2004). Fewer than ten strains are available in pure culture, and most of those are magnetite-producing α-Proteobacteria of the genus *Magnetospirillum* from freshwater environments. A few strains of marine magnetite producing magnetic bacteria are available in culture (Bazylinski *et al.,* 1988; Sakaguchi *et al.,* 2002; Spring and Bazylinski, 2000). These strains are all microaerophiles when growing on O_2, and some can grow anaerobically on N_2O (Bazylinski *et al.,* 1988). All are capable of oxidising but not reducing inorganic sulphur compounds, with the exception of the freshwater sulphate-reducing rod *Desulfovibrio magneticus* (Sakaguchi *et al.,* 2002). Greigite producing magnetic bacteria have not yet been isolated in axenic cultures and their phylogeny is unknown (Simmons *et al.,* 2004), with the exception of the many-celled magnetotactic prokaryote (MMP), which has been identified as one of the δ-Proteobacteria by fluorescent *in situ* hybridisation (FISH) (de Long *et al.,* 1993).

Table 1.1 Some characteristics of magnetic bacteria that have been isolated from the environment over the years.

Organism	Family	Organism characteristics	Magnetosome characteristics	Reference
Magnetic				
Magnetospirillum magnetotacticum MS-1	α-proteobacteria	Gram negative, spirillum, obligate microaerobe	magnetite, cubo-octahedral habit	Blakemore (1975)
Bilophococcus magnetotacticus	α-proteobacteria	Gram negative, coccoid	magnetite, hexagonal prismatic habit	Moench (1988)
Magnetic vibrio MV-1	α-proteobacteria	Gram negative, vibrioid-helicoid	magnetite, elongated hexagonal habit	Bazylinski *et al.* (1988)
Magnetospirillum gryphiswaldense MSR-1	α-proteobacteria	Gram negative, spirillum, obligate microaerobe	magnetite, cubo-octahedral habit	Schliefer *et al.* (1991)
Magnetospirillum magneticum AMB-1	α-proteobacteria	Gram negative, spirillum, facultative anaerobe	magnetite, cubo-octahedral habit	Matsunaga *et al.* (1991)
Magnetococcus sp. MC-1	α-proteobacteria	Gram negative, coccoid	magnetite, pseudo-hexagonal prismatic habit	Meldrum *et al*. (1993)
Magnetic vibrio MV-2	α-proteobacteria	Gram negative, vibrioid-helicoid	magnetite, cubo-octahedral habit	Meldrum *et al.* (1993)
Magnetic vibrio MV-4	α-proteobacteria	Gram negative, vibrioid-helicoid, bipolar flagella	magnetite, cubo-octahedral habit	Meldrum *et al.* (1993)
Magnetic bacterium RS-1*	δ-proteobacteria	Gram negative rod/helicoid, sulphate reducing, anaerobe	magnetite, single domain,	Sakaguchi *et al.* (1993)
Magnetobacterium bavaricum	Nitrospira	Gram negative rod, nitrite-oxidiser	magnetite, bullet shaped	Spring *et al.* (1993)
Magnetospirillum sp. MGT-1	α-proteobacteria	Gram negative, spirillum, facultative anaerobe		Burgess *et al.* (1993)
multicellular magnteic procaryote	δ -proteobacteria	Gram negative, coccoid (pyrimidal)	greigite/magnetite	Lins and Farina (1999)
Magnetospirillum sp. SAR-1				Venter *et al.* (2004)
Magnetospirillum strain WM-1	α-proteobacteria	Gram negative, spirillum, obligate microaerobe	magnetite, cubo-octahedral habit	Li *et al.* (2007)
non-magnetic				
Geobacter metallireducens GS-15	δ-proteobacteria	Gram negative, rod, insoluble metal reducing, anaerobe	extracellular magnetite	Lovely *et al.* (1987)
Thermophilic Fe(III)-Reducing Bacteria			extracellular magnetite	Liu *et al.* (1997)
TOR-39	δ-proteobacteria	Thermophilic fermentative	extracellular magnetite	Zhang *et al.* (1998)

*RS-1 is unusual in that it is the only dissimilatory sulphate reducing magntic bacterium to produce magnetite as opposed to the expected greigite crystals. Therefore disrupting the correlation between a-proteobacteria production of magnetite and d-proteobacteria production of greigite.

1.1.3 Magnetotaxis in bacteria

Early observations prompted the model that bacteria in the northern hemisphere predominantly swim in a northerly direction whilst in the southern hemisphere they predominantly swim in a southerly direction in response to geomagnetic fields (Blakemore *et al.*, 1980). Magnetotaxis was believed to be a behaviour whereby magnetic bacteria orient and migrate along magnetic field lines that lead down to ideal conditions in microaerobic sediments where the cells can adhere (Frankel and Bazylinski, 2001) (Figure 1.4). If the cells are displaced they can use their magnetotactic response to find ideal conditions again.

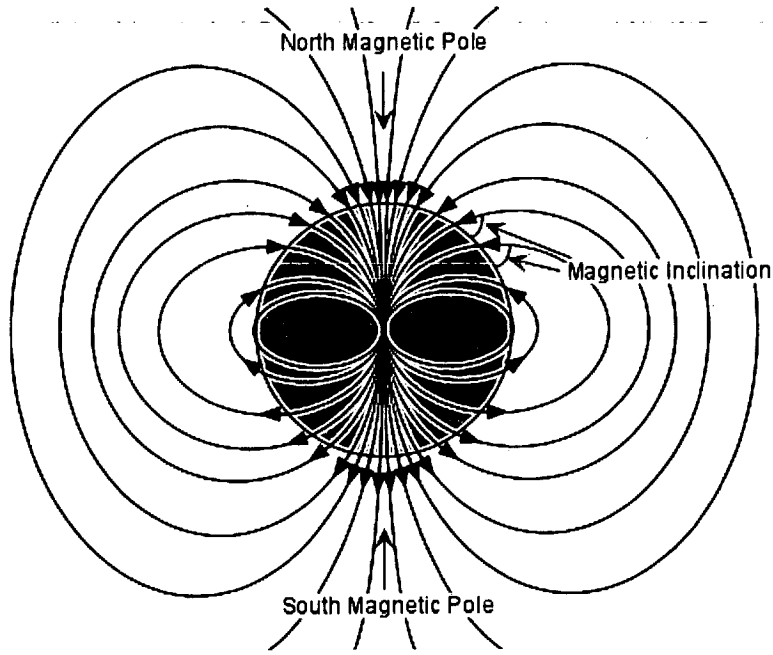

Figure 1.4 The Earth's magnetic field (earthsci.org/education/teacher/basicgeol/platec/platec.html)

Magnetotaxis results from passive alignment of the bacterial cell along geomagnetic field lines while it swims, due to torque experienced through the effect geological magnetic lines have on the magnetosomes. "Magnetotaxis" is the term that describes the behaviour of magnetic bacteria but it is a misnomer (Bazylinski, 2004). The tactic response of the magnetic bacterial species or strains have been identified to have either a *"two-way"* (typified by *Magnetospirillum* spp.) or *"one-way"* (typified

by MC-1 and other marine species) swimming behaviour along local geomagnetic field lines. To illustrate this more clearly, when cells are observed under the influence of a magnet in a droplet of water the magnetic spirilla can be found in equal numbers on opposite sides of the drop whilst the magnetic cocci are found all together on one side of the drop (Figure 1.5).

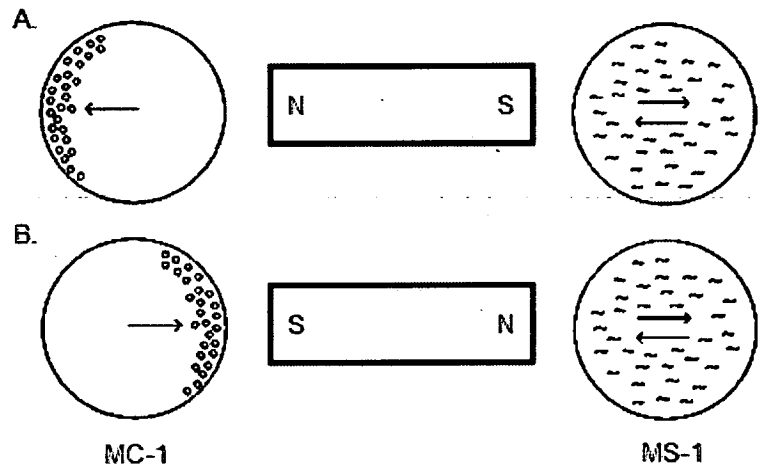

Figure 1.5 The difference in the one way response of *Magnetococcus* MC-1 and the two way response of MS-1. (A) The magnet is positioned in a North-South direction and is then inverted to a (B) South-North direction. Note the distribution of each species in their respective drops. (Plate and legend are courtesy of Dennis Bazylinski with slight adaptation).

Through further observations it was found that magnetic bacteria use the magnetotactic response in conjunction with an aerotactic response (Blakemore *et al.*, 1980) which at the time seemed to help explain the advantage of magnetotaxis to bacteria living in the anoxic zone and the reason why some species form bands at a particular point in test tubes. Blakemore *et al.* (1980) provides experimental results to illustrate this behaviour and describes polar magneto-aerotaxis where cells use a magnetic field to provide both an axis and direction of motility; and axial magneto-aerotaxis where cells use a magnetic field to provide only an axis to travel along in either direction to find the correct oxygen level in the gradient (Figure 1.6).

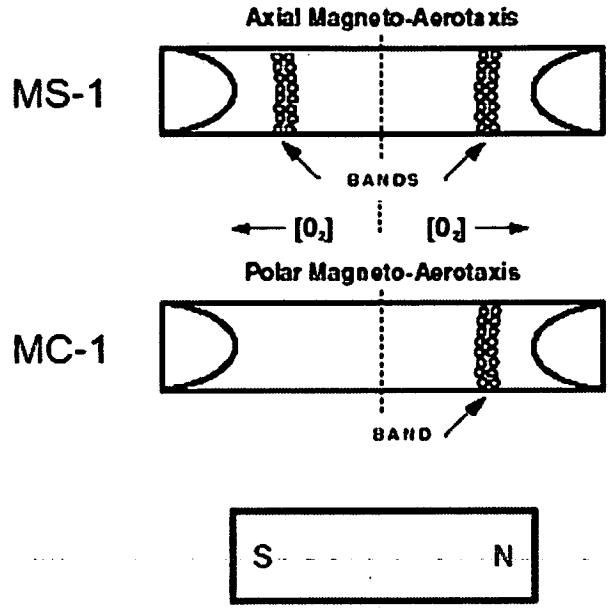

Figure 1.6 The difference in the axial magneto-aerotaxis of MS-1 and the polar magneto-aerotaxis of MC-1. This figure depicts an experiment that was carried out in a flat capillary tube containing appropriate medium where a double oxygen gradient was formed at each open end of the tube. Note how MS-1 travels in both directions following the line of the magnet to the appropriate oxygen concentration whilst MC-1 travels to the correct oxygen concentration at the north pole of the magnet. (Plate and legend are courtesy of Dennis Bazylinski with slight adaptation).

Essentially, magnetotaxis increases the efficiency of aerotaxis in vertical concentration gradients by reducing a three dimensional search to a single dimension (Blakemore *et al.*, 1980). There are perhaps other forms of chemotactic response that work in conjunction with magnetotaxis to aid magnetic bacteria living in anaerobic environments (Bazylinski, 2004). So perhaps it would be more fitting that this section was entitled "Magneto-chemo-taxis in bacteria".

The coexistence of magnetotactic bacteria with opposing polarities in the same redox environment has been identified (Simmons *et al.*, 2006). This discovery conflicts with current models of the adaptive value of magnetotaxis in magnetic bacteria where bacteria thriving at the same redox levels might be attracted either north or south in the same hemisphere. Those swimming south in the northern hemisphere would, according to the long respected model, essentially be swimming away from their ideal survival conditions, and vice versa for bacteria living in the southern

hemisphere. It is important to understand that the behaviour of a magnetic bacterium *in situ* could differ from behaviour in the laboratory due to the fact that magnetotactic bacteria at the chemocline of a stratified water column rarely, if ever, experience atmospheric oxygen levels like those in the standard laboratory assay for polarity. It is also likely that they experience chemical gradients, particularly iron and sulphur species, not present in a drop of water exposed to air in a laboratory assay (Simmons *et al.*, 2006).

1.1.4 Alternative evolutionary requirements for magnetosome formation

A further suggestion to account for the selective advantage for forming magnetosomes based on available publications include the magnetosomes' potential contribution to iron homeostasis and detoxification within the cell as suggested by the sensitivity to iron of the non-magnetic mutant, *Magnetospirillum gryphiswaldense* MSR-1B (Schübbe *et al.*, 2003).

Another suggestions is that perhaps magnetosomes function as an iron store just as it has been documented that magnetic bacteria harbour poly(3-hydroxybutyrate) (PHB) inclusion bodies containing a carbon source that can be hydrolysed under starvation periods (Schultheiss *et al.*, 2005). There is some evidence to show that magnetic bacteria in the wild may sometimes be present in a non-magnetic state (Sakaguchi *et al.*, 1996) whilst in laboratory culture magnetic bacteria biomineralise iron as long as there is iron present in the culture medium. Single domain crystals may be the most advantageous way for the cell to pack iron for storage and the behaviour induced by magnets in a laboratory may be caused by an artefact that has been the basis of models on the magnetotactic response of magnetic bacteria. Fridge magnets that can be used in a laboratory to induce a magnetotactic response have a magnetisation far greater than that of the Earth's magnetic field, which averages about 50,000 nT, the equivalent of 0.5 Gauss. An average sised fridge magnet has a magnetisation of c. 10 Gauss.

1.1.5 Evolution of magnetosomes and magnetoreception in migratory organisms

There was controversy surrounding the sense of magnetoreception (Kirschvink *et al.*, 2001). Up to the 1970s it was believed that studying magnetic effects on organisms was the work of charlatans as magnetoreception is not a sense that humans are necessarily aware of experiencing. Also, the lack of clear and simple biological transduction mechanisms led to a number of competing biophysical hypotheses (Table 1.2).

Table 1.2 Hypotheses regarding magnetoreception in migratory organisms explained in terms of basis and evidence (Lohman and Johnsen, 2000; Kirschvink *et al.*, 2001; Bisio *et al.*, 1999, Mora *et al.*, 2004).

Electromagnetic induction	**Basis** An electron moving through a magnetic field experiences a force perpendicular to both its motion and the direction of the field. **Evidence** Rays and sharks are highly sensitive to electrical fields generated by the tissues of prey. In principle this is sufficient for the detection of the Earth's magnetic field.
Chemical magnetoreception	**Basis** Nuclear and electron spins may be influenced by chemical reactions triggered by weak magnetic fields. **Evidence** Electrophysical responses to magnetic fields have been detected in several parts of the avian nervous system that receive projections from the nervous system.
Magnetomechanical magnetoreception	**Basis** Magnetic crystals exert a torque on secondary receptors as the particles align with the geomagnetic field. **Evidence** Trout and pigeons contain magnetosomes in cells that are innervated by a branch of the fifth cranial nerve.

Steady magnetic fields produce a distortion of the molecular energy distribution including spatial and directional current asymmetries (Bisio *et al.*, 1999). Considering this, it is hypothesised that magnetoreception aids a response to geomagnetic fields that may influence the direction taken by migrating organisms. Kirschvink and Walker (1986) believe the most plausible structures for use as magnetoreceptors in higher organisms as well as in bacteria are single-domain magnetosome organelles. Electromagnetic induction, chemical magnetoreception and magnetosome based magnetoreception support hypotheses for magnetoreception (Lohman and Johnsen, 2000). The diversity associated with magnetosomes including the magnetic properties of paramagnetic and multi-domain particles are in keeping with postulations that magnetoreceptors are specialised for discrete functions where some may monitor magnetic field direction and others magnetic field intensity (Kirschvink *et al.*, 2001). Hypotheses regarding magnetoreception in migratory organisms explained in terms of basis and evidence are presented in Table 1.2.

Reference has been made to birds, amphibians, marine turtles and arthropods that use the geomagnetic force to orient in conjunction with sight (Kimchi and Terkel, 2001). Photo-magnetoreceptive animals also have the ability to orient in the absence of light. For example, migratory birds in the northern hemisphere appeared to follow their predicted northern flight path in clear skies (Gudmundsson and Sandberg, 2000). In overcast skies approximately half the birds broke away and started following a southern flight path, in the direction of wintering grounds in the southern hemisphere. This seems to reflect magneto-chemo-taxis in bacteria from northern and southern hemispheres in a hanging drop laboratory assay (Simmons *et al.*, 2006) (Section 1.1.3; Figures 1.4; Figure 1.6). In the absence of usual cues the magnetoreception appeared to govern orientation.

Behavioural experiments incorporating the use of a strong magnetic field and a maze carried out on the blind mole rat (*Spalax ehrenbergi*) showed that under the Earth's natural magnetic field mole rats show a preference for building nests in the southern sector of the maze and when the magnetic field was shifted 180°, the mole rat's preference also shifted 180° to the northern sector (Kimchi and Terkel, 2001).

Magnetoreception is now well established in virtually all major groups of animals (Wiltschko and Wiltschko, 1995), and specialised cells containing single-domain chains of magnetite are the best candidates for the receptor cells (Walker *et al.*, 1997; Kirschvink, 1997; Lohman and Johnsen, 2000). From an evolutionary perspective, it seems that magnetite-based magnetoreception, and hence magnetite biomineralisation, date back at least to the last common ancestor of Chordata, Mollusca, and Arthropoda (~600 to 900 Myr ago) (Kirschvink, 2000).

Magnetic bacteria were discussed for the first time in 1975 (Blakemore, 1975). In 1983 Magnetotactic Multicellular Aggregates (MMAs) were discovered in the oxic-anoxic transition zone (OATZ) that co-ordinately and simultaneously divided on reaching an upper sise limit (Lins and Farina, 1999). Seven years on further reports of MMAs revealed that individual cells in aggregates are connected by the presence of cell-to-cell junctions and it was concluded that these MMAs were best described as a many-celled magnetotactic prokaryote; and that specialised intercellular membrane junction-like structures in prokaryotes may have preceded those in eukaryotes (Rodgers *et al,* 1990). These discoveries and the potential of magnetosomes as biological bar magnets gave strength to hypotheses of magnetoreception using inbuilt systems in migratory animals.

The possibility of magnetotactic bacteria incorporating themselves into eukaryotic cells through endosymbiosis exists (Kirschvink *et al.*, 2001). Kwang Jeon witnessed all the initial stages of endosymbiosis occurring between bacteria and amoeba that he was studying (Jeon 1987, Jeon, 2000; Margulis and Sagan, 1997). Large, free-living amoebae are inherently phagocytic on microbes that they digest in phagolysosomes. An unidentified Gram-negative, rod-shaped bacterium that spontaneously infected a strain of *Amoeba proteus* came to survive inside them. These bacteria established a stable symbiotic relationship with amoebae that resulted in phenotypic modulation of the host and mutual dependence for survival (Jeon, 2000). The widespread distribution of organisms (prokaryotes, protists, chordates and arthropods) reported

to be magnetoreceptive argues that this sense evolved prior to the radiation of the animal phyla and shares a common origin.

Ferromagnetic particles have been removed from the upper beak area of the bobolink – a migratory bird, whilst similar particles have been removed from the olfactory lamellae of trout (Lohman and Johnsen, 2000). In the brown trout, it was shown that magnetically-sensitive nerves in the ophthalmic branch of the trigeminal nerve connect to specialised, tri-lobed cells in the olfactory laminae which contain magnetite crystals (Walker *et al.,* 1997). Similarly, behavioural work with migratory organisms has shown that brief magnetic pulses are able to alter their magnetic responses, confirming that a ferromagnetic material like magnetite is indeed part of the magnetic sensory system.

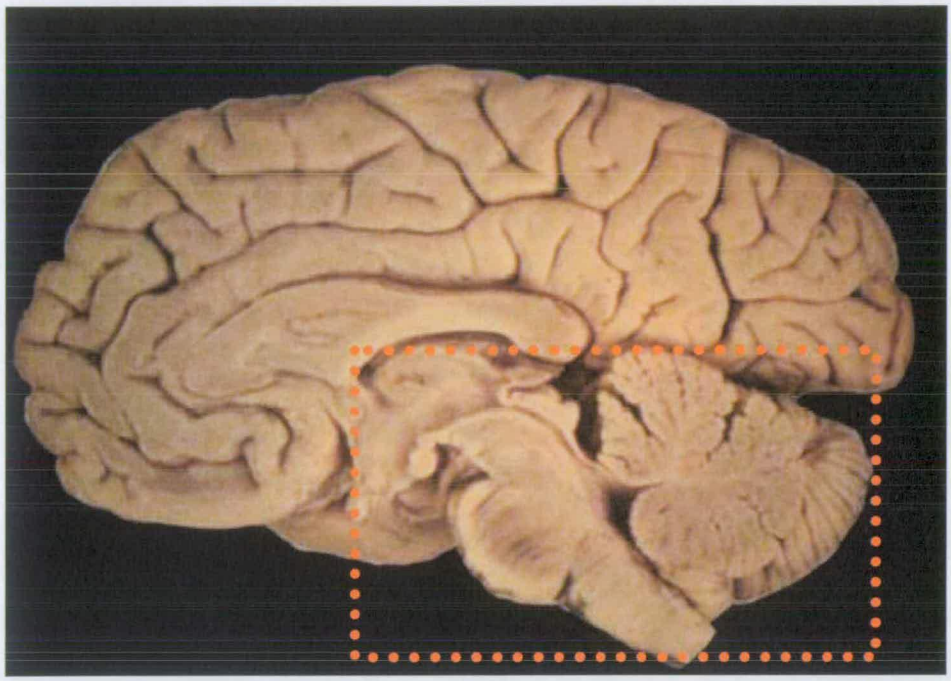

Figure 1.7 The distribution of magnetosomes in the human brain highlighted withing the red dashed line. This region is also in keeping with isolation of magnetosomes from migratory animals (Plate courtesy of the University of Edinburgh)

Further documented examples of magnetosome harbouring organisms include honeybees, pigeons, turtles, protoctists, a variety of pelagic fish, butterflies, newts, shrimps, barnacles, bats and rodents (Gould *et al.*, 1978; Walcott *et al.*, 1979; Kirschvink, 1981; Kirschvink and Gould, 1981; Walker *et al.*, 1984, 1988; Kirschvink *et al.*, 1985 a, b, c; MacFadden and Jones, 1985; Buskirk and O'Brien,

1985; Perry *et al.*, 1985, Buehler and Wasilewski, 1985; Bauer *et al.*, 1985; Mather, 1985; Torres de Araujo *et al.*, 1986, Vali *et al.*, 1987; Mann *et al.*, 1988, Lohman *et al.*, 2000, Phillips *et al.*, 2001).

A diffuse and homogenous distribution of single domain magnetite crystals, with a minimum of 5 million magnetite crystals per gram of tissue in human central lobes, cerebellum, basal ganglia and midbrain were identified (Kirschvink *et al.*, 1992) (Figure 1.7). The samples bore a remarkable resemblance to single domain crystals removed from bacteria, fish and other organisms. In terms of phyletic diversity, magnetite may soon rank as the fourth-most abundant biogenic mineral after calcite, aragonite (calcium carbonate forms), and opal (silica) (Chang and Kirschvink, 1989).

Each region of the brain mentioned above is involved in sensory processing and instinctual behaviour as opposed to intellectual puzzle solving.

1.1.6 The influence of magnetosomes on theories of the origin of life

Some planetary scientists showed particular interest in bacterial magnetosomes towards the end of the 1980s (Funaki *et al.*, 1989). Magnetofossils found on the Martian meteorite ALH84001 (Figure 1.8) fuelled controversial debates on extraterrestrial life and panspermia theories. The Panspermia hypothesis refers to the inevitable transfer of life from planet to planet based on the infinite extent and duration of the Universe (Raulin-Cerceau *et al.*, 1996). The arrival of the Big Bang theory and Louis Pasteur's refutation of the spontaneous generation of life detracted from Panspermia and swayed popular belief toward the assumption that life originated on Earth (Kirchvink *et al.*, 2002; Raulin-Cerceau *et al.*, 1996). Davis and McKay (1996) discuss many theories related to the origins of life under extraterrestrial and terrestrial headings and explain how there is no consensus relating to the theories of the origins of life.

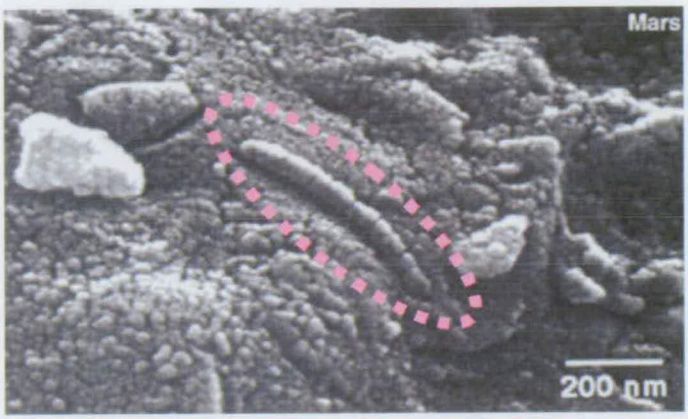

Figure 1.8 Structures in Martian meteorite ALH84001 resembling magnetosome chains. (http://www.britannica.com/ebc/art/print?id=70954&articleTypeId=0)

Adding to the debate of the origin of life was initiated by the discovery of Martian meteorite ALH84001. Much of the controversy surrounding ALH84001 is due to the lack of determination of the iron oxide crystals' organic or inorganic origin (Buseck *et al.*, 2001). The broad range of sises and shapes of crystals uncovered on ALH84001 is problematic to the crystals' positive identification. Once identified a decision concerning their biogenic or geological deposition could be made (Buseck *et al.*, 2001; Kirschvink *et al.*, 2002; Posfai *et al.*, 1998). If magnetofossils on the meteorite are positively identified as biogenic in origin, theories of the origins of life would require reshaping.

1.1.7 Magnetosomes as markers of paleoenvironmental change

The beginning of the 1980s saw noticeable interest in bacterial magnetosomes with regard to the geological history of our planet (McCrea, 1981; Lovlie and Larsen, 1981; Kirschvink, 1982; Wisnioweiki *et al.*, 1983; Kirschvink and Chang, 1984; Robinson, 1986; Chang *et al.*, 1987, Snowball *et al.*, 2002; Berquo *et al.*, 2004; Chang *et al.*, 1989).

Magnetosome particles behave as dipole magnets and contribute significantly to the magnetisation of sediments (Stolz, 1993). Magnetic concentration, grain sise and mineralogy; and the inclination, declination and intensity studies of Lake Baikal, Siberia, have provided useful information regarding paleoenvironmental change, in

particular limnological and climatic change (Peck and King, 1996). Limnology is defined as the study of freshwater systems with particular emphasis on their history, geology, biology, physics, and chemistry of lakes. In this instance the changes were mapped by studying the chemistry of magnetofossils and the level of dissolution that they had gone through related to oxidised and reduced conditions. The magnetosomes tend to dissolve under reduced conditions. The correlation between concentration of magnetosomes and the percentage of total organic carbon (TOC) as an indicator of organic productivity in lakes indicates the importance of magnetosomes as markers (Snowball *et al.*, 2002). Their results show that over long time scales the organic productivity is partly driven by temporal variations.

The dipole orientation of magnetofossils buried deep in sediments is one of several markers that have contributed information relating to the positional history of plate tectonics (Williams and Jercinovic, 2002). To understand the basic theory one needs to imagine populations of magnetic bacteria dying and lysing over time to release their magnetic particles that fall to rest with their axes in alignment with the Earth's magnetic poles. As the plates move over time the magnetosomes that have settled on them misalign with the magnetic poles to reveal how many degrees out of line they are.

1.1.8 Magnetosomes as a platform technology with great scope for commercialisation

Magnetic particles are already being used in applications such as magnetic carriers in immunoassay and drug delivery, molecular and cell separation systems, and magnetic memory in electronic applications. Further visions of their use have been recognised in automotive, audio-visual and information recording, molecular biology, pharmaceuticals and diagnostics industries (Schüler, 1999; Bisio *et al.*, 1999; Matsunaga *et al.*, 2007). Bacterial magnetosomes have been recognised in the material sciences as a resource worth harnessing for uses in applications stated above, i.e., electronics, automotive, audio-visual, information recording, molecular biology (Nakamura *et al.*, 1991; Nakamura *et al.*, 1993; Nakamura and Matsunaga,

1993; Sode *et al.*, 1993; Takeyama *et al.*, 1995), pharmaceuticals, diagnostics industry and so forth.

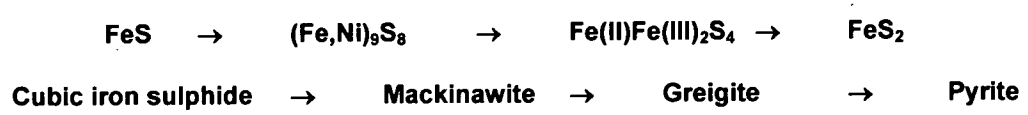

Figure 1.9 Chemical formulas for compounds formed in the reaction sequence from iron sulphide to pyrite.

The conversion of mackinawite to greigite and ultimately to pyrite has been observed extracellularly in the dissimilatory, sulphate-reducing bacterium *Desulfovibrio desulfuricans* (Posfai *et al.*, 1998). The same reaction occurs at low temperatures in nonbiological reactions when excess S or S^{2-} is present (Figure 1.9). The greigite producing magnetotactic bacteria are probably dissimilatory sulphate-reducers living where there are relatively high concentrations of H_2S. Posfai *et al.* (1998) demonstrates that the same inorganically driven iron sulphide reaction sequence occurs in the magnetotactic bacteria as in the geological environment. However, in bacteria the sequence is under strict control and truncated at greigite thus preventing the development of non-magnetic pyrite (Bertani *et al.*, 2001; Okuda and Fukamori, 2001). Strategies for aerobic magnetite production will be presented later in Sections 1.2.4.1 and 1.2.4.2.

Presently, the ferrite industry meets the demands for nano-sised magnetite particles by chemical synthesis. This involves the co-precipitation of Fe (II) and Fe (III) in alkaline solution (Figure 1.10).

Figure 1.10 A chemical equation representing ion transfer during the co-precipitation of Fe (II) and Fe (III) in alkaline solution.

For the past 60 years the ferrite industry has tried and failed to attain the high quality of form associated with bacterial magnetosomes (Kirschvink *et al.*, 2002). The chemical techniques required to prepare high quality magnetite particles by these techniques requires strict control over pH, temperature and pressure during the reaction process (Schüler, 1999). Much energy and time are therefore devoted to the preparation of nano-sised magnetite particles with well-defined shape and sise. Leaders in the field (e.g. Bazylinski, Frankel, Kirschvink, Matsunaga and Schüler) believe that additional biological controls would yield greater advantages during nano-particle manufacture (See section 1.2.6).

1.1.9 Bioremediation

Magnetotactic bacteria have the ability to sequester copious amounts of iron from low concentrations in the environment (Schüler, 1999; Stolz, 1993). Growth conditions do not appear to affect the sise and morphology of the crystals but the number of magnetosomes in a cell may vary considerably (Schüler, 1999). This point is commercially relevant to the industrial synthesis of magnetosomes (Section 1.1.8). Due to the large surface area to volume ratio magnetosomes are useful carriers for the immobilisation of relatively large quantities of bioactive substances that may then be separated by magnetic fields.

With the development of techniques for manipulation of magnetosome genes into other species (Okuda and Fukamori, 2001; Ochman *et al.*, 2000) it may be possible to engineer organisms for bioremediation of contaminated aquifers, landfills, or any other environment that these organisms might be induced to migrate to (Urban, 1998). Magnetotactic bacteria have been shown to be useful for the removal of heavy metals and radionuclides from wastewater (Schüler, 1999); the role of magnetotactic bacteria in bioremediation is strengthened due to the observation that magnetosomes contain iron sulphides as mineral phases but can also incorporate other metals like copper (Lins and Farina, 1999).

In recent years there has been an increasing global interest in interactions of heavy metals within microorganisms (Pümpel *et al.*, 1995). The pollution of the environment with heavy metals has led to the selection of heavy metal resistant microorganisms in the soil and water of industrial regions. In many cases, resistance to heavy metals is encoded on plasmids, which can be used for the creation of novel microbial strains with high detoxifying activity against heavy metals (Aleem *et al.*, 2003; Llamas *et al.*, 2000). The study of the ability of magnetic bacteria to partition various metals coupled with either the loosening of laws related to the release of genetically modified organisms or development of immobilisation matrices to reach basic government guideline standards may be invaluable to the clean up of polluting toxic metals on a global scale.

1.2 UNDERSTANDING THE SUBCELLULAR ORGANISATION OF THE BACTERIAL MAGNETOSOME

The availability of the complete genomes of the magnetotactic *alphaproteobacteria*, *Magnetospirillum magnetotacticum* MS-1, and magnetic coccus MC-1 (http://www.jgi.doe.gov/JGI_microbial/html/index.html) allowed increased study of magnetosome formation at the genomic level at the turn of the century (Grünberg *et al.*, 2001). Research on the genome of MC-1 was overshadowed by a focus on three magnetic spirilla, *Magnetospirillum magnetotacticum* MS-1 (USA), *Magnetospirillum magneticum* AMB-1 (Japan) and *Magnetospirillum gryphiswaldense* MSR-1 (Germany) because of the relative ease found whilst culturing them. In turn each of these spirilla has yielded characteristics that are revolutionising our understanding of magnetosome formation at a molecular level.

Figure 1.11 A pellet of isolated magnetosomes in a microfuge tube sticking to a permanent magnet. (Plate courtesy of Dirk Schüler).

Much of the initial work carried out by groups interested in magnetosome synthesis used high magnification imaging and magnetosome isolation (Figure 1.11) for structural composition analysis of the magnetosome membrane and the crystals within them. Protein work led on from structural composition analysis and this work focused on isolating the magnetosome crystals to determine what proteins were most closely associated with them. The discovery of the chromosomal magnetosome

island, discussed in section 1.2.2, and genetic techniques developed for *Magnetospirillum* spp. facilitated studies on the putative function of magnetosome associated proteins. As magnetosomes are biogenically produced the consensus in the field was that the magnetosome membrane assists in anchoring the particles at designated positions in the cell and also provides the location for nucleation and growth of the crystals thus advantageously increasing their net magnetisation (Frankel and Bazylinski, 2001).

1.2.1 The conformation and composition of the magnetosome

Each magnetosome is composed of an intracellular magnetic iron mineral crystal (magnetosome crystal). These particles are enclosed by lipids including glycolipids, sulpholipids, and phospholipids similar to those of the cytoplasmic membrane (magnetosome membrane) (Refer to Sections 1.1.1 and 1.1.2).

1.2.1.1 The magnetosome membrane

The protein and lipid composition of the magnetosome membrane of *Magnetospirillum magnetotacticum* MS-1 were found to have similarities to other biological cell membranes (Gorby *et al.,* 1988). However, most proteins detected in the envelopes of purified magnetosomes were of a mass (but not a quantity) similar to those of the cytoplasmic membrane, whilst two unnamed, uncharacterised proteins (15 kDa and 33 kDa) were unique to the magnetosome envelope.

1.2.1.2 Magnetosome crystals

A variety of magnetosome crystal structures have been noted (Figure 1.12) such as truncated octahedrons, parallelipeds, hexagonal prisms, tear- and flake- shaped particles and on rare occasions, twinned particles from a diverse range of organisms not necessarily in pure culture (Posfai *et al.*, 1998; Stoltz, 1993). The crystals arguably range in diameter from less than 40 nm to greater than 100 nm depending on species. The sise of the crystal imparts an influence on the magnetic properties of the crystal as outlined in Table 1.3.

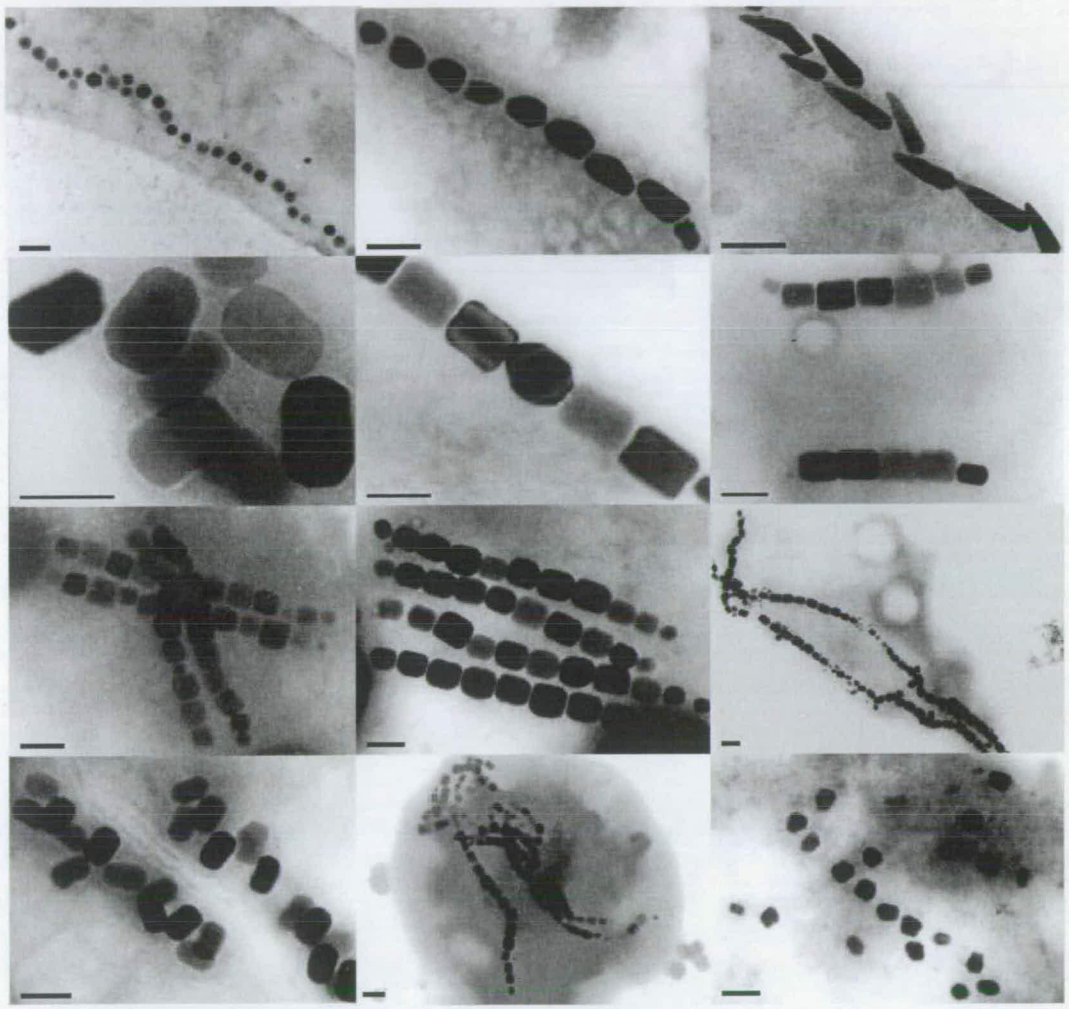

Figure 1.12 Micrographs showing the diversity of magnetosome crystals found in various magnetotactic bacteria from different environments (bar represents 0.1 micrometer). Most of the bacteria shown have not been isolated in pure culture. (Plate and legend courtesy of Dirk Schüler, www.mikrobiologie.biologie.uni-muenchen.de/index.php?showpage=68)

The Goldilocks Principle has been used to explain the strong selective pressure that constrains the sise and morphology of a functional magnetosome more commonly to that of the single-domain particle (Stolz, 1993). If the particles are too small (superparamagnetic particles), they do not have enough mass to overcome the energy of thermal vibration to maintain a stable magnetic moment; and if the particles are too big (multi-domain particles), domain walls form with randomly oriented magnetic domains resulting in a weak total magnetic moment. That leaves single domain particles "just right" for magnetotaxis and indeed magnetoreception assuming magnetosomes in bacteria are biomineralised for the purpose of navigation (refer to Section 1.1.3).

Table 1.3 Some magnetic properties of ferromagnetic particles (based on information in Kirschvink and Walker, 1986; Frankel and Bazylinski, 2001; and Stolz, 1993). (Plate adapted courtesy of Dennis Bazylinski.)

Superparamagnetic particles 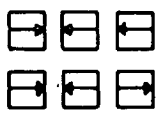	Less than 35 nm in size these particles are uniformly magnetised but the direction of the magnetic moment is not stable in relation to the crystal's axis. Any small magnetic or thermal fluctuation will cause the magnetic moment to wander.
Single-domain particles 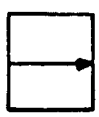	Measuring 35 nm to 100 nm in size these particles are uniformly magnetised with a stable magnetic moment throughout the particle volume in relation to the crystal's axis. These particles will rotate like compass needles in an external magnetic field and can produce a measurable torque on neighbouring structures. Net magnetisation increases per unit volume of these particles.
Multi-domain particles 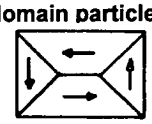	Generally >100 nm, these particles form internal domains that have atomic moments aligned in randomly varying directions. Net magnetisation per unit volume of these particles is negligible.

Magnetosomes more commonly assume the form of magnetite (Fe_3O_4) in oxic environments or, may also assume the form of greigite (Fe_3S_4) in sulphidic environments (Posfai *et al.*, 1998) whilst the controlled biomineralisation of magnetite and greigite in the same magnetotactic bacterium has also been reported (Bazylinski *et al.*, 1995). Bacteria isolated from sulphidic environments have also

been found to contain pyrite (FeS_2) along with greigite (Mann *et al.*, 1990), whilst monoclinic pyrrhotite (Fe_7S_8) has been identified in an uncultured rod (Farina *et al.*, 1990). Evidence of mackinawite ($(Fe,Ni)_9S_8$), an intermediate in the synthesis of magnetic greigite, and the non-magnetic pyrite (FeS_2) and pyrrhotite ($Fe_{(1-x)}S$ (x = 0 to 0.2)) formed after the reduction of greigite have been reported (Posfai *et al.*, 1998) (refer to Section 1.1.8, paragraph 2). Intermediates in greigite formation were located in the magnetosomes at the ends of what was to become a linear chain perhaps indicating the formation of the magnetosomes from a single point extending out in two directions. A variable amount of up to 10 % of copper in the composition of iron-sulphur magnetosome crystals has been reported (Posfai *et al.*, 1998). The transition of greigite to pyrite is not advantageous for the navigation of magnetic bacteria as pyrite is a non-magnetic material. The selective advantage of magnetosome crystals is discussed in Section 1.1.3.

1.2.2 Isolation of genes involved in magnetosome formation

The first example of gene transfer using Tn5 insertions in a magnetic bacterium was reported of the isolation of three genomic fragments from *Magnetospirillum magneticum* AMB-1 involved in the synthesis of magnetosomes (Matsunaga *et al.*, 1992). Two of the isolated fragments were restriction mapped and the position of the transposon insertion was determined. Hybridisation studies revealed that high homology existed between the genomes of *Magnetospirillum magneticum* AMB-1 and *Magnetospirillum magnetotacticum* MS-1.

PCR was used to amplify the 16s rRNA gene from the chromosome of *Magnetospirillum magneticum* AMB-1 and then to sequence it. For the first time the phylogenetic relationship between the three *Magnetospirillum* sp. was studied. Unexpectedly *Magnetospirillum magneticum* AMB-1 is more closely related to *Magnetospirillum magnetotacticum* MS-1 compared to the more aerotolerant *Magnetospirillum gryphiswaldense.* This was a surprise as *Magnetospirillum magneticum* AMB-1 is capable of growing aerobically and is oxidase positive.

A low-resolution physical genome map of *Magnetospirillum magnetotacticum* MS-1 was constructed using pulsed field gel electrophoresis (PFGE) (Bertani *et al.*, 2001). They determined the sise of the genome to be 4.3 Mb which today is presented as 9.2 Mb at the National Centre for Biotechnology Information (NCBI) (http://www.ncbi.nlm.nih.gov/genomes/framik.cgi?db=genome& gi=5016).

Magnetospirillum magnetotacticum MS-1 belongs to the α-subgroup of the *Proteobacteria* of which some members are photosynthetic (Bertani *et al.*, 2001). As most of the genes involved in photosynthesis are clustered in superoperons, occupying about 1% of the genome (Bertani *et al.*, 2001), it may be that the genes involved in magnetite synthesis cluster in a similar way. Some members of the α-proteobacteria have been physically characterised and found to have unusual genome structure, including linear and multiple chromosomes (Jumas-Bilak *et al.*, 1998). Dean and Bazylinski (1999) studied magnetic marine vibrio strains and found no unusual structures. The genome sises of MV-1, MV-2 and MV-4 were given as

approximately 3.6, 3.7 and 4.5 Mb respectively, but there was no genetic characterisation.

Prior to the discovery of definitive evidence of the biogenic control of magnetosome synthesis it had been postulated that the process was under biogenic control. It was also postulated that the formation and alignment of iron sulphide crystals were each under separate control as observed by the accumulation of non-magnetic sulphides in the vesicle and the alignment of the vesicle prior to the crystals becoming magnetic in a magnetic Deltaproteobacterium (Posfai *et al.*, 1998). The presence of vesicles containing no magnetic crystals has been documented in wild type *Magnetospirillum magnetotacticum* MS-1 cells starved of iron, whilst in a non-magnetic mutant similar vesicles were not present (Balkwill *et al.,* 1980; Gorby *et al.,* 1988). Repeated observations of the consistent morphology associated with magnetosome crystals found in varying species allowed models for the exertion of a high degree of genetic control over magnetosome vesicle and crystal formation to be developed (Frankel and Bazylinski, 2001).

Magnetosome chains were fractionated and separated by SDS-PAGE electrophoresis (Grünberg *et al.*, 2001). N-terminal amino acid sequencing was performed on several major magnetosome membrane specific polypeptides and from these sequences long non-degenerate primers were designed based on codon usage bias found in previously analysed genes from *Magnetospirillum* species. These oligonucleotides were labelled and directly used as probes for hybridisation for magnetosome associated genes and MamA, MamB, MamC and MamD were eventually identified.

The previously unreported genes (*mamA, mamB, mamC* and *mamD*) of *Magnetospirillum gryphiswaldense* were involved in magnetosome formation and their characteristics were comparable to equivalent proteins from *Magnetospirillum magnetotacticum* MS-1 and magnetic coccus strain MC-1 (Grünberg *et al.*, 2001). The *mamB* gene of *Magnetospirillum gryphiswaldense* MSR-1 was located 1,120 bp downstream of *mamA*. Both genes were part of a region containing several ORFs of

collinear orientation. Genes that were homologous to *mamA* and *mamB* were found in the same chromosomal region of *Magnetospirillum magnetotacticum* MS-1 (contig 3824) and strain MC-1 (contig 431) (Figure 1.13). Grünberg *et al.* (2001) tabulated the arrangement of ORFs in the chromosomal *mamAB* gene clusters and the characteristics of the corresponding predicted proteins of *Magnetospirillum gryphiswaldense* MSR-1, *Magnetospirillum magnetotacticum* MS-1 and strain MC-1 (Figures 1.13 and 1.14). In *Magnetospirillum gryphiswaldense* MSR-1, *mamA* and *mamB*, together with at least eight other ORFs arranged in a collinear fashion implied an operon-like structure. This organisation was identical to that of *Magnetospirillum magnetotacticum* MS-1, which was part of a larger cluster comprising 16 consecutive ORFs with transcription running in the same direction. In both organisms the *mamB* gene and the two ORFs preceding it overlapped by a single nucleotide, respectively. They pointed out that the two genes were organised similarly in magnetic coccus strain MC-1, together with seven consecutive ORFs extending over 11 kilobases. The chromosomal *mamAB* clusters in the three strains were characterised by the presence of one or several members of various classes of homologous genes. Several of these classes corresponded to the gene *lemA or* genes encoding proteins with TPR motifs, or homology to CDF family proteins or HtrA family proteins.

The tetratricopeptide repeat (TPR family) is a ubiquitous motif found in a number of proteins that are functionally unrelated (Blatch and Lässle., 1999). TPR motifs mediate a variety of different protein-protein interactions with partner proteins and proteins containing TPR are involved in a diverse spectrum of cellular functions with the majority of them participating in cell cycle control, transcription and splicing events, protein transport especially protein import, regulatory phosphate turnover, and protein folding. There are more than 50 proteins present in organisms as diverse as bacteria and humans containing TPR motifs.

Cation diffusion facilitator (CDF family) proteins occur ubiquitously in eukaryotes, bacteria and archaea and are involved in the transport of various heavy metals. HtrA proteins are widely distributed in *Escherichia coli* and other bacteria. They are heat

shock induced serine proteases that are active in the periplasm where their main function is to degrade misfolded proteins. Although little is known about the *lem*A gene, in the plant pathogen *Pseudomonas syringae* pv. syringae it is required for disease lesion formation on bean plants and appears to be positively auto-regulated (Hrabak and Willis, 1992). As a LemA homologue (MamP) is located on the magnetosome island that in turn is vital to the biomineralisation of iron this indicates that LemA is involved in iron sequestration in *Pseudomonas syringae* pv. syringae.

The discovery of a genetic region involved in magnetosome synthesis proved to be a great advance in understanding the genetic control of magnetosome formation in *Magnetospirillum gryphiswaldense* MSR-1 (Schübbe, *et al.,* 2003) and other magnetic bacteria. The finding resulted in the isolation and characterisation of the *Magnetospirillum gryphiswaldense* MSR-1B, non-magnetic mutant derived from the wild type. Most important to the scientific community's understanding of the genetic control that magnetic bacteria have over the organisation of their magnetosomes were comparative results from work carried out on a library of bacterial artificial chromosomes (BACs) from the wild-type and non-magnetic mutant. This landmark discovery was popularly known as the "chromosomal magnetosome island" and supported earlier and contemporary work that attempted to understand the genetics and proteomics of magnetosome organisation in magnetic bacteria (Arakaki *et al.,* 2003; Bertani *et al.,* 1997; Gorby *et al.,* 1988; Grünberg *et al.,* 2001; Grünberg *et al.,* 2004; Okuda *et al.,* 1996; Okamura *et al.,* 2001; Schleifer *et al.,* 1991; Schüler, 2002; Schultheiss and Schüler, 2003).

A 35 kilobase region comprised of 37 open reading frames (ORFs), of which 16 contained domains of recognised function, most of which are divided between three operons (*mms6*, *mamDC* and *mamAB*) was described (Schübbe *et al.,* 2003), outlined in Figure 1.14. Many of the genes without recognised function were putatively considered to be specific to magnetosome organisation through identification of homologous genes in other magnetic bacteria, specifically, *Magnetococcus* MC-1 (genome sequence available online, www.ncbi.nlm.nih.gov), magnetic vibrio MV-1 (direct communication with Prof. Dennis Bazylinski), *Magnetospirillum magnetotacticum* MS-1 (genome sequence available online, www.ncbi.nlm.nih.gov) (Bertani *et al.,* 1997) and *Magnetospirillum magneticum* AMB-1 (genome sequence available online, www.ncbi.nlm.nih.gov).

Although the three clusters (*mms6*, *mamDC* and *mamAB*) identified in the 37 kb region of *Magnetospirillum gryphiswaldense* MSR-1 were also present in the other *Magnetospirillum* species and *Magnetococcus* MC-1 the sequence of genes was incontiguous compared to regions from *Magnetospirillum gryphiswaldense* MSR-1

as can be seen to a certain extent in the *mamAB* operon depicted in Figure 1.13. This mosaic-like structure resembles many of the characteristics of a genome island suggesting that magnetosome formation in bacteria is the result of horizontal gene transfer (Schübbe *et al.,* 2003). Comparison has been made between this magnetosome island and pathogenicity islands where presence or absence of a pathogenicity island determines the success or failure of host colonisation between serovars (Schubert *et al.,* 2004). Further evidence to suggest that magnetosome formation in microorganisms has separate evolutionary origins or is the result of lateral gene transfer is the division of iron –oxide and –sulphide assimilators respectively into α- and δ- subdivisions of the Proteobacteria (De Long *et al.,* 1993), the Nitrospira and members of the Eukaryota (Mann *et al.* 1990).

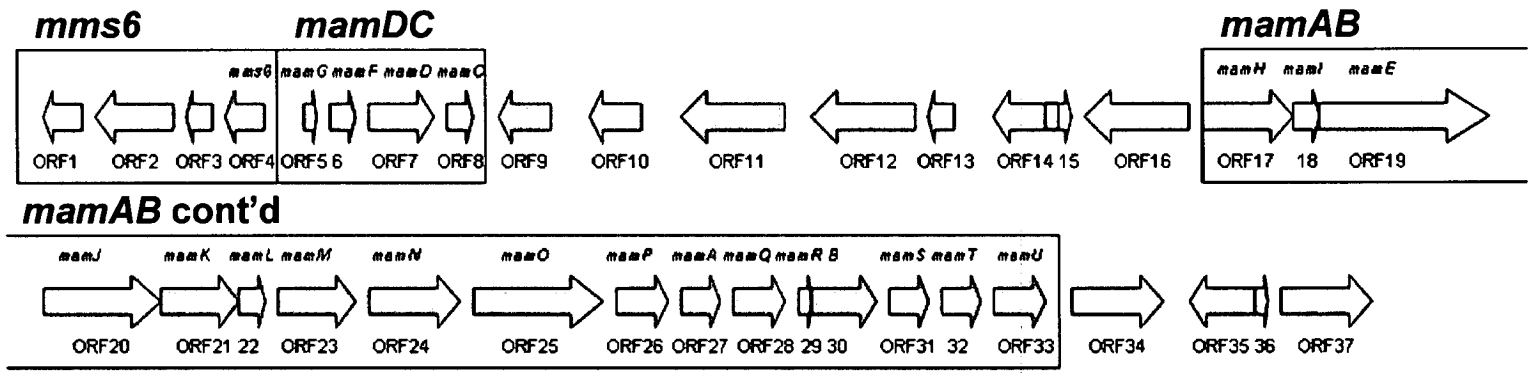

Magnetosome associated clusters

mms6 (ORF1 – ORF4)

mamDC (ORF5 – ORF8)

mamAB (ORF17 – ORF33)

☐ Sequences containing domains of recognised function (Psi- and Phi- Blast)

ORF9 – Iron ABC transporter

ORF11 – CueR type Helix-turn-helix transcription regulator / Transposase / Integrase

ORF12 – N-terminal chemotaxis domain (CheY) with a central haemerythin domain

ORF13 – Haemerythrin domain

ORF19 – Trypsin-like serine protease (DegQ, DegP, HtrA)

ORF21 – Actin structure domain (MreB)

☐ Cont'd

ORF23 – Cation efflux pump (CzcD)

ORF24 – Anion permease (ArsB, HhaD, YbiR, CitT)

ORF25 – Trypsin-like serine protease

ORF26 – Trypsin-like serine protease / PDZ domain (DegP, HtrA)

ORF 27 – Tetracopeptide repeat (TPR) domain / Flp pilus assembly protein (TadD)

ORF28 – LemA amino terminal predicted tranmembrane helix that is possibly extracellular and potentially involved in nodule formation in plants in *Pseudomonas syringae*

ORF30 – Cation efflux pump (CzcD)

ORF33 – Sphingosine kinase and enzymes related to eukaryotic diaglycerol kinase (lipid metabolism)

ORF35 – Full length transposase domain

ORF37 – Full length transposase domain

Figure 1.14 Depiction of the molecular organisation of the chromosomal magnetosome island of *Magnetospirillum gryphiswaldense* MSR-1. Three prominent operons are outlined (*mms6, mamDC* and *mamAB*. ORFs containing sequences of recognised function are also pointed out. (Based on information reported by Schübbe, *et al.*, 2003 and Grünberg *et al.*, 2001).

its preference for intermediate O_2 concentrations. It synthesises magnetic particles in the cell with a diameter ranging from c. 40-100 nm.

1.2.3.2 *Magnetospirillum magneticum* AMB-1

Magnetospirillum magneticum AMB-1 was isolated in 1991 (Matsunaga and Okamura, 2003). *Magnetospirillum magneticum* AMB-1 is good to work with due to the fact that it is far more oxygen tolerant than other magnetotactic species and forms colonies on the surface of agar plates (Matsunaga *et al.*, 1991). AMB-1 is a magnetic bacterium that synthesises cubo-octahedral crystals of magnetite. It is an obligatory respirer, has a chemoorganoheterotrophic mode of nutrition and uses organic acids as sources of energy and carbon. The cells form more magnetosomes when grown with nitrate and synthesise magnetite without molecular oxygen (Matsunaga and Tsujimura, 1993). Growth and inhibition studies show that *Magnetospirillum magneticum* AMB-1 can use nitrate as a terminal electron acceptor although the products of nitrate reduction were not reported.

1.2.3.3 *Magnetospirillum gryphiswaldense* MSR-1

Dirk Schüler and his team preferred working with *Magnetospirillum gryphiswaldense* as they found it easier to cultivate than most other magnetotactic bacteria, which facilitates its physiological and biochemical analysis (Grünberg *et al.*, 2001; Grünberg *et al.*, 2001). *Magnetospirillum gryphiswaldense* synthesises up to 60 cubo-octahedral crystals of magnetite. However, Schübbe *et al.* (2003) observed frequent spontaneous loss of magnetic phenotype in stationary-phase cultures of *Magnetospirillum gryphiswaldense* MSR-1.

1.2.4 Strategies for uptake of iron from the environment by magnetic bacteria

Generally speaking most magnetic bacteria synthesise magnetic crystals under microaerobic conditions. Cells of the species *Magnetospirillum magnetotacticum* MS-1 require molecular oxygen for magnetosome production which is inhibited at headspace oxygen concentrations of greater than 5 or 6 % (Blakemore *et al.*, 1985). Cells of other species including marine vibrio MV-1, *Magnetospirillum magneticum* AMB-1 and *Magnetospirillum* sp. MGT-1 do not require oxygen for magnetite synthesis since they produce magnetite not only when grown microaerobically but

when grown anaerobically with nitrous oxide or nitrate, as the terminal electron acceptor (Bazylinski *et al.,* 1988; Burgess *et al.*, 1993).

Bacteria take up iron prior to the formation of magnetosomes. Unbound Fe (II) is very soluble (Nielands, 1984) and highly bioavailable. With regard to Fe (III), it is so insoluble that most microbes rely on iron chelators that bind and solubilise it. These chelators, called siderophores, are defined as low molecular weight (<1 kDa), specific ligands that facilitate the solubilisation and transport of Fe (III) (Geurinot, 1994). They are generally produced under iron-limited conditions, and high iron concentrations repress their synthesis.

The nature and distribution of major iron compounds in *Magnetospirillum magnetotacticum* MS-1 was examined using ^{57}Fe Mössbauer spectroscopy (Frankel *et al.,* 1983). A model was proposed in which Fe (III) is taken up by the cell by non-specific means and reduced to Fe (II) as it enters the cell. It is then reoxidised to form a low-density hydrous Fe (III) oxide that is then dehydrated to form a high-density Fe (III) oxide (ferrihydrite) that was detected in cells. In the last step, one third of the Fe (III) ions in ferrihydrite are reduced and with further dehydration magnetite is produced (Refer to Section 1.1.8).

1.2.4.1 A siderophore mediated approach to iron uptake

Fe (III) is actively taken up with siderophore mediatation in *Magnetospirillum magnetotacticum* MS-1 and the marine vibrio MV-1 (Figure 1.16) (Paoletti and Blakemore, 1986; Calugay *et al.,* 2003; Dubbels *et al.,* 2004) although it is not known what proportion of the iron in the magnetosomes is taken up as Fe (III) by these organisms. That said, Nakamura *et al.* (1993) did not detect siderophore production by *Magnetospirillum magneticum* AMB-1 and concluded that Fe (III) uptake by cells was mediated by a periplasmic binding protein dependent iron transport system. In the case of siderophore activity, siderophore-bound Fe (III) is probably reduced to Fe (II). At least 70% of the iron in the culture medium that is used to grow strain MV-1 is present as Fe (II), so it is likely that much of the iron that is taken up by this strain is of the form Fe (II). A periplasmic, multicopper-

containing Fe (II) oxidase has been purified from this organism that could be involved in the transport of iron into the cytoplasm (Dubbels *et al.,* 2004).

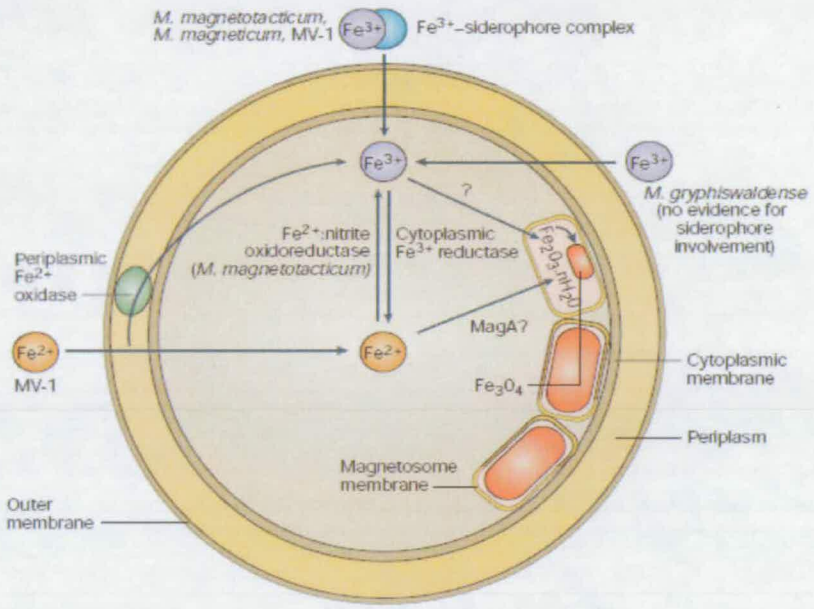

Figure 1.16 Representation of possible reactions leading to magnetite biomineralisation in known, cultured species of magnetotactic bacteria (Plate from Bazylinski and Frankel, 2004).

A cytochrome cd_1 with Fe (II):nitrite oxidoreductase activity capable of Fe (II) oxidation was found and purified from *Magnetospirillum magnetotacticum* MS-1 (Yamazaki *et al.,* 1995), cytoplasmic Fe (III) reductase activity is present in strain MV-1 (Dubbels *et al.,* 2004) and a cytoplasmic Fe (III) reductase has been purified from *Magnetospirillum magnetotacticum* MS-1 (Naguchi, 1999). Iron that is transported into the magnetosome membrane vesicle in *Magnetospirillum magnetotacticum* MS-1 is then thought to form a high-density hydrous Fe (III) oxide (ferrihydrite; $Fe_2O_3 \cdot nH_2O$); reduction of one-third of the Fe (III) ions and adjustment of the pH may result in nucleation of the magnetite crystal within the magnetosome vesicle (Frankel *et al.,* 1983). The nucleation step might involve the adsorption of aqueous Fe (II) ions onto the surface of the hydrous iron oxide (Mann and Frankel, 1989; Cornell and Schwertmann, 2003). There is no definitive result regarding proteins directly involved in the oxidation and reduction of iron for magnetosome synthesis. There is a great number of enzymes with oxidation and reduction

potential utilised by cells for their basic metabolism making directed effort to pinpoint a specific protein an arduous task.

1.2.4.2 A non-siderophore approach to iron uptake

Fe (III) is actively taken up by cells of *Magnetospirillum gryphiswaldense* MSR-1, with no evidence of the involvement of a siderophore under microaerobic conditions (Figure 1.16) (Schüler and Baeurlein, 1996). The inorganic synthesis of magnetite at neutral pH is known to be thermodynamically favoured compared to that of other crystalline iron oxide phases like Fe_2O_3 (Bell *et al.,* 1987). On this basis a model was proposed for *Magnetospirillum gryphiswaldense* MSR-1 where the development of microaerobic conditions directly affects the physiochemical conditions in the interior of magnetosome vesicles, favouring the precipitation of magnetite. By monitoring microaerobic growth and the uptake of iron and magnetite crystal formation of *Magnetospirillum gryphiswaldense* MSR-1 using a radioactive tracer method for iron transport and a differential light-scattering technique for magnetism it was observed that magnetite formation was tightly coupled to a drastic increase in iron uptake whereas the iron content of nonmagnetic cells was very similar to that reported for other non-magnetic bacteria (Hartman and Braun, 1981; Lankford, 1973). It appeared that the iron taken up by the cells was rapidly converted to magnetite without delay which does not support the idea that the formation of magnetite crystals is preceded by the accumulation of a large iron pool stored in non-magnetic form. The regulation of iron uptake in cells was indicated by the higher potential of iron depleted cells to accumulate iron compared to cells replete with iron.

1.2.5 Transport of iron from the cytosol into the magnetosome

1.2.5.1 *magA*

A 2975 bp genomic DNA fragment from the Tn5 flanking region of a *Magnetospirillum magneticum* AMB-1 mutant was sequenced (Nakamura *et al.,* 1995a; Nakamura *et al.,* 1995b). Three open reading frames were found with putative ribosome binding sites. The *magA* gene was 1305 bp and the putative MagA (434 aa) protein was predicted to have a molecular weight of 46.8 kDa. After performing homology searches on sequence databases MagA was found to have high sequence homology to KefC, potassium ion-translocating protein from *Escherichia*

coli, and NapA, a Na^+/H^+-antiporter from *Enterococcus hirae*. A functional promoter located upstream from the gene was present and its transcription was regulated by environmental iron concentration. MagA was expressed in *Escherichia coli* and isolated vesicles showed the ability to accumulate iron. These results indicated that *magA* was related to iron metabolism.

Using transposon mutagenesis methods in *Magnetospirillum magneticum* AMB-1 the molecular mechanisms of magnetite biomineralisation were examined (Nakamura *et al.*, 1995a; Nakamura *et al.*, 1995b). It was found that *Magnetospirillum magneticum* AMB-1 in contrast to *Magnetospirillum magnetotacticum* MS-1 does not encode siderophore production, secretion and utilisation generally incorporated for iron uptake by microorganisms. The appearance of *mag*A expression appeared to be regulated in a similar way to iron uptake genes from *Escherichia coli* although without a domain similar to the Fur-binding region near the *mag*A it seemed likely that *Magnetospirillum magneticum* AMB-1 had an alternative system to the Fur-regulation and iron uptake systems. Direct iron uptake measurements in membrane vesicles confirmed that the *mag*A gene product functions as an iron transporter in *Escherichia coli* verifying that the putative MagA protein is located in the inner membrane in *Escherichia coli*. It was concluded that MagA protein was possibly an iron transport channel protein and coupled to ATPase. Two hypotheses for energy coupling (Nakamura *et al.*, 1995a; Nakamura *et al.*, 1995b) include –

1 direct driving of iron transport by ATPase, with a protein encoded by the second ORF in their cloned *NcoI*-BamHI restriction fragment functioning as the ATPase or an ATPase derived from *Escherichia coli* interacting with MagA;

2 an indirect ATPase coupling with MagA functioning as an Fe^{3+}/H^+-antiporter driven by the proton motive force of F_1F_0-ATPase, which was compared to the KefC protein of *Escherichia coli* and the NapA protein of *Enterococcus hirae*.

1.2.5.2 MagA-Luc fusion

A *magA-luc* fusion was constructed to investigate the effect of iron on MagA regulation (Nakamura *et al.,* 1995b). The *magA* gene was upregulated at low concentrations of iron (33 μM) and was not completely repressed under iron sufficient conditions. Luciferase activity was detected in the cytoplasm, cell membrane, and magnetic particle membrane subcellular fractions indicating that the MagA-Luc fusion may function as an iron translocating protein which is integrated into the cell and magnetosome membranes of *Magnetospirillum magneticum* AMB-1. If so MagA transports iron from the environment into the cytoplasmic space across the cell membrane into the cytoplasm and from the cytoplasm into the magnetosome membrane.

1.2.5.3 Bacterioferritin (Bfr)

In *Magnetospirillum magnetotacticum* MS-1, there was some evidence that the MagA protein first isolated from *Magnetospirillum magneticum* AMB-1, functioned as an H^+/Fe (II) antiporter. The involvement of the *bfr* and *mag*A operons of *Magnetospirillum magnetotacticum* MS-1 in the synthesis of magnetite were investigated (Bertani *et al.,* 2001). The *mag*A gene, first isolated in *Magnetospirillum magneticum* AMB-1 (Matsunaga *et al.,* 1991; Matsunaga *et al.,* 1997), was believed to express a component of the magnetosome membrane that surrounded each magnetite crystal. The *bfr* operon of *Magnetospirillum magnetotacticum* MS-1 was found to be tightly linked and encode subunits of the iron storage protein, bacterioferritin that may be the source of the iron that is converted to magnetite (Bertani *et al.,* 1997).

The *Magnetospirillum magnetotacticum* MS-1 *bfr* genes were mapped within a 670 kb segment of the genome to a 170 kb band whilst *mag*A was mapped to an adjacent 500 kb region (Bertani *et al.,* 1997; Bertani *et al.,* 2001). The *Magnetospirillum magnetotacticum* MS-1 *bfr* genes (*bfr1 and bfr2*) overlap by one nucleotide (ORFs – bp 766-1257; bp 1257-1736) and this overlap may function to keep the two genes together or to play a regulatory role in determining the relative amounts of the subunits that are made. It was reported that *Magnetospirillum*

magnetotacticum MS-1 Bfr was composed of two subunits rather than one (Bertani *et al.,* 1997; Bertani *et al.,* 2001) and the author compared this to GenBank organisms that also produce two Bfr subunits. The genes encoding the two subunits of the compared organisms do not overlap.

1.2.5.4 Fur

The strict control of iron homeostasis is mediated by the Fur (ferric uptake repressor) repressor, which is highly conserved among various bacterial species. Fur represses iron uptake genes in the presence of excessive iron concentration (Bagg and Neilands, 1987; Panina *et al.,* 2001), and is activated by excess iron. Iron is an essential element for the survival and pathogenesis of bacteria but excessive iron can react with superoxide and hydrogen peroxide to form hydroxyl radicals, which can directly damage DNA and proteins. Thus, the presence of Fur-binding sites overlapping promoter regions is an indication that a gene is regulated by iron concentration.

Two putative Fur-binding sites with better than 50% identity with the Fur-box consensus sequence were found in the *bfr*2 sequence (Bertani *et al.,* 1997), although they are within the gene at bp 1065-1083 and bp 1098-1116, as found in the *Azotobacter vinelandii bfr* gene (Grossman *et al.,* 1992). The subunits were produced as individual proteins from cloned *Magnetospirillum magnetotacticum* MS-1 DNA expressed in an *Escherichia coli* host. These observations were extended to *Magnetospirillum magneticum* AMB-1, and a non-magnetic relative, Ai. The two *Magnetospirillum* strains are very closely related. Only 8 bp out of 1424 of the 16S rDNA of MS-1 and AMB-1 were found to be different whereas there are 96 differences out of 878 bp between MS-1 and Ai (Burgess *et al.,* 1993). The arrangement of the *bfr* genes in MS-1 and AMB-1 was identical. In Ai, however, although the genes for the two subunits were in the same order (*bfr*2 upstream of *bfr*1) they were separated by 16 bp (Bertani *et al.,* 2001).

A *Magnetospirillum gryphiswaldense* MSR-1 *fur* disruption mutant was constructed (Huang *et al.,* 2007). The mutant was unable to form magnetosomes but its growth

was not affected. It remained unknown whether the magnetosome deficiency resulted from the oxidative stress or repression of enzymes related to magnetosome synthesis or from the lack of cellular iron. These findings suggest that Fur maintains a tight balance between iron metabolism and oxidative stress and strengthens the relationship between Fur, Bfr and MagA in iron sequestration for magnetosome synthesis.

1.2.5.5 MamB and MamM

Other proteins possibly responsible for, or involved in, iron transport into the magnetosome membrane vesicle are MamB and MamM, which are abundant in the magnetosome membranes of *Magnetospirillum gryphiswaldense* MSR-1 (Schübbe *et al.,* 2003). These proteins have homology to a heavy metal ion transporter, CzcD, from other bacteria, eg. *Natranaerobius thermophilus* JW/NM-WN-LF, Pelobacter *propionicus* DSM 2379 and *Geobacter* sp. FRC-32. MamB, MamM and CzcD each contain domains that deal with the transport of cobalt, zinc, cadmium and iron, categorised under the cation efflux superfamily (NCBI BLAST-blast.ncbi.nlm.nih.gov).

Magnetospirillum gryphiswaldense MSR-1 deletion mutants of *mamM* and *mamB* were constructed to study the effect of magnetite biomineralisation *in vivo* (Junge *et al.,* 2006). Preliminary results showed that the absence of either of these proteins resulted in cells that did not form magnetic crystals and were also impaired in iron accumulation. Complementation studies were yet to be conducted to demonstrate whether the deletions can be functionally restored by wild type alleles of *mamM* and *mamB* of *Magnetospirillum gryphiswaldense* MSR-1 as well as homologues from other magnetic and non-magnetic bacteria although preliminary results of GFP fusions suggest that the localisation of MamM and MamB is not restricted to the magnetosome membrane, as MamM-GFP has also been detected in the cytoplasmic membrane during the cell cycle. These results indicate that MamM and MamB have essential roles in magnetite biomineralisation and are likely have a role in iron transport across the magnetosome membrane by active transport.

1.2.6 Genes directly involved in iron crystal formation

Magnetosome chains were isolated to examine them for organic structures that might act as regulators for sise and shape of the magnetic crystals in order that they maintain a single domain in *Magnetospirillum magneticum* AMB-1 (Arakaki *et al.*, 2003). Four proteins, designated Mms5, Mms6, Mms7 and Mms13, were tightly bound to the magnetite crystal (Arakaki *et al.*, 2003). These proteins have a common sequence motif (LGLGLGLGAWGPXXLGXXGXAGA) and respectively Mms5 and Mms13 are homologous to MamC, Mms6 is homologous to ORF4 and Mms7 is homologous to a highly acidic C-terminal region of MamD in *Magnetospirillum gryphiswaldense* MSR-1. Mature Mms6 consists of a hydrophobic domain in the N-terminal region, which is thought to be the transmembrane region and the C-terminal domain is highly acidic (Arakaki *et al.*, 2003). Lysine, tyrosine and arginine are contained in the middle and C-terminal domains which were also noted in Mms5, Mms7 and Mms13. It is the hydrophilic domain in mineral associated proteins that captures metal ions or interacts with the mineral phase. When Mms6 is present *in vitro* magnetite precipitates with cuboidal morphology and 20-30 nm diameters are found with the magnetic precipitates whereas in the absence of Mms6 the magnetic particles are heterogenous in sise (1-100 nm in diameter) and shape (Arakaki *et al.*, 2003). Most recently it was discovered that MamGFDC in *Magnetospirillum gryphiswaldense* regulates the sise of magnetosome crystals (Scheffel *et al.*, 2008). This finding may provide a powerful strategy for the precise control of the particle sise considerable that would interest in a number of technological applications (See section 1.1.8).

1.2.7 Magnetosome vesicles are present prior to magnetosome formation

1.2.7.1 MamA (MAM22/Mms24)

Magnetospirillum magneticum AMB-1 was grown in the absence of iron and the presence of magnetosome vesicles in the absence of magnetite was observed (Komeili *et al.*, 2004). Non-polar deletions of *mamA* (*mam22/mms24*) were constructed and mutants were functionally complemented with a MamA-GFP fusion. The deletion mutant was found to contain vesicles although they did not appear to be able to function for the production of magnetite. After complementation with a

MamA-GFP fusion a very distinct localisation was observed depending on the growth stage of the cells. MamA-GFP localised to a thin spotted line extending from one end of the cell to the other in nearly all of the cells indicating the interaction of MamA with the magnetosome and other parts of the cell. On occasion MamA also appeared to localise to the cell membrane. As the cells entered stationary phase localisation became more punctuated and at the stationary phase cells contained from one to four foci. This localisation pattern was seen in cells grown with or without iron confirming the presence of vesicles prior to iron crystal formation. It was suggested that the dynamic pattern of MamA localisation suggests that various parts of the same cell have different properties throughout the growth cycle of magnetotactic bacteria.

The protein structure of MAM22 (molecular mass, 22 kDa) (MamA/Mms24), a magnetosome associated protein, was determined in *Magnetospirillum magnetotacticum* MS-1 and was found to contain tetratricopeptide (TPR) motifs (Okuda *et al.*, 1996). As mentioned previously the tetratricopeptide repeat is a ubiquitous motif found in a number of proteins that are functionally unrelated (Blatch and Lässle., 1999).

The gene, *mam*22 (*mamA/mms24*), was expressed in *Escherichia coli* (Okuda and Fukamori, 2001). The protein was purified and was found to have a tendency for self-aggregation in the presence of NaCl. The structural features of the motif suggested that MAM22 monomers interact with each other *via* the distribution of charges so the addition of NaCl would drown out the negative/positive charges to induce its aggregation by hydrophobic interactions between the putative TPR motifs. These properties were very similar to those of hydrophobic colloids that also have a tendency to be coagulated with NaCl. It was postulated that the magnetosome protein MAM22 had a functional role as a receptor for the cytoplasmic proteins that were transferred in the magnetosome; or interacted with proteins that were present in the contiguous magnetosome particle or cytoplasmic membrane resulting in holding the magnetosome chain structure. The diversity associated with TPR motifs makes

the complete characterisation of MAM22 involvement in magnetosome organisation a difficult task.

1.2.7.2 MpsA

MpsA has a role in mediating invagination of the cytoplasmic membrane to form the magnetosome membrane by acylation (Matsunaga *et al.,* 2000). The *mpsA* gene was cloned and characterised in *Magnetospirillium magneticum* AMB-1. This was done by first isolating proteins *via* SDS-PAGE and by determining the N-terminal amino acid sequence of one of these proteins (34.5 kDa) a pair of PCR primers was designed that amplified a 105 bp fragment of AMB-1 genomic DNA. The complete sequence of the gene (954 bp) was determined *via* gene walking and anchored PCR. An *mpsA-luc* gene fusion was constructed and expressed in *Magnetospirillium magneticum* AMB-1 following conjugation. Homology was identified between *mpsA* and acetyl-CoA carboxylase and decarboxylases of other Gram-negative bacteria. It was concluded that the total protein content of the cell membrane and magnetosome membrane is comparable and although a greater mass of MpsA partitions to the cell membrane it clearly has a preference for the magnetosome membrane in spite of being hydrophilic and is therefore believed to be associated with the magnetosome membrane. Parallels were drawn to ADP-ribosylation factor on specific eukaryote membranes which requires acylation for membranal invagination and how fatty acyl-CoA stimulates budding of transport vesicles from donor golgi cisternae in cell-free systems.

1.2.7.3 Mms16

Mms16 is a 16 kDa protein with GTPase activity (Okamura *et al.,* 2001) and contains a domain that categorises the protein in the Phasin 2 superfamily. Phasin proteins describes a group of small proteins found associated with inclusions in bacterial cells. Most associate with polyhydroxyalkanoate (PHA) inclusions, the most common of which consist of polyhydroxybutyrate (PHB). These are designated granule-associate proteins or phasins. Mms16 was found to be the most abundant of five proteins isolated from the magnetosome membrane of *Magnetospirillum magneticum* AMB-1 (Matsunaga *et al.,* 2000). It shows similar properties to eukaryotic small GTPases that control priming and trafficking of budding vesicles

which led to the hypothesis that the magnetosome membrane is derived from the cytoplasmic membrane through an invagination process. GTPase activity is required for magnetosome synthesis as GTPase inhibition experiments indicated whereby the higher the concentration of inhibitor (nucleotide competitors), the more the magnetism of the cells decreased, and interrupted chains of magnetosomes were observed through microscopy studies.

The gene, *mms16,* has GTPase activity in *Magnetospirillum gryphiswaldense* MSR-1. The activator of polyhydroxybutyrate (PHB) degradation in *Rhodospirillum rubrum* was examined (Handrick *et al.*, 2004). The gene in question, *apdA* (activator of polymer degradation), was cloned and expressed in *Escherichia coli.* The amino acid sequence of ApdA was 55% similar to the amino acid sequence of Mms16 although it did not demonstrate any GTPase activity. PHB is a compound that stores carbon and energy in many bacteria and can account for up to 90% of the cellular dry weight during unbalanced growth. Accumulated PHB can be hydrolysed by the cell during starvation or by other organisms after its release from the accumulating organism. Mms16 of *Magnetospirillum gryphiswaldense* MSR-1 can functionally replace ApdA in *Rhodospirillum rubrum* (Handrick *et al.*, 2004 a, Handrick *et al.*, 2004 b). Fusions of *apdA* and *mms16* to *gfp* and *yfp* were functionally expressed and both fusions colocalised with PHB granules after conjugative transfer to *Rhodospirillum rubrum.* In conclusion, ApdA *in vivo* is a PHB-bound phasin-like protein in *Rhodospirillum rubrum.* The function of Mms16 in *Magnetospirillum gryphiswaldense* MSR-1 needs further clarification as it may instead be a PHB-bound phasin in magnetospirilla, which also produce PHB granules.

1.3 ACTIN, BACTERIAL ACTIN-LIKE PROTEINS AND MamK

This section is aimed at providing a general understanding of the localisation pattern, function and behaviour of actin, known bacterial actin-like proteins and how the understanding of MamK prior to the beginning of this work relates to them and magnetosomes. Work by other groups has increased our understanding of MamK since the beginning of 2006 and their findings will be discussed later alongside the findings of this work in the results and discussion sections.

1.3.1 Actin

A broad review of actin is available where the actin cytoskeleton is described as a highly dynamic network composed of actin polymers and a large variety of associated proteins (Schmidt and Hall, 1998). The main functions of the actin cytoskeleton are to mediate cell motility and cell shape changes during the cell cycle and in response to extracellular stimuli, to organise the cytoplasm, and to generate mechanical forces within the cell. The reshaping and functions of the actin cytoskeleton are regulated by signalling pathways.

Actin is a ubiquitous protein involved in the formation of filaments that have a major architectural role determining the shape and motility of a eukaryotic cell at many points during its existence. For example, actin interactions with myosin provide the basis of muscular contraction and many aspects of cell motility (Halliburton, 1887; Straub, 1942). Generally, each actin monomer binds one molecule of ATP and either calcium or magnesium ions. Actin exists as a monomer in low salt concentrations, but filaments form rapidly as salt concentration rises (Straub, 1942), with the consequent hydrolysis of ATP to ADP and inorganic phosphate producing a conformational change in the subunits of the monomer that affect the dynamics of polymerisation (Otterbein *et al.* 2001). A simplified model of the actin polymerisation process can be seen in Figure 1.17.

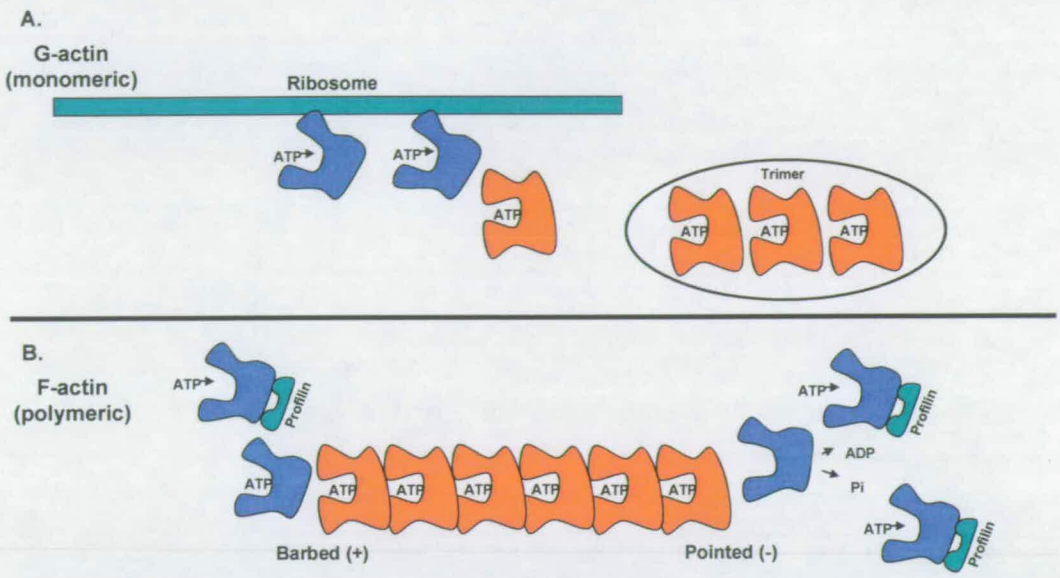

Figure 1.17 Simplification of the process of actin polymerisation. (A) As actin is expressed from the ribosome it binds ATP. Nucleation starts with the association of three monomers into a trimer. (B) Some time after the association of a unit to the plus end of the polymer ATP is immediately hydrolysed to ADP and Pi. This hydrolysis reduces the binding strength between units. The ADP and Pi remain trapped until the unit is free to disassociate at the minus end. Disassociation stimulates the exchange of bound ADP for ATP through interactions with other proteins, notably profilin that prevents denaturation of monomers during nucleotide exchange, thus perpetuating the process. (Dr Sutherland Maciver, University of Edinburgh, personal communication)

Actin polymerisation is partly regulated by capping proteins. For example, CapZ is a microfilament capping protein located in the Z-line of skeletal muscle, made up of two subunits that selectively bind to the positive ends of actin filaments, stabilising them and preventing depolymerisation (Casella *et al.*, 1986), whilst some actin-binding proteins have control to prevent actin polymerisation (McLaughlin *et al.*, 1993). Actin binding proteins also play a part in initiation, cleavage and cross-linkage of the polymers (Korn *et al.* 1987; Schmidt and Hall, 1998).

Research in actin slumped in the years surrounding 1970 (Leavitt, 2005). Many molecular biologists from the 1970's did not find actin very interesting and sometimes referred to it as a wonderful protein standard for marking a gel (43 kDa) whilst its messenger RNA is useful as a hybridisation control in a Northern blot (Leavitt, 2005). Actin has been described as orienting landmarks for all the other visible proteins or messenger RNAs separated by one or other laboratory technique

until 1975 when it was found that the organisation of actin in the cytoplasm was altered vastly when the cells became cancerous (Weber *et al.*, 1975). Indeed, mutations in the actin protein sequence can lead to fatal heart attacks (Møgensen *et al.* 1999) and other physiological problems brought on by actin not functioning correctly in its various roles.

Electron microscopy and X-ray diffraction have shown that F-actin consists of two protofilaments that are twisted gently around one another to form a right-handed double helix (Figure 1.18) (Holmes *et al.*, 1990). The subunits in each actin protofilament have a 55 Å spacing (Steinmetz, *et al.* 1998); the helical pitch is variable due to the flexibility of the protofilaments (Egelman *et al.* 1982).

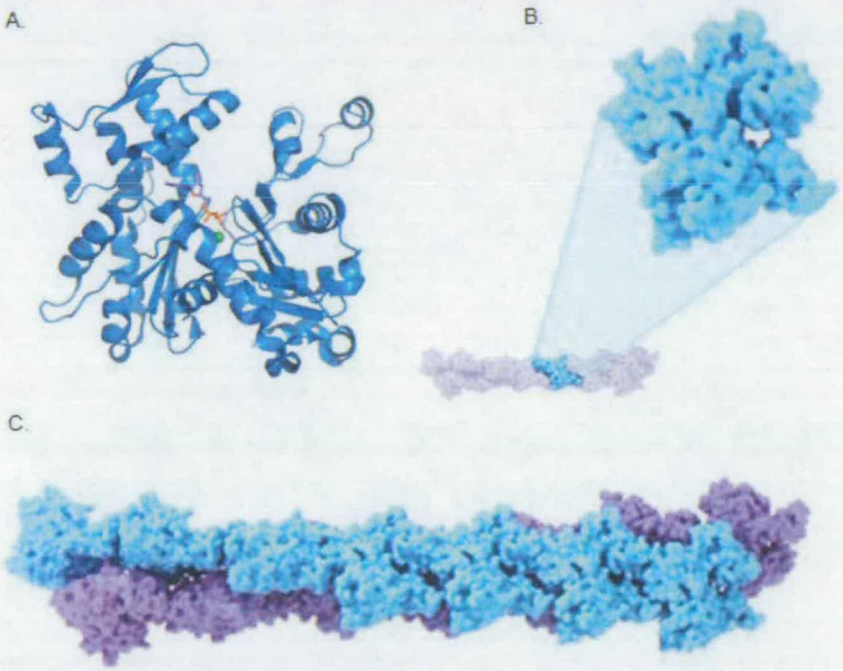

Figure 1.18 The conformation of actin. (A) The crystal structure of uncomplexed actin in the ADP state with the divalent cation highlighted in green (Thomas Splettstoesser, 2006, http://en.wikipedia.org/wiki/ Image: Actin_with_ADP_highlighted.png) (also, Otterbein *et al.*, 2001). (B) The positioning of an actin monomer within one protofilament of an actin filament (ghr.nlm.nih.gov/handbook/illustrations/actin.jpg). (C) The double helix conformation of two actin protofilaments (one blue and one purple) to make an actin filament (ghr.nlm.nih.gov/handbook/illustrations/actin.jpg).

1.3.2 MreB and Mbl

It is well documented that eukaryotic cells use cytoskeletal polymers and molecular motors for structure, motility of intracellular constituents and motility of the cells themselves. It has only recently been recognised that bacteria also harbour cytoskeletal systems and intracellular organelles, contrary to the belief that bacterial intracellular constituents float in the cytosol whilst the cell wall determines cell shape. MreB contributes its role alongside Mbl in *Bacillus subtilis* in determining bacterial shape (Doi *et al.*, 1988; Jones *et al.*, 2001) and contributing understanding to the rising numbers of bacterial cytoskeletal proteins.

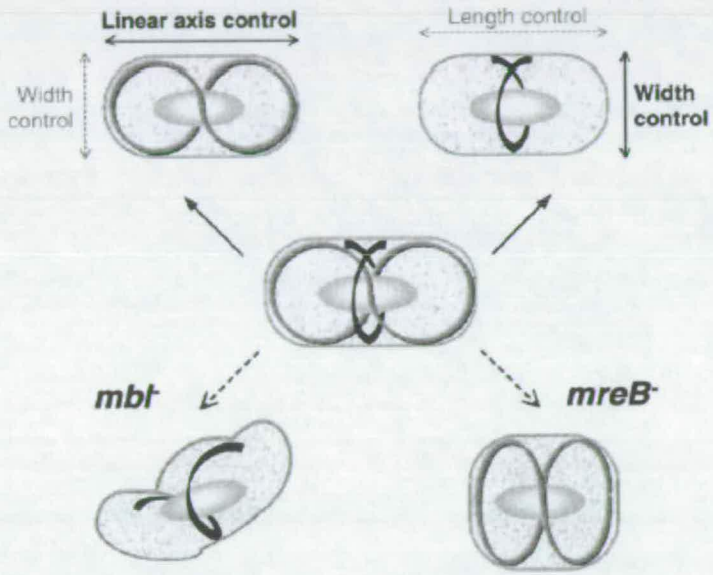

Figure 1.19 A schematic model for shape control by MreB and Mbl. The shape of the wild-type cell (center) is maintained by the combined action of the MreB (black) and Mbl (grey) helical filaments. The two systems are mainly responsible for width control and linear axis control, respectively, as indicated above. In the absence of one of the genes (below), the remaining structure exerts partial control over shape giving a characteristic aberrant morphology. The nucleoid (oval in the middle of the cell) is shown only to provide perspective. (Figure and legend taken directly from Jones *et al.* (2001).)

MreB is essential in *Bacillus subtilis*, as indicated by the failure of deletion mutants to survive beyond 5 generations (Jones *et al.*, 2001). They found that loss of MreB affected the ability of the cells to control their width (Figure 1.19). It was found that in the Mbl deletion mutant cells were bent and twisted at irregular angles and that the main effect of the loss of Mbl was in the longitudinal axis during cell growth (Figure

1.19). Using bioinformatics it was found that MreB and Mbl existed only in non-coccoid bacteria suggesting the spherical shape as the default setting in bacteria lacking MreB.

MreB and Mbl have complementary and contrasting roles in *Bacillus subtilis* and through protein localisation with GFP fusions it has been shown that MreB and Mbl each forms a distinct filamentous helical structure lying close to the cell surface. The distribution of MreB and Mbl in different species of bacteria, and the sequence similarity with eukaryotic actins, suggest that the MreB-like proteins have a cytoskeletal, actin- like role in bacterial cell morphogenesis.

The *mreB* gene is located in the gene cluster *mre* (murein cluster e) and *mre* together with *mrd* is the principal operon involved in determination of cell shape in bacteria (van den Ent *et al.,* 2001). MreB from *Thermotoga maritima* assembles into filaments with a subunit repeat similar to that of F-actin (Figure 1.20 and 1.21) (van den Ent *et al.,* 2001). There is agreement between species regarding the localisation of MreB to the cytoplasmic membrane and the formation of helical actin-like filaments likely to be involved in the spatial distribution of proteins involved in maintaining shape in non-coccoid cells (Jones *et al.,* 2001; van den Ent *et al.,* 2001). MreB forms two-stranded filaments similar to F-actin apart from the fact that they do not twist together in helical formation (van den Ent *et al.,* 2001). The two-stranded filaments can associate into pairs and larger bundles whilst *in vitro* observations show that nucleation and polymerisation rates exceed those of actin (Esue *et al.* 2005; van den Ent *et al.,* 2001). In comparison to actin, MreB forms polymers in the presence of ATP or GTP and in the absence of magnesium over a wide pH range with the optimum being pH 6.0 – 7.0 (van den Ent *et al.,* 2001). MreB from *Thermotoga maritima* was found to polymerise in NaCl at concentrations up to 4 M perhaps because thermophilic organisms often have a high salt content to prevent losing too much water in high temperatures (van den Ent *et al.,* 2001). MreB configures itself in a number of polymeric forms (van den Ent *et al.,* 2001) outlined in Figure 1.22. (van den Ent *et al.,* 2001)

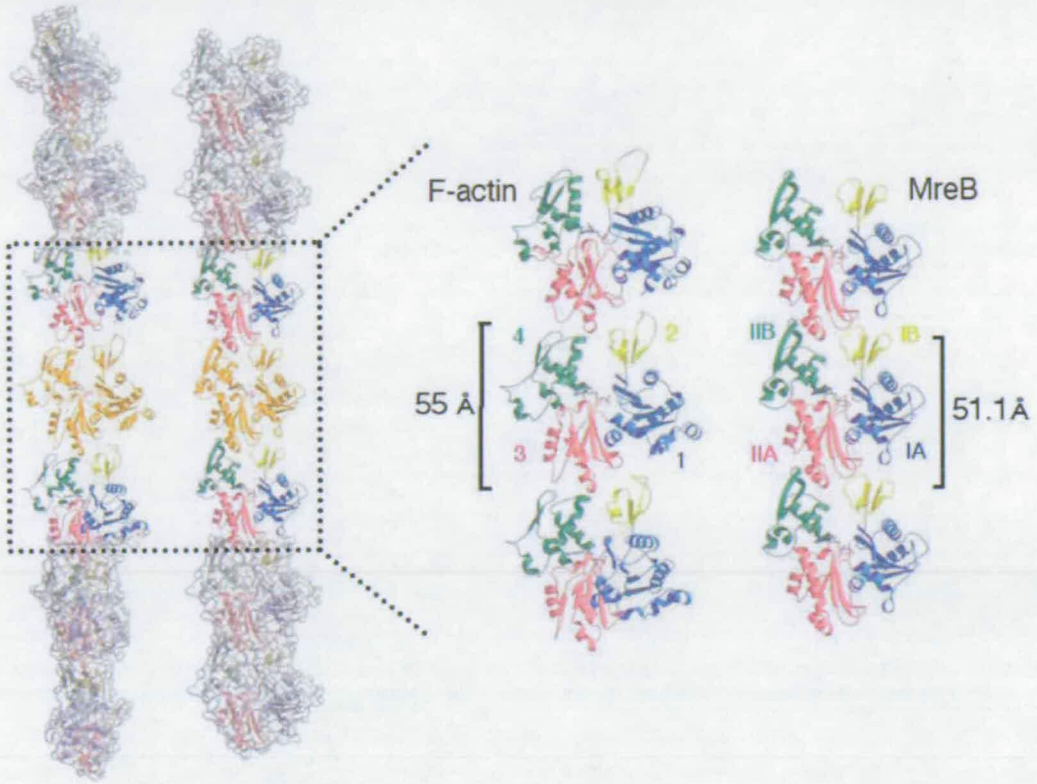

Figure 1.20 Ribbon diagrams showing comparisons between the crystal structures of F-actin and MreB. Both crystal forms (HRES, NATI) contain planar protofilaments. A striking similarity can be observed between F-actin and MreB although MreB protofilaments have no or much less twist. Residues at the bottom of subdomains IA and IIA (1 and 3 in actin) insert into the cleft formed by subdomains IB and IIB (2 and 4 in actin). This is essentially the same interaction that has been proposed for the longitudinal interaction in the two strands of F-actin shown in Holmes *et al.* (1990). The protofilament repeat is 51.1 Å as measured in crystal form NATI. In the trigonal crystal form the protofilament axis is aligned with the crystallographic cell axis *a*. (Figure and legend adapted from van den Ent *et al.* (2001) and http://www2.mrc-lmb.cam.ac.uk/SS/Lowe_J/group/MreB.html)

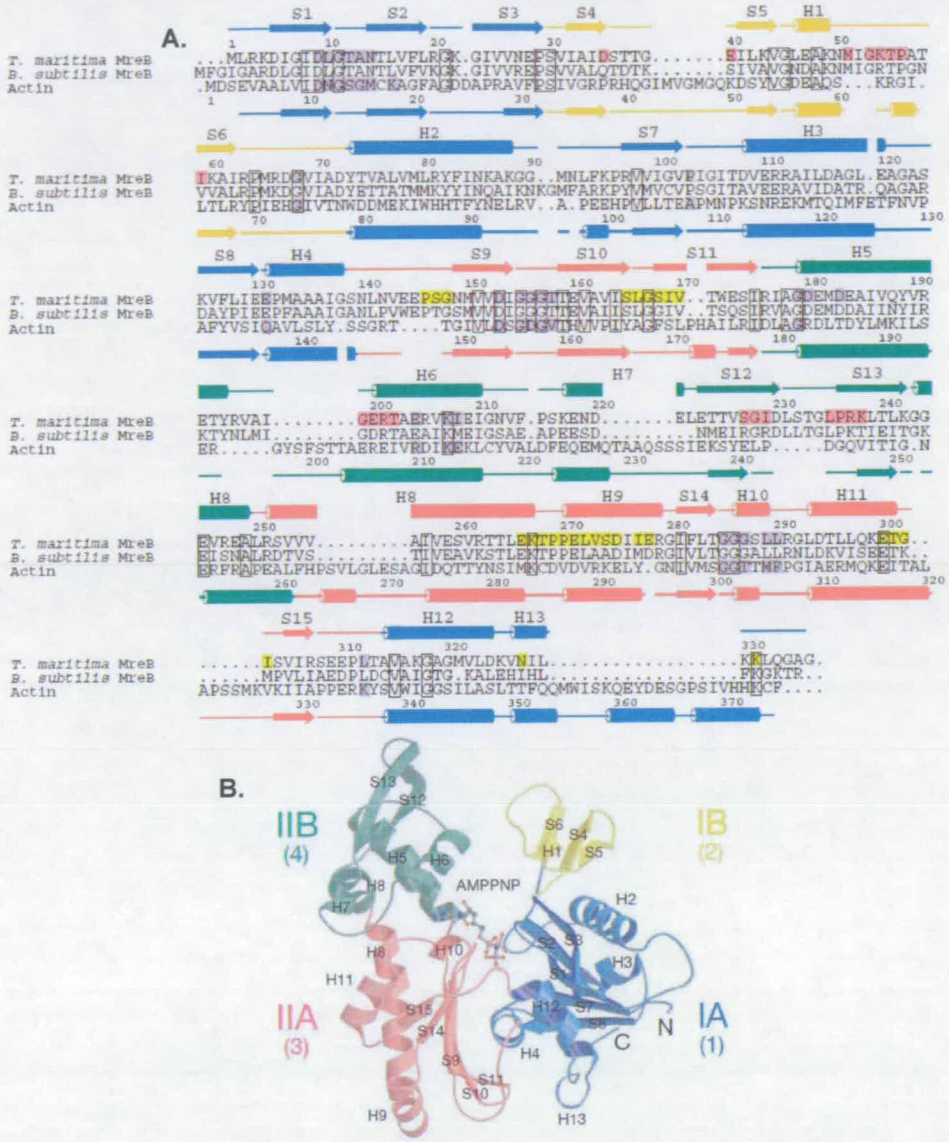

Figure 1.21. (A) Sequence alignment of MreB1 from *T. maritima* to *B. subtilis* MreB and structure-based sequence alignment to yeast actin. Secondary structural elements are shown according to DSSP output of MreB and actin. Helix and strand colours refer to the domain colours in 1.21 b. Active site residues in MreB and actin are highlighted in light purple. Protofilament contacts from one subunit to the next are marked in yellow; residues involved in protofilament contacts to the previous subunit are coloured pink. Boxed residues are conserved in all three sequences. Sequence identity is 56% between the two MreB proteins and 15% between MreB and actin. (B) Ribbon representation of the crystal structure of MreB complexed with AMPPNP and magnesium. MreB is a member of the actin family of proteins, showing the typical four-domain architecture. AMPPNP binds in a cleft between domains I and II. The four subdomains IA, IB, IIA and IIB correspond to subdomains 1, 2, 3 and 4 in actin. (Plate and legend adapted from van den Ent 2001.)

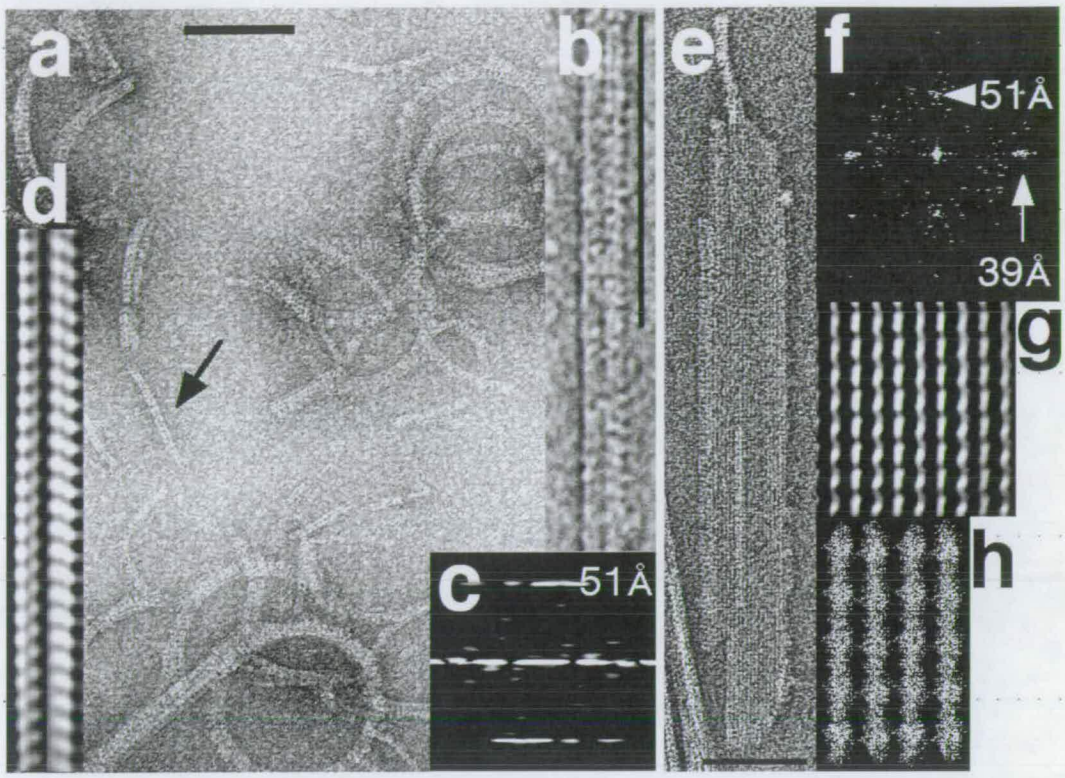

Figure 1.22 Negatively stained MreB filaments. (a) Typical view of MreB filaments when salt and neutral pH is used. MreB (1 mg ml^{-1}) was incubated for 30 min at 37 °C in 100 mM Tris-HCl, pH 7.5, 100 mM NaCl, 3 mM $CaCl_2$, 2 mM ATP (buffered) and 4 mM $MgCl_2$. Scale bar, 100 nm. The filament indicated with an arrow is the same filament that is shown at a higher magnification in (b). (b) "Double" filament formed at high pH. MreB (1 mg ml^{-1}) was incubated for 30 min at 37 °C in 100 mM BICINE, pH 9.0, 100 mM NaCl, 2 mM ATP (buffered) and 4 mM $MgCl_2$. Scale bar, 100 nm. (c) Diffraction image of the polymer in (b) showing the first strong layer line at 51 Å. (d) Filtered image of (b), treating both filaments separately. The polymer is about 160 Å wide, which suggests four single protofilaments in total (each 40 Å). (e) Electron micrograph of a negatively stained MreB sheet. MreB (1 mg ml^{-1}) was incubated for 30 min at 37 °C in 100 mM Tris-HCl, pH 7.5, 25 mM NaCl, 2 mM ATP (buffered) and 4 mM $MgCl_2$. The protofilaments are aligned vertically in the MreB sheet. Scale bar, 100 nm. (f) Diffraction image of sheet in (e). The longitudinal repeat is 51 Å, the lateral spacing is 39 Å. (g) Filtered image of sheet in (e). (h) The protofilaments found in the crystals of MreB fit well with the filtered image in (g). The longitudinal repeat of 51 Å in the sheets is the same as in the crystals (Figure 1.20). The lateral spacing in the sheets suggests that the protofilaments interact with their flat sides. (Figure and legend taken directly from van den Ent *et al.*, 2001).

1.3.3 FtsA

Cell division in *Escherichia coli* (and other bacteria) is a complex process involving the formation of a septum at the correct time and place for successful cell division (de Boer *et al.*, 1990; Dewar *et al.*, 1992). Genetic studies have identified a number of genes (*ftsA, ftsI, ftsL, ftsQ, ftsN, ftsW*, and *ftsZ*) which are essential for this process (Bi and Lutkenhaus, 1992). Among these genes, *ftsZ* and *ftsA* encode cytoplasmic proteins and the remainder encode membrane proteins. The capacity of a bacterial cell to divide by making septa at new, central sites in the cell is determined by the levels of FtsA (an actin-like protein) and FtsZ (a tubulin-like protein) (Begg *et al.*, 1998).

Bacillus subtilis FtsA is targeted to division sites in both vegetative cells where division septa form exclusively at the mid-cell, and sporulating cells where FtsA is recruited to potential division sites at one cell pole (Figure 1.23) suggesting that FtsA may play an important role in the generation of asymmetry in this system (Feucht *et al.*, 2001). FtsA is present in much higher quantities in *Bacillus subtilis* than in *Escherichia coli*, with approximately one molecule of FtsA for five of FtsZ, and may be able to form a complete circumferential ring at the cell division site giving it a direct structural role in cell division (Feucht *et al.*, 2001). FtsA behaves as a dimer with ATP-binding and -hydrolysis activities suggesting that ATP hydrolysis by FtsA is required, together with GTP hydrolysis by FtsZ (Bramhill and Thompson, 1994; Mukherjee and Lutkenhaus, 1994) for cell division in *Bacillus subtilis* (Feucht *et al.*, 2001).

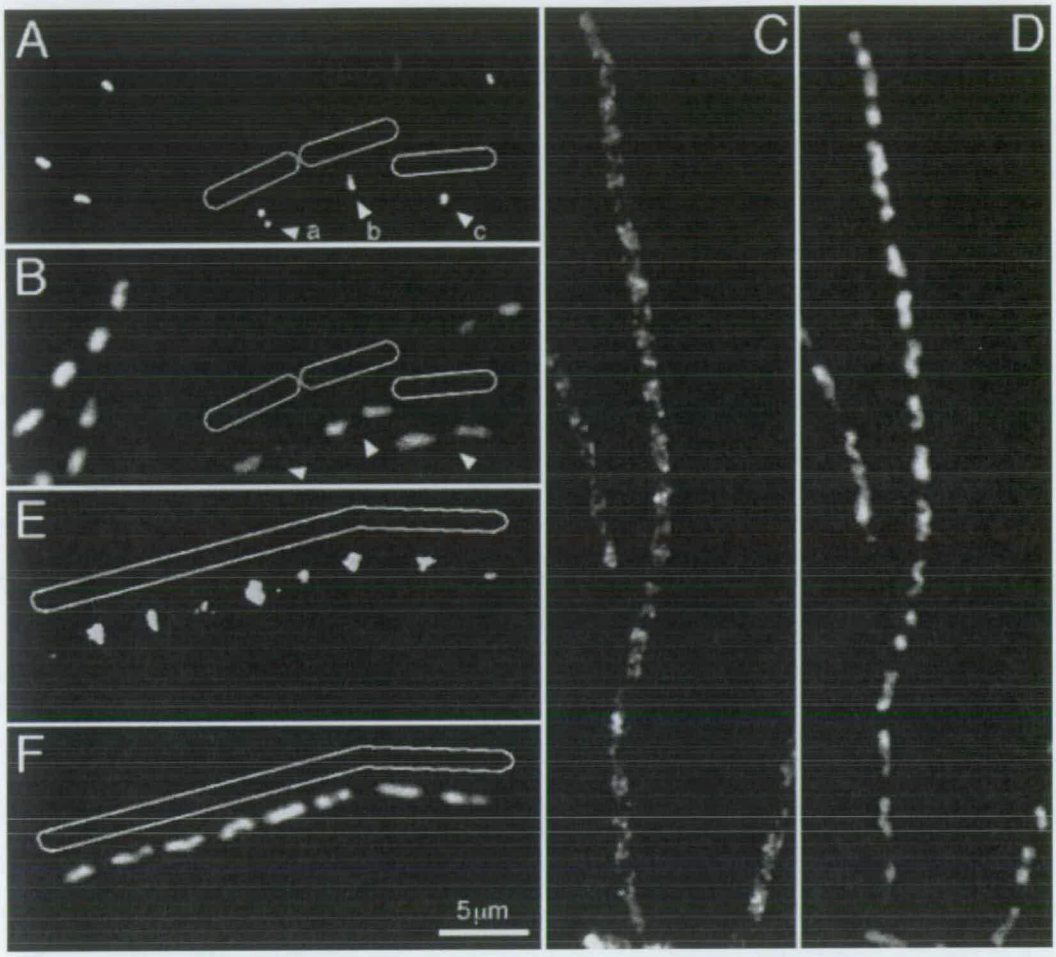

Figure 1.23 Immunolocalisation of FtsA in wild type and division mutants. Fluorescence micrographs of cells stained for DNA with DAPI (B, D and F) and immunostained with affinity-purified antibodies against the *B. subtilis* FtsA protein (A, C and E). Cells of vegetatively growing *Bacillus subtilis* SG38 (A and B), FtsZ-repressed cells grown in the absence of IPTG (C and D) and *divIB* (supporting FtsZ cell division machinery) mutant cells are shown. Arrows in A and B point to cells with different FtsA localisation patterns: (a) pair of dots (b) transverse band and (c) single, central dot. Cartoons have been placed near some of the cells illustrating their outlines. (Direct from Feucht *et al.*, 2001)

The crystal structure of FtsA was solved and proved to share the same core domain architecture and nucleotide binding site with actin despite the low similarity between their amino acid sequences (van den Ent and Löwe, 2000) (Figure 1.24). FtsA has a domain not observed in the crystal structure of actin or any of the bacterial-actin proteins examined in this way.

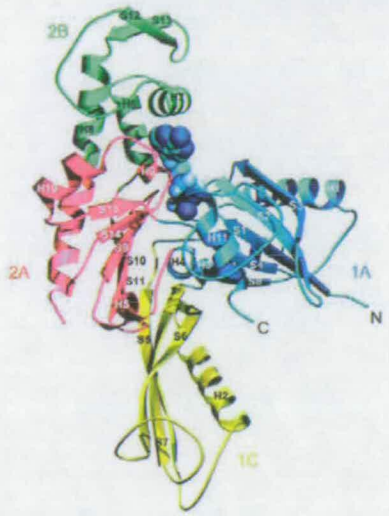

Figure 1.24 Ribbon plot of the crystal structure of FtsA. The structure is divided into four domains, in analogy to the actin family of proteins, which are designated 1A (blue), the FtsA-specific domain 1C (yellow), subdomain 2A (red) and subdomain 2B. Secondary structure elements are labelled according to their order of appearance in the primary sequence of FtsA (Figure 4). Mg-ATP is depicted in purple. (Plate taken directly from van den Ent and Löwe, 2000).

During sedimentation velocity analysis in an analytical ultracentrifuge it was observed that after the addition of ATP and Mg^{2+} a very large structure was formed that sedimented very fast, suggesting the association of FtsA monomers either into aggregates or into high molecular weight polymers (Lara *et al.*, 2004). These complexes were large enough to be pelleted using a tabletop centrifuge, and were formed only in the presence of ATP and Mg^{2+} and no precipitation was observed in the absence of either of the two. Electron microscopy analysis of the samples in the presence of ATP showed that the complexes formed were long curved polymers (Figure 1.25). Most of the polymeric material was composed of large complex helices, formed by a pair of paired filaments (2 + 2) in a corkscrew-like structure (Figure 1.25 b). Although the structures were quite regular, they were often bent, and the filaments were often aggregated forming long bundles. Measurements were taken from different areas of the micrographs (Figure 1.25 b). The average width of the double filament was 8.08 ± 0.81 nm and the helical turn was 69.5 ± 6.6 nm. The *Thermotoga maritima* FtsA monomer has a length of approximately 9 nm and a diameter of 5 nm in the central and wider region, although it is narrower at both extremes. This suggests that each single protofilament might be a polymer formed by

monomeric subunits interacting in a head-to-tail manner, and that the subunits might be oriented with the longer axis approximately parallel to the axis of the protofilament.

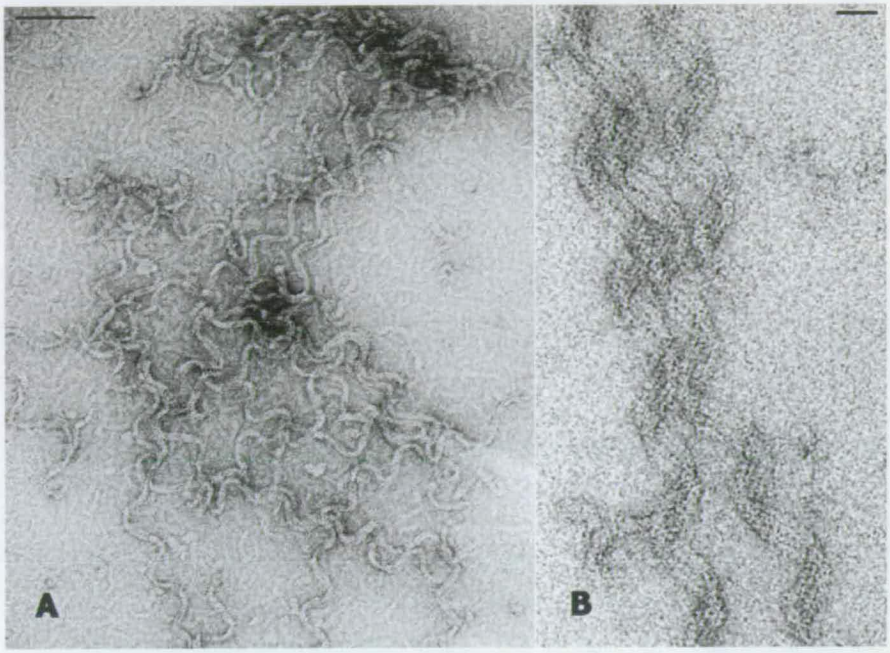

Figure 1.25 Micrographs of the FtsA polymers. FtsA (0.5 mg ml-1) was incubated with 2 mM ATP, applied to copper grids and negatively stained (Lara *et al.*, 2004) (the scale bar on the upper left side represents 100 nm) (A). Detail of an image taken with minimal dose mode (the scale bar on the upper right side represents 20 nm) (B). Plate and legend from Lara *et al.*, 2004)

FtsA was able to bind different nucleotides and its polymerisation activity in the presence of various nucleotides was studied (Lara *et al.*, 2004). Polymer formation was observed in the presence of either 5 mM ATP or GTP, in agreement with the results of nucleotide binding. FtsA was also able to polymerise in the presence of 5 mM ADP and the nonhydrolysable ATP analogues, ATP-g-S or AMP-PNP. A relatively low level of polymerisation was observed with AMP or AMP-PCP, although no binding was detected in competition assays.

1.3.4 ParM

A model has been proposed of the separation and movement of plasmid molecules to the cell poles in preparation for cell division and the involvement of ParM in that process has been described (Møller-Jensen *et al.,* 2002). ParM is required to actively segregate the R1 plasmid prior to cell division. ParM forms filamentous structures extending along the longitudinal axis of *Escherichia coli* (Figure 1.26). When ParM was expressed in the cell without the ParR-*parC* complex fluorescent foci were observed but ParM was unable to filament. Localisation work on ParM, ParR and *parC* showed that *in vivo* polymerisation of ParM relied on the presence of the ParR-*parC* (M for motor; R for repressor; C for centromere-like region) complex and is perhaps analogous to the eukaryotic mitotic spindle apparatus.

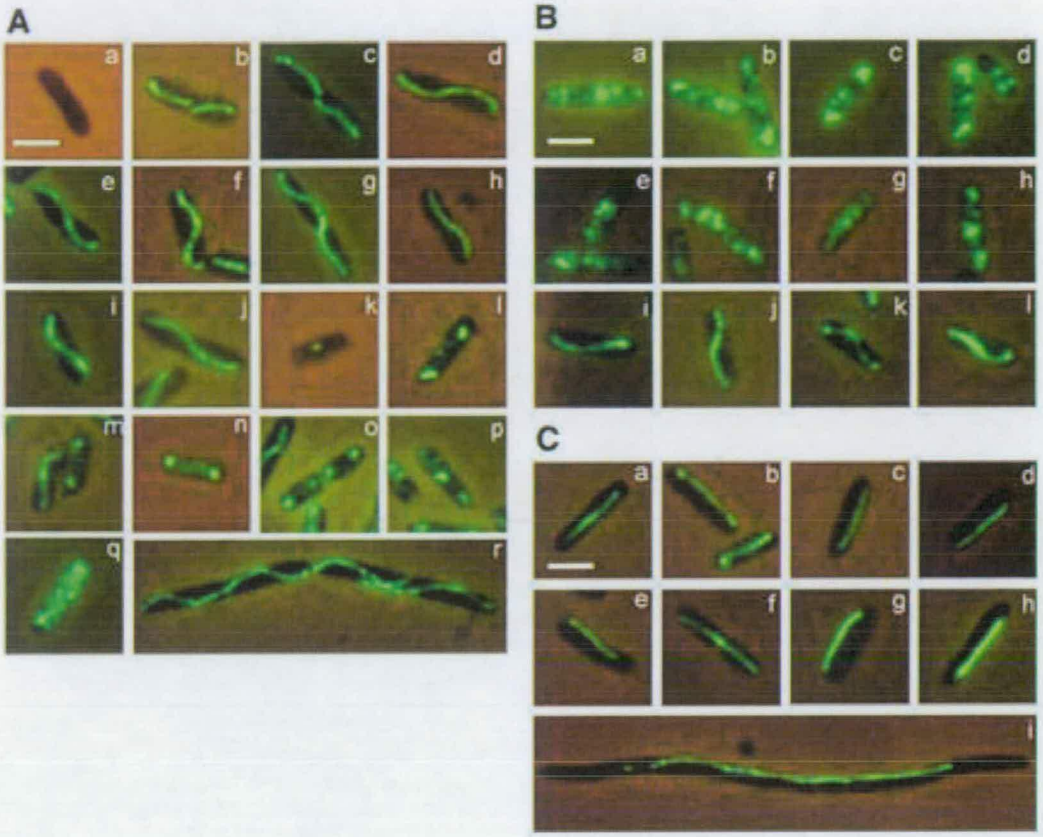

Figure 1.26 Images depicting localisation of ParM in *Escherichia coli*. The scale bar represents 2 µm. (A) Phase contrast and immunofluorescence microscopy of ParM localisation in *Escherichia coli* MC1000 where ParM is shown to form intracellular actin-like filaments. This work was carried out by use of a number of plasmids outlined in tabular form in Møller-Jensen *et al.* (2002) and Jensen and Gerdes (1997). (a) Control cell lacking of ParM and the ParR-parC complex. (b–r) Cells expressing ParM and the ParR-parC. (r) Filamentous phenotype of *Escherichia coli* MC1000/pKG491 obtained by addition of 10 g/ml cephalexin to the growth medium 90 min prior to fixation. (B) Phenotypes of *Escherichia coli* MC1000 expressing ParM only, ParM and ParR, and ParM with the ParR-*parC* complex showing that polymerisation of ParM depends on the ParR–*parC* complex. (a–d) ParM localisation in the absence of *parR* and *parC*, (e–h) in the presence of parR, or (i–l) parR–parC on a second plasmid. (C) Phenotypes where mutation of the ParM ATPase active site changes filament dynamics and morphology. (a–c) Cells expressing mutated ParM (where the 170 aspartate residue was changed to the small uncharged amino acid, alanine) along with the ParR-*parC* complex; (d–f) Cells expressing conservatively mutated ParM (where aspartate residue 170 was changed to glutamic acid) with the ParR-*parC* complex; (g and h) cells expressing mutated ParM (alanine) and ParM (glutamic acid) in the absence of ParR and parC respectively; (i) filamentous cell of *Escherichia coli* MC1000 expressing the glutamic acid substitution after addition of 10 g/ml cephalexin to the growth medium for 90 min prior to fixation. (Figure and legend adapted from Møller-Jensen *et al.* (2002).)

In vitro experiments showed that polymerisation requires ATP and magnesium ions (Møller-Jensen *et al.,* 2002). The ParM filaments were measured with a width of 7 nm compared to F-actin (two protofilaments) with a width of 6.5 nm and MreB with a width of 3.9 nm (Steinmetz *et al.*, 1998; van den Ent *et al.*, 2001).

1.3.5 MamK and its role as a novel bacterial actin-like protein

The functional and biochemical characterisation of MamK is important in order to distinguish its behaviour compared to other homologous proteins of varying function, e.g. Hsp70, hexokinase, sugar kinases and other actin-like proteins (Kabsch and Holmes, 1995). The bacterial actin-like rod shape determining protein (Daniel and Errington, 2003), MreB, is currently recognised as being most closely related to Eukaryotic actin (van den Ent *et al.*, 2001). However, phylogenetic analysis has revealed that MamK is slightly more homologous to actin than MreB. Equally, this close relationship raises questions of the ability of MamK to treadmill or to behave as a track for motor proteins as previously questioned of MreB (van den Ent *et al.*, 2001).

Very little was known about MamK at the outset of work contributing to this thesis. The *mamK* gene was first discussed as comprising part of the *Magnetospirillum gryphiswaldense* MSR-1 magnetosome island (Schübbe, *et al.,* 2003). Schübbe, *et al.* (2003) commented on the homology between MamK and MreB and how the putative function of MamK is to provide a cytoskeletal structure that has a role in the linear organisation of the magnetosome chain thus maximising the net magnetisation. MamK protein sequence has homology to actin-like cytoskeletal proteins in organisms from each of the phylogenetic kingdoms.

Since the beginning of 2006 reports have shown that the MamK protein is associated with the magnetosome vesicle of magnetotactic bacteria and is partly responsible for the linear arrangement of the magnetosomes within the cell as without MamK the magnetosomes lose their linear arrangement (Komeilli, *et al.*, 2006; Pradel, *et al.,* 2006; Scheffel, *et al.,* 2006). These reports, contributing to the understanding of the functional characterisation of MamK, will be discussed in more detail in comparison to the findings presented in this thesis.

1.4 SUMMARY

This introduction has given a comprehensive background to a contemporary understanding of magnetic bacteria and bacterial actin-like proteins in preparation for the presentation of novel results of *in vitro* behaviour of recombinant MamK. In magnetic bacteria there is high interspecies sequence homology between magnetosome specific proteins so it is reasonable to speculate that these proteins are functionally transposable. Some of the work carried out on *Magnetospirillum* spp. considers the potential of systems with secondary and tertiary involvement in magnetosome synthesis, such as chemotaxis, or different strategies for iron uptake between magnetic species; or paralogous functions like those of MreB and other actin-like proteins compared to MamK. Comparison of the mosaic structures of magnetosome islands shows that the magnetosome island of *Magnetospirillum gryphiswaldense* MSR-1 differs from that of *Magnetospirillum* sp. AMB-1 and MS-1 all of which differ from that of *Magnetococcus* MC-1, all of which differ again from the marine vibrio MV-1 evident from the inability to locate genes based on known sequences from the aforementioned species (work in progress, Bruce Ward and Denis Trubytsin). Investigations remain to find all the genes involved in magnetosome synthesis and to elucidate the smallest number of genes required for *in vitro* magnetosome formation. Magnetic bacteria have various strategies for iron uptake and so it might be misleading to assume that information derived from a study on one species is true for another.

2 METHODS AND MATERIALS

2.1. ORGANISMS AND THEIR GROWTH

2.1.1. *Magnetospirillum gryphiswaldense* MSR-1

Magnetospirillum gryphiswaldense MSR-1 (DSMZ) was grown on activated charcoal medium that contained per litre 2.38 g HEPES, 3 g sodium pyruvate, 0.10 g yeast extract, 3 g soybean peptone, 0.34 g $NaNO_3$, 0.10 g KH_2PO_4, 0.15 g $MgSO_4.7H_2O$, 3 g activated charcoal adjusted to pH 7.0 with NaOH and autoclaved (Schultheiss and Schüler, 2003). After autoclaving 20 µM filter sterile ferric quinate and 1 mM filter sterile DTT (final concentrations) were added. A solid version of this medium was prepared by adding 15 g of agar. This strain was incubated aerobically at 26 °C or in a microaerobic cabinet under 5 % (v/v) CO_2: 94 % (v/v) N_2: 1 % (v/v) O_2 at 28.4 °C.

2.1.2. *Escherichia coli* S17λpir

Escherichia coli S17λpir (*Tpr Smr, recA thi pro hsdR M+ RP4:2-Tc:Mu:Km Tn7 pir*) was transformed with the suicide vector, pK19*mobsacB*, for conjugation with wild-type *Magnetospirillum gryphiswaldense* MSR-1 during *mamK* disruption experiments.

2.1.3. *Escherichia coli* JM109, DH5α, and BL21(DE3)p*LysS*

Escherichia coli JM109 (*endA1, recA1, gyrA96, thi, hsdR17 (rk–, mk+), relA1,supE44, Δ(lac-proAB), [F', traD36, proAB, laq*I^q*ZΔM15])* (Promega) (Yanisch-Perron *et al.*, 1985). JM109 is used to select the recombinant DNA using the activity of β-galactosidase (α-complementation) recovered with *lacZ*α peptide of the vector DNA and *lacZ*ΔM15 coded in F' episome in this strain. This strain carries F' episome and it is useful for the preparation of ssDNA as well as gene library construction and subcloning.

Escherichia coli DH5α (*F-, φ80dlacZΔM15, Δ(lacZYA-argF)U169, deoR, recA1, endA1, hsdR17(rk-, mk+), phoA, supE44, λ-, thi-1, gyrA96, relA1*) host for Blue/White screening utilising the activity of β-galactosidase (α-complementation) in combination with use of pUC vectors. As this strain does not

carry *lacI*^{q}, basically IPTG is not needed. Therefore, DH5α allows easy selection of recombinant DNA with X-Gal when constructing a gene library or subcloning recombinant plasmids. During this work *Escherichia coli* JM109 and *Escherichia coli* DH5α were used interchangeably.

Escherichia coli BL21(DE3)p*LysS* (F–, *omp*T, *hsd*S_B (r_B–, m_B–), *dcm*, *gal*, λ(DE3), p*LysS*, Cm^r) (Promega) cells can be used with protein expression vectors that are under the control of the T7 promoter, such as pET28a and pT7-7. This strain is lysogenic for lambda-DE3 (Studier and Moffatt, 1986), which contains the T7 bacteriophage gene 1, encoding T7 RNA polymerase (Davanloo, *et al.,* 1984) under the control of the *lac* UV5 promoter. *Escherichia coli* BL21(DE3)p*LysS* also contains the p*LysS* plasmid, which carries the gene encoding T7 lysozyme. T7 lysozyme lowers the background expression level of target genes under the control of the T7 promoter but does not interfere with the level of expression achieved following induction with IPTG.

Escherichia coli JM109 (Promega)/DH5α and *Escherichia coli* BL21(DE3)p*LysS* (Promega), used for cloning and expression of MamK respectively, were grown on Luria Bertani broth (LB) solid and liquid media. During expression experiments *Escherichia coli* BL21(DE3)p*LysS* was grown on 2 x TY containing (per litre): 16 g bactone-tryptone, 10 g bacto-yeast extract and 5 g NaCl. In all cases, unless stated otherwise, the cells were incubated at 37 °C, whilst liquid cultures were placed on a shaker at 200 rpm.

Table 2.1 summarises the strains used in this work.

Table 2.1 Summary of strains used in this work

Strain	Features	Source
Magnetospirillum gryphiswaldense DSM 6361	Type strain	DSMZ
Escherichia coli JM109	endA1 glnV44 thi-1 relA1 gyrA96 recA1 $mcrB^+$ Δ(lac-proAB) glnV44 e14- [F' traD36 $proAB^+$ $lacI^q$ lacZΔM15] hsdR17($r_K^-m_K^+$)	Promega
Escherichia coli DH5α	F^-, φ80d*lacZ* ΔM15, Δ(*lacZYA-argF*)U169, *deoR*, *recA* 1, *endA* 1, *hsdR* 17(rk^-, mk^+), *phoA*, *supE* 44, λ^-, *thi*-1, *gyrA* 96, *relA* 1	Invitrogen
Escherichia coli S17 λ pir	*Tpr Smr, recA thi pro hsdR M+ RP4:2-Tc:Mu:Km Tn7 pir*	Dirk Schüler
Escherichia coli BL21 (DE3) pLysS	F^- ompT gal dcm lon $hsdS_B(r_B^- m_B^-)$ λ(DE3) pLysS(cm^R)	Novagen

2.1.4. Competent cells for transformation with constructs

2.1.4.1. Preparation of competent cells using TSS

Competent cells were prepared using 1x TSS from sterile component parts by mixing 5 ml 40 % polyethylene glycol (PEG) , 17 ml LB, 1 ml 1 M $NaCl_2$ and 1 ml dimethyl sulphoxide (DMSO). LB (50 mls) was inoculated from an overnight culture and incubated to OD_{600} 0.6 and put on ice in 1.5 ml aliquots in microfuge tubes. Cells were pelleted at 4293 *x g* in a microcentrifuge, the supernatant was removed and then the cells were resuspended in 100 microlitres of 1x TSS (taking care not to disturb the sediment). The cells were left on ice for an hr for immediate use or storage at -80° for use later.

2.1.4.2. Preparation of competent cells using $CaCl_2$

Competent cells were prepared using $CaCl_2$ by inoculating LB (5 ml) with 0.2 ml of an overnight culture of incompetent cells. The cells were incubated to OD_{600} 0.5, put on ice in 1.5 ml aliquots in microfuge tubes and transferred to the cold room for the following procedures at 4 °C. The cells were pelleted at 4293 *x g* in a microcentrifuge; the supernatant was removed and the cells were resuspended in 1 ml of ice cold 0.2 M $CaCl_2$. The resuspended cells were on ice for 45 min after which they were pelleted again at 4293 *x g*, the supernatant was removed and the cells were resuspended in 0.1 ml of ice cold $CaCl_2$ and incubated for 1 hr for immediate use.

2.1.5. Transformation of cells

Cells were made competent as mentioned above. Ligation product (between 3 – 10 µl) or plasmid DNA (3 µl) was mixed with the cells and incubated on ice for 30 min. After incubation on ice 900 ml LB was added to the culture which was then incubated for 1 hr at 37 °C (*Escherichia coli)* or 4 hr at 26 °C (*Magnetospirillum gryphiswaldense*) and plated to the appropriate medium.

2.1.6. Biparental conjugation

Magnetospirillum gryphiswaldense MSR-1 was grown microaerobically in 250 ml activated charcoal liquid medium and concentrate to an OD_{600} 0.8. The growth of *Escherichia coli* S17 λPir carrying pK19*mobsacB*::*mamK*-Gm^R-*mamK* was synchronised to OD_{600} 0.8 to coincide with harvesting and concentration of *Magnetospirillum gryphiswaldense* MSR-1. Cells from 1.5 ml aliquots of the culture were microcentrifuged at 4293 *x g* for 3 min, the supernatant was discarded and the cells were resuspended in activated charcoal liquid medium. The cells were mixed (Figure 2.2) to promote the transfer of the suicide vector by conjugation.

Table 2.2 Mixtures for transfer of pK19*mobsacB*::*mamK*-Gm^R-*mamK* by biparental conjugation

Conjugation	5 µl *Escherichia coli*	45 µl *Magnetospirillum gryphiswaldense*
Control 1	5 µl *Escherichia coli*	45 µl activated charcoal medium
Control 2	5 µl activated charcoal medium	45 µl *Magnetospirillum gryphiswaldense*

The cell mixtures were vortexed and spotted onto sterile nitrocellulose filter paper (Whatman), on an activated charcoal medium plate and incubate at 26 °C overnight to promote conjugation. The inoculated filter paper from overnight cultures was resuspended in 1 ml of activated charcoal liquid medium by vortexing, the filter paper was removed and the cells were pelleted at 4293 *x g* for 3 min. The pelleted cells were resuspended in 200 µl activated charcoal liquid medium and plated to solid activated charcoal medium containing 25 µg/ml gentamycin and incubated microaerobically overnight at 26 °C for single crossover selection purposes. Single crossovers were to be plated to activated charcoal medium containing 25 µg/ml gentamycin and 5 % sucrose).

2.2. PLASMIDS

2.2.1. pK19*mobsacB*

The pK19*mobsacB* (Integration vector, Km^r $oriV_{Ec}$ *oriT sacB*) (donated by Dirk Schüler) plasmid is a mobilisable suicide vector for allelic exchange in *Magnetospirillum gryphiswaldense* MSR-1 (Schultheiss *et al.*, 2004).

2.2.2. pBBR1MCS-2 and -5

The pBBR1MCS-2 and pBBR1MCS-5 plasmids are derivatives of the broad-host-range cloning vector pBBR1MCS as outlined by Kovach *et al.* (1995). The gentamycin resistance cassette of pBBR1MCS-5 was used as a selectable marker and to create a chromosomal disruption of *mamK* from *Magnetospirillum gryphiswaldense* MSR-1. The pBBR1MCS-2 was used to carry *mamK-egfp* to complement and show localisation of MamK expression in wildtype cells.

2.2.3. pGemT Easy Vector

The pGEM®-T Easy Vector System (Promega) facilitates the direct insertion of PCR products for cloning in *Escherichia coli* JM109. The pGEM®-T Easy Vector Systems takes advantage of the template independent addition of a single deoxyadenosine onto the 3'-end of PCR products by some thermostable DNA polymerases such as Roche Taq. These PCR fragments are ligated to linearised vector DNA that has a single 3'-terminal thymidine added to both ends. Recombinants were identified by blue/white colony selection and restriction enzyme analysis.

2.2.4. pT7-7

The pT7-7 vector is a derivative of pBR322 plasmid carrying a T7 promoter (Tabor, 1985).

2.2.5. pET28a

The pET28a vector is a derivative of pBR322 carrying N-terminal His-tag and T7 promoter. The pET-28a(+) vectors carries an N-terminal

His•Tag®/thrombin/T7•Tag® configuration plus an optional C-terminal His•Tag sequence.

2.2.6. pEGFP-N1

The vector, pEGFP-N1 (Clontech), was used as a source of the *egfp* gene for fusion with *mamK* for expression in pT7-7 and pET28a. The *egfp* gene encodes a red-shifted variant of wild-type GFP (Prasher, *et al.*, 1992; Chalfie, *et al.*, 1994; Inouye and Tsuji, 1994) which has been optimised for brighter fluorescence and higher expression in mammalian cells. (Excitation maximum = 488 nm; emission maximum = 507 nm.) Genes cloned into the multiple cloning site of pEGFP-N1 are expressed as fusions to the N-terminus of EGFP if they are in the same reading frame as EGFP and there are no intervening stop codons. The pEGFP-N1 vector contains a bacterial promoter that expresses kanamycin resistance for compatible cloning in *Escherichia coli* JM109.

Green fluorescent protein (GFP) is c. 26 kDa and has a typical beta barrel structure, consisting of one β-sheet with alpha helices containing the fluorophore running through the center (Yang *et al.*, 1996). While the tightly packed barrel shell protects the fluorophore from quenching by the surrounding microenvironment, the inward facing sidechains of the barrel induce specific cyclisation reactions in the tripeptide Ser65–Tyr66–Gly67 that lead to fluorophore formation. This occurs in a series of discrete steps with distinct excitation and emission properties. This process is referred to as maturation and generally takes 30 mins to occur which is important to consider when viewing GFP under the microscope.

Table 2.3 summarises the plasmids used in this work.

Table 2.3 Summary of plasmids used in this work

Plasmid	Features	Source	Reference
pGEMT Easy Vector System II	Rapid ligation of sticky-ended PCR products, blue/white screening	Promega	
Suicide vector for homologous recombination of *mamK* Gm^R disruption mutation			
pK19mobsacB	Kanamycin resistance, *SacB* for sucrose intolerance	Dirk Schüler	
pBBR1MCS-5	Gentamycin resistance	Dirk Schüler	Kovach *et al.* (1995)
Broad-host range mamK-egfp complimentation			
pBBR1MCS-2	Kanamycin resistance	Dirk Schüler	Kovach *et al.* (1995)
pEGFP-N1	Ampicillin resistance	Clontech	
MamK over expression and protein-protein interactions			
pT7-7	Ampicillin resistance, T7 promoter	Chris French	Tabor *et al.* (1985)
pET28a	Kanamycin resistance, T7 promoter, N-terminal His-tag	Novagen	

2.3. CLONING

Prior to cloning bioinformatics work was carried out on *mamK* nucleotide sequences and MamK amino acid sequences. We used of the National Centre for Biological Information (www.ncbi.nlm.nih.gov) and the European Bioinformatics Institute (www.ebi.ac.uk) sequence databases and online sequence analysis tools such as BLAST and ClustalW. The downloadable sequence analysis software, Vector NTI (Invitrogen, www.invitrogen.com) was useful. Other useful online resources were Prosite and ProtScale from the ExPASy Proteomics Server (expasy.org), the Institute for Genomic Research (www.tigr.org/) (now part of the Craig J. Venter Institute), and TMPRED Transmembrane regions detection hosted by the Swiss Institute of Bioinformatics (http://www.ch.embnet.org/index.html).

Table 2.4 summarises clones used in this work.

Table 2.4 Summary of clones used thoughout this work

Suicide vector for homologous recombination of mamK Gm^R disruption mutation		
pK19*mobsacB*::*mamK*-Gm^R-*mamK*	In frame *mamK* disruption with a gentamycin cassette for homologous recombination into the MSR-1 chromosome	This work
Broad-host range *mamK-egfp* complimentation in pBBR1MCS-2		
pEGFP-N1::*mamK*	Template for amplification of *mamK-egfp* for insertion into pBBR1-MCS-2	This work
pBBR1MCS-2::*mamK-egfp* 1	Complementation of the chromosomal *mamK* mutant from 27 base pairs upstream from the start site annotated in acc no BX571797	This work
pBBR1MCS-2::*mamK-egfp* 2	Complementation of the chromosomal *mamK* mutant from the start site annotated in acc no BX571797 for insertion into	This work
pBBR1MCS-2::*mamK-egfp* 3	Complementation of the chromosomal *mamK* mutant from 36 base pairs downstream from the start site annotated in acc no BX571797. This position is equivalent to that of *Magnetospirillum magneticum AMB-1.*	This work
pBBR1MCS-2::(RBS)*mamK-egfp*	Complementation of the chromosomal *mamK* mutant from 36 base pairs downstream from the start site annotated in acc no BX571797. This position is equivalent to that of *Magnetospirillum magneticum* AMB-1 and also includes an *E. coli* ribosome binding site for localisation in *E. coli.*	This work
MamK overexpression		
pT7-7::*mamK*	Overexpression of recombinant MamK	This work
pT7-7::*mamK* (cys)	Overexpression of recombinant MamK with an additional cysteine residue at the C-terminal for attachment of a pyrene probe for conformational change light scattering	This work
pT7-7::*mamK-egfp*	Overexpression of MamK-EGFP for expressionand visualisation of the localisation fo MamK *in vivo* and *in vitro*	This work
pET28a::*mamK*	Overexpression of MamK with N-terminal His-tag for ease of purification and protein-protein interactions	This work
pET28a::*mamK-egfp*	Overexpression of MamK-EGFP for expression and visualisation of the localisation of MamK *in vivo* and *in vitro* and for ease of purification	This work

2.3.1. Suicide vector for chromosomal MamK disruption in *Magnetospirillum gryphiswaldense* MSR-1

The MamK suicide vector, pK19*mobsacB*::*mamK*-Gm^R-*mamK* (Table 2.5), was created for chromosomal insertion of a gentamycin disrupted *mamK* sequence for in frame replacement of wild type *mamK* by homologous recombination into the *Magnetospirillum gryphiswaldense* MSR-1 chromosome.

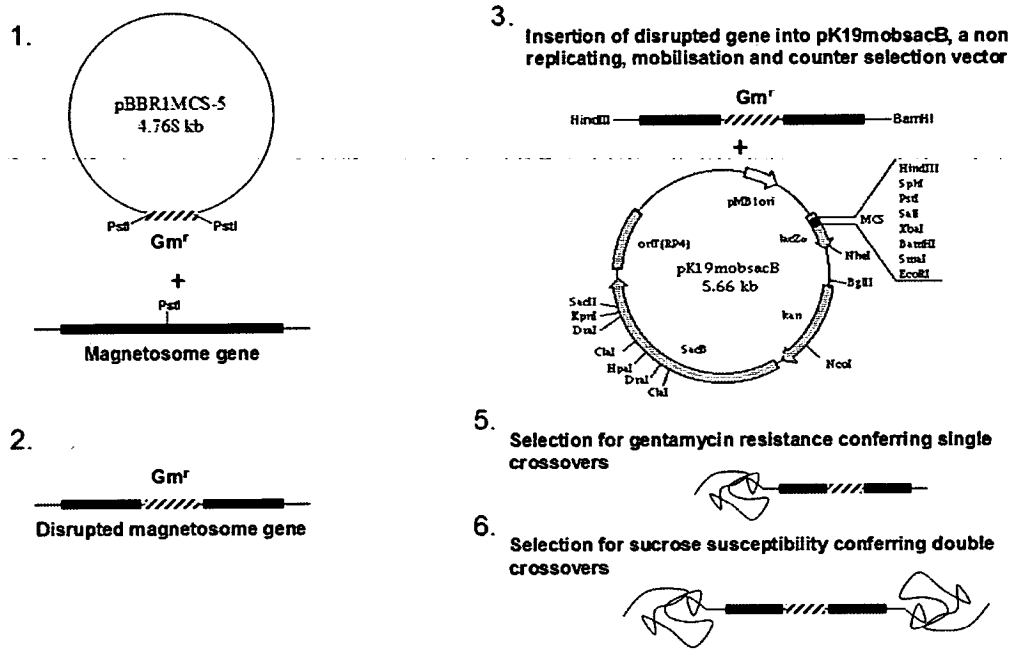

Figure 2.1 Schematic diagram of a knockout mutagenesis method in *Magnetospirillum gryphiswaldense* MSR-1. The gentamycin resistance cassette of vector pBBR1MCS-5 was inserted at a naturally occurring PstI site in *mamK* (1) resulting in the disruption of the *mamK* gene (2). The disrupted *mamK* gene was inserted into the suicide vector, pK19*mobsacB*, at the HindIII/BamHI position (3). Following conjugation *Magnetospirillum gryphiswaldense* MSR-1 *mamK* single cross over mutants were selected for using gentamycin (5) and double crossovers were to be selected for using replica plating and sucrose susceptibility (6) (Based on work by Schultheiss *et al.*, 2004)

The method was adapted from Schultheiss *et al.* (2004) (Figure 2.1). MamK has a naturally occurring PstI site. Primers 1 and 2 (Table 2.5), and 3 and 4 (Table 2.5) were designed to clone the gentamycin resistance cassette from pBBR1-MCS-5 and *mamK* from wild type *Magnetospirillum gryphiswaldense* MSR-1 respectively in pGemT Easy Vector. A HindIII/BamHI restriction digest was conducted on the

mamK clone for insertion into the HindIII/BamHI sites of pK19*mobsacB*. PstI restriction digests were carried out on the gentamycin resistant clone and pK19*mobsacB*::*mamK* for insertion of the gentamycin resistance cassette into the naturally occurring PstI site of *mamK*. At this stage the suicide vector was ready for homologous recombination into the *Magnetospirillum gryphiswaldense* MSR-1 genome. Transformation of cells was conducted by conjugation and selection methods described under Section 2.1 of the materials and methods section. Cells were plated on to activated charcoal agar containing 25 µg/ml gentamycin and incubated under microaerobic conditions outlined in section 2.1.1 for at least 3 weeks with regular observation as advised by Dirk Schüler.

2.3.2. MamK insertion into a broad host range vector for localisation in the *mamK* mutant

Two methods were used to construct the clone for the localised complementation of MamK in *Magnetospirillum gryphiswaldense* MSR-1. The first method was based on work by Scheffel *et al.* (2006). Primers 5 and 6, and 7 and 8 (Table 2.5) were used to clone *mamK* from *Magnetospirillum gryphiswaldense* MSR-1 and *egfp* from pEGFP-N1. The products of each of these reactions were mixed together and used as template for a PCR reaction using primers 5 and 8 where the 3′ and 5′ regions of *mamK* and *egfp* respectively would form a bridge resulting in an in frame *mamK-egfp* fusion for insertion into the HindIII/XbaI sites of pBBR1MCS2 for localisation of MamK in the wild type.

The second method resulted in four constructs each with a variation in their start site based on available sequence information of the *Magnetospirillum gryphiswaldense* MSR-1 genome and questionability regarding the presence of a ribosome binding site in pBBR1MCS-2. Forward primers 9, 10, 11 and 12 (Table 2.5) were set up in individual PCR reactions with reverse primer 13 resulting in 4 *mamK* pGemT Easy clones. These primers resulted in the broad host range constructs, pBBR1MCS-2::*mamK-egfp* 1, 2, 3 and pBBR1MCS-2::(RBS)*mamK-egfp* (Table 2.4) HindIII/BamHI restriction digests were carried out on the clones and they were inserted into the corresponding sites of pEGFP-N1. The pEGFP-N1::*mamK* clones were used as template in reactions with the respective forward primers and reverse

primer 8 (Table 2.5). The products of these reactions were cloned in pGemT Easy followed by restriction digests with HindIII and BamHI for insertion of the *mamK-egfp* fusion into pBBR1MCS-2 for localisation of MamK in the wild type *Magnetospirillum gryphiswaldense* MSR-1.

Table 2.5 Summary of primers for *mamK* chromosomal disruption work

No.	Descriptive name	Oligonucleotide sequence	Tm (°C)	Use	Origin
Suicide vector preparation					
1	pBBR1MCS-5 Gm^R cassette forward *PstI*	5'- CTGCAGGACGCACACCGTGGAAA	64.7	Cloning of the gentamycin cassette from pBBR1MCS-5 for in	This work
2	pBBR1MCS-5 Gm^R cassette reverse *PstI*	5'- CTGCAGGCGGCGTTGTGACAATTT	64.7	frame insertion into a naturally occurring *PstI* site in *mamK*	This work
3	*mamK* chromosomal disruption forward *HindIII*	5'- AAGCTTGGATTGATCTGTTAGC	47.0	Cloning of *mamK* for insertion into pK19mobsacB suicide vector	This work
4	*mamK* chromosomal disruption reverse *BamHI*	5'- GGATCCGACCGGAAACGTCAC	55.2	for homologous recombination on the MSR-1 chromosome	This work
a Broad-host range *mamK-egfp* complimentation preparation (each primer was designed to clone *mamK-egfp* in one reaction for direct insertion into pBBR1MCS-2)					
5	*mamK* fusion PCR forward *HindIII*	5'- AAGCTTCTGTGGATTGATCTGTTAGCACG	65.5	Primes *mamK* from the start site annotated in acc no BX571797 for insertion into pBBR1MCS-2	This work
6	*mamK-egfp* fusion PCR bridge	5'- CCCTTGCTCACCATTCACTGACCGGAAACGTCA	65.5	Provides a bridge between *mamK* and *egfp* during fusion PCR	Method adapted from Scheffel *et al.* (2005)
7	*mamK-egfp* fusion PCR bridge	5'- CGTTTCCGGTCAGTGAATGGTGAGCAAGGGCGA	65.7	Provides a bridge between *mamK* and *egfp* during fusion PCR	Method adapted from Scheffel *et al.* (2005)
8	*egfp* fusion PCR reverse *XbaI*	5'- TCTAGATTACTTGTACAGCTCGTCCATGC	65.0	Primes *egfp* from pEGFP-N1 for insertion into pBBR1MCS-2	This work
b Broad-host range *mamK-egfp* complimentation preparation (each primer was designed to clone *mamK for insertion into* pEGFP-N1)					
9	*mamK-EGFP* complimentation forward *HindIII 1*	5'- AAGCTTATGCTGAAGATAAGAATAAATAGAGACCT	61.6	Primes *mamK* 27 base pairs upstream from the start site annotated in acc no BX571797	This work
10	*mamK-EGFP* complimentation forward *HindIII 2*	5'- AAGCTTCTGTGGATTGATCTGTTAGCACG	65.5	Primes *mamK* from the start site annotated in acc no BX571797 for insertion into pBBR1MCS-2	This work
11	*mamK-EGFP* complimentation forward *HindIII 3*	5'- AAGCTTATGAGTGAAGGTGAAGGCCA	64.6	Primes *mamK* 36 base pairs downstream from the start site annotated in acc no BX571797. This position is equivalent to that of *Magnetospirillum magneticum* AMB-1	This work
12	RBS *mamK-EGFP* complimentation forward *HindIII*	5'- AAGCTTAAGGAGGGACAAAATGAGTGAAGGTGAAG	60.2	Includes an *E. coli* RBS for localisation in *E. coli* and primes *mamK* 36 base pairs downstream from the start site annotated in acc no BX571797.	This work
13	*mamK-EGFP* complimentation reverse BamHI	5'- GGATCCTGACCGGAAACGTCACC	64.3	Cloning of *mamK* for insertion into pEGFP-N1	This work

2.3.3. Cloning for overexpression of MamK and its fusions and mutants

2.3.3.1. Native MamK

Five clones were constructed for overexpression of MamK, MamK-EGFP and MamK(cys) (Table 2.4). As before, pGemT was used to clone PCR products before restriction digestion and ligation to the target vector. The restriction sites for primers were chosen based on their compatibility with both pT7-7 and pET28a (Table 2.6). As the start site of pT7-7 and pET28a is conveniently incorporated into an NdeI site on the vector the forward primer 14 (Table 2.6) incorporated an NdeI site and was designed to express the protein in frame with this. Reverse primer 15 (Table 2.6) incorporated a HindIII site and was used to clone *mamK* for overexpression of native form protein or His-tagged protein in pT7-7 and pET28a respectively.

2.3.3.2. MamK-EGFP fusion

Forward primer 14 and reverse primer 16 (Table 2.6), that incorporated a SalI restriction site, were used in a reaction with pBBR1MCS-2::*mamK-egfp* 1 (Table 2.4) or the clone, pEGFP-N1::*mamK* (Table 2.4), used as an intermediate in the construction of this broad host range vector. This combination of primers produced a clone that overexpressed *mamK-egfp* in pT7-7 and pET28a.

2.3.3.3. MamK-cys

Forward primer 14 and reverse primer 17 (Table 2.6) were used to construct pT7-7::*mamK*-cys (Table 2.4). Primer 17 codes for the transcription of a cys residue at the C-terminus of MamK thus increasing the length of the protein by one amino acid.

Table 2.6 Summary of primers for overexpression

No.	Descriptive name	Oligonucleotide sequence	Tm (°C)	Use	Origin
14	*mamK* over expression forward *NdeI*	5'- CATATGTGGATTGATCTGTTAGCACGC	65.0	Primes *mamK* for overexpression in pT7-7 or pET28a	This work
15	*mamK* over expression reverse *HindIII*	5'- AAGCTTCAAAATGACATCCCCCATCA	65.4	Primes *mamK* for overexpression in pT7-7 or pET28a	This work
16	*mamK-egfp* fusion over expression reverse *SalI*	5'- GTCGACTTACTTGTACAGCTCGTCCATGC	65.0	Primes *mamK-egfp* fusion from pEGFP-N1 or pBBR1MCS-2 for insertion into pT7-7 or pET28a	This work
17	*mamK-cys* over expression reverse *HindIII*	5'- ATCCCCCATCAACACTGACC	65.9	Primes *mamK* encoding a C-terminal cysteine residue for attachment of pyrene or rhodamine fluorescent probes	This work

2.4. DNA WORK

2.4.1. Genomic DNA purification

Genomic DNA was isolated using the Wizard Genomic Kit (Promega). The manufacturer's instructions were followed except that 10 ml of *Magnetospirillum gryphiswaldense* was substituted for 1 ml of *Escherichia coli* culture.

2.4.2. Silica solution for plasmid DNA purification

Silica (1 g) (Sigma S-5631) was suspended in 10 ml PBS and left for 2 hr. The supernatant was removed and the silica resuspended in PBS and again left for 2 hr. The beads were sedimented at 604 *x g* in a microcentrifuge after which the supernatant was removed and the silica resuspended in 3 M KI and stored at 4 °C.

2.4.3. Wash buffer for plasmid DNA purification

Components were mixed (50 mM NaCl, 2.5 mM EDTA, 10 mM Tris-HCl pH 7.5 and 50 % v/v EtOH) and stored at -20 °C.

2.4.4. 10 mM Tris pH 8.0 Elution buffer

A 1 M stock solution of Tris pH 8.0 was prepared by adding 88.8 g of tris HCl and 53 g of tris base to 700 ml dH_2O with mixing and made up to 1 litre with dH_2O. Diluting 1 ml of the 1 M stock solution in 99 ml dH_2O resulted in 10 mM Tris pH 8.0.

2.4.5. 20x TAE for electrophoresis gels

Tris base (48.4 g) and Na_2EDTA (3.72 g) were dissolved in 400 ml of dH_2O. Acetic acid (11.4 ml) was added and mixed in a fume head and the solution was made up to 500 ml with dH_2O.

2.4.6. Agarose gel electrophoresis (0.8 % agarose)

20x TAE (13.5 ml) was added to dH_2O (270 ml) to make 1x TAE. Agarose (240 mg) was added to 30 ml of 1x TAE in a 50 ml Ehrlenmeyer and microwaved on high for 1 minute to dissolve it and then poured into the gel cast.

2.4.7. PCR reactions for Roche Taq experiments

Table 2.7 Volumes of reagents used for PCR experiments.

	µl
water	31
buffer	5
dNTP (10 mM)	1
template	2
primer F (10 mM)	5
primer R (10 mM)	5
Taq DNA polymerase	1
	50

2.4.8. Plasmid DNA mini-preparation

Three solutions were prepared prior to beginning DNA mini-preparations. Solution 1 contains 5 µl/ml of 5 mg/ml RNAse of which 100 µl is required per prep. Solution 2 contains water, 0.4 M NaOH and 10 % SDS at a ratio of 4:5:1 v/v respectively (i.e. for six preps use 0.56 ml water, 0.7 ml 0.4 M NaOH and 0.14 ml 10 % SDS). Solution 3 is made up of 3 M potassium acetate and 2 M acetic acid and can be kept at 4 °C.

Transformed overnight cultures were aliquoted to a microfuge tube in 1.5 ml volumes and pelleted at 4293 *x g* for 3 min. The supernatant was discarded and the cells resuspend in 0.1 ml of solution 1 by pipetting up and down. Solution 2 (0.2 ml) was added to the cells and mixed by inversion until the solution appeared clear and viscous. Solution 3 (0.15 ml) was added from 4 °C and mixed immediately by inversion until a precipitate formed. The DNA mini-preparations were incubated on ice for 10 min with mixing after 5 min followed by microcentrifugation at 11,340 *x g* for 3 min. The supernatant (c. 0.42 ml) was transferred to a fresh tube avoiding as much of the precipitate as possible, the precipitate was discarded. Ethanol was added to the supernatant (0.92 ml 100 % EtOH) (c. v/v 2.2:1 EtOH: supernatant) and incubated on ice for 10 min or in a freezer overnight. The DNA mini-preparations

were spun at 11,340 *x g* for 10 min to pellet the DNA. The supernatant was discarded carefully without disturbing the pellet. The pellet was washed with 0.2 ml 70 % EtOH, centrifuged at 11,340 *x g* for 1 minute and the supernatant was discarded. The DNA mini-preparations were centrifuged briefly once again to remove as much supernatant as possible. The pellets were dissolved in EB pH 8.0 and stored at -20 °C.

2.4.9. Restriction digests

Restriction digests were prepared at a (v/v) ratio of 6:2:1:1 dH_2O: DNA: 10x reaction buffer: digestion enzyme respectively. Double digests (i.e. digests using two enzymes) share the assigned ration of 1 (e.g. 6 µl water, 2 µl DNA, 1 µl buffer and 0.5 µl of each enzyme).

2.4.10. pGemT Easy ligation

Ligations to the pGemT Easy vector were prepared by mixing 5 µl 2x ligase buffer, 3 µl DNA, 1 µl vector and 1 µl T4 DNA ligase followed by incubation overnight at 4 °C. Remember that if PCR was done using Roche Taq there is no need to digest the insert or vector prior to ligation due to the AT overhangs of pGEMT Easy.

2.4.11. Ligation of purified DNA to vector

Ligations of purified DNA fragments to vectors were prepared by mixing 4 µl DNA, 4 µl vector, 1 µl 10x ligase buffer and 1 µl T4 DNA ligase followed by overnight incubation at 16 °C.

2.4.12. DNA purification using glass beads

DNA was purified using a silica solution (Section 2.4.2) from either agarose gel (e.g. digested DNA) or liquid (e.g. PCR reaction).

From a gel the DNA band of interest was cut from an agarose gel and placed in a pre weighed microcentrifuge tube. The gel slice was weighed and 3x its weight in mg of 6 M NaI was added to the tube which was then incubated in a water bath at 55 °C until the gel slice has completely melted (c. 5 min)

From liquid the volume of the soluble DNA was accounted and 3 x its volume of 6 M NaI was added.

After incubation the silica solution was added (e.g. 5 µl depending on the volume of DNA) and incubated on ice for 10 min with mixing after 5 min to keep the silica suspended. The tubes were microcentrifuged to pellet the silica and the supernatant was discarded. The pellet was washed in ice cold buffer (0.25 ml) (-20 °C) (Section 2.4.3) followed by microcentrifugation three times. The silica pellet was resuspended by pipetting in EB (e.g. 10 µl or double the volume of glass beads used) (Section 2.4.4). The suspension was incubated at 55 °C in a water bath for 10 min, with mixing after 5 min. The solution was microcentrifuged and the supernatant containing the DNA was transferred to a fresh tube.

2.4.13. Loading buffer for electrophoresis gels

Mix 600 µl 50% glycerol, 100 µl 10 % SDS, 300 µl 20x TAE and enough bromophenol blue to colour the solution in a microfuge tube and store at 4 °C.

2.4.14. BDV3.1 DNA sequence reactions and PCR program

Mix 5 µl plasmid template, 2 µl BDV3.1, 2.5 µl distilled water and 0.5 µl primer. Set up the PCR program to run Stage 1 at 96 °C for 1 minute, Stage 2 (x 25) at 96 °C for 30 seconds, 50 °C for 15 seconds and 60 °C for 4 min, and Stage 3 to hold at 4 °C.

2.5. PROTEIN WORK

2.5.1. Storage of cell extracts

Cultures were harvested and resuspended in *Escherichia coli* lysis buffer containing 50 mM Tris HCl pH 8.0, 1 mM EDTA, 100 mM NaCl. Lysozyme was added to the suspension at a final concentration of 1 mg/ml along with a protease inhibitor cocktail (Sigma P8465). The suspension was incubated at room temperature for one hr and then frozen for storage at – 20 °C.

2.5.2. Preparation of Tris-glycine electrophoresis buffer

A 5 x stock was prepared by mixing 15.1 g tris base, 94 g glycine and 1 g SDS in 1 l of dH_2O. The buffer was used at 1 x and was prepared by diluting 200 ml of the 5 x stock with 800 ml of dH_2O.

2.5.3. Preparation of the resolving gel (12 %)

The resolving gels were cast with a 12 % SDS content per gel containing 1.8 ml 30 % bis-acrylamide (Ultra pure protogel, EC-890, National Diagnostics), 1.4 ml water, 1 ml Tris-HCl pH 8.8, 40 µl 10 % SDS, 40 µl 10 % APS and 10 µl TEMED. Of this solution 3.2 ml was poured into the cast.

2.5.4. Preparation of the stacking gel (5 %)

The stacking gels were cast with a 5 % SDS content per gel containing 830 µl 30% bis-acrylamide, 3 ml water, 630 µl Tris-HCl pH 6.8, 50 µl 10 % SDS, 50 µl 10 % APS and 5 µl TEMED.

2.5.5. Stain for SDS-PAGE gels

Stain was prepared by mixing 500 ml water, 400 ml methanol, 100 ml acetic acid and 1 g of Coomassie Brilliant Blue.

2.5.6. Destain for SDS-PAGE gels

Destain was prepared by mixing 500 ml water, 400 ml methanol and 100 ml acetic acid. Destain can be reused after filtering through activated charcoal to remove the coomassie stain.

2.5.7. SDS-PAGE

SDS-PAGE was carried out using a PROTEAN mini gel system at 200 V and 50 mA for 1 hr. After electrophoresis the gels were stained (Section 2.5.5) and destained (Section 2.6.6).

2.5.8. Denaturation/renaturation

A culture (50 ml) expressing MamK was aliquoted to microfuge tubes in 1.5 ml volumes was lysed microcentrifuged at 11,340 *x g* for 10 min following which the supernatant was discarded. The pellet was resuspended in 150 µl 6 M guanidine-HCl and incubated at room temperature for 1 h. The suspension was microcentrifuged for 10 min at 11,340 *x g*. The supernatant was removed to a fresh microfuge tube. The supernatant underwent slow dilution with 50 mM Tris-HCl pH 7.5. Samples were then viewed by phase contrast and fluorescence microscopy.

2.5.9. Inclusion body preparation

Cell extracts from 50 ml cultures were thawed and sonicated to get maximum lysis of cells. Three buffers were pre-prepared. Buffer 1 contained 20 mM Tris pH 8.0, 0.2 M NaCl, 1 % (w/v) sodium deoxycholate and 2 mM EGTA; buffer 2 contained 0.25 % (w/v) deoxycholate, 1 mM EGTA, 10 mM Tris pH 8.0; and buffer 3 contained 8 M urea, 10 mM Tris pH 8.0, 1 mM sodium azide and 1 mM EGTA. Firstly, the pellet from the sonicate, that can be assumed to contain protein inclusion bodies, was resuspended in 50 ml of inclusion body buffer 1 and incubated for 15 to 30 min at room temperature. The suspension was centrifuged for 5 min at 5590 *x g* after which the supernatant was removed. The pellet was then washed in buffer 2 by repeating resuspension and centrifugation at 5590 *x g* for 5 min (x 3). Finally, the pellet was dissolved in buffer 3.

2.5.10. Chromatography

MamK was prepared for chromatography first by carrying out an inclusion body preparation on ice and then by overnight dialysis in a buffer containing 10 mM Tris pH 8.0, 0.2 mM $CaCl_2$ and 2 mM DTT at 4° C. ATP or GTP at 0.2 mM was added to this buffer in order to test different methods of purifying MamK.

2.5.10.1. Ion exchange chromatography

MamK in buffer 3 was dialysed overnight in the same buffer used to equilibrate the column (10 mM Tris pH 8.0, 0.2 mM $CaCl_2$ and 2 mM DTT, 1 mM NaN_3 without the addition of NTP or with the addition of either 0.2 mM ATP or GTP). The ion gradient buffer was the same as the equilibration buffer but with the addition of 0.5 M KCl. The dialysed solution was loaded on to a DE53 column (column sise, 2.5 cm x 10 cm; volume, 39 cm^3; flowrate, 0.5 ml/min; gradient 0 – 0.5 M KCl). The ion gradient was applied to the column after 160 ml had passed through the column. Approximately 5 ml fractions were collected. Protein concentration was monitored at 280 nm.

2.5.10.2. Sise exclusion chromatography

Fractions containing MamK were collected from the ion exchange column, pooled and concentrated using a protein concentration column (VIVASPIN6 at 4000 *x g*; VIVASPIN50 at 6383 *x g*, Sartorius) to a volume of 1 ml and loaded onto a Sephacryl-300 (Pharmacia) sise exclusion column. The sise exclusion column was packed with Sephacryl 300 (GE Healthcare) in all cases (column sise, 1.6 cm x 70 cm; volume, 175 cm^3; flowrate, 0.5ml/min). The column was equilibrated with 10 mM Tris pH 8.0, 0.2 mM $CaCl_2$, 50 mM NaCl, 2 mM DTT and either 0.2 mM ATP, 0.2 mM GTP or no NTPs. Approximately 5 ml fractions were collected and protein concentration was monitored at 280 nm.

MamK was dialysed overnight using 10 mM Tris pH 8.0, 0.2 mM $CaCl_2$ and 2 mM DTT containing or not containing 0.2 mM ATP or GTP and the column was equilibrated overnight with the same buffer.

2.5.11. Crystallisation

MamK was purified by inclusion body preparation and column chromatography. The protein was concentrated to 8 mg/ml using a VIVASPIN6 in the presence of 150 mM NaCl. Crystallisation screens were carried out using the hanging drop vapour diffusion method in Linbro trays at 4 °C. Hanging drops of 4 µl were prepared by adding 2 µl of protein to 2 µl of well solution (Structure Screen 1,

Molecular Dimensions Ltd, Cat. No. MD1-01, Batch 008). Trays were examined for crystals periodically.

2.5.12. Microscopy

2.5.12.1. Phase contrast microscopy

Wet mounts were prepared and viewed under 400 x or 1000 x magnification on a Eclipse E 200, Nikon.

2.5.12.2. Fluorescence microscopy

Wet mounts were prepared and viewed under 400 x and 1000 x on a Metalux II (Leitz Wetzlar) with assistance from Dr. Garry Blakely. Samples were also viewed at 400 x using an Axiovert 200 (Zeiss) with a Samrock dichroic GFP filter set to obtain bright field and fluorescent images for processing with Metamorph v. 6.3 r2 with assistance from Mr. Martin White, University of Edinburgh.

2.5.12.3. Transmission electron microscopy (TEM)

Recombinant MamK was purified and dialysed into 10 mM Tris pH 8.0. Samples were incubated for at least 2 hr in the presence of 2 mM $MgCl_2$. The samples were diluted 100 fold into dH_2O in order to reduce the $MgCl_2$ concentration to prevent the formvar coating from splitting.

Sample volumes of 20 µl were applied to formvar coated copper grids and incubated at room temperature for 20 min to allow time for sheets to sediment on to the grid. Excess liquid was blotted off with filter paper. The samples were stained with 2 % (w/v) uranyl acetate for 30 min. Excess uranyl acetate was blotted off with filter paper and the samples were left to dry overnight. Images were captured on a Kodak SO-163 electron image film in a Philips CM120 biotwin transmission electron microscope with the assistance of Mr. Steve Mitchell, University of Edinburgh. Further images were captured after the same preparation method in a JEOL 1200 EXII transmission electron microscope operated at an accelerating voltage of 120 kV and micrographs were recorded on 2k x 2k Gatan digital camera with the assistance of Dr. David Bhella and Dr. Worawit Suphamungmee, University of Glasgow.

2.5.12.4. Atomic force microscopy (AFM)

AFM was performed using NP-20 cantilevers (c) in tapping mode on a Veeco multimode controller Nanoscope 3a with the assistance of Dr. Nhan Pham, University of Edinburgh.

2.5.13. Light scattering and fluorescence

Inclusion body buffer 3 containing MamK (0.125 – 0.25 μg/ml) was dialysed overnight in 10 mM Tris pH 8.0, 2 mM DTT and 2 mM NaN_3 without the addition of NTP or with the addition of either 0.2 mM ATP or GTP. Light scattering assays were conducted in a Perkin Elmer LS55 Luminescence Spectrometer. Light scattering data were collected under the time drive mode with an excitation wavelength of 350 nm. Tryptophan fluorescence data were collected under scan mode at 290 – 800 nm with excitation at 270 nm. MamK was observed in buffers under conditions with and without nucleotides (ATP and GTP), $MgCl_2$, $CaCl_2$, EGTA and 1M Tris. Pyrenyl MamK fluorescence data were collected under scan mode at 390 - 500 nm with excitation at 365 nm.

2.5.14. Coupling of MamK-cys to fluorescent probes

Five methods of preparing fluorescently probed MamK with a C-terminal cys mutation were carried out (Table 2.8). For each method light scattering experiments were carried out to test for polymerisation of MamK-cys/aggregation on addition of $MgCl_2$. The fluorescence spectrum of pyrenyl-MamK-cys was measured for some preps to test whether pyrene had coupled to the C-terminal cys residue of the protein.

Table 2.8 Summary of methods for binding of fluorescent probes to MamK-cys protein.

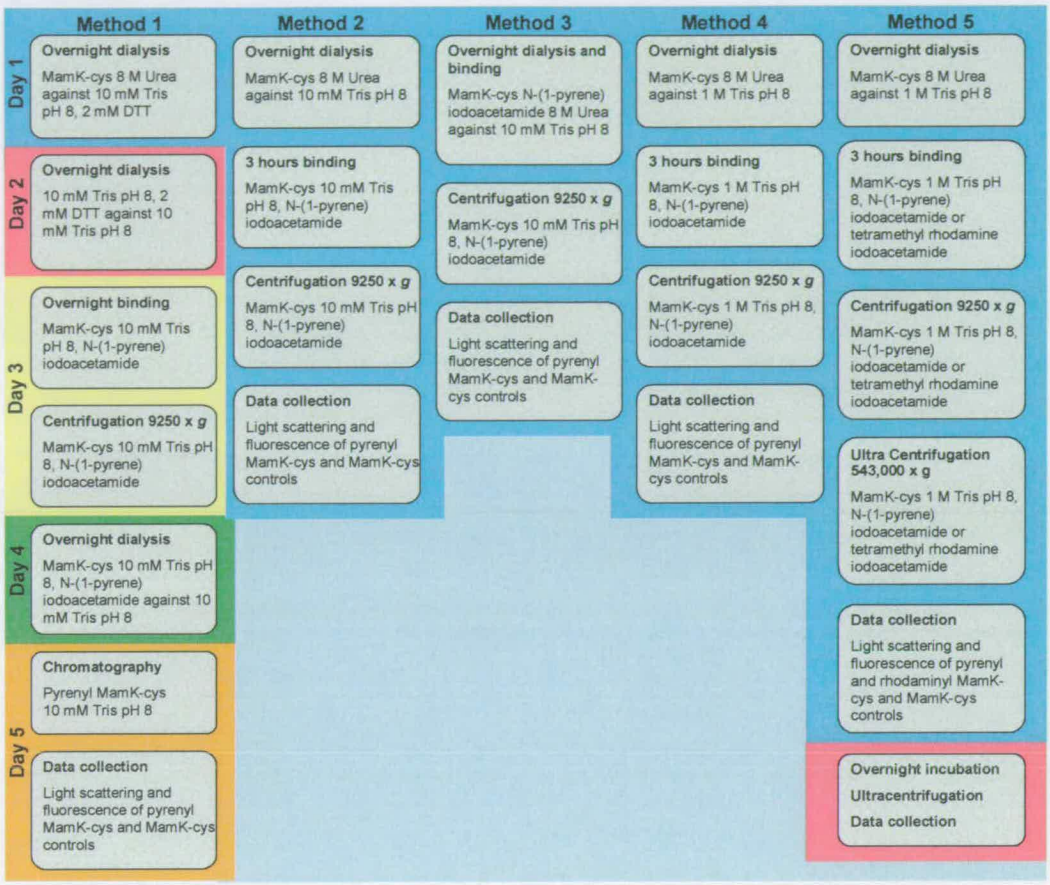

2.5.14.1. Method 1

MamK-cys was dialysed overnight at 4° C from 8 M urea into 10 mM Tris pH 8.0, 2 mM DTT followed by another overnight dialysis into 10 mM Tris pH 8.0. A soupçon of N-(1-pyrene)iodoacetamide was solubilised in 100 µl DMF, added to the protein suspension and incubated overnight at 4° C. The mixture was centrifuged at 9250 *x g* for 25 min. The pellet was discarded and the supernatant was loaded to a Sephacryl 300 sise exclusion column. Spectrophotometric readings of fractions were taken at A_{280} to locate the protein peaks

2.5.14.2. Method 2

The same stock of MamK-cys in 8 M urea as before was dialysed overnight into 10 mM Tris pH 8.0. A soupçon of N-(1-pyrene)iodoacetamide was solubilised in 100 µl DMF of which all was added to the protein suspension and incubated for 3 hr at 4° C. The mix was centrifuged at 9250 *x g* for 25 min. The pellet was discarded

and fluoro- and spectrophoto- metric readings of a 20-fold dilution of the supernatant were taken.

2.5.14.3. Method 3

Samples of MamK-cys were split and dialysed overnight at 4 °C from 8 M urea into 10 mM Tris pH 8.0. One sample contained N-(1-pyrene)iodoacetamide and the control did not. Samples were examined by SDS-PAGE. The samples were centrifuged at 9250 *x g* for 25 min to remove any precipitated compound. The pellet was discarded and fluoro- and spectrophoto- metric readings of a 20-fold dilution of the supernatant were taken.

2.5.14.4. Method 4

MamK-cys was dialysed overnight at room temperature from 8 M urea into 1 M Tris pH 8.0 as 1 M Tris has been shown to keep actin in a disassociated form (Pinder *et al.*, 1995). The sample was split and incubated for 3 hr at 4 °C with rotation, one with N-(1-pyrene)iodoacetamide and one without. Samples were examined by SDS-PAGE. Following incubation the samples were centrifuged at 9250 *x g* for 25 min to remove any precipitate. The pellet was discarded and fluorometric and spectrophotometric readings of a 20-fold dilution into 10 mM Tris pH 8.0 were taken. MamK-cys and pyrenyl MamK-cys samples were incubated for 2 hr after the addition of $MgCl_2$ after which fluorescence readings were taken. The samples were then centrifuged at 9250 *x g* in a microcentrifuge and further fluorescence readings were taken.

2.5.14.5. Method 5

MamK-cys was dialysed overnight at room temperature from 8 M urea into 1 M Tris pH 8.0 (Pinder *et al.*, 1995). The sample was split and incubated for 3 hr at room temperature with rotation, one with N-(1-pyrene)iodoacetamide, one with tetramethyl rhodamine iodoacetamide and one without a fluorescent label. Following incubation the samples were centrifuged at 9250 *x g* for 25 min to remove any precipitate. The pellet was discarded and the supernatant was centrifuged at 543000 *x g* in a TLA100 for one hr at 4 °C. The supernatant was removed immediately after centrifugation and retained along with the resuspended pellet for

fluoroscopy and spectroscopy. Fluorometric and spectrophotometric readings of 20-fold dilutions into 10 mM Tris pH 8.0 were taken from each sample. The samples were incubated overnight at room temperature in 1 M Tris pH 8.0 and 15 mM $MgCl_2$. Following incubation the samples were centrifuged at 543000 *x g* in a TLA100 ultracentrifuge and the pellet washed three times with 1 M Tris pH 8.0 and resuspended in 1 M Tris pH 8.0 by vortexing at room temperature for two hr.

2.5.15. Coupling of MamK to CNBr-activated sepharose 4B

CNBr-activated sepharose 4B (1 g for 5 ml of ligand solution, 1 g gives about 3.5 ml swollen gel) was suspended in 1 mM HCl. The gel was washed for 15 min on a sintered glass filter (~ 200 ml/g of dry sepharose 4B). The OD_{280} readings were taken of the ligand and a sample was kept for SDS-PAGE. The ligand was dissolved in coupling buffer (0.1 M $NaHCO_3$ pH 8.3 and 0.5 M NaCl), or the protein was dialysed overnight in 1 litre of this buffer if it was already in solution. The ligand solution was mixed with the CNBr-activated sepharose 4B gel in a stoppered vessel and rotate end-over-end overnight at 4° C. The following day the sepharose was pelleted by centrifugation at 9250 *x g* and the supernatant removed being sure to read the optical density to compare it to the reading from the previous day. This gives an idea of how much protein has bound to the sepharose. Excess ligand was washed away with coupling buffer and any remaining active groups were blocked with 0.1 M Tris-HCl pH 8.0 for 16 hr at 4° C. The product was washed with three cycles of alternating pH. Each cycle should consist of a wash with acetate buffer (0.1 M AcONa pH 4 and 0.5 M NaCl), followed by a wash with a Tris buffer (0.1 M Tris-HCl pH 8.0 and 0.5 M NaCl). The product was stored in the Tris buffer with additional 0.5 mM DTT at 4 °C.

The binding of recombinant MamK to sepharose 4B results in matrices to be used for column chromatography. A column was packed and equilibrated with 10 mM Tris pH 8.0. *Magnetospirillum gryphiswaldense* MSR-1 crude cell extract was dialysed overnight in 10 mM Tris pH 8.0. Following dialysis the crude cell extract was loaded to the column. A 1 M KCl buffer was prepared to create a gradient to elute

MamK and interacting proteins. Fractions are examined by spectrophotometry at an absorbance of 280 nm for the presence of protein.

2.5.16. Raising anti-MamK antibodies

An inclusion body preparation was carried out on cells expressing MamK. The protein was dialysed from 8 M urea into 10 mM Tris pH 8.0. A 5 ml aliquot of the protein was used as antigen to raise anti-MamK sheep antibodies (work carried out by Dr. Maggie Chambers, Diagnostic Scotland).

2.5.17. Western blot analysis

Proteins were separated by SDS-PAGE and transferred to a nitrocellulose membrane by electroblotting for 1 hr at 200 mA in 1 x transfer buffer (3.02 g/l Tris, 14.26 g/l glycine). The membrane was placed in 2 % blocking agent (100 ml 2 % (w/v) dried non fat milk, 0.2 % (v/v) Tween 20 in TBS, 1 mM NaN_3) made up in TBS (50 mM Tris pH 8.0, 150 mM NaCl) and incubated for 1-2 hr at room temperature. The blocked membrane was rinsed (2 x 5 min) in TBS and 0.2 % Tween 20 (TBST). The primary and secondary antibodies were diluted to working concentrations (anti-*mamK*, 2:1000 dilution; anti-goat HRP, 1:25000) in TBST. The blocked washed blot was incubated with primary antibody for 1 hr at room temperature then rinsed (4 x 5 min) in TBST. The blot was then incubated with secondary antibody for 1 hr then rinsed (4 x 5 min) in TBST. In a dark room, the blot was transferred to a ten-fold dilution of 1:1 (v/v) ECL detection reagent (LumiGLO) for 1 min. Excess solution was removed and the blot was wrapped in clingfilm and exposed to X-ray film for 1 min.

2.5.18. Pierce® protein quantification

Protein was quantified by Bradford assay as outlined by Pierce®.

2.5.19. N-terminal sequencing

Immobilised protein samples were solubilised for Edman degradation and degradation products were analysed on an Applied Biosystems Procise 4HT microsequencer using the method of Hayes *et al.* (1989) (work carried out by Dr. Andy Cronshaw, ICMB sequencing service, University of Edinburgh).

3 SEQUENCE ANALYSIS OF MamK

3.1 BACKGROUND

The amino acid sequence of MamK has been identified as having homology to actin and bacterial cytoskeleton proteins. The putative function of MamK is to provide a cytoskeletal structure that has a role in the linear organisation of the magnetosome chain thus maximising the net magnetisation of magnetosomes within the cells of magnetic bacteria. There are no reports of sequence comparisons of MamK so work was carried out here to verify the differentiation of MamK into a clade distinct from actin and other bacterial cytoskeletal proteins. This chapter describes amino acid sequence comparison of MamK from *Magnetospirillum gryphiswaldense* MSR-1 to MamK amino acid sequences from other magnetic bacteria and amino acid sequences from evolutionarily distinct cytoskeletal proteins.

3.2 RESULTS

3.2.1 The emergence of a clade closely related to MamK

Basic local alignment was conducted on *Magnetospirillum gryphiswaldense* MSR-1 MamK amino acid sequence using the default settings of the protein-protein BLAST algorithm (Altschul *et al.*, 1990). The three most significant alignments were with actin-like ATPases from *Magnetospirillum magneticum* AMB-1 with 94 % identity (Bits, 670; E-value 0.0), *Magnetospirillum magnetotacticum* MS-1 with 94 % identity (Bits, 619; E-value, 8e-176), and *Magnetococcus* sp. MC-1 with 51 % identity (Bits, 354; E-value, 5e-96). The following four most significant alignments were with actin-like ATPases from Deltaproteobacterium MLMS-1 with scores ranging from 49 % identity (Bits, 326; E-value, 2e-87) to 51 % identity (Bits, 236; E-value, 2e-60). The remaining sequence alignments were annotated as MreB, the bacterial cell shape determining protein and had identity of 29 % (Bits, 84.3; E-value, 1e-14) or less. The three most significant alignments were with amino acid sequences from magnetic bacteria whereas the following four most significant alignments were with amino acid sequences from Deltaproteobacterium MLMS-1. The Deltaproteobacterium MLMS-1 hits are curious as this bacterium has not been reported to be magnetic so should not express magnetosome specific proteins (Dr.

John Stolz, Duquesne University, personal communication). A further search showed that Deltaproteobacterium MLMS-1 also has amino acid sequences defined as MreB and FtsA that are distinct from the sequences that showed more homology to MamK.

To show differentiation of the most significant basic local alignments for *Magnetospirillum gryphiswaldense* MSR-1 MamK, this and the seven homologous amino acid sequences from the aforementioned protein-protein BLAST were aligned with actin and other bacterial actin-like (MreB, FtsA and ParM) amino acid sequences from various organisms using ClustalW2 (Higgins *et al.,* 1994). The sequence comparison included MreB and FtsA homologues from the proteome sequences of *Magnetospirillum magnetotacticum* MS-1 and Deltaproteobacterium MLMS-1 to investigate whether MamK had paralogy to these cytoskeletal proteins.

Sequences were input in FASTA format to ClustalW2 under default settings except for the "pir" format output. The "pir" format output was copied and re-entered to the ClustalW2 algorithm where the output was according to similarity ("alignment") as an "nj" (neighbour joining) tree type. The sequences were firstly tested under conditions that corrected distances. Setting the algorithm to "distance corrections" corrects multiple substitutions (Higgins *et al.*, 1994). As sequences diverge, more than one substitution occurs at many sites but only one difference is seen when looking at the present day sequences. Choosing to correct distances has the effect of stretching branch lengths in trees (especially long branches). The results (Figure 3.1) showed that MamK grouped with the three most significant basic local alignments from magnetic bacteria. These results also showed that all the actin-like MLMS-1 sequences that showed homology to MamK grouped with MamK indicating that they may be part of the MamK clade or that they form a distinct but closely related clade. Further to this the FtsA homologues from *Magnetospirillum magnetotacticum* MS-1 and Deltaproteobacterium MLMS-1 actin-like MLMS-1 sequence fell into their expected clades whilst the respective MreB homologues appeared to group with the MreB clade but on closer examination they are more distantly related compared to MreB from *Escherichia coli, Bacillus subtilis* and *Thermotoga maritima.*

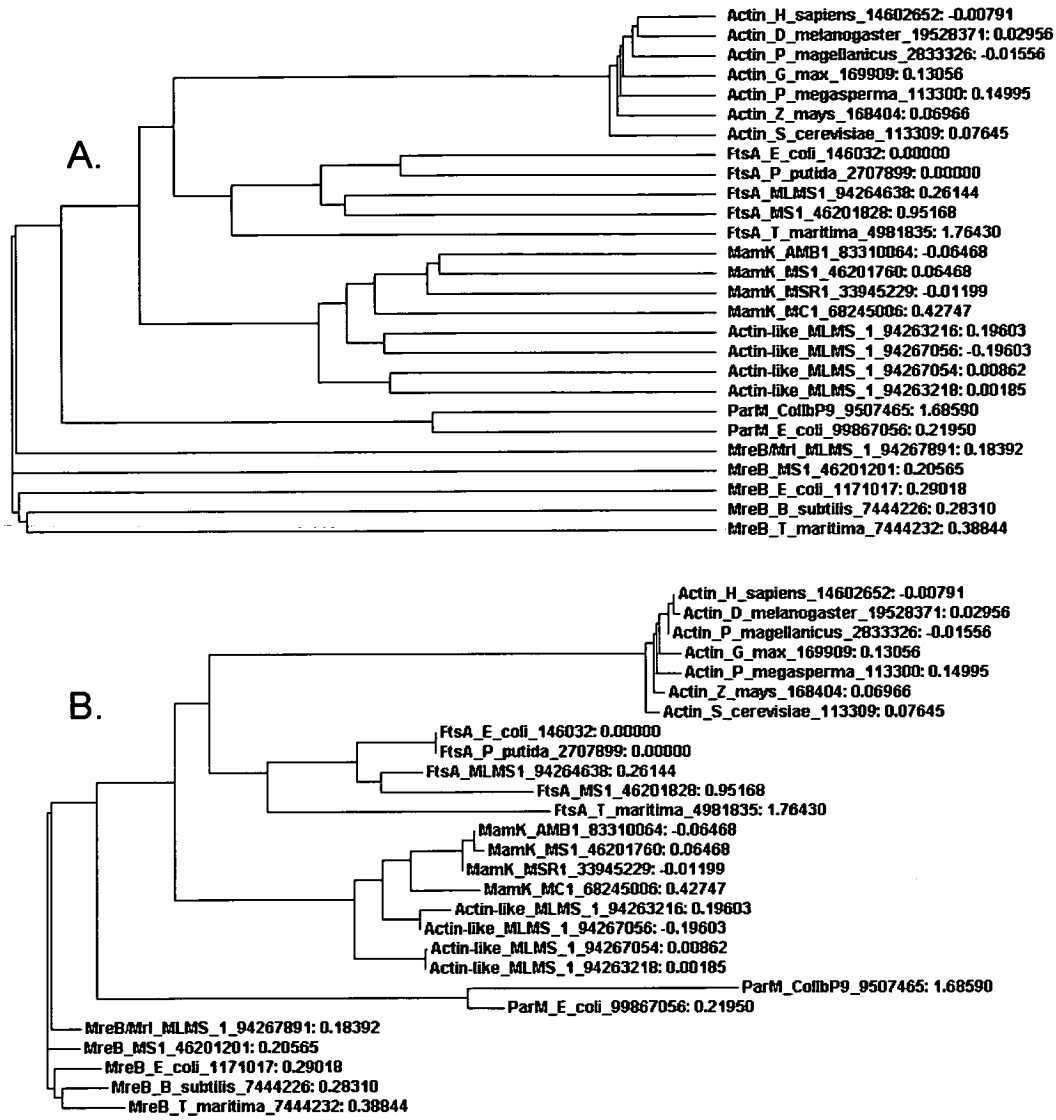

Figure 3.1 A cladogram (A) and a phylogram (B) illustrating the division of actin and bacterial actin-like amino acid sequences whilst correcting for multiple substitutions in the amino acid sequences. The annotation follows the form of protein_organism_NCBI GI no: distance score} Clade.

Another test was performed on the sequences as before except this time rather than correcting for distances between sequences, gaps in the sequences were ignored (Figure 3.2). This time the MreB homologues from *Magnetospirillum magnetotacticum* MS-1 and Deltaproteobacterium MLMS-1 actin-like MLMS-1 the sequences grouped more closely into the MreB clade. The FtsA clade changed position from diverging with actin (Figure 3.1) to diverging with MreB (Figure 3.2). Choosing to "ignore gaps" means that any alignment positions where any of the

sequences have a gap will be ignored (Higgins *et al.*, 1990). This means that 'like' is compared to 'like' in all distances and the most ambiguous parts of the alignment, which are often concentrated around gaps are thrown away. The disadvantage of this is that much of the data may be thrown away if there are many gaps.

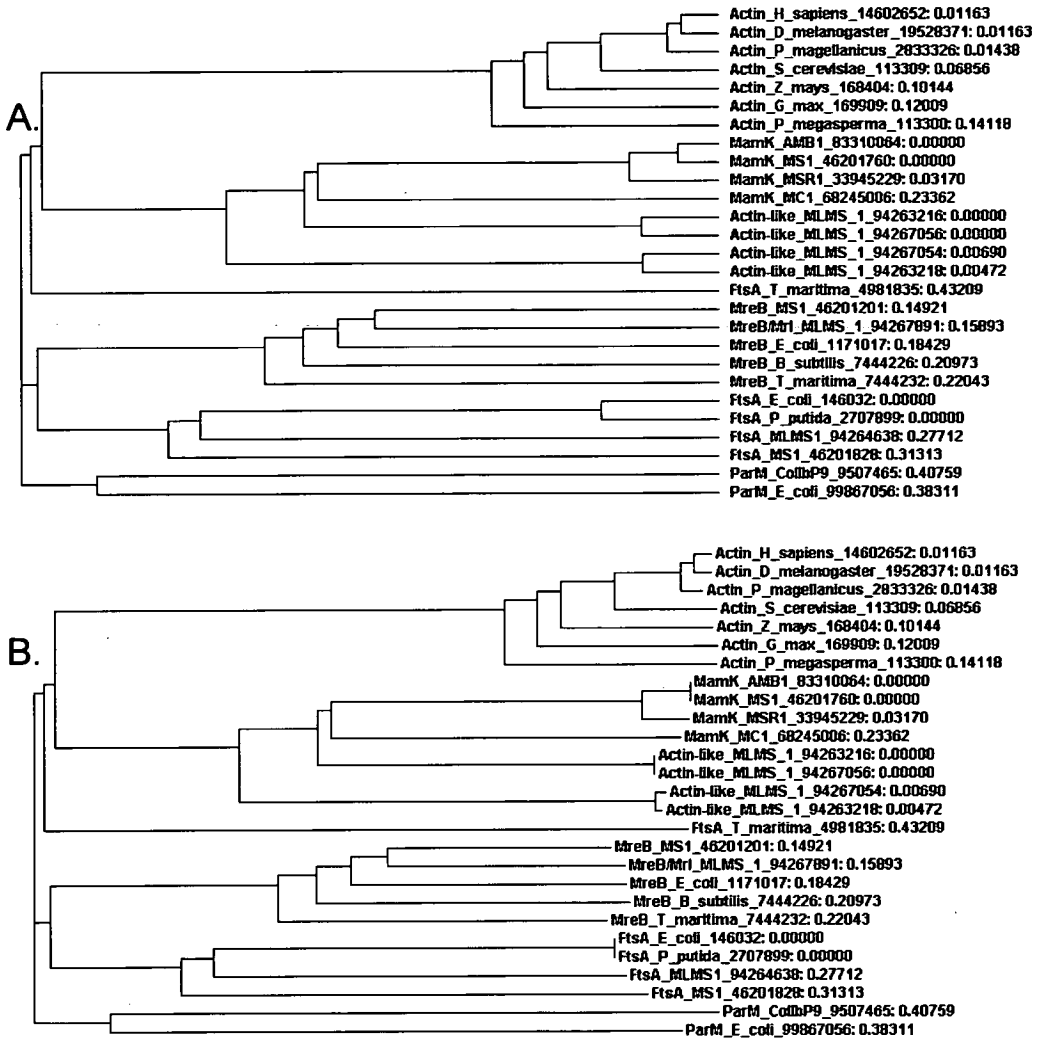

Figure 3.2 A cladogram (A) and a phylogram (B) illustrating the division of actin and bacterial actin-like amino acid sequences whilst ignoring gaps in the amino acid sequences. The annotation follows the form of protein_organism_NCBI GI no: distance score} Clade.

The amino acid sequences of the *Magnetospirillum gryphiswaldense* MSR-1 magnetosome island (GI:33945208) were compared to the Deltaproteobacterium MLMS-1 proteome to investigate the possibility of further magnetosome associated proteins using genome BLAST. Scores ranging between 30% and 49 % identity

were returned for ORF9, MamE, MamJ, MamK, MamM and MamB. Orf9 had homology to extracellular solute-binding protein with 48% identity (Bits, 296; E-value, 2e-81). MamE revealed three sequences with homology to the PDZ domain of trypsin-like serine proteases, such as DegP/HtrA, which are oligomeric proteins involved in heat-shock response, chaperone function, and apoptosis with scores between 48% identity (Bits, 153; E-value, 9e-38) and 49 % identity (Bits 135; E-value of 2e-32). MamJ showed 30 % identity (Bits 27.3, E-value, 5.2) to a small region of a conserved hypothetical protein. MamK was homologous to four sequences ranging from 50 % identity (Bits, 320, E-value, 2e-88) to 25 % identity (Bits, 65.9; E-value, 1e-11). MamM had homology to a cation efflux pump predicted to transport cobalt, zinc or cadmium cations with 33 % identity (Bits 155; E-value, 8e-39) and 33 % identity (Bits 155; E-value, 1e-38) whilst MamB had homology to the same sequences but with 30 % identity (Bits 171; E-value, 1e-43) and 30 % identity (Bits 171; E-value, 2e-43). These sequence homologies are relatively consistent with domains that have been identified in magnetosome associated proteins Orf9 (ABC-type iron transporter), MamE (trypsin like-serine protease), MamJ (methyl-accepting chemotaxis domain at the N-terminus and a haemerythrin domain at the C-terminus), MamK (actin-like), and MamM and MamB (Co/Zn/Cd cation transporter). This result suggests that *Deltaproteobacterium* MLMS-1 may harbour inclusions with a similar process of formation to magnetosomes of magnetic bacteria.

3.2.2 MamK amino acid sequence comparison

The alignment of the eight amino acid sequences from the MamK clade (Section 3.1, Figure 3.1 and Figure 3.2) was examined for homologous residues using ClustalW2. The sequences were submitted to the algorithm using the default setting except for the output which was set at "pir". The "pir" output was re-submitted for tree building under the default and this resulted in the alignment presented in Figure 3.3. As presented earlier *Magnetospirillum gryphiswaldense* MSR-1 MamK has greatest homology to *Magnetospirillum magneticum* AMB-1 MamK and *Magnetospirillum magetotacticum* MS-1 MamK amino acid sequences, followed by *Magnetococcus* MC-1 MamK and then the amino acid sequences from *Deltaproteobacterium*

MLMS-1. The *Magnetospirillum magneticum* AMB-1 and *Magnetospirillum magetotacticum* MS-1 MamK sequences score 100 % for sequence similarity and in turn *Magnetospirillum gryphiswaldense* MSR-1 MamK scores 85 % for sequence similarity with the preceeding magnetospirilla (Table 3.1). Each of the other sequences tested score less than 50 % similarity with the *Magnetospirillum* spp.

Table 3.1 The % similarity of homologous MamK sequences with *Magnetospirillum* spp.

Organism number	*Magnetospirillum* sp.	% similarity AMB-1	MS-1	MSR-1
1	*Magnetospirillum magneticum* AMB-1		100	85
2	*Magnetospirillum magetotacticum* MS-1	100		85
3	*Magnetospirillum gryphiswaldense* MSR-1	85	85	
4	*Magnetococcus* MC-1	47	47	46
5	MLMS-1_94263216	42	42	43
6	MLMS1_94263218	36	36	36
7	MLMS1_94267054	36	36	36
8	MLMS1_94267056	33	33	33

In Figure 3.3 the annotated start site for each sequence is underlined. The start sites of *Magnetospirillum magneticum* AMB-1, *Magnetococcus* MC-1 and Deltaproteobacterium MLMS-1 sequences MLMS1_94263218 and MLMS1_ 94267054 share the same annotated start position.

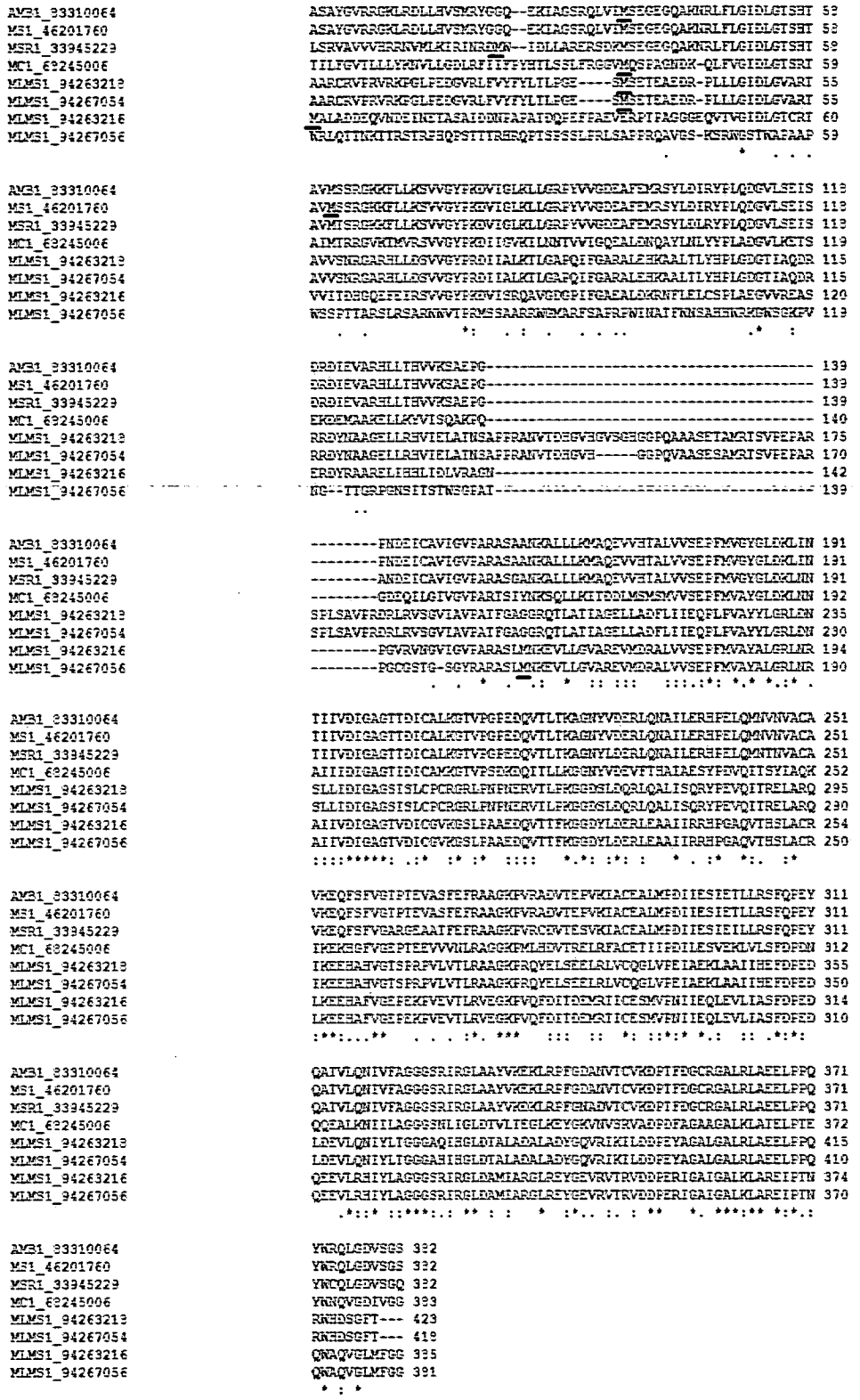

Figure 3.3 Multiple sequence alignments for sequences with high homology to *Magnetospirillum gryphiswaldense* MSR-1. Annotated start sites are underlined.

3.2.3 Conserved active site residues in actin and MreB compare well to MamK amino acid sequence

Tertiary conformations of actin and MreB and their active site residues are well documented (van den Ent *et al.,* 2001; Kabsch and Holmes, 1995; Vorbiev *et al.,* 2003; Martin *et al.,* 2006; Nolen and Pollard, 2007). Sequence comparison of MamK to MreB and actin was conducted to highlight shared conserved residues and to analogously infer the role of conserved regions in MamK through available literature on actin and MreB sequences. Sequence alignments were prepared using ClustalW2 similarly to those illustrated in Figure 3.3 except the *Deltaproteobacterium* MLMS-1 sequences MLMS1_94263218, MLMS1_94267054 and MLMS1_94267056 were removed from the selection whilst *Homo sapien* actin (GI:14602652), *Drosophila melanogaster* actin (GI:19528371), *Placopecten magellanicus* actin (GI:2833326), *Saccharomyces cerevisiae* actin (GI:113309), *Bacillus subtilis* MreB (GI:7444226) and *Thermotoga maritima* MreB (GI:7444232) amino acid sequences were added to the selection.

Figure 3.4 shows the results of the multiple sequence alignments of variants of MamK, actin and MreB to highlight conserved residues. Fifteen highly conserved residues were identified and these are labelled with letters of the alphabet. Many of the residues labelled in Figure 3.4 correspond to residues and regions of known function in *Saccharomyces cerevisiae* actin and *Thermotoga maritima* MreB (van den Ent *et al.,* 2001; Kabsch and Holmes, 1995; Vorbiev *et al.,* 2003; Martin *et al.,* 2006; Nolen and Pollard, 2007).

Many of the conserved residues are involved in the coordination of the nucleotide (ATP or GTP) in *Saccharomyces cerevisiae* actin and *Thermotoga maritima* MreB (van den Ent *et al.,* 2001; Kabsch and Holmes, 1995; Vorbiev *et al.,* 2003; Martin *et al.,* 2006; Nolen and Pollard, 2007). In Figure 3.4 highly conserved nucleotide coordinating residues are highlighted by (a) (actin residues 11-16, 18; MreB residues 9-14), (d) (actin residue 74; MreB residue 68), (f) (actin residue 108; MreB residue 103), (g, h, i) (actin residues 154, 156-159; MreB residues 153, 155-158), (j) (actin residues 182; MreB residue 179-180, 183), (l, m) (actin residues 301-303, 306-306;

MreB residues 285-287, 289-290) and (n) (actin residues 336, MreB residues 312) (van den Ent *et al.* 2001). There are further *Saccharomyces cerevisiae* actin and *Thermotoga maritima* MreB sites involved in nucleotide binding that have not fully aligned and these include actin residue 137 and MreB residue 131 situated between (f and g) where the MreB residue corresponds to conserved residues in MamK, and actin residues 206, 213-214 and MreB residues 104, 107-108) between (j and k) where the actin residues 213-214 correspond to conserved residues in MamK.

More specifically *Saccharomyces cerevisiae* actin residue 157-159 (i) were postulated to couple the γ-phosphate release to opening the cleft of actin whilst residue 161 may play a role in activating and/or positioning a nucleophilic water molecule located near the γ-phosphate (Kabsch and Holmes, 1995; Vorbiev *et al.,* 2003; Martin *et al.,* 2006; Nolen and Pollard, 2007). The adenosine group fits into a hydrophobic pocket which corresponds to residues 210-214 (between Figure 3.4 j and k), that have conserved or conserved substitute residues in the MamK sequences, where residue 214 forms a hydrogen bond to the O_2 atom of the ribose and also a salt bridge to a residue across one helical turn to residue 210, residues 302-306 (Figure 3.4 l and m) and residue 336 that does not appear to correspond to residues in MamK or MreB in Figure 3.4 (Kabsch and Holmes, 1995). Actin residues 14-16 (Figure 3.4 a) correspond to where the β-phosphate forms hydrogen bonds with the amides of the three residues whilst residue 303 (Figure 3.4 m) is in close proximity to the α-phosphate (Kabsch and Holmes, 1995). Ca^{2+} is bound in a pocket by the phosphate moiety and residue 11 (before Figure 3.4 (a) where semi reserved substitutions are observed for each sequence), 137 (that does not show similarity to the other clades), and 154 (Figure 3.4 g) whilst Mg^{2+} is bound by residues 11 and 137 only (Kabsch and Holmes, 1995).

Actin residues 69-78 (including Figure 3.4 c and d) correspond to the sensor loop which is postulated to detect and relay conformational differences between ADP- and ATP-actin from the nucleotide cleft to other parts of the molecule (Graceffa and Dominguez, 2003; Otterbein *et al.,* 2001; Rould *et al.* 2006, Nolen and Pollard, 2007). In actin the bilobed domains are connected at residues 137-144 that shows

semi conserved substitutions between sequences at residue 140, and 338 to 348 that shows highly conserved sequence at Figure 3.4 (o) (Kabsch and Holmes, 1995).

Actin residues 262-274 (Figure 3.4 k) correspond to the hydrophobic plug which is a region that is generally accepted to refold in F-actin and to be essential for the interactions between the two strands of the double-stranded F-actin (Holmes *et al.*, 1990). The actin residue 33 (Figure 3.4 b) marks the beginning of the next subdomain in actin (Graceffa and Dominguez, 2003).

Protofilament contacts have been observed in *Thermotoga maritima* MreB (van den Ent *et al.*, 2001). These include MreB residues with protofilament contacts from one subunit to the next which are 146-148, 165-170, 266-275 (containing a residue with conserved substitutions in Figure 3.4), 277-278, 300-303 (flanked by residues with conserved substitutions), 326 and 330 which are divided by a residue with conserved substitutions. Protofilament contact residues from one subunit to the previous subunit include 35, 40, 50, 53-56 and 59, all between Figure 3.4 b and c, a region interspersed with residues of conserved or semi conserved substitutions. Residues 199-202, 227-229 and 335- 338 are interspersed with residues of conserved or semi conserved substitutions some of which have been noted to be involved in nucleotide binding in MreB (104, 107-108) and actin (206, 213-214).

The only conserved residue to elude a functional description in the literature is highlighted by Figure 3.4 e.

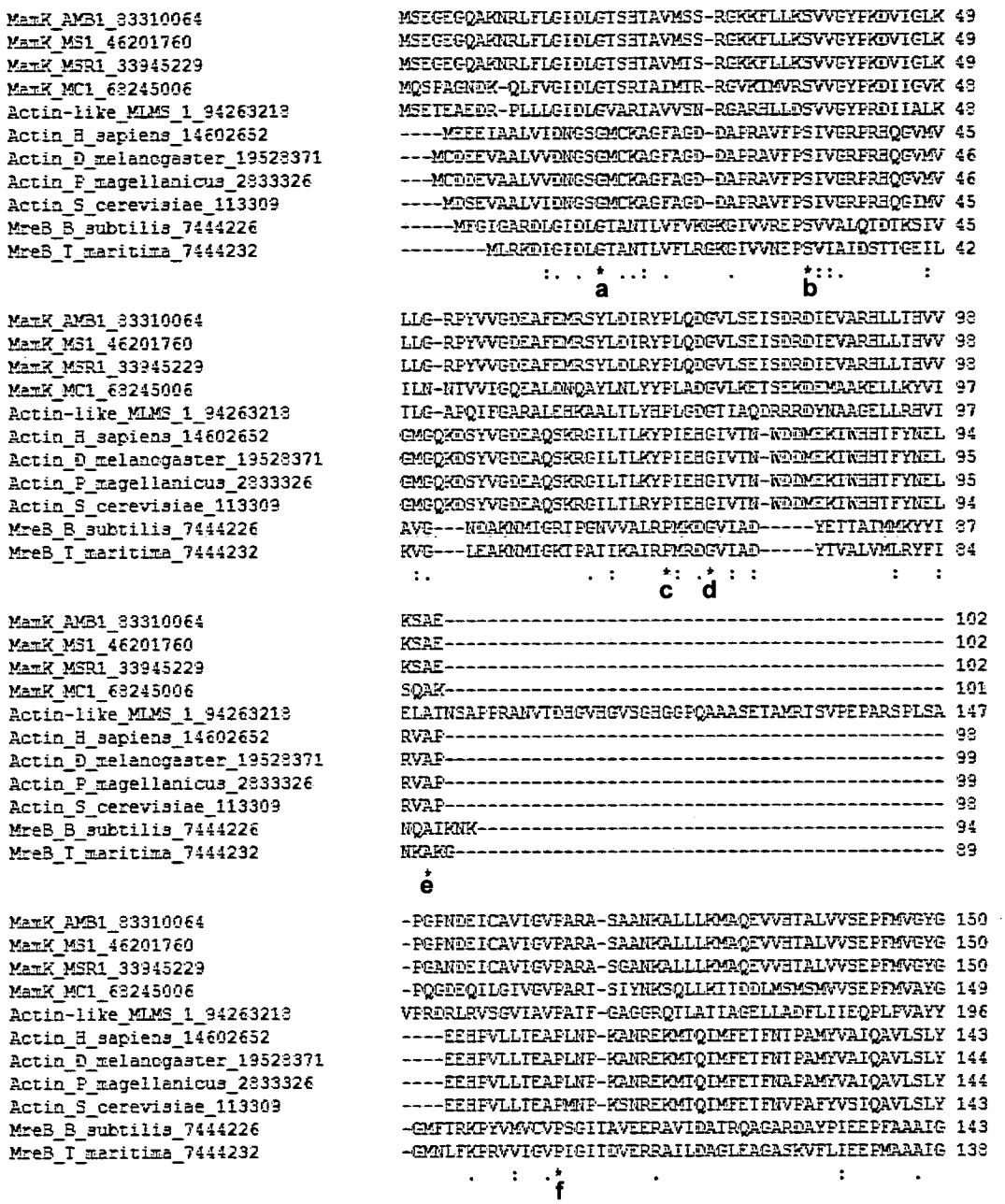

a nucleotide coordination (β-phosphate)	**f** nucleotide coordination	**k** nucleotide coordination (adenosine group) hydrophobic plug
b marks the next subdomain protofilament contact	**g** nucleotide coordination (cation binding)	**l** nucleotide coordination (hydrogen bond and salt bridge)
c sensor loop protofilament contact	**h** nucleotide coordination	**m** nucleotide coordination (α-phosphate) (hydrogen and salt bridge involvement)
d nucleotide coordination sensor loop	**i** nucleotide coordination (γ-phosphate release)	**n** nucleotide coordination
e unknown significance	**j** nucleotide coordination (adenosine group)	**o** connection of bilobed domains

note:
There are further residues in actin and MreB with known function that have not fully aligned (see text)

Continued...

Figure 3.4 Multiple sequence alignments of variants of MamK, actin and MreB to highlight conserved residues.

Figure 3.4 Continued...

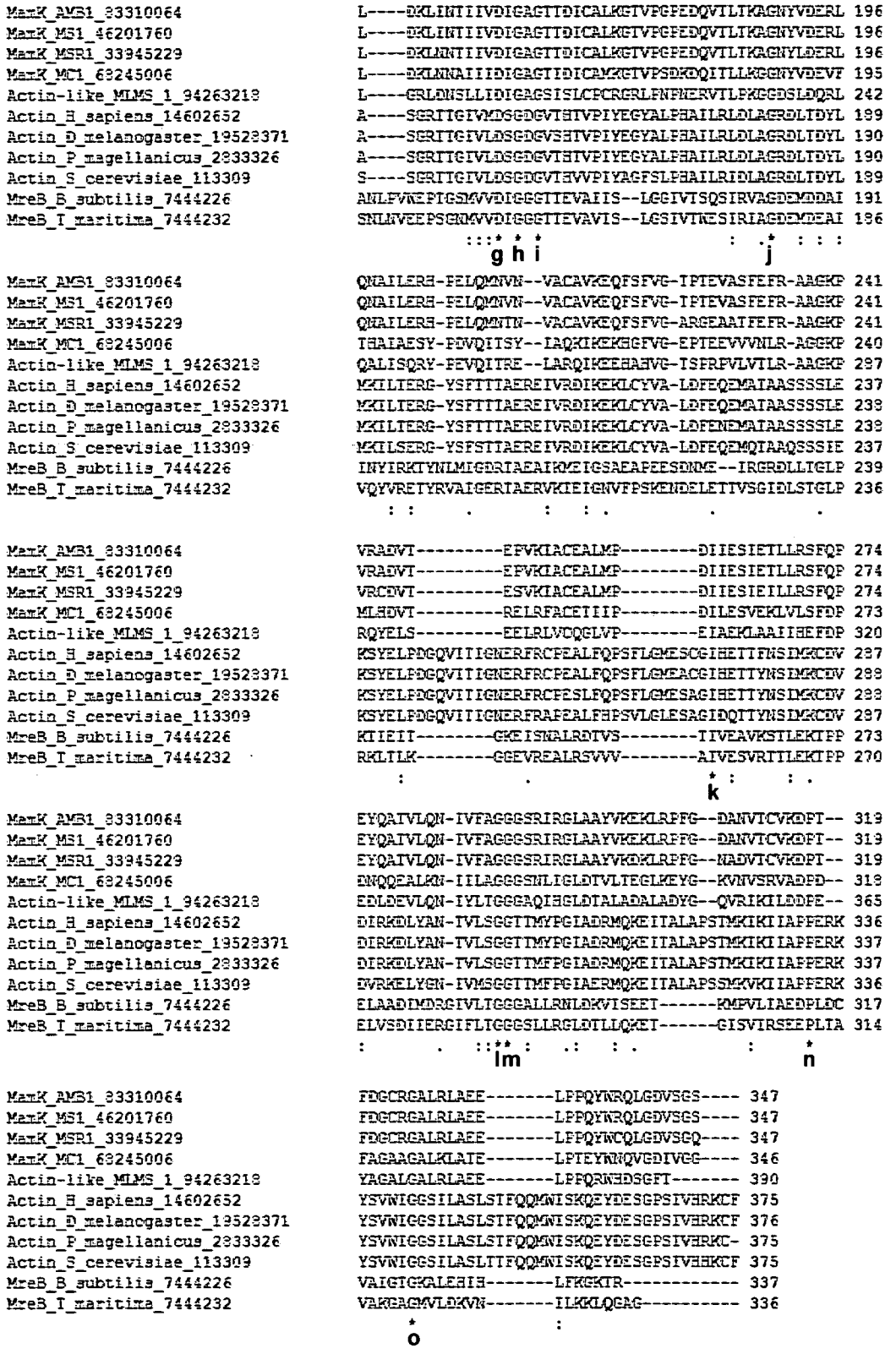

3.2.4 MamK amino acid sequence predictions compared to actin and MreB

Online tools (ProtParam, ProtScale and TmPred) were used to make predictions regarding the amino acid sequence of MamK. The MamK predictions were compared to those of MreB and actin in order to judge how to proceed when expressing and purifying MamK. Amino acid sequence outputs were calculated from the default setting on each occasion. The amino acid sequence of *Magnetospirillum gryphiswaldense* MSR-1 MamK (GI: 33945208) is 360 amino acids long and theoretically has a molecular weight of 39.2 kDa, a pI of 5.45, a half life of 30 hr *in vitro* and an instability index of 39.92 thus classifying it as stable (ProtParam, www.expasy.ch/tools/protparam.html). Theoretically, MamK has a 51.7 % chance of being insoluble when expressed in *Escherichia coli* (ProtScale, expasy.org/tools/protscale.html), and is highly unlikely to have transmembrane helices (TmPred, www.ch.embnet.org/ software/ TMPRED_ form.html). These parameters compare well with those of *Oryctolagus cuniculus* smooth muscle actin (GI:1701) and *Thermotoga maritima* MreB (GI:7444232) as outlined in Table 3.5 so it is likely that methods used to characterise actin and MreB are also relevant to MamK.

Table 3.2 Comparison of protein parameters between MamK, actin and MreB using online resources.

	M. gryphiswaldense MamK GI:33945208	*O. cuniculus* Smooth muscle actin GI:1701	*T. maritima* MreB GI: 7444232
Amino acids	360	377	336
kDa	39.2	42.1	35.8
pI	5.45	5.24	5.34
In vitro half life	30 h	30 h	30 h
Instability index	39.92 (stable)	36.65 (stable)	27.75 (stable)
Transmembrane helices	none	none	none

3.3 DISCUSSION

3.3.1 The emergence of a clade closely related to MamK

Amino acid sequence comparison of MamK showed the protein to have homologues in other magnetic bacteria that fall into distinct clades indicating a separate function compared to other bacterial cytoskeletal proteins (Figures 3.1 and 3.2). Surprisingly, MamK homologues were highlighted in Deltaproteobacterium MLMS-1, a bacterium that is so far understood to be non-magnetic (Dr. John Stolz, Duquesne University, personal communication) (Section 3.2.1). Deltaproteobacterium MLMS-1 is a Gram-negative, chemoautotrophic, motile curved rod that grows by oxidising sulphide to sulphate while reducing arsenate to arsenite (Heoft *et al.*, 2004). The presence of a MamK homologue in Deltaproteobacterium MLMS-1 indicates the possible isolation of a novel magnetic bacterium or the emergence of a novel clade more closely related to MamK than other clades of bacterial cytoskeletal protein.

Homologues of genes encoding magnetosome associated proteins (Orf9, MamE, MamJ, MamK, MamM and MamB) were also found on the chromosome of Deltaproteobacterium MLMS-1 but they do not appear to cluster together on the MLMS-1 genome as they do in magnetotactic bacteria further suggesting that MLMS-1 is not magnetotactic. Work has already begun to test the ability of MLMS-1 to form magnetosomes (Dr. John Stolz, Duquesne University, personal communication).

Close MamK homologues could have the ability to position a variety of bacterial inclusions, or have multiple functions from species to species. Examination of the MamK-like protein from MLMS-1 and its functional characterisation would add to understanding the evolution and multiple functions of actin from its bacterial ancestry. Future work may demonstrate that bacterial cells contain a complicated matrix of highly homologous polymerising structural proteins that can be compared to the many functions of actin in Eukaryotic cells.

3.3.2 MamK amino acid sequence

MamK forms a clade that is distinct from other cytoskeletal proteins. The amino acid sequences of the three *Magnetospirillum* spp., *Magnetococcus* MC-1, and the

four Deltaproteobacterium MLMS-1 MamK homologues were compared to identify the most likely start position for the expression of native MamK (Figure 3.3). The results show that the most commonly annotated start site shared by the sequences is that annotated for *Magnetospirillum magneticum* AMB-1 and closer observation shows that from this point all three of the *Magnetospirillum* spp. MamK amino acid sequences are virtually identical suggesting that native *Magnetospirillum gryphiswaldense* MSR-1 MamK is expressed from the equivalent position. Work, such as purification, microscopy and light scattering, following the expression of *Magnetospirillum gryphiswaldense* MSR-1 MamK, as annotated in the magnetosome island sequence file (BX571797), had already started yielding interesting results so a decision was made to continue working with the protein at hand. These results will be discussed throughout the following chapters. Statistical predictions (Table 3.2) of the behaviour of *Magnetospirillum gryphiswaldense* MSR-1 MamK compared to *Oryctolagus cuniculus* smooth muscle actin and *Thermotoga martima* MreB were conducted and showed similar results further indicating that approaches used to work with actin and MreB were likely to be applicable to *Magnetospirillum gryphiswaldense* MSR-1 MamK.

3.3.3 Conserved functional regions of MamK

MamK from the three *Magnetospirillum* spp. and *Magnetococcus* MC-1, the Deltaproteobacterium MLMS-1 actin-like protein (GI no: 94263218) with the highest homology to MamK, four actin amino acid sequences and two MreB amino acid sequences were compared to observe sequence similarities in active sites that are known for actin and MreB (Figure 3.4). Conserved active sites were highlighted based on results from a number of previous studies (van den Ent *et al.*, 2001; Kabsch and Holmes, 1995; Vorbiev *et al.*, 2003; Martin *et al.*, 2006; Nolen and Pollard, 2007). The degree of conservation of active site amino acid residues was not sufficient for strong conclusions to be drawn, but was clear that, in important regions, MamK generally has a high degree of conservation with MreB and/or actin. Conserved regions presented in Figure 3.4 are also conserved in other bacterial cell cycle proteins, sugar kinases and heat shock proteins all of which are members of the ATPase family (Bork *et al.* 1992). From Figure 3.4 it is clear that use of the

annotated MS-1 start site (Figure 3.3) would lead to omission of residues near the N-terminus which, in MreB and actin, are involved in binding of the α-phosphate of the NTP ligand (van den Ent *et al.,* 2001; Kabsch and Holmes, 1995; Vorbiev *et al.,* 2003; Martin *et al.,* 2006; Nolen and Pollard, 2007). It has been demonstrated that when MamK is expressed according to the *Magnetospirillum magnetotacticum* MS-1 annotation polymers fail to form *in vivo* (Pradel *et al.*, 2006). This work concluded that the most likely start site for MamK expression in *Magnetospirillum magnetotacticum* MS-1 is that shown for *Magnetospirillum magneticum* AMB-1 (Pradel *et al.*, 2006).

4 *IN VIVO* STUDIES OF MAMK

4.1 BACKGROUND

MamK was putatively believed to maintain the linear positioning of the magnetosomes within the cells of magnetic bacteria. If this were true successful functional disruption of MamK on the *Magnetospirillum gryphiswaldense* MSR-1 chromosome followed by functional complementation with fluorescent MamK would demonstrate obvious phenotypes. This chapter outlines work towards the *in vivo* characterisation of MamK in *Magnetospirillum gryphiswaldense* MSR-1.

4.2 RESULTS

4.2.1 Deletion of *mamK* in *Magnetospirillum gryphiswaldense* MSR-1

The MamK suicide vector, pK19*mobsacB*::*mamK-Gm*^{R}*-mamK*, was created for chromosomal insertion of a gentamycin disrupted *mamK* sequence for in frame replacement of wild type *mamK* by homologous recombination into the *Magnetospirillum gryphiswaldense* MSR-1 chromosome. The method was adapted from Schultheiss *et al.* (2004) (Figure 4.1). Primers with PstI sites were designed to amplify the gentamycin resistance cassette from pBBR1MCS-5 for insertion into a naturally occurring PstI site in *mamK*. The disrupted *mamK* was then inserted into the mobilisable suicide vector pK19*mobsacB* (Section 2.3.1). The mobilisable vector was cloned in *Escherichia coli* S17 λpir in preparation for conjugation with *Magnetospirillum gryphiswaldense* MSR-1. Conjugants were screened on a number of occasions but did not result in any colonies indicating single or double crossovers.

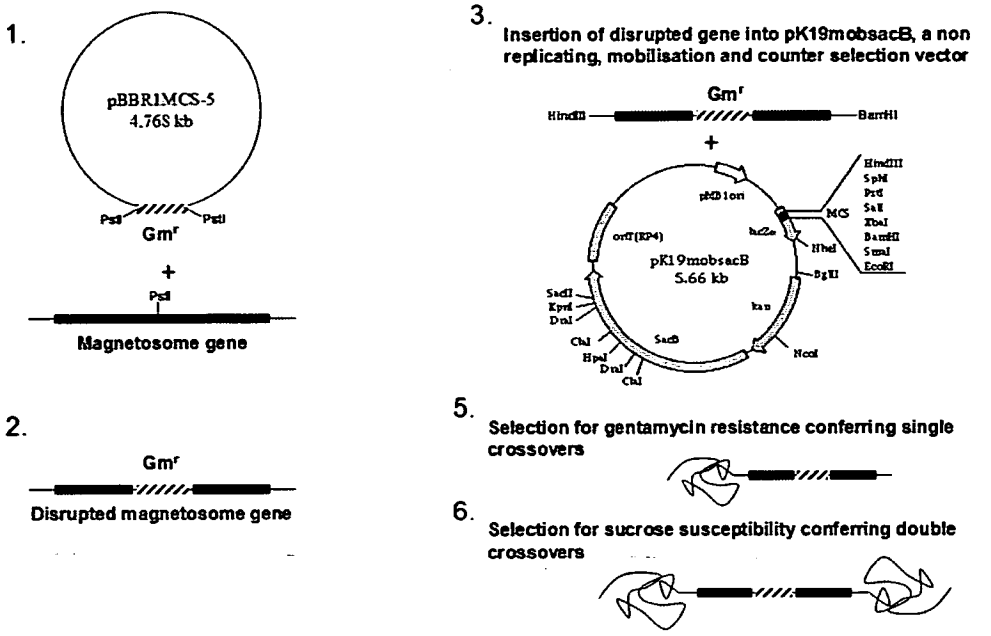

Figure 4.1 Schematic diagram of a knockout mutagenesis method in *Magnetospirillum gryphiswaldense* MSR-1 (Schultheiss *et al.*, 2004) (Figure 2.1).

4.2.2 Construction of MamK-EGFP fusion constructs for complementation

Start sites for MamK translation were indicated by amino acid sequence alignments described earlier (Section 3.2.2). Primers were initially designed to amplify *Magnetospirillum gryphiswaldense* MSR-1 *mamK* and *egfp* (from pEGFP-N1), fuse them and clone them in pBBR1MCS-5 for *in vivo* complementation of the *Magnetospirillum gryphiswaldense* MSR-1 *mamK* disruption mutant. Initial experiments with this construct did not result in fluorescence when expressed in *Escherichia coli.* In an attempt to trouble shoot the lack of fluorescence further constructs were made based on other potential start sites located 27 base pairs upstream of the MSR-1 start site and a potential start site that is equivalent to the AMB-1 start site and a construct with an engineered *Escherichia coli* ribosome binding site upstream of the AMB-1 start site. Subsequently four broad host range constructs translating *Magnetospirillum gryphiswaldense* MSR-1 MamK from each of three annotated start sites were constructed.

Two methods were used to achieve an in frame *mamK-egfp* fusion on a broad host range vector for complementation and localisation of MamK. The first method was based on work by Scheffel *et al.* (2006) where the reverse primer for the gene of

interest (*mamJ* in their case) and the forward primer for the *egfp* gene contained complementary overlapping sequences to form a bridge when the products of the initial PCR were mixed as template for fusion PCR. When trying to achieve a similar result with *mamK* alterations were made to the annealing temperature but this repeatedly resulted in multiple DNA bands after agarose gel electrophoresis, none of which were the expected sise of the fusion product. If this method had been successful it would have been quicker than the standard laboratory method.

The slower standard method resulted in *mamK-egfp* fusions that were successfully inserted into the broad host range vector as indicated by sequencing and restriction pattern. Attempts to visualise MamK-EGFP expression from pBBR1MCS-2 in *Escherichia coli* JM109 and BL21(DE3)p*LysS* under a fluorescence microscope at 1000 x magnification were disappointing. No foci were apparent regardless of the start site or the coding of a ribosome binding site. In order to test that the fusion was correct nested PCR was conducted using pBBR1MCS-2::*mamK-egfp* 1 as template to amplify *mamK-egfp* from the *Magnetospirillum gryphiswaldense* MSR-1 annotated start site. Primers 14 and 15 (Table 2.6) were designed to make insertion of *mamK* according to the MSR-1 annotation into the NdeI and HindIII positions for overexpression from expression vector pT7-7 in *Escherichia coli* BL21(DE3)p*LysS*. Overexpression of the fusion in pT7-7 resulted in fluorescent inclusion bodies (Figure 4.2) suggesting that there was in frame translation of the protein from the pT7-7 start site or possibly from the start site for AMB-1 which is also present in this construct, 13 codons downstream of the MSR-1 start site. The inclusion bodies were always confined to one pole of the cell.

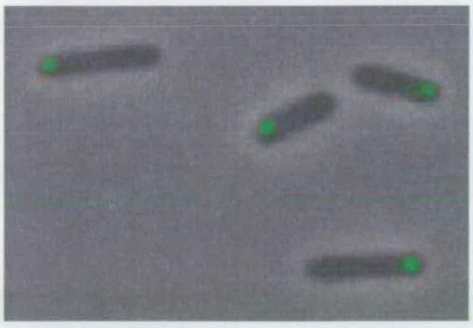

Figure 4.2 Merged phase contrast/fluorescence microscopy image showing MamK-EGFP inclusion bodies in *Escherichia coli* BL21(DE3)p*LysS*.

The reason for apparent lack of expression of the fusion from pBBR1MCS-2 is unclear. Neither Kovach *et al.* (1995), Schultheiss *et al.* (2004) nor Scheffel *et al.* (2006) discuss further steps required to express their fusions in pBBR1MCS-2 indicating that straightforward insertion of their respective fusions into the broad host range vector was enough for them to achieve their anticipated results. The sensitivity of the microscope must also be taken into consideration as the concentration of protein expressed from a T7 promoter will far exceed what would be expected from a low copy number broad host range vector. Resolving difficulties associated with visualising the fusion expressed from pBBR1MCS-2 was set aside to focus on screening for a deletion mutant and overexpression of recombinant MamK from T7 promoters.

4.3 DISCUSSION

4.3.1 *In vivo* localisation and functional characterisation of MamK

The generation time of wild type *Magnetospirillum gryphiswaldense* MSR-1 has been recorded at 8.9 hr (Schübbe *et al.*, 2003) under ideal liquid culture conditions. Crossovers should be allowed three weeks growth before screening and even then mutants are not guaranteed (Dr. Dirk Schüler, Max-Planck-Institute for Marine Biology, personal communication). Multiple attempts at transposon mutagenesis and screening for disrupted *mamK* crossovers yielded no gentamycin-resistant colonies. On reflection the concentration of antibiotics, although correct for selection of the suicide vector in *Escherichia coli*, may have been too high for selection in *Magnetospirillum gryphiswaldense* MSR-1 on solid medium.

During the screening process for this thesis results regarding *in vivo* characterisation of *mamK* in *Magnetospirillum magneticum* AMB-1 were released (Komeilli *et al.*, 2006). Their findings showed the phenotype of the MamK wild-type compared to the deletion and complementation strains (Figure 4.3). The deletion mutant contained magnetosomes without a linear arrangement. After complementation of the mutant with a functional MamK-GFP fusion they observed the realignment of the magnetosomes and the localisation of MamK-GFP in the cell. This validated our

experimental strategy but made completion of these experiments seem less important.

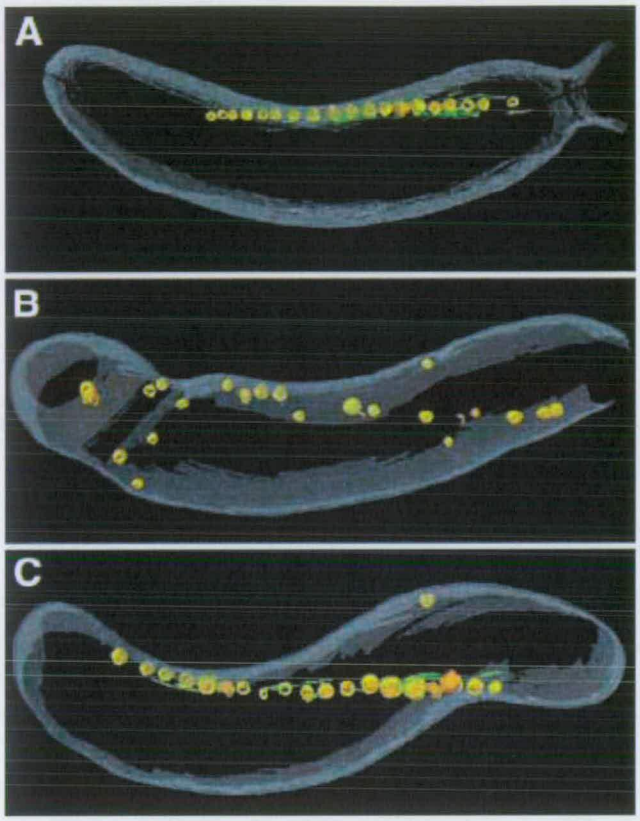

Figure 4.3 Schematic diagrams showing three dimensional reconstructions of *Magnetospirillum magneticum* AMB-1 harbouring wild-type *mamK* (A), a *mamK* deletion (B), and a *mamK-gfp* complementation on a broad host range plasmid (C). The cell membrane (grey), magnetosome membrane (yellow), magnetite (orange), and magnetosome-associated filaments (green) are rendered. (B) Δ*mamK* mutant, where magnetosomes appear disordered and no filaments are found in their vicinity. (C) Δ*mamK* cell expressing *mamK-gfp* on a plasmid showing full reversal of the mutant phenotype. (Taken directly from Komeilli *et al.*, 2006)

Using electron cryotomography to observe the magnetosome chain the magnetosomes appeared to be permanent invaginations of the inner membrane rather than a step in the development of a cytoplasmic vesicle and they are flanked by a network of cytoskeletal filaments, as indicated by the loss of filamentous structures in the *mamK* deletion mutant (Komeilli *et al.*, 2006) (Figure 4.4). This is contrary to the long-term acceptance that magnetosomes pinch off and are separate from the cell membrane (Bazylinski and Frankel, 2004). The fact that the magnetosomes are

invaginations of the cell membrane provides an alternative strategy of transport of iron into the cell compared to systems discussed in Chapter 1.

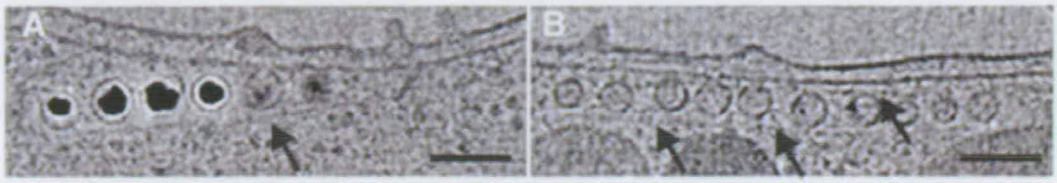

Figure 4.4 Micrographs of magnetosome chains flanked by long cytoskeletal filaments (➔). (A) The magnetosome chain containing magnetite crystals (B) Similar view of a magnetosome chain grown in the absence of iron, which prevents the formation of magnetite crystals. Arrows point to the long filaments. (Plate and legend taken directly from Komeili *et al.*, 2006)

These findings present a problem in evaluating the evolutionary relationship between magnetosomes and eukaryotic intracellular organelles (Komeilli *et al.*, 2006). It was discussed that as magnetosomes do not separate from the cell membrane, they might be analogous to photosynthetic membranes in bacteria; and they may also represent a step in the development of mechanisms for membrane bud formation before the evolution of membrane fission. The observations of the close proximity of MamK to the cell membrane raises attention to the differentiation of biochemical processes of MamK in order to facilitate its organisation independent of MreB, which also localises at the inner membrane.

The work presented by Komeilli *et al.* (2006) prompted work contributing to this thesis to focus more on *in vitro* characterisation of MamK. Efforts to achieve a *mamK* mutation in *Magnetospirillum gryphiswaldense* MSR-1 or resolve difficulties we encountered with expression of the recombinant MamK-EGFP fusion from the broad host range vector were abandoned. After this descision three further papers were released shedding light on *in vivo* localisation and functional characterisation of MamK (Scheffel *et al.*, 2006; Scheffel and Schüler, 2007; Pradel *et al.*, 2006).

Further characterisation of the function of MamK was incidentally reported after work on a *mamJ* deletion mutant (Scheffel *et al.*, 2006). A *Magnetospirillum gryphiswaldense* MSR-1 *mamJ* chromosomal deletion was made and found to lose the linear arrangement of magnetosomes (Figure 4.5). These results suggest that MamK has a close relationship with MamJ in maintaining the linear arrangement of

the magnetosomes and closer examination of the *mamJ* and *mamK* nucleotide sequences shows that their products are co-transcribed (Scheffel *et al.*, 2006).

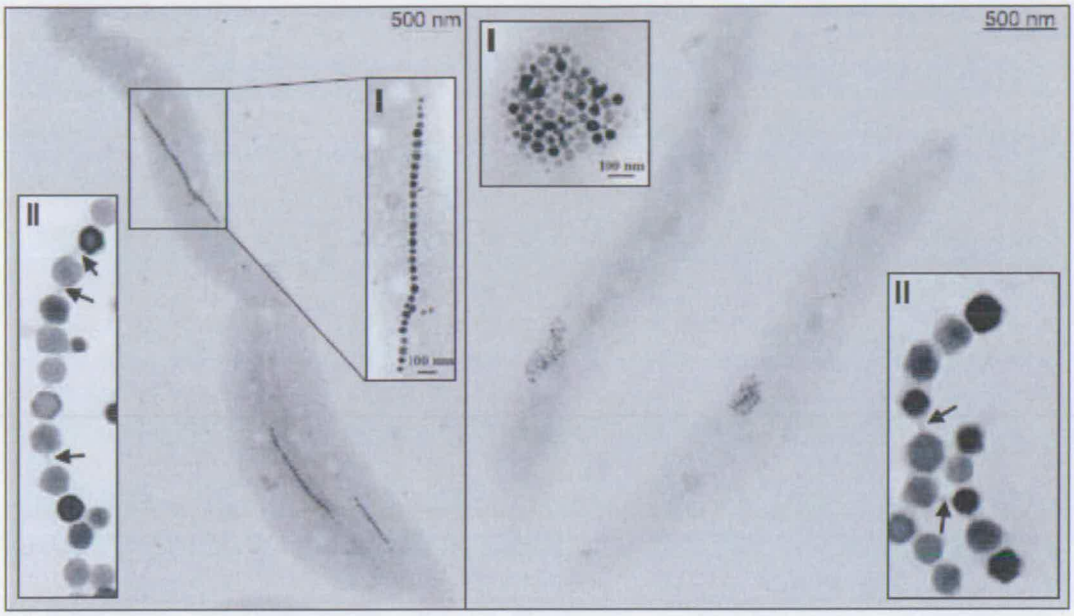

Figure 4.5 Images depicting micrographs of MamJ wild type (I) and deletion mutant (II) phenotypes. Insets show (I) magnification of magnetosome organisation and (II) magnetosome membranes forming junctions (arrows) between isolated crystals. (Plate and legend from Scheffel *et al.* (2006))

Examination of the sequence of MamJ reveals a protein of 466 amino acids with 4.75 sequence repeats and 2 predicted (www.ch.embnet.org / software / TMPRED_ form.html) transmembrane helices running from amino acids 356-375 and 399-418 (Figure 4.6).

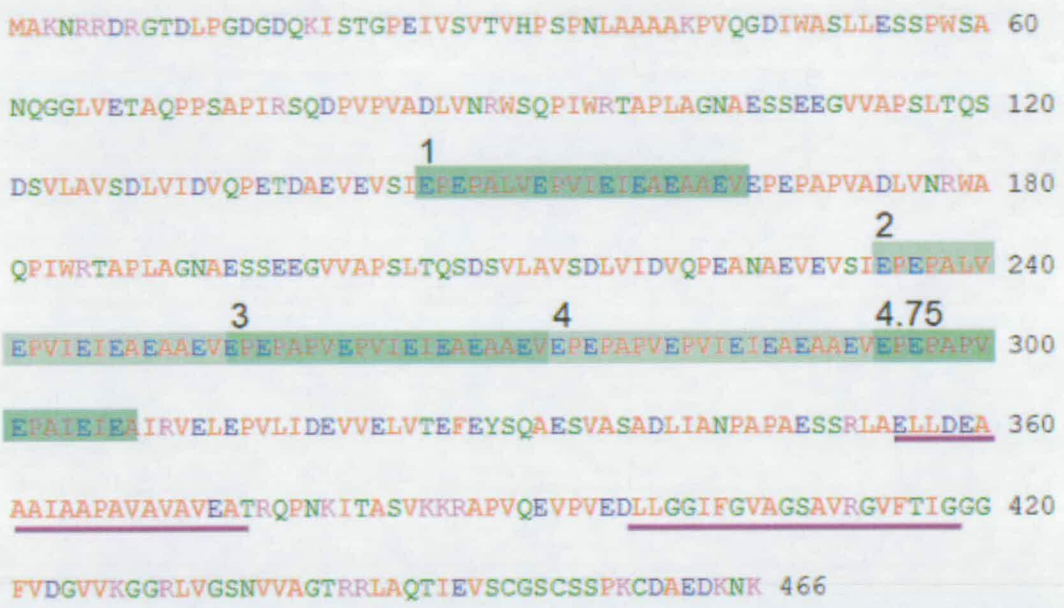

Figure 4.6 MamJ amino acid sequence highlighting 4.75 obvious sequence repeats (EPEPA.VEP.IEIEAEAAEV) and two transmembrane helices (underlined in purple).

In Figure 4.5 II (Scheffel *et al.*, 2006) attention is brought to magnetosome membrane junctions between magnetosome crystals. A model is proposed where MamJ acts as a tether between the MamK cytoskeleton and the magnetosome membrane whereby the sequence repeats wrap around the MamK structure and the transmembrane helices imbed themselves in the magnetosome membrane (Figure 4.7).

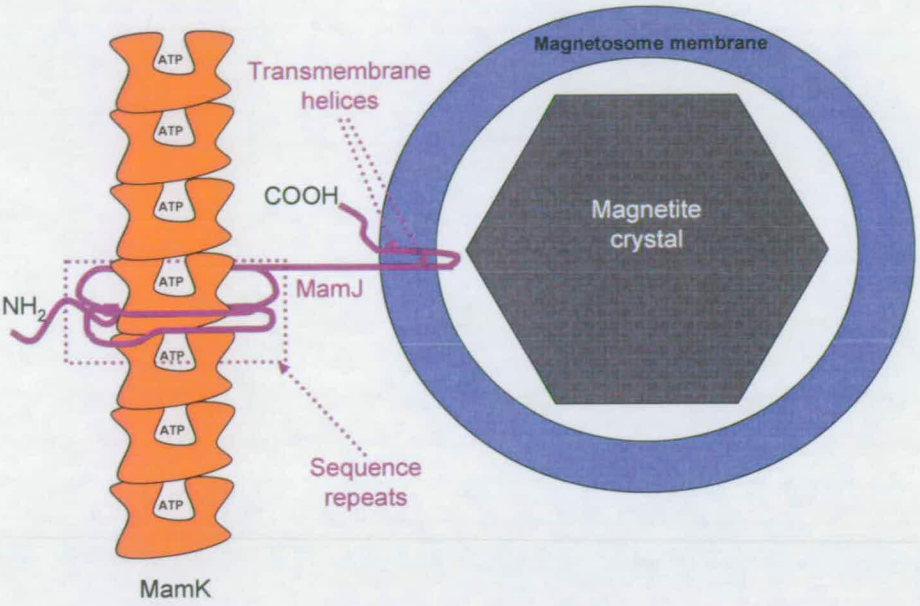

Figure 4.7 A model for the interaction of MamK, MamJ and the magnetosome membrane where the acidic repeat winds around MamK filaments thus anchoring the magnetosomes in a linear organisation.

Several functional MamJ variants from *Magnetospirillum gryphiswaldense* and other magnetotactic bacteria share an acidic and repetitive central domain, which displays an unusual intra- and interspecies sequence polymorphism thought to be caused by homologous recombination between identical copies of Glu- and Pro-rich repeats (Scheffel and Schüler, 2007). It was presented that surprisingly *mamJ* mutant alleles in which the central domain was deleted retained their potential to restore chain formation in a *mamJ* deletion mutant, suggesting that the acidic domain is not essential for MamJ to function. Results of two-hybrid experiments indicate that MamJ physically interacts with MamK, and two distinct sequence regions within MamJ were shown to be involved in binding to MamK. Mutant variants of MamJ lacking either of the binding domains were unable to functionally complement the *mamJ* deletion mutant. In addition, two-hybrid experiments suggest that both MamK-binding domains of MamJ confer oligomerisation of MamJ. Domains were revealed that were required for the functions of the MamJ protein in chain assembly and maintenance and provide the first experimental indications for a direct interaction between MamJ and the cytoskeletal actin-like protein MamK. This shows

that the model in Figure 4.7 is not entirely correct as the acidic repeat is not essential to MamK-MamJ interactions.

Magnetospirillum magneticum AMB-1 MamK was investigated using immunogold staining of ultrathin frozen sections and fluorescence microscopy (Pradel *et al.*, 2006). They found that MamK alone (i.e. independent of other actin-like proteins and magnetosome proteins) is sufficient to direct the assembly of straight mosaic filaments and that the properties and the biosynthesis of the MamK filaments is different to those of MreB and ParM and appears to be optimally adapted for the linear organisation of the magnetosome chain. Further to this, the gold particles were observed to align to areas without magnetosomes implying that MamK filament localisation is independent of the magnetosomes.

The kinetics of MamK assembly was examined in *Escherichia coli* using the tightly controlled expression of a MamK-GFP fusion under the control of an arabinose promoter (Pradel *et al.*, 2006). Time-lapse images were taken every 15 min to follow the assembly of the MamK filaments in *Escherichia coli*. A fluorescent focus was seen appearing 30 min after the induction of MamK-GFP expression. Additional foci appeared 45 min after induction in the same cell and in another septating cell. After 75 min short threads were observed that elongated proportionally with time to reach distinct filamentous appearance. The filaments were described as exhibiting different intensities in different areas. In some cases one short filament seemed to disassociate and reassociate to another filament, in a septating cell the old filament seemed to end at the septum with short smear fibres on the other side of the septum initiating the assembly of a new filament in the daughter cell without alignment with the old one (Pradel *et al.*, 2006). These results indicate that MamK polymerisation is highly dynamic and a kinetically asymmetrical system undergoing continuous rearrangement (Pradel *et al.*, 2006).

Studying MamK polymerisation in *Escherichia coli* has draw backs as the protein may be under cellular controls that are not relevant to the species origin of the protein. Proteolysis work conducted on G-actin using a number of enzymes found in

either Eukaryotes and/or bacteria revealed that there are sites, generally closer to the N-terminus, that are sensitive to proteolysis (Mornet and Ue, 1984; Carbonell and Villaverde, 2002). The work conducted by Pradel *et al.*, 2006 does not discount the potential involvement of protease activity during the low level expression of MamK in *Escherichia coli* that might have contributed to what appears to be dynamic expression. Work examining the kinetics of MamK expression in magnetic bacteria has not yet been fully raised but so far MamK appears as a stable undynamic structure within the cells of magnetic bacteria. Considering the function of MamK to provide a structure for magnetosomes to align against there does not seem to be a firm reason for MamK to be highly dynamic.

Assembly of actin is a multiple-step process including nucleation, elongation, and remodelling. In eukaryotic cells, both actin filaments and microtubules are structurally and kinetically polarised so that one end of the polymer elongates faster than the other (Alberts *et al.*, 1999). The asymmetry of actin assembly may explain the position of MamK-EGFP foci at one pole of *Escherichia coli* in this study (Figure 4.2), also observed by Pradel *et al.* (2006), although fluorescent filaments were not observed.

5 PURIFICATION OF MamK

5.1 BACKGROUND

MamK purification was undertaken as the first step towards *in vitro* characterisation of MamK. The protein was expressed using a T7 promoter in *Escherichia coli* BL21(DE3)p*LysS*. Under these conditions it had already been shown in Section 4.2.2 that inclusion bodies were repeatedly observed and confined to one pole of the cell. This chapter describes methods used to purify MamK and an attempt to crystallise it from highly concentrated protein.

5.2 RESULTS

5.2.1 Cloning and expression of recombinant *mamK*

The pT7-7::*mamK-egfp* clone has been introduced in Section 4.2. Parallel work was also carried out to clone pT7-7::*mamK*, pET28a::*mamK* and pET28a::*mamK-egfp*, pET28a introduces a His-tag.. Conveniently the *mamK* and *mamK-egfp* fragments were interchangeable between pT7-7 and pET28a so the cloning procedure was straightforward. The clones were confirmed to be correct by restriction patterns and nucleotide sequencing. Whole cell, supernatant and pelleted fractions were analysed by SDS-PAGE and showed the majority of MamK to be present in the pellet (Figure 5.1). Expression of *mamK* resulted in strong bands in keeping with the expected sise of the protein (39 kDa) and a pelleting assay of the whole cell crude extract showed that MamK sedimented into the pellet fraction as would be expected of inclusion bodies.

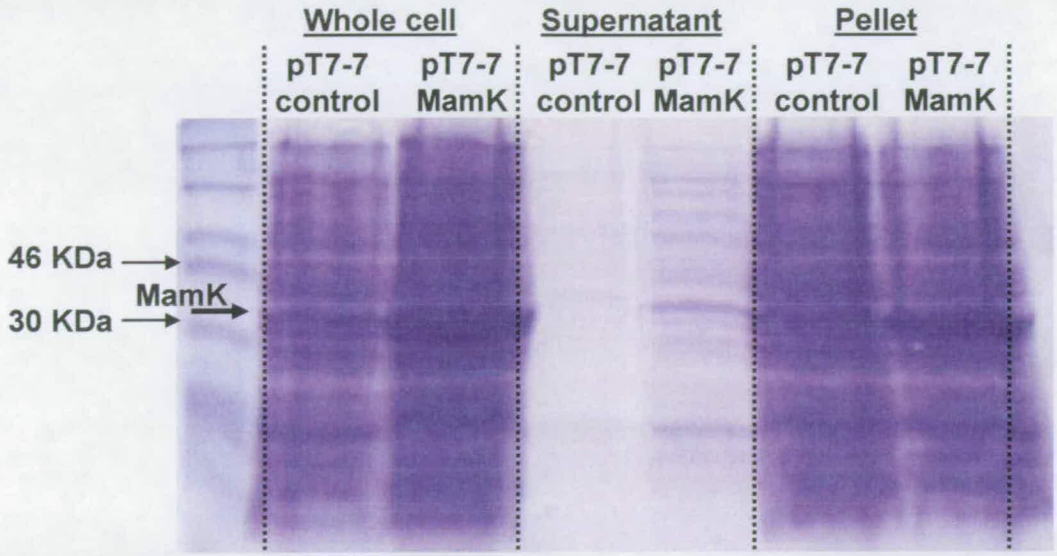

Figure 5.1 SDS-PAGE showing and expression of recombinant MamK from the T7 promoter of pT7-7 alongside a negative control. MamK can be seen most strongly in the pelleted fraction. The marker is New England Biolabs pre-stained protein marker.

Interestingly when MamK was expressed in pET28a after 3 hr induction chained cells were observed at 400 x magnification under phase contrast (Figure 5.2) although the reason for this is unclear. It may be due to the His residues of the expression vector, pET28a, causing some sort of conformational change in MamK that causes the protein to interfere with cell division in the host.

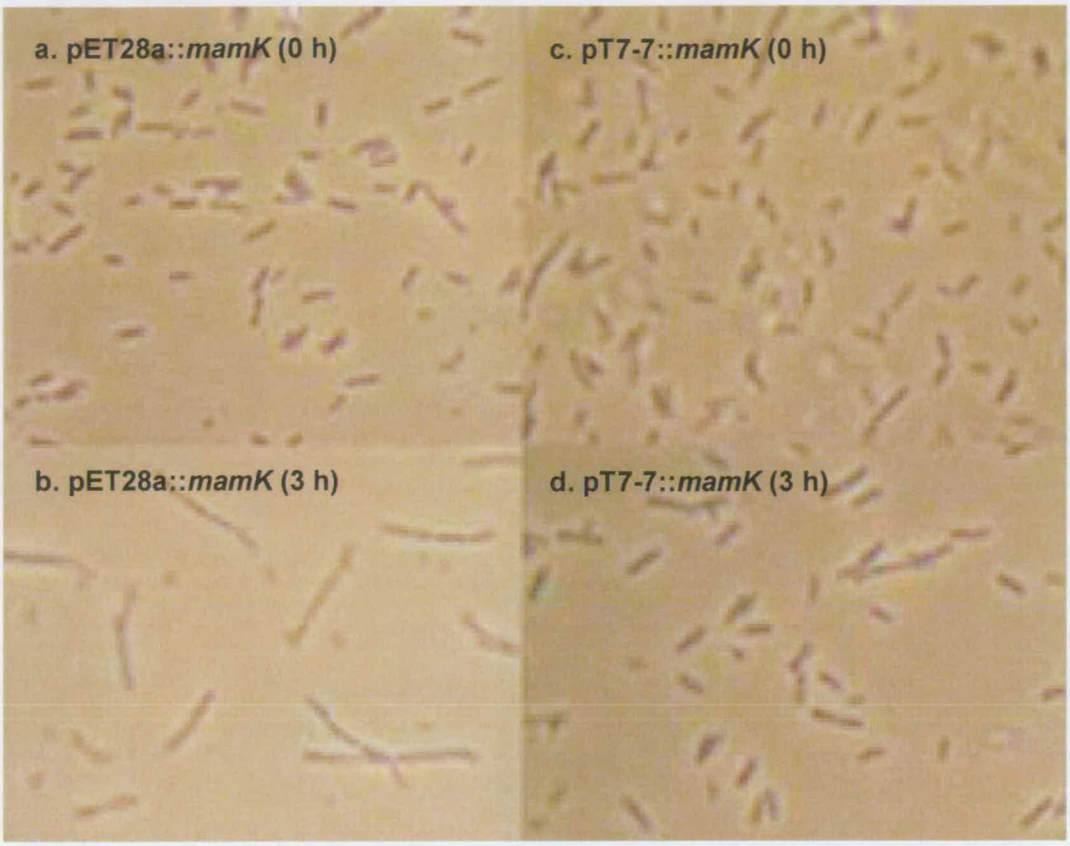

Figure 5.2 Phase contrast microscopy of cells expressing MamK from pET28a and pT7-7.

5.2.2 Purification of recombinant MamK

Two approaches were applied to purify MamK. One investigated the ability to denature and renature the insoluble protein using guanidine hydrochloride thus purifying it directly from whole cell extract. The other method made use of an inclusion body preparation that results in the isolation of inclusion bodies from crude cell extract before total denaturation and renaturation prior to column chromatography.

5.2.2.1 Denaturation and renaturation of MamK directly from crude cell extract using guanidine hydrochloride

Recombinant MamK was overexpressed in *Escherichia coli* for purification from crude cell extract by denaturation in 6 M guanidine hydrochloride followed by renaturation by slow dilution in 50 mM Tris-HCl pH 7.5. This method had worked well for haemerythrin purification by fellow laboratory members (Lucy Bellamy and Chris French, unpublished).

The first attempt using this method was on recombinant MamK overexpressed from pT7-7. After incubation of the insoluble fraction of the crude cell extract in 6 M guanidine hydrochloride the sample was centrifuged. It was anticipated that lipids and membrane proteins would sediment whilst leaving MamK in solution. On dilution of the 6 M guanidine hydrochloride with 50 mM Tris pH 7.5 the protein was anticipated to renature in an active and soluble state. Whilst slowly (20 µl every 10 min) diluting the 6 M guanidine hydrochloride with the Tris buffer a precipitate started to form in the tube (just visible at c. 2.6 M guanidine hydrochloride). Under microscopic analysis the precipitate appeared to contain large fibers suggesting the ability of MamK to self assemble (Figure 5.3).

Figure 5.3 Phase contrast microscopy at 1000 x magnification showing putative MamK polymers under 1000 x phase contrast after a denaturation/renaturation experiment.

The same experiment was repeated on MamK-EGFP to ascertain whether or not the fibers from the recombinant MamK sample were MamK. The result supported the previous observation (Figure 5.3 and Figure 5.4). As the fibres extended beyond the field of view they were followed and seemed to stretch out over the expanse of the slide. The fluorescence images in Figure 5.4 show the scale of polymerisation in comparison to the cells that had expressed the protein as inclusion bodies.

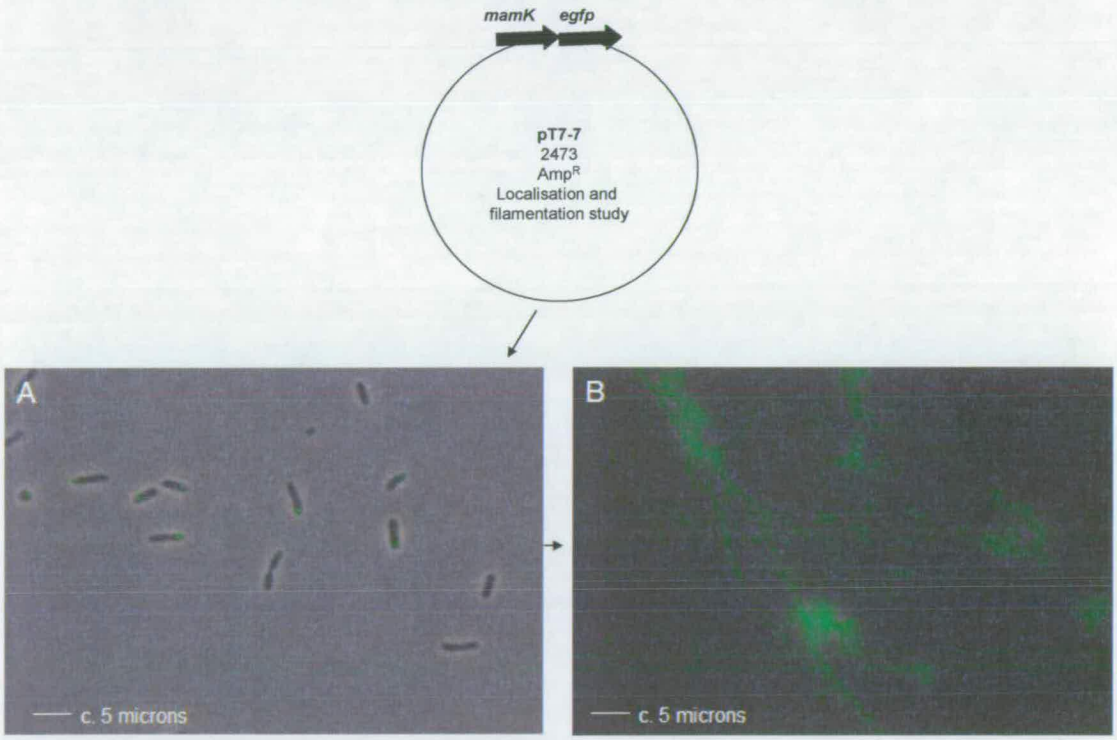

Figure 5.4 Merged phase contrast/fluorescence microscopy at 1000 x magnification showing *Escherichia coli* BL21(DE3)p*LysS* harbouring MamK-EGFP inclusion bodies (A) and filaments under 1000 x fluorescence microscopy after a denaturation/renaturation experiment (B).

5.2.2.2 The inclusion body preparation and column chromatography method

As the denaturation/renaturation method resulted in protein that was not soluble this method was exchanged for purification by inclusion body preparation and column chromatography. Preparation of inclusion bodies and column chromatography are well established methods for the purification of proteins overexpressed in *Escherichia coli* (Singh and Panda, 2005). The cells were harvested, sonicated and the pellet fraction was washed several times. After the inclusion body preparation wash steps the inclusion bodies were denatured in 8 M urea followed by renaturation by overnight dialysis into refolding buffer. The inclusion body preparation resulted in relatively pure recombinant MamK solubilised in 8 M urea (Figure 5.5). Recombinant MamK was refolded by dialysis into the same buffer (10 mM Tris pH 8.0, 2 mM DTT, 2 mM $CaCl_2$, 0.2 mM ATP/GTP) intended to equilibrate the column. Putative MamK breakdown products were consistently observed during SDS-PAGE.

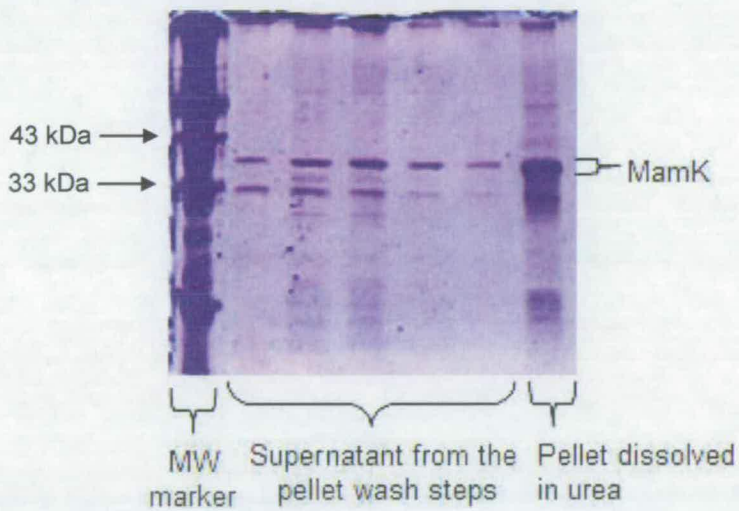

Figure 5.5 Samples of supernatant from each inclusion body preparation wash step (1 x step 1, 4 x step 2) and a sample of MamK once the pellet is dissolved in 8 M urea after SDS-PAGE. The molecular marker was prepared in the lab.

So far in actin and bacterial actin-like protein purification the presence of ATP or GTP assists in the correct folding of the protein and contributes to polymer formation. It was observed that MamK precipitated during dialysis when the protein was at concentrations approaching 750 μg/ml. It was also observed that the

appearance of the precipitate differed depending on the presence or absence of ATP or GTP which can be seen in Figure 5.6. The precipitate observed without NTP contained small homogenous aggregates, difficult to measure by eye, giving the solution a milky appearance; the precipitate in the presence of GTP contained aggregates of approximately 1 mm diameter; whilst the precipitate in the presence of ATP contained the largest aggregates, averaging approximately 5 mm in diameter.

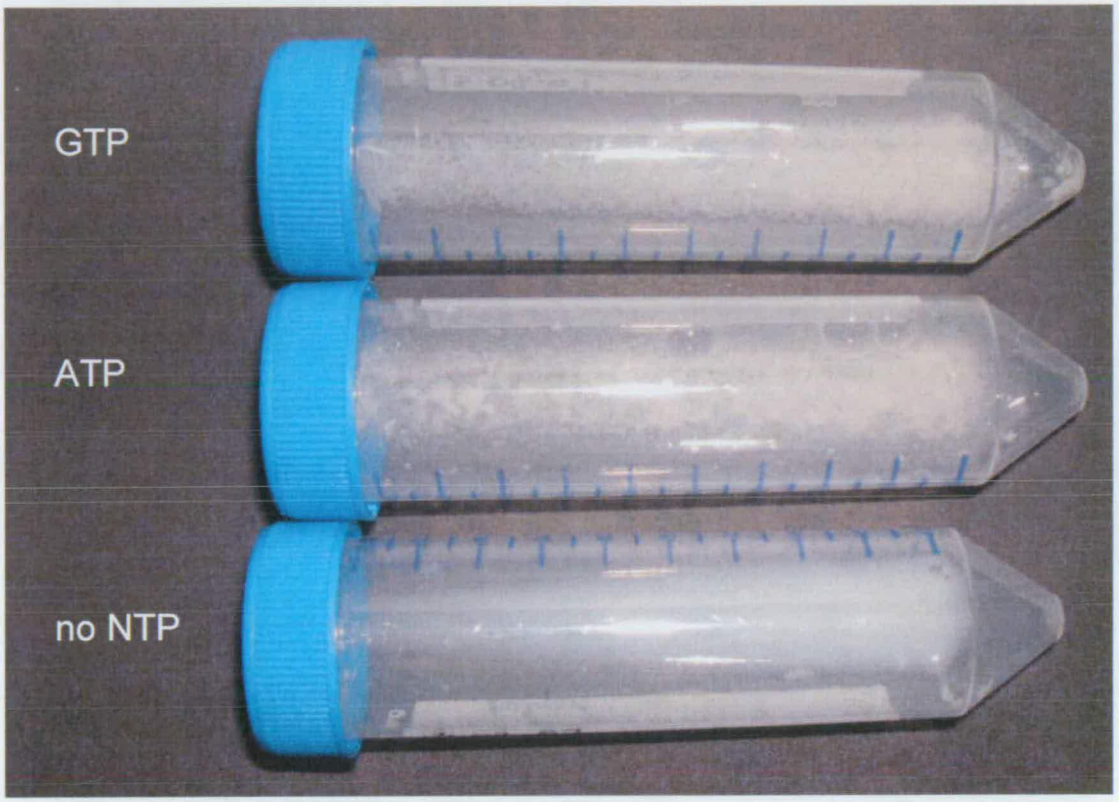

Figure 5.6 MamK after dialysis into 10 mM Tris pH 8.0, 2 mM $CaCl_2$, 2 mM DTT containing either 0.2 mM ATP, 0.2 mM GTP or no NTP.

Differences in the samples with and without $MgCl_2$ were observed under phase contrast microscopy at 400 x magnification (Figure 5.7). When MamK was dialysed without NTP the precipitate appears to aggregate more once $MgCl_2$ is added whereas the fields of view are similar for MamK dialysed with ATP or GTP before and after the addition of $MgCl_2$. Filaments are noticeable in the samples dialysed with ATP that are not dissimilar to those observed during the guanidine hydrochloride denaturation/renaturation of MamK from crude cell extract (Figures 5.3 and 5.4). It is clear that MamK has different biochemical behaviour to actin as the purification

process used so far is routinely used for actin where the protein is maintained in a soluble form in up to 6 mg/ml when dialysed in the presence of $CaCl_2$ and ATP (Shetterline and Sparrow, 1994).

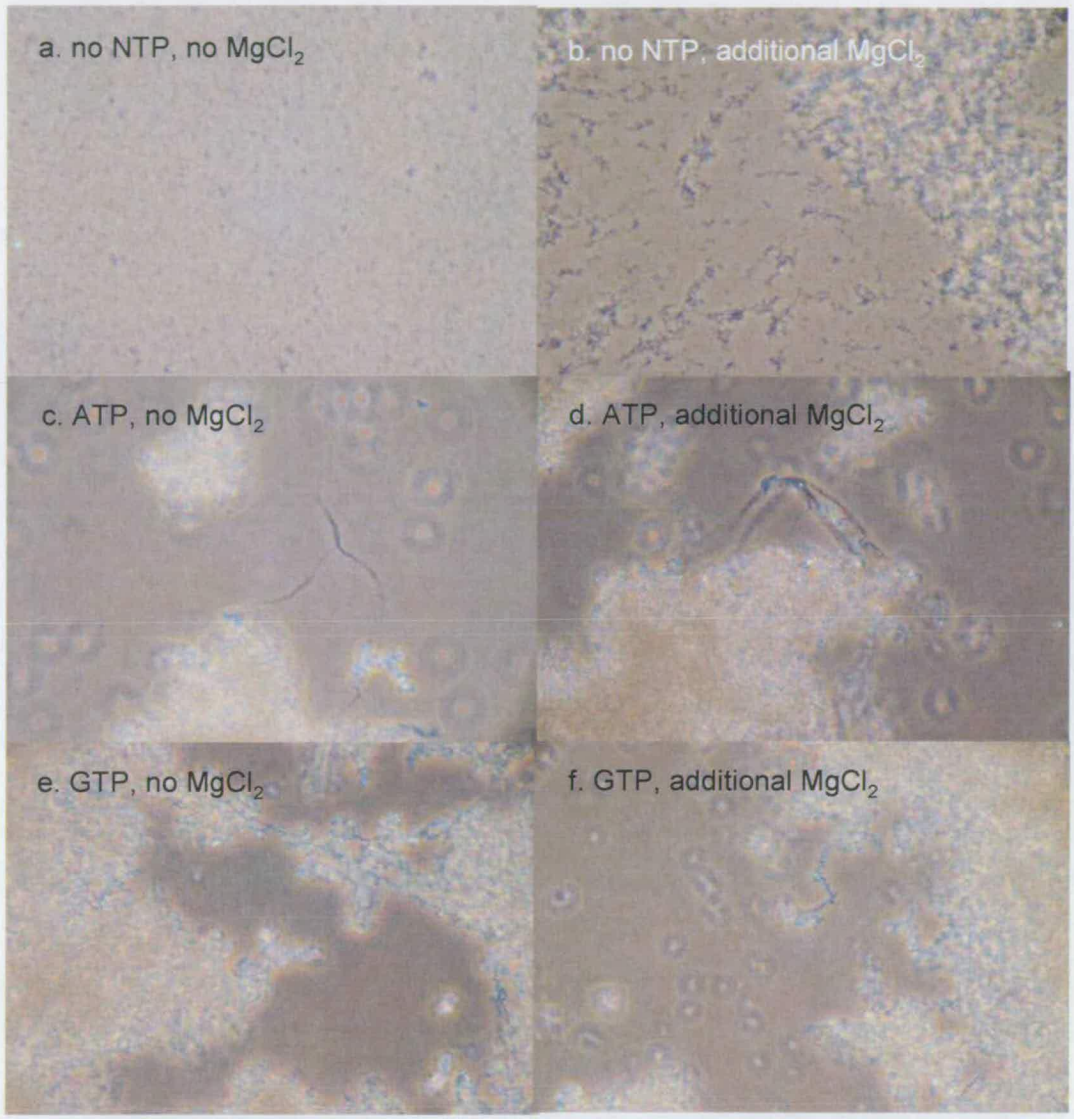

Figure 5.7 MamK after dialysis into 10 mM Tris pH 8.0, 2 mM $CaCl_2$, 2 mM DTT containing either 0.2 mM ATP, 0.2 mM GTP or no NTP before and after the addition of 2 mM $MgCl_2$ under phase contrast at 400 x magnification. These pictures are representative of a number of experiments.

After dialysis the soluble fraction of protein was loaded to a preswollen DEAE-cellulose (DE-53, Whatman) column for anion exchange column chromatography (Figure 5.8). The column was equilibrated in the same buffer used for the dialysis of each sample. A salt gradient was applied to the column to elute the protein and

absorbance of 280 nm of the eluted fractions was read on a spectrophotometer to locate the protein.

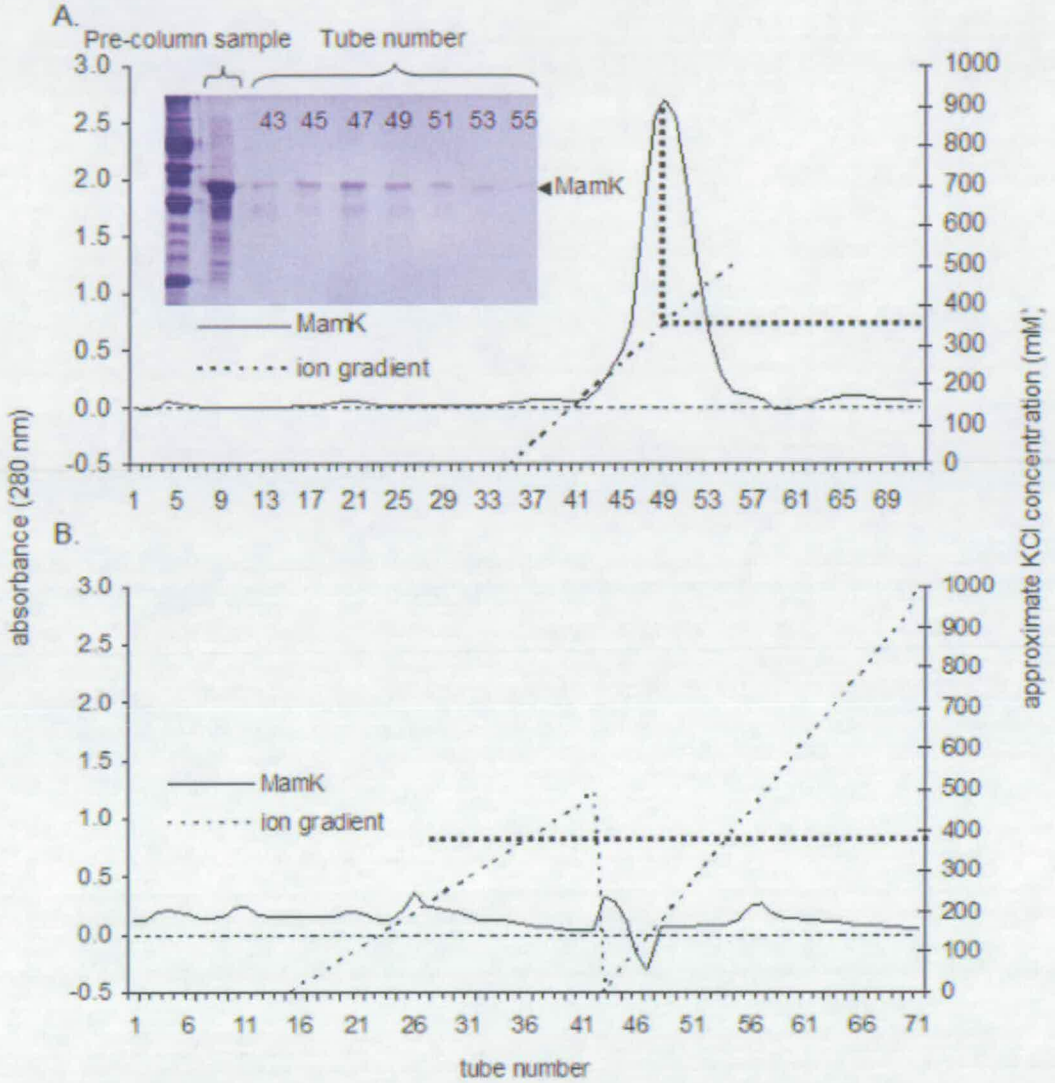

Figure 5.8 A_{280} data of fractions collected from a DE53 ion exchange column during purification of MamK with and without ATP. A. The inset illustration of the SDS-PAGE shows the pre-column sample from the inclusion body preparation and samples corresponding to various fractions of the peak. MamK was eluted between approximately 150 and 450 mM KCl. These results are indistinguishable from MamK purification in the presence of GTP. B. shows results for MamK dialysis and purification without the presence of NTPs. There is no distinguishable peak that yields MamK bands through SDS-PAGE (not shown here). Two salt gradients were applied the first of which had a 500 mM maximum and the second a 1 M maximum of KCl.

It was observed that when ATP or GTP was present a clear peak was identified in the spectrophotometric data that contained protein that when analysed by SDS-PAGE was consistent with the expected sise of monomeric MamK (39 kDa) and a total

protein concentration of over 500 µg/ml (Figure 5.8 a). When NTP was omitted the fate of MamK was undetermined (Figure 5.8 b). Fractions from the small peaks were analysed by SDS-PAGE and they did not reveal bands consistent with what would be expected of MamK. If MamK had not bound to the column it is likely that a peak would have eluted in the void volume so it is possible that MamK bound irreversibly to the column. If large filaments/aggregates formed MamK might have failed to pass through the column for physical reasons.

After ion exchange chromatography the fractions revealing the strongest bands corresponding to MamK after SDS-PAGE were pooled, concentrated and loaded to a sise exclusion column for further purification (Figure 5.9).

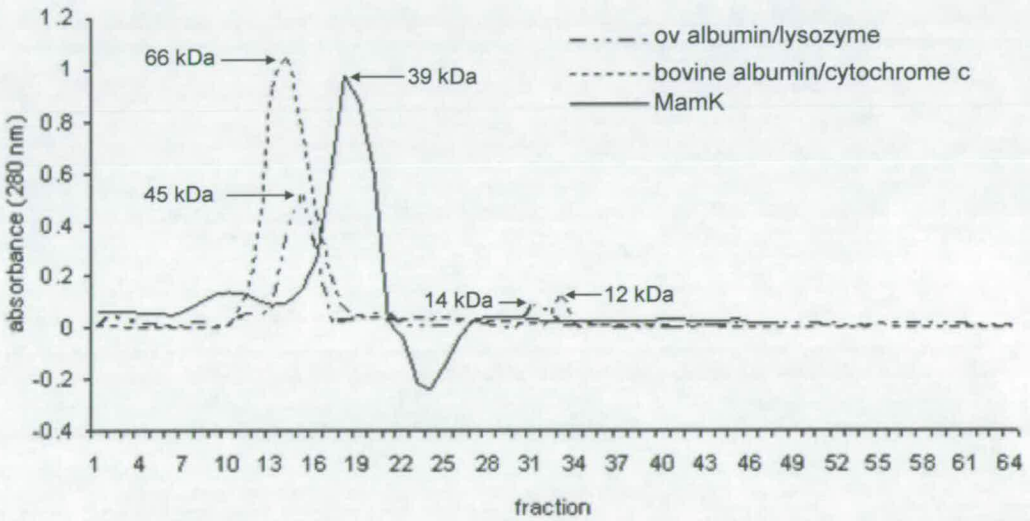

Figure 5.9 A_{280} data of fractions collected from a sise exclusion column during purification of MamK with ATP.

As expected, eluted fractions contained protein detected by taking absorbance readings. The peak corresponded to the expected sise for monomeric MamK (39 kDa) compared to readings taken for bovine albumin (66 kDa), ovalbumin (45 kDa), lysozyme (14 kDa) and cytochrome c (12 kDa) (Figure 5.9).

5.2.3 Crystallisation of recombinant MamK

Recombinant MamK was purified and concentrated to 8 mg/ml with the addition of 150 mM NaCl to the buffer. Physiological salt concentrations maintain some proteins in a soluble monomeric form by preventing precipitation due to non-specific ionic interactions. Crystallisation screens were carried out using the hanging drop vapour diffusion method in Linbro trays and incubated at 4 °C (Table 5.1). Droplets were examined for crystals and observations were recorded after 3, 5 and 28 weeks using a stereomicroscope. Crystals were not obtained although sphaerulite forms were observed. Attaining soluble MamK at a concentration high enough to continue investigations was unsuccessful for reasons that are unclear.

Table 5.1 The conditions per well of MamK crystallisation plates and observations after 3, 5 and 28 weeks incubation at 4 °C (S – Sphaerulite, F – Filament, C – Clear) Unless indicated otherwise by abbreviation samples appeared amorphous.

Sample	Sample solution			observations week 3	5	28
1	0.2 M Calcium chloride dihidrate	0.1 M Na acetate trihydrate pH 4.6	30 % v/v 2-methyl-2,4 pentanediol			
2	0.2 M Ammonium acetate	0.1 M Na acetate trihydrate pH 4.6	30 % w/v PEG 4000			
3	0.2 M Ammonium sulphate	0.1 M Na acetate trihydrate pH 4.6	30 % w/v PEG 4000			
4		0.1 M Na acetate trihydrate pH 4.6	2.0 M Sodium formate			F
5		0.1 M Na acetate trihydrate pH 4.6	2.0 M Ammonium sulphate			
6		0.1 M Na acetate trihydrate pH 4.6	8 % w/v PEG 4000			
7	0.2 M Ammonium acetate	0.1 M tri-Sodium citrate dihydrate pH 5.6	30 % w/v PEG 4000			
8	0.2 M Ammonium acetate	0.1 M tri-Sodium citrate dihydrate pH 5.6	30 % v/v 2-methyl-2,4 pentanediol			
9		0.1 M tri-Sodium citrate dihydrate pH 5.6	20 % v/v 2-propanol, 20 % w/v PEG 4000			
10		0.1 M Na citrate pH 5.6	1.0 M ammonium dihydrogen phosphate			
11	0.2 M Calcium chloride dihidrate	0.1 M Na acetate trihydrate pH 4.6	20 % v/v 2-propanol			
12		0.1 M Na cacodylate pH 6.5	1.4 M Na acetate trihydrate			
13	0.2 M tri-Sodium citrate dihydrate	0.1 M Na cacodylate pH 6.5	30 % v/v 2-propanol			
14	0.2 M Ammonium sulphate	0.1 M Na cacodylate pH 6.5	30 % w/v PEG 8000	S		S
15	0.2 M Magnesium acetate tetrahydrate	0.1 M Na cacodylate pH 6.5	20 % w/v PEG 8000			
16		0.1 M Na cacodylate pH 6.5	30 % v/v 2-methyl-2,4 pentanediol			
17	0.2 M Sodium acetate trihydrate	0.1 M Imidazole pH 6.5	1.0 M Na acetate trihydrate			
18	0.2 M Zinc acetate dihydrate	0.1 M Na cacodylate pH 6.5	30 % w/v PEG 8000			
19	0.2 M Calcium acetate hydrate	0.1 M Na cacodylate pH 6.5	18 % w/v PEG 8000			
20	0.2 M Magnesium chloride hexahydrate	0.1 M Na cacodylate pH 6.5	18 % w/v PEG 8000			
21	0.2 M Calcium chloride dihydrate	0.1 M Hepes pH 7.5	30 % v/v 2-methyl-2,4 pentanediol			
22	0.2 M Magnesium chloride hexahydrate	0.1 M Hepes pH 7.5	30 % v/v 2-propanol			
23	0.2 M Calcium chloride dihidrate	0.1 M Hepes pH 7.5	28 % w/v PEG 400			
24	0.2 M Magnesium chloride hexahydrate	0.1 M Hepes pH 7.5	30 % w/v PEG 400			
25		0.1 M Hepes pH 7.5	20 % v/v 2-propanol			
26		0.1 M Hepes pH 7.5	0.8 M K, Na tartrate tetrahydrate			
27		0.1 M Hepes pH 7.5	1.5 M Lithium sulphate monohydrate			
28		0.1 M Hepes pH 7.5	0.8 M Sodium dihydrogen phosphate, 0.8 M K dihydrogen phosphate			
29			1.4 M tri-Sodium citrate dihydrate			
30		0.1 M Hepes pH 7.5	2 % w/v PEG 400, 2.0 M ammonium sulphate			S
31		0.1 M Hepes pH 7.5	10 % v/v 2-propanol, 20 % w/v PEG 4000			
32		0.1 M Hepes pH 7.5	2.0 M Ammonium sulphate			
33	0.2 M Magnesium chloride hexahydrate	1.0 M Tris pH 8.5	30 % w/v PEG 4000			
34	0.2 M tri-Sodium citrate dihydrate	1.0 M Tris pH 8.5	30 % w/v PEG 400			
35	0.2 M Lithium sulphate monohydrate	1.0 M Tris pH 8.5	30 % w/v PEG 4000			
36	0.2 M Ammonium acetate	1.0 M Tris pH 8.5	30 % v/v 2-propanol			
37	0.2 M Sodium acetate trihydrate	1.0 M Tris pH 8.5	30 % w/v PEG 4000			
38		1.0 M Tris pH 8.5	8 % w/v PEG 8000	F	F	
39		1.0 M Tris pH 8.5	1.0 M ammonium dihydrogen phosphate			
40			0.4 M K, Na tartrate tetrahydrate			F
41			1.4 M ammonium dihydrogen phosphate			
42	0.2 M Ammonium sulphate		30 % w/v PEG 8000			
43	0.2 M Ammonium sulphate		30 % w/v PEG 4000		S	
44			2.0 M Ammonium sulphate	S	S	
45			4.0 M Sodium formate		S	F
46			20 % w/v PEG 8000	C		
47			30 % w/v PEG 1500	C		
48			0.2 M Magnesium formate			
49	0.2 M Lithium sulphate monohydrate		2 % w/v PEG 8000			
50	0.2 M Lithium sulphate monohydrate		15 % w/v PEG 8000			

5.2.4 Western blotting with anti-MamK polyclonal antibodies

Anti-MamK polyclonal antibodies were raised and tested by western blotting for binding to recombinant MamK expressed in *Escherichia coli* cells (Figure 5.10). Western blotting showed that anti-MamK bound to recombinant MamK, His-tagged MamK and the MamK-EGFP fusion protein although the signal is less for the MamK-EGFP fusion protein. The anti-MamK polyclonal antibodies also appear to bind to MamK breakdown products.

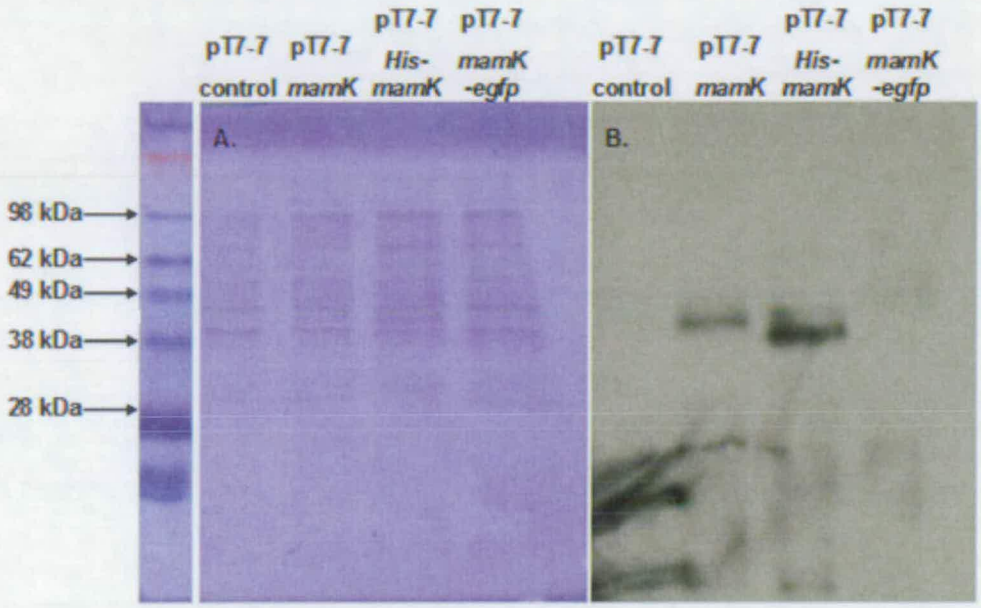

Figure 5.10 SDS-PAGE (A) and subsequent western blot (B) of MamK forms expressed in *Escherichia coli* BL21 (DE3) p*LysS* cells. The protein standard is relavant only to the SDS-PAGE gel. The molecular standard is SeeBlue Plus2 Pre-stained standard (Invitrogen).

A magnetically enriched culture of *Magnetospririllum gryphiswaldense* MSR-1 was grown and the cells were pelleted to maximise the concentration of native MamK. Recombinant MamK was purified from *Escherichia coli* and western blotting was performed to compare the sise of recombinant MamK to *Magnetospirillum gryphiswaldense* MSR-1 native MamK (Figure 5.11). Each attempt revealed a signal for recombinant MamK but no signal of the expected sise for native MamK. A signal at the top of the native MamK lane was observed on many occasions although this could be caused by non-specific binding of the luminescent probe. Either the

anti-MamK polyclonal antibodies are not specific to native MamK or the native MamK has not migrated through the gel.

Figure 5.11 Western blot of recombinant MamK compared to native MamK.

5.3 DISCUSSION

5.3.1 Insoluble protein and the purification of MamK

A method allowing purification of MamK from inclusion bodies by denaturation and renaturation in guanidine hydrochloride caused precipitation of protein to occur. The precipitate was observed under phase contrast at 400 x magnification and filaments extending out of view from one side of the field to the other were observed. The same method of purification was conducted on MamK-EGFP and observations were made under phase contrast and fluorescence microscopy at 400 x magnification with similar results. For the purpose of biochemical characterisation it was important to purify MamK in a soluble and active form. Fluorescent filaments were observed extending out of view from one side of the field to the other.

Inclusion body preparations were conducted on recombinant MamK as part of a method regularly used for the purification of overexpressed protein from *Escherichia coli*. The inclusion body preparation was then dialysed into an appropriate buffer for column chromatography. This method proved to work well for MamK which was not unexpected considering the similarities it has with actin. It was found that when ATP or GTP was present MamK migrated through the column during ion exchange chromatography and in the absence of NTP the fate of MamK was undetermined. This suggested that ATP or GTP was required to keep MamK in a soluble and monomeric form as has been observed for actin (Shetterline and Sparrow, 1994). MamK eluted during gel filtration chromatography in fractions containing protein that would be expected size considering the molecular weight of MamK compared to albumin, cytochrome c and lysozyme standards. Breakdown products were regularly observed during inclusion body preparations and column chromatography and it was decided that inclusion body preparations were sufficient to purify MamK for light scattering assays. This decision limited loss of MamK during column chromatography and the time required to prepare MamK samples for assays.

5.3.2 Crystallisation of MamK

MreB crystals were reported to grow in 10 % PEG 8000, 200 mM NaCl and 0.1 M CAPS, pH 10.5 using the sitting drop vapour diffusion technique (van den Ent *et al.*, 2001). MamK does not behave as MreB under the same crystallisation conditions

(Prof. Linda Amos, University of Cambridge, personal communication). MamK crystals were not observed in trays although sodium formate, PEG 8000 and PEG 4000 were common denominators in samples containing sphaerulite or filamentous forms (Table 5.1, Section 3.4.1.4) so optimising conditions with these reagents may be worthwhile. Further work is required to optimise the conditions required to concentrate MamK highly enough to set up more crystallisation conditions.

5.3.3 Western blotting with anti-MamK polyclonal antibodies

Western blotting was undertaken using anti-MamK polyclonal antibodies raised in a sheep in order to compare the kDa of recombinant MamK to native MamK from *Magnetospirillum gryphiswaldense* MSR-1. The antibodies showed specificity for recombinant MamK forms and did not bind to native MamK. On closer examination of western blots there appeared to be a signal at the top of the *Magnetosprillum gryphiswaldense* MSR-1 lane suggesting that native MamK had not migrated through the gel or that there had been non-specific binding fo the luminescent probe.

Interestingly, magnetosomes were isolated from *Magnetospirillum gryphiswaldense* and prepared for SDS-PAGE using either 2% Triton X-100, 2% Tween 20, 500 mM octylglucoside, 5% SDS, 5 M urea, or 2 M NaCl, shaken at room temperature for 2 h and centrifuged for 30 min at 13,000 *x g* (Grünberg *et al.*, 2004). Under these conditions the membrane structure enveloping the crystals was not entirely removed (Figure 5.12). Even after boiling with 1 % SDS, which led to instant agglomeration of particles, traces of organic material remained attached to the crystals and a residual tendency to form chains was observed, although the particles were tightly spaced due to the magnetosome membrane solubilisation. In another study immunoelectron microscopy images of purified magnetosomes using anti-recombinant MamK antibody show that the 5-nm gold particles are distributed along the surfaces of the magnetite particles in the magnetosome chains (Taoka *et al.* 2007) which is consistent with the observation by Grünberg *et al.* (2004) (Figure 5.12). The magnetosome pellets were analysed by SDS-PAGE after extensive washing and bands were excised for N-terminal sequencing (Figure 5.13) the results of which do

not include MamK suggesting that MamK had not soubilised to migrate through the gel.

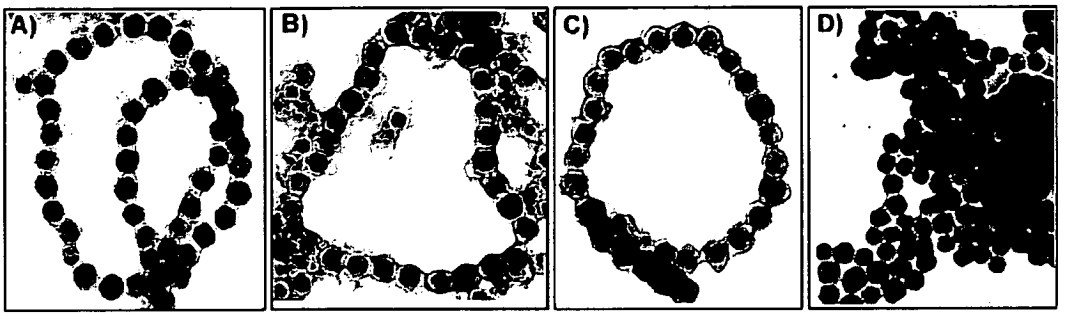

Figure 5.12 Electron micrographs of isolated magnetosome particles. (A) Untreated magnetosomes; (B) magnetosomes after treatment with Triton X-100; (C) magnetosomes after tryptic digestion; (D) magnetosomes after boiling with 1% SDS. (Plate and legend taken directly from Grünberg et al., 2004.)

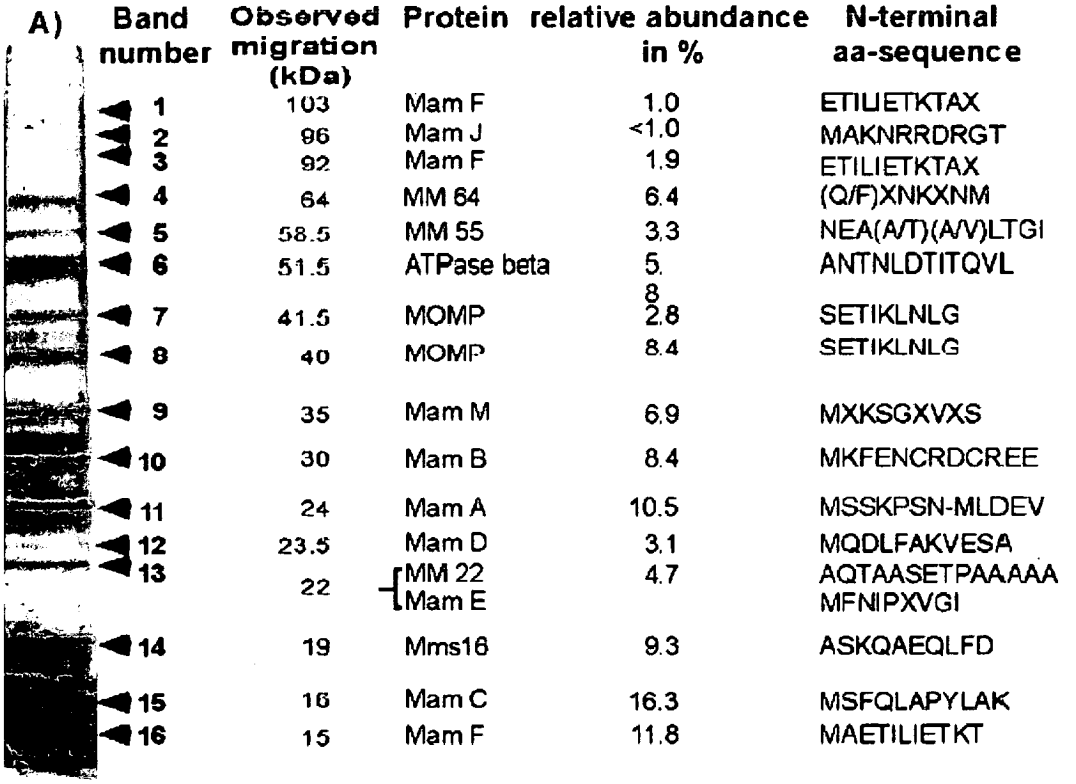

A) Band number	Observed migration (kDa)	Protein	relative abundance in %	N-terminal aa-sequence
1	103	Mam F	1.0	ETILIETKTAX
2	96	Mam J	<1.0	MAKNRRDRGT
3	92	Mam F	1.9	ETILIETKTAX
4	64	MM 64	6.4	(Q/F)XNKXNM
5	58.5	MM 55	3.3	NEA(A/T)(A/V)LTGI
6	51.5	ATPase beta	5.8	ANTNLDTITQVL
7	41.5	MOMP	2.8	SETIKLNLG
8	40	MOMP	8.4	SETIKLNLG
9	35	Mam M	6.9	MXKSGXVXS
10	30	Mam B	8.4	MKFENCRDCREE
11	24	Mam A	10.5	MSSKPSN-MLDEV
12	23.5	Mam D	3.1	MQDLFAKVESA
13	22	MM 22 / Mam E	4.7	AQTAASETPAAAAA / MFNIPXVGI
14	19	Mms16	9.3	ASKQAEQLFD
15	16	Mam C	16.3	MSFQLAPYLAK
16	15	Mam F	11.8	MAETILIETKT

Figure 5.13 Summary of MMPs detected by Coomassie blue staining in 1D SDS–16% PAGE gels. (Plate and legend taken directly from Grünberg et al., 2004.)

6 STUDY OF MamK POLYMERISATION *IN VITRO*

6.1 BACKGROUND

During purification actin is routinely dialysed into 10 mM Tris pH 8.0, 2 mM DTT, 0.2 mM $CaCl_2$ and 2 mM ATP prior to column chromatography and this was practiced in early MamK purification experiments. During early biochemical assays, which are described in this chapter, it was realised that $CaCl_2$ caused polymerisation of MamK which differs from the behaviour of actin as Ca.ATP will keep actin in a soluble monomeric form up to concentrations of 6 mg/ml (Shetterline and Sparrow, 1994). Once this was realised MamK was purified using buffer without $CaCl_2$. Microscopic observations showed that NTP was not required to fold MamK and that $MgCl_2$ or $CaCl_2$ appeared to be the limiting factors in MamK polymerisation.

Well established techniques to biochemically characterise actin were applied to progress further in understanding MamK. The process of *in vitro* polymerisation of MamK was investigated by microscopy and time course light scattering under conditions of altered ATP, GTP, Mg^{2+}, and Ca^{2+} concentrations. The findings of these experiments are described in this chapter.

6.2 RESULTS

6.2.1 Visualisation of structures formed by MamK

6.2.1.1 Macroscopic MamK structures

When crude cell extracts containing MamK were left at room temperature for several days macroscopic filaments several cm in length and approximately 1 mm in diameter were observed to form in a spiral pattern along the walls of 50 ml Falcon tubes above the air-liquid interface (Figure 6.1). These were extremely resistant to detachment, but after washing the polymers with dH_2O and boiling the filaments in SDS-PAGE sample buffer, followed by SDS-PAGE and mass spec analysis, it was found that these structures were composed of a protein of Mr c. 4 kDa lower than that of MamK. Analysis of this material by mass spectrometry yielded peptides from the MamK amino acid sequence (MOWSE score 9.72, 2 % covering, tolerance 50 ppm).

Figure 6.1 *In vitro* polymerisation of recombinant MamK in a Falcon tube from *Escherichia coli* crude cell extract. (A) shows polymerisation of MamK in a Falcon tube after incubation of c. 200 µ l of crude extract of cells that had expressed native MamK. (B) Shows SDS-PAGE of the filaments performed three months after the filaments formed. The outlined band, which corresponds to the expected sise for MamK, was sent for mass spectrophotometry for identification purposes.

6.2.1.2 Phase contrast and fluorescence microscopy of recombinant MamK

It was observed that MamK has different biochemical behaviour to actin during dialysis and column chromatography experiments. The presence of Ca.ATP maintains actin in a soluble monomeric form, which is not true for MamK. Further dialyses of MamK after inclusion body preparations were performed using buffer omitting $CaCl_2$ (10 mM Tris pH 8.0, 2 mM DTT) and regardless of the addition or omission of ATP or GTP MamK was not observed to polymerise under phase contrast microscopy until the addition of 2 mM $MgCl_2$ or the addition of 2 mM $CaCl_2$ suggesting that the cations are the limiting factor for MamK polymerisation. In contrast to earlier purification attempts using guanidine hydrochloride where MamK appeared to polymerise into filaments (Section 5.2.2.1, Figures 5.3 and 5.4),

the MamK purified by inclusion body preparation polymerises into sheets on addition of $MgCl_2$ or $CaCl_2$.

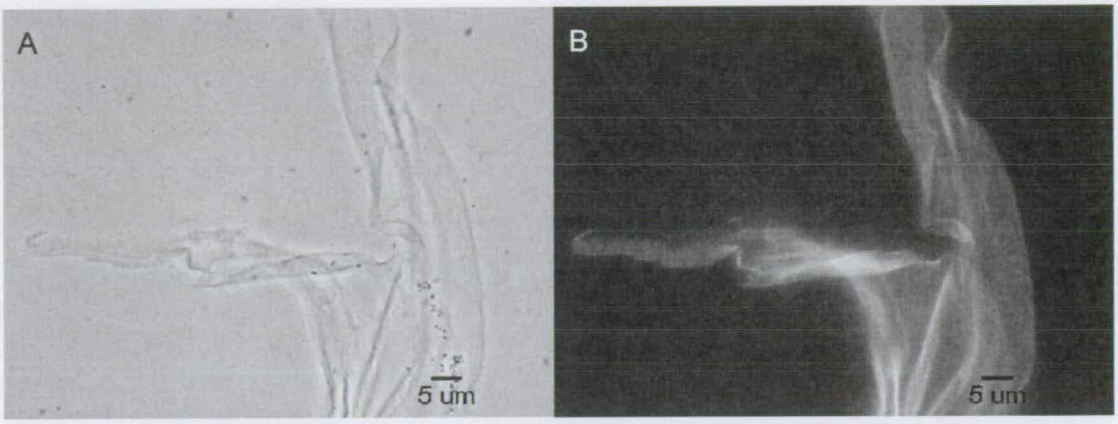

Figure 6.2 MamK-EGFP images under phase contrast (A) and fluorescence microscopy (B) taken at 400 x magnification after dialysis with the addition of 0.2 mM $MgCl_2$. These images are representative of repeat experiments.

At concentrations between 3 μM and 19 μM purified recombinant MamK and MamK-EGFP form what appear to be sheets regardless of the presence ATP or GTP or absence of NTPs. To confirm that the sheets were composed of MamK, the MamK-EGFP fusion was examined under fluorescence microscopy (Figure 6.2). Visible sheets were chosen randomly and all were over 200 μm in depth as measured using a confocal fluorescence microscope. Sheet fragments had a range of sises from 2 μm to those extending out of the field of view making measurements difficult. This was particularly true of samples that did not contain NTP. It was repeatedly qualitatively noted that the presence of sheets in NTP-free samples appeared at a higher frequency compared to sheets in MamK samples containing ATP or GTP.

6.2.1.3 TEM of negatively stained recombinant MamK sheets

Recombinant MamK was purified by inclusion body preparation and dialysed into 10 mM Tris pH 8.0 and 2 mM DTT. The volume of the dialysed protein solution was divided in two to provide positive and negative controls for overnight incubation at 4 °C with $MgCl_2$. Overnight incubation allowed plenty of time for the polymerisation process to stabilise. Observation of the presence of sheets was verified by phase contrast microscopy and showed that only the sample containing

$MgCl_2$ contained them. On inversion of the tube the solution containing $MgCl_2$ was more viscous compared to the negative control which is a property that has been used to quantify actin polymerisation in the past (Cooper *et al.,* 1983; Pinder *et al.*, 1994).

Centrifugation was performed to sediment sheets of MamK. The supernatant was removed to another tube and the pellet was washed and resuspended in an equivalent volume of dH_2O. Ten-fold dilutions were performed on the pellet and the supernatant. Samples from each dilution were applied to grids, stained with 2 % uranyl acetate and examined at up to 65000 x magnification.

The supernatant that was diluted 100 x yielded the greatest success (Figure 6.3). The micrograph depicted in Figure 6.3 was taken at 65000 x magnification (Mr. Steve Mitchell, University of Edinburgh) and reveals parallel lines in keeping with what might be expected if MamK formed sheets. It would seem that although the image is heavily stained with a lot of protein present the repetitive structure to the right of the micrograph label is very promising (Figure 6.3 a) whilst Figure 6.3 d, although containing larger parallel repeat structures, appears to be more consistent with an artefact caused by a poorly aligned microscope (Dr. Carolyn Moores, University College London, personal communication). Figure 6.3 b and c also appear to represent repetitive structures of a similar sise to Figure 6.3 a.

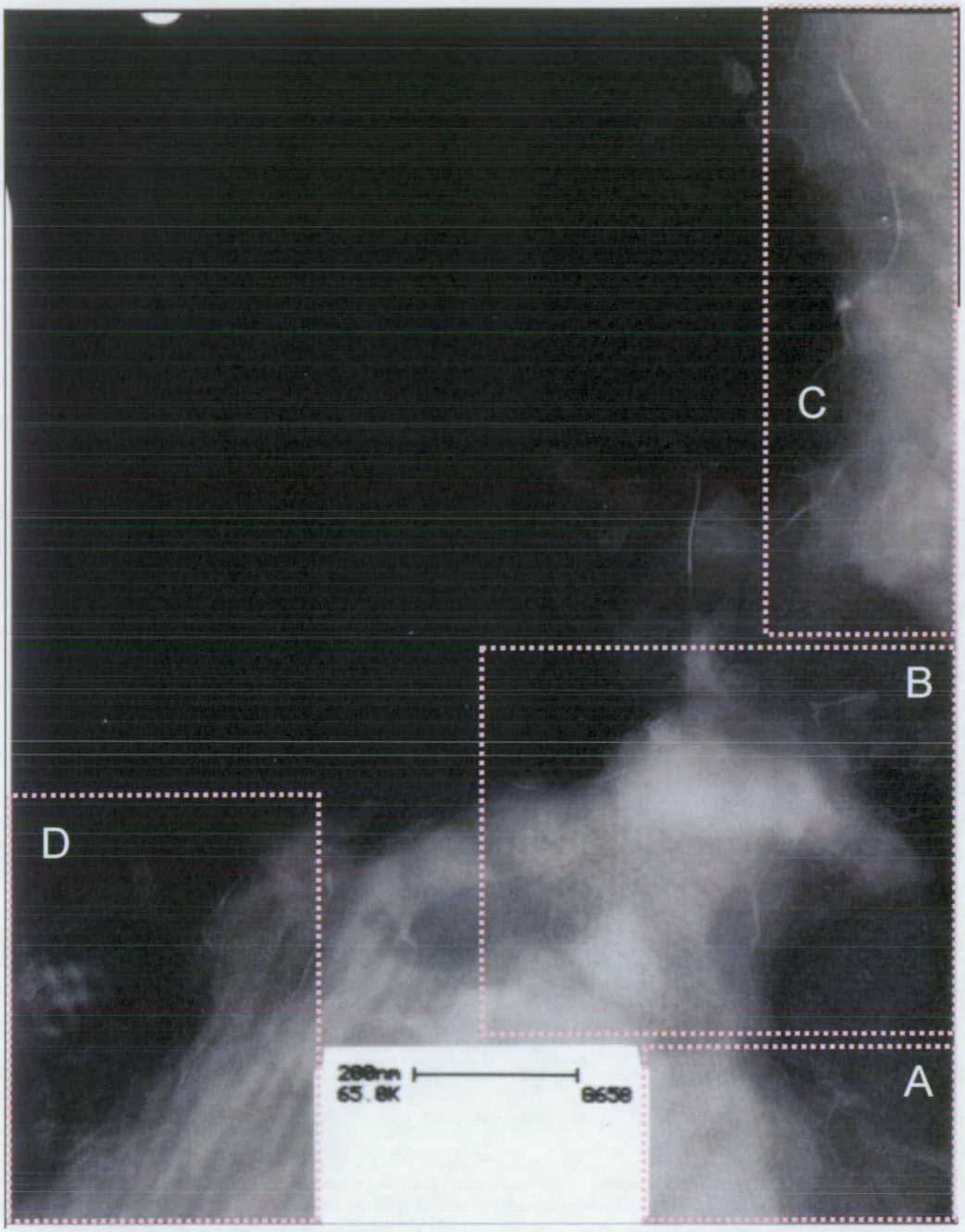

Figure 6.3 Micrograph of negatively stained sheets of recombinant MamK taken at 65000 x magnification (bar = 200 nm) (Mr. Steve Mitchell, University of Edinburgh)

Figure 6.4 depicts the most promising area from the micrograph (Figure 6.3 a). After tracing over the parallel lines in Figure 6.4 the pattern of the structure becomes clearer. It is as though three sheets are resting one on top of the other with each

rotated out of alignment with the other by approximately 60°. Roughly calculated the length of the repeat is approximately 7 nm.

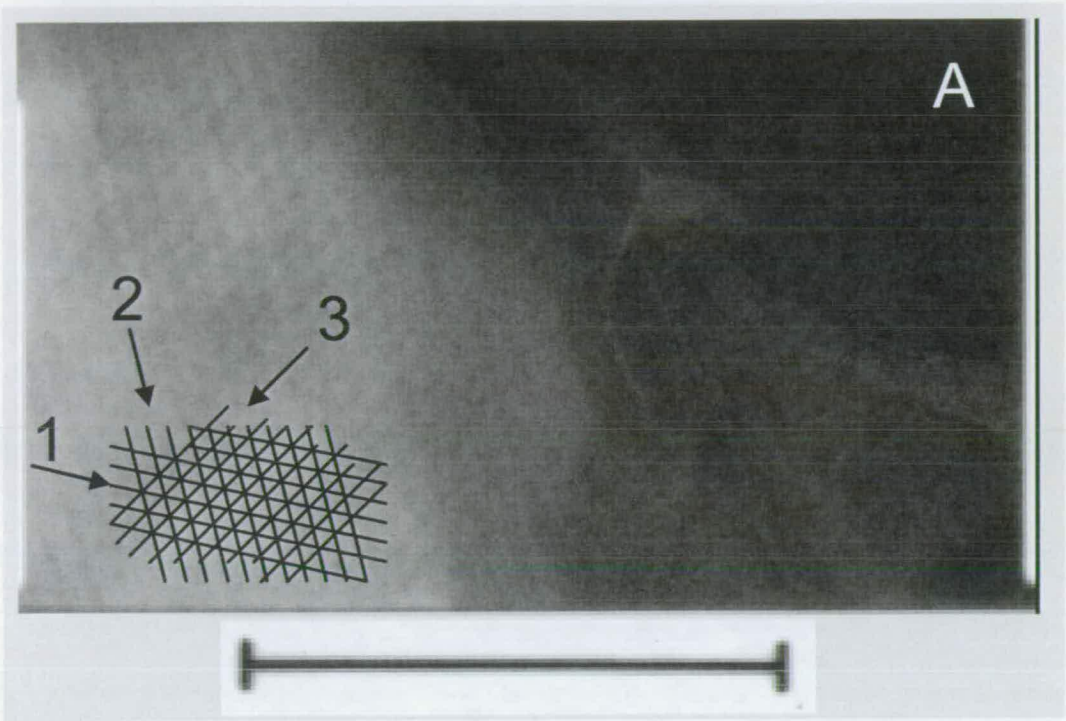

Figure 6.4 Enlargement of section (A) from the micrograph depicted in Figure 6.3 (bar = 200 nm). The lines represent parallel lines picked out of the pattern and due to their direction suggest that there are three visible sheets resting on each other.

Figure 6.5 shows images taken of a MamK sheet with assistance from Dr. David Bhella and Dr. Worawit Suphamungmee at the University of Glasgow. The images in Figure 6.5 were prepared the same way as the image in Figure 6.3. The initial picture was taken at 100000 x magnification (A) after which other areas of the same sheet were examined at higher magnifications (B, 200000 x; C, 200000 x; D, 400000 x). The dappling effect is an artefact produced by the and is not representative of the MamK sample (Fiugre 6.5). It is possible to make out parallel lines that indicate substructures especially in areas adjacent to where the folds are most obvious. Unfortunately these substructures are obscured by the dappled artefacts on the grid.

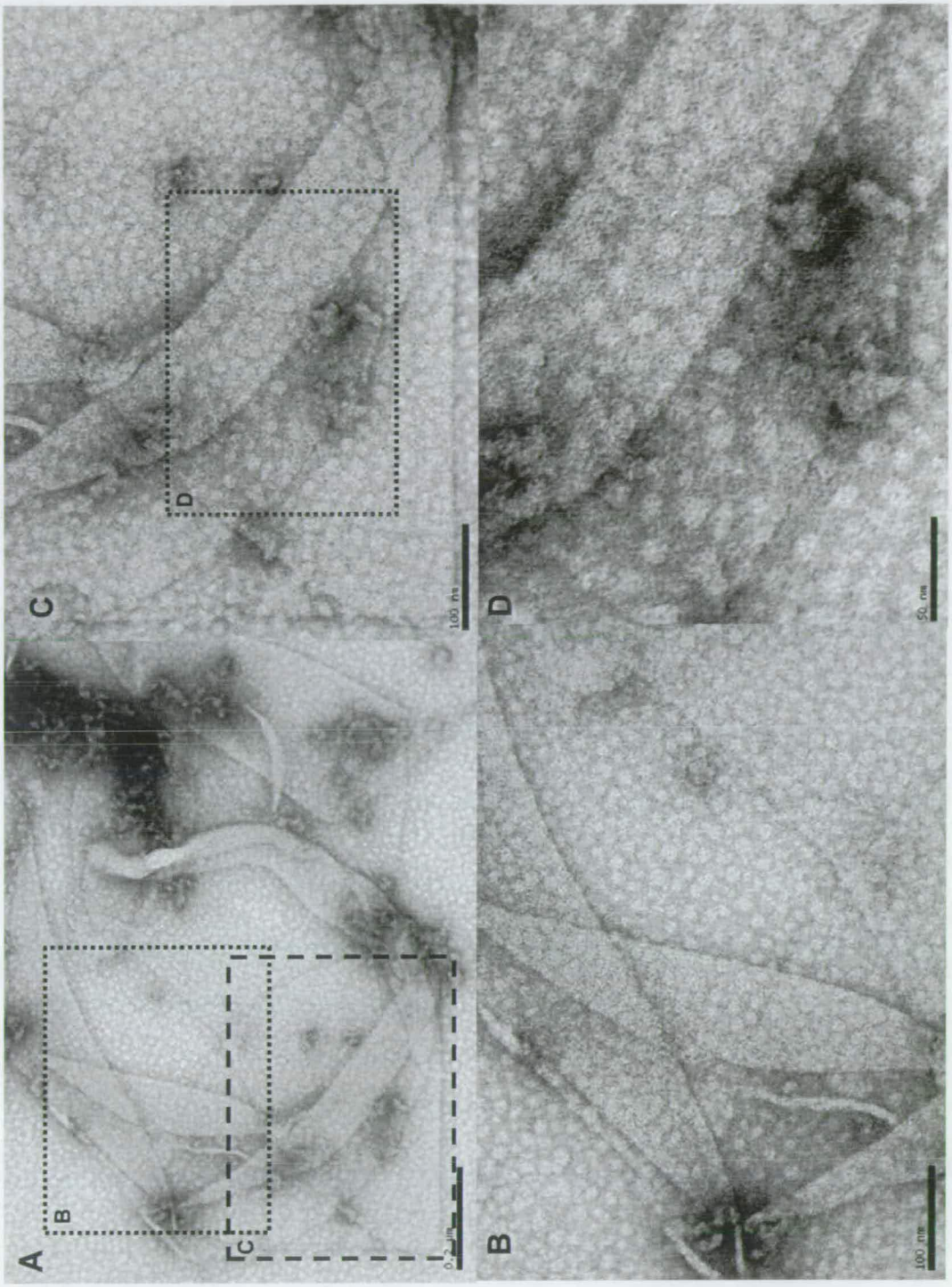

Figure 6.5 Folds in a MamK sheet (A, 100000 x magnification) viewed at various magnifications (B, 200000 x; C, 200000 x; D, 400000 x). The boxes highlight the areas that were viewed at the higher magnification.

Further images of MamK were taken at 200000 x magnification at the University of Glasgow (Figure 6.6) where the circular artefacts are not present as in Figure 6.5. It is also possible to make out parallel lines with the potential of being polymeric substructures although there is less certainty compared to Figures 6.3, 6.4 and 6.5.

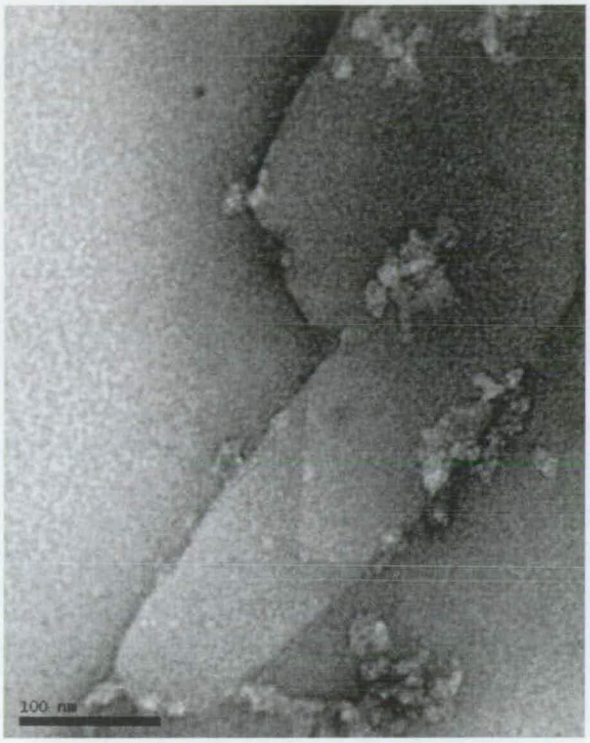

Figure 6.6 A MamK sheet fragment (200000 x magnification).

6.2.1.4 Atomic force microscopy (AFM) of MamK

Atomic force microscopy using tapping mode was conducted on MamK sheets but due to the lack of obvious repetitive structures or pattern our findings were very difficult to interpret (Figure 6.7). A cantilever was used with resolution at 20 nm and although this resolution is not optimal when looking for structures that are 5 nm wide. Experience showed that had the edge of the sample or an isolated filament been found it may have yielded a clear result. Unlike light microscopy or TEM only small areas (5 micrometers squared) can be observed at a time which makes locating areas of most interest a labour intensive task.

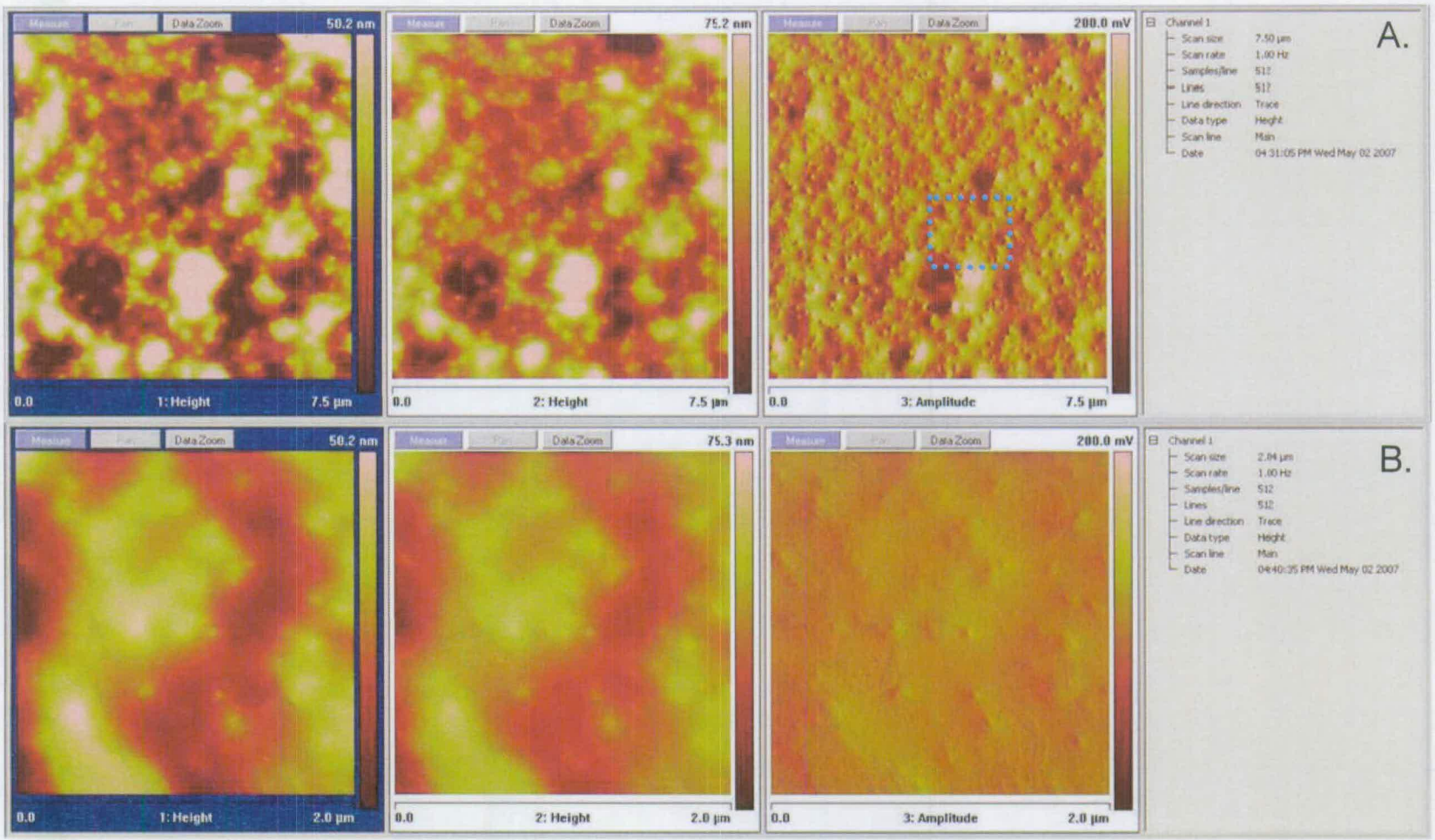

Figure 6.7 Data screens from atomic force microscopy of MamK sheets. (A) shows the field of view over 7.5 µm². (B) shows an enlargement of the highlighted area in (A) covering a 2.0 µm² area.

6.2.2 Light scattering and tryptophan fluorescence

Light scattering is a well established method used to investigate the polymerisation properties of actin. For actin these properties have been characterised under various conditions using criteria such as (1) time course of polymerisation; (2) elongation rate constants; (3) intrinsic viscosity; and (4) critical concentration (Cooper *et al.*, 1983; Pinder *et al.*, 1994). The work described in this section focussed on time course experiments and touched a little on the critical concentration of MamK in that the critical concentration of MamK appears to be higher than that of F-actin (Dr. Sutherland Maciver, University of Edinburgh, personal communication).

Intrinsic tryptophan fluorescence of proteins offers an alternative to the use of extrinsic probes for monitoring local structural changes around labelled residues (Burstein *et al.*, 1973; Doyle *et al.*, 2001; Eftink and Ghiron, 1976, Eftink and Ghiron, 1977). In actin, the intrinsic fluorescence of tryptophan has been used to monitor changes associated with divalent cation exchange and actin polymerisation (Selden *et al.*, 1994). These conformational changes result in changes in tryptophan fluorescence that can be used to map changes to specific sites on actin.

For example, actin contains four tryptophan residues, W79, W86, W340, and W356, all located in subdomain 1 of the protein. Replacement of each of these residues with either tyrosine (W79Y and W356Y) or phenylalanine (W86F and W340F) generated viable proteins in the yeast *Saccharomyces cerevisiae*, which, when purified, allowed the analysis of the contribution of these residues to the overall tryptophan fluorescence of actin (Doyle *et al.*, 2001). The sum of the relative contributions of these tryptophans was found to account for the intrinsic fluorescence of wild-type actin, indicating that energy transfer between the tryptophans is not the main determinant of their quantum yield, and that these mutations induce little conformational change to the protein. This was borne out by virtually identical polymerisation rates and similar myosin interactions of each of the mutants and the wild-type actin. In addition, these mutants allowed the dissection of the microenvironment of each tryptophan as actin undergoes conformational changes

upon metal cation exchange and polymerisation. Based on the relative tryptophan contributions determined from single residue alteration, a triple residue alteration of yeast actin was generated that showed small intrinsic fluorescence changes and was thought to prove useful for studies of actin interactions with actin-binding proteins.

In this work the recombinant MamK has one tryptophan residue located 10 residues in from the C-terminus. Changes in tryptophan fluorescence after the addition of $MgCl_2$ may help to distinguish between polymerisation and aggregation of the protein.

6.2.2.1 Polymerisation of recombinant MamK

Early light scattering polymerisation assays were carried out on MamK at concentrations ranging between 3 μM and 6.5 μM. MamK was dialysed from a buffer containing 8 M urea to a buffer containing 10 mM Tris pH 8.0, 2 mM DTT, 0.2 mM $CaCl_2$, and no NTP, 0.2 mM ATP or GTP (Figure 5.6 and 5.7). Preliminary results showed that the addition of 2 mM $MgCl_2$ caused an immediate increase in light scattering regardless of the presence or absence of ATP or GTP. This is in contrast to actin which has an absolute requirement for ATP to polymerise. There was a reproducible positive correlation between the increase in concentration of $MgCl_2$, from 5 mM to 10 mM to 15 mM, and the increase in light scattering (Figure 6.8 b). It was observed that the addition of $CaCl_2$ also caused a similar increase in light scattering so further experiments were conducted on protein purified in buffer lacking $CaCl_2$.

Leaving $CaCl_2$ out of the dialysis buffer did not alter previous observations of the positive correlation between the increases in light scattering with an increase in $MgCl_2$ concentration. Additionally, light scattering increased on the addition of $MgCl_2$ to MamK that was not dialysed in the presence of NTP (Figure 6.8 b) suggesting that MamK, unlike reports of actin and other actin-like proteins, does not require NTP for refolding or polymerisation events and in this form it spontaneously folds and polymerises in the presence of divalent cations as suggested by column chromatography and microscopy results.

Tryptophan fluorescence scans were conducted at 290 – 800 nm with excitation at 270 nm (Figure 6.8 a). The difference in fluorescence before and after the addition of $MgCl_2$ was insignificant as curves were produced that are virtually indistinguishable from each other (Figure 6.8 a) regardless of variation in protein concentration per batch and $MgCl_2$ concentration compared to the more dramatic results from visible light scattering (Figure 6.8 b). There are no significant differences in tryptophan fluorescence before or after the addition of divalent ions, but there is a time dependent increase in 90° light scattering indicating a polymerisation or precipitation event. These results suggest that the MamK tryptophan residue is not positioned in such a way to reveal the behaviour of the protein under various treatments. The high peak at 550 nm in Figure 6.8 is an artefact created by the fluorometer used to carry out the assay.

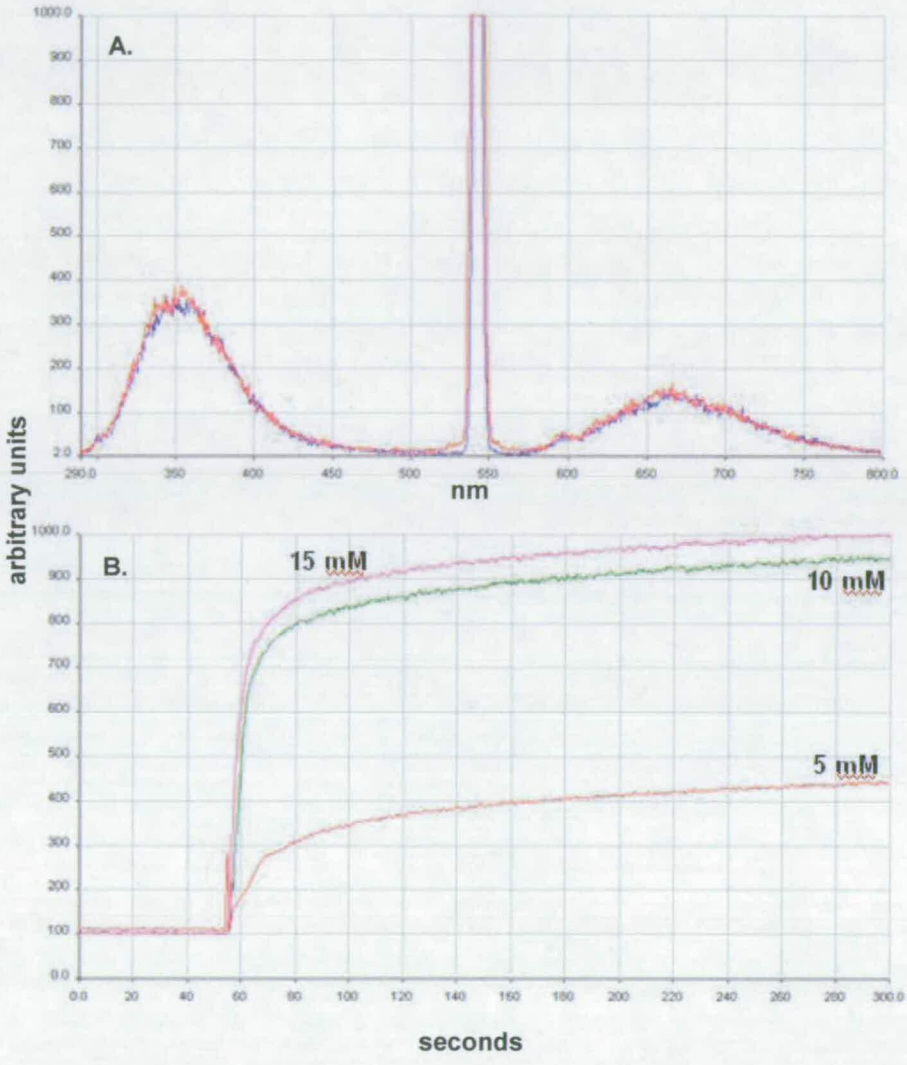

Figure 6.8 Tryptophan fluorescence readings at 290 – 800 nm with excitation at 270 nm (A) and light scattering readings of recombinant MamK at 300 nm after the addition of various concentrations of $MgCl_2$ (B).

6.2.2.2 Depolymerisation of recombinant MamK

MamK samples with 15 mM $MgCl_2$ and 15 mM $CaCl_2$ discussed alongside Figure 6.9 were incubated at room temperature for 3 hr to allow polymerisation to reach steady state as judged by the lack of fluctuation in the reading. The samples were diluted ten-fold to attain readings within the range of the y-axis of the graph. All light scattering depolymerisation assays were carried out on MamK at concentrations ranging from 1 – 2 μM (Figure 6.9). It was observed that a decrease in light scattering did not occur after diluting MamK to between 1 and 2 μM suggesting that MamK has a lower critical concentration than F-actin (Dr. Sutherland Maciver, University of Edinburgh, personal communication) or that depolymerisation is much slower. The addition of 50 mM EGTA decreased MamK light scattering slowly under both divalent cation treatments suggesting that divalent cations are required for polymerisation of MamK, and that the polymerisation/precipitation is reversible to some extent. EGTA has a greater affinity for Ca^{2+}, although in the absence of Ca^{2+} it will chelate Mg^{2+} with a two-fold lower affinity (www.sigmaaldrich.com/ Brands/ FlukaRiedel_Home/ Bioscience/ BioChemika_Ultra/ Chelators.html).

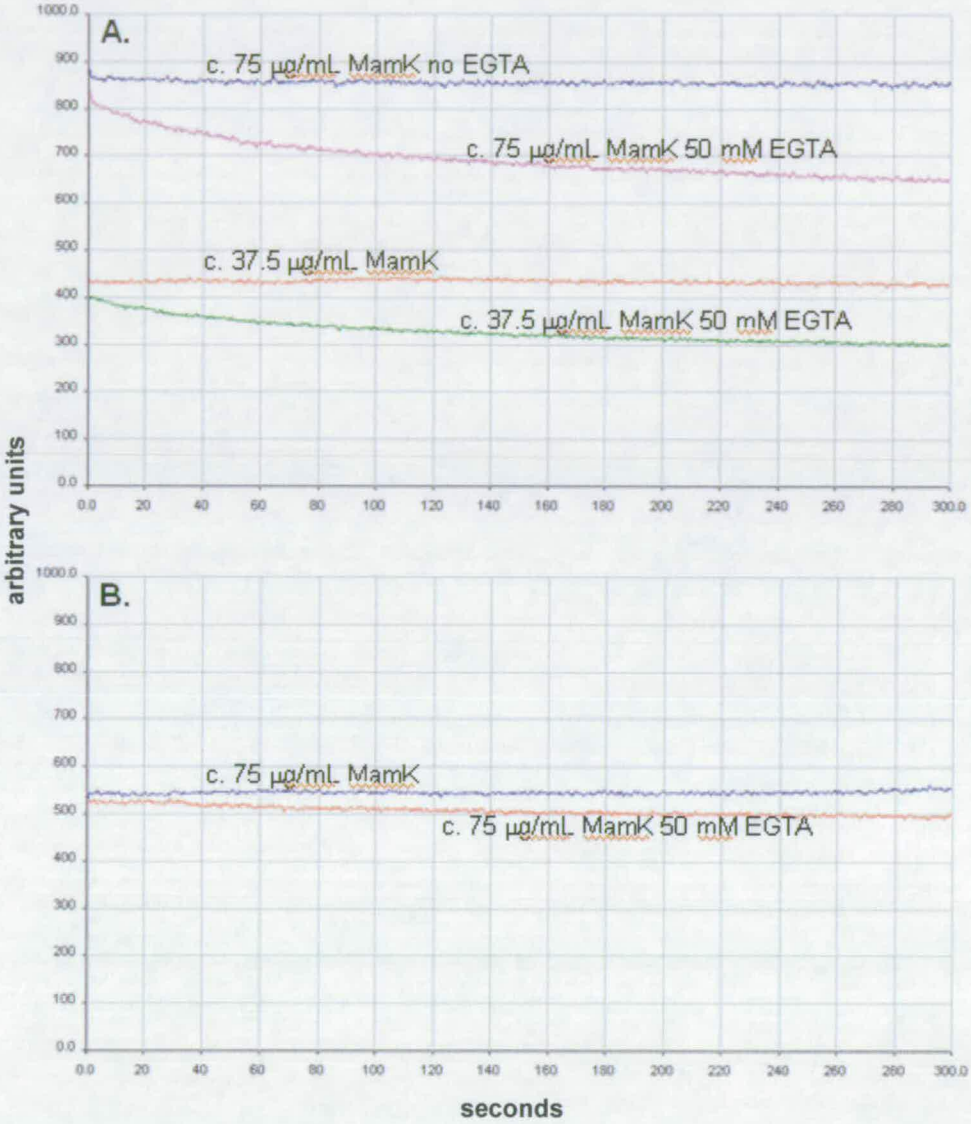

Figure 6.9 Light scattering readings taken from recombinant MamK samples incubated in the presence of 15 mM $CaCl_2$ (A) or $MgCl_2$ (B) for two hr. The samples were diluted and 50 mM EGTA was added to observe depolymerisation. Readings were taken at 300 nm over a period of 300 seconds.

6.2.3 Light scattering and fluorescence of fluorescently labelled MamK-cys

Tryptophan fluorescence failed to yield results that might contribute to understanding local structural changes in MamK under various conditions (Figure 6.8 a). In assays carried out on actin, the pyrene label is bound to the penultimate cysteine residue. MamK does not have a penultimate cysteine residue, so a mutation was engineered

that added a cysteine residue to the C-terminus of MamK to be available for fluorescence labelling, thus extending the MamK amino acid sequence by one amino acid. The method used for binding pyrene to actin was used for binding pyrene to MamK-cys to fluorescently label it. It was hoped that fluorescence readings would be obvious enough to indicate any local structural changes in MamK.

The fluorescence of pyrene-labelled actin is much higher after polymerisation (Cooper *et al.,* 1981). The polymerisation properties of pyrene actin were characterised in detail and it was reported that native and pyrene actin are identical using the following criteria: (1) the time course of polymerisation; (2) the elongation rate constants; (3) the intrinsic viscosity; and (4) the critical concentration. Native and pyrene actin copolymerise. Fluorescence of polymerised pyrene actin is 7-10 times higher than monomer. The fluorescent signal is proportional to polymer weight concentration and is insensitive to filament length distribution. Bleaching can be minimised by appropriate filters to allow continuous monitoring of signal. Measurements do not influence polymerisation kinetics. It was established that pyrene actin fluorescence is a valid assay for actin polymerisation that is more sensitive than any other current assay (Cooper *et al.,* 1981).

Five methods were tested based on the method of fluorescently labelling actin to fluorescently label MamK-cys with either N-(1-pyrene) iodoacetamide or tetramethyl rhodamine iodoacetamide (Table 6.1). The lack of success of the first method suggested that labelling MamK-cys was not going to be as straightforward as labelling actin.

Table 6.1 Summary of methods to fluorescently label MamK-cys

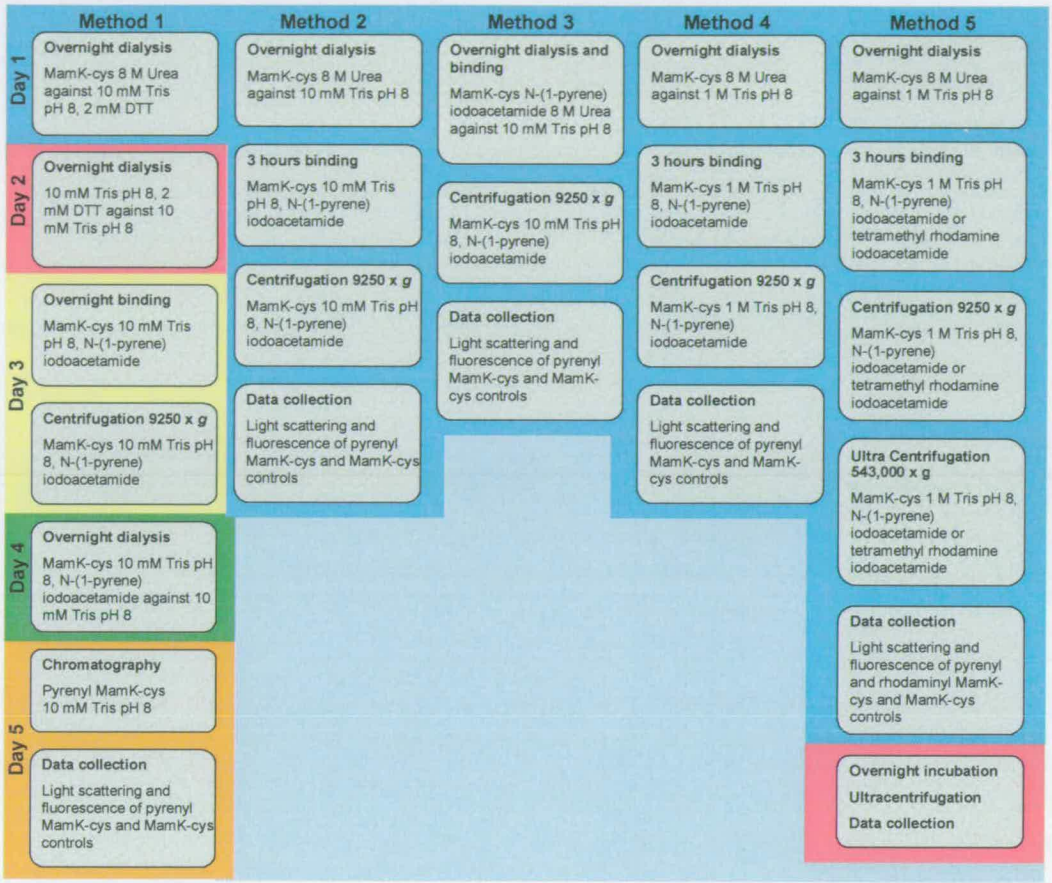

6.2.3.1 Result 1

Method 1 used the most steps in labelling the C-terminal cysteine residue with N-(1-pyrene) iodoacetamide. The procedure lasted 5 days. For this method MamK-cys was purified by inclusion body preparation and dialysed overnight from 8 M urea into 10 mM Tris pH 8.0 and 2 mM DTT to refold the protein. A second overnight dialysis into 10 mM Tris pH 8.0 in preparation for labelling with N-(1-pyrene) iodoacetamide took place. MamK-cys was incubated overnight with N-(1-pyrene) iodoacetamide for it to attach to the C-terminal cysteine residue. The first centrifugation step was carried out to sediment N-(1-pyrene) iodoacetamide as it precipitates on addition to 10 mM Tris pH 8.0. The sample was dialysed overnight against 10 mM Tris pH 8.0 to remove unbound pyrene. The protein was then loaded

to a sise exclusion column for further separation from unbound pyrene prior to light scattering and fluorescence results.

After each dialysis step the soluble MamK-cys concentration decreased as indicated by the density of the protein bands after SDS-PAGE. Either protease inhibitors were insufficient to prevent proteolysis or the protein was polymerising/precipitating out of solution. Protein fractions yielded a very small peak from which samples were examined by SDS-PAGE. The bands were not visible to the naked eye. Fluorescence and light scattering results were taken and there was no increase in the curve after the addition of $MgCl_2$. These results suggest a lack of protein after column chromatography. Repeating the method showed that the protein concentration, which was initially c. 500 μg/ml, had depleted so much by the time it came to load the column that it was likely that the protein would not elute in a sufficient amount to carry on with fluoroscopy or spectroscopy.

6.2.3.2 Result 2

In an effort to prevent loss of protein from solution the method was adjusted to minimise dialysis and incubation steps. The procedure was shortened to 1 day. The results obtained using method 1 indicated that speed was important for the preparation of fluorescently labelled MamK-cys as the soluble protein concentration diminished over time.

In method 2 MamK-cys was purified by inclusion body preparation and dialysed overnight from 8 M urea directly into 10 mM Tris pH 8.0 skipping the second dialysis step into an intermediate buffer. The sample was then incubated with N-(1-pyrene) iodoacetamide for 3 hr at 4 °C to bind the compound to the terminal cysteine residue. The sample was centrifuged at 9250 *x g* for 10 min to sediment N-(1-pyrene) iodoacetamide precipitate. The supernatant was removed and light scattering and fluoroscopy polymerisation experiments were conducted.

In order to get a reading on the y-axis of the graph between 0 and 1000 arbitrary units (Figure 6.10) MamK-cys and pyrenyl MamK-cys were diluted 20-fold to

c. 25 μg/ml. The need to dilute the protein indicates the presence of insoluble material (polymers or aggregate). MamK-cys and pyrenyl MamK-cys give similar increases in light scattering to those obtained in earlier native MamK experiments where addition of $MgCl_2$ was made (Figure 6.8 b). Fluorescence results (examples of which are shown later) showed greater fluorescence readings from the pyrenyl MamK-cys sample compared to the MamK-cys control although neither curve increased on the addition of $MgCl_2$. The difference in the curve is likely to be due to the precipitation or self polymerisation of pyrenyl MamK-cys out of solution as only the initial concentration of the protein inclusion body preparation was monitored prior to the addition of pyrenyl MamK-cys.

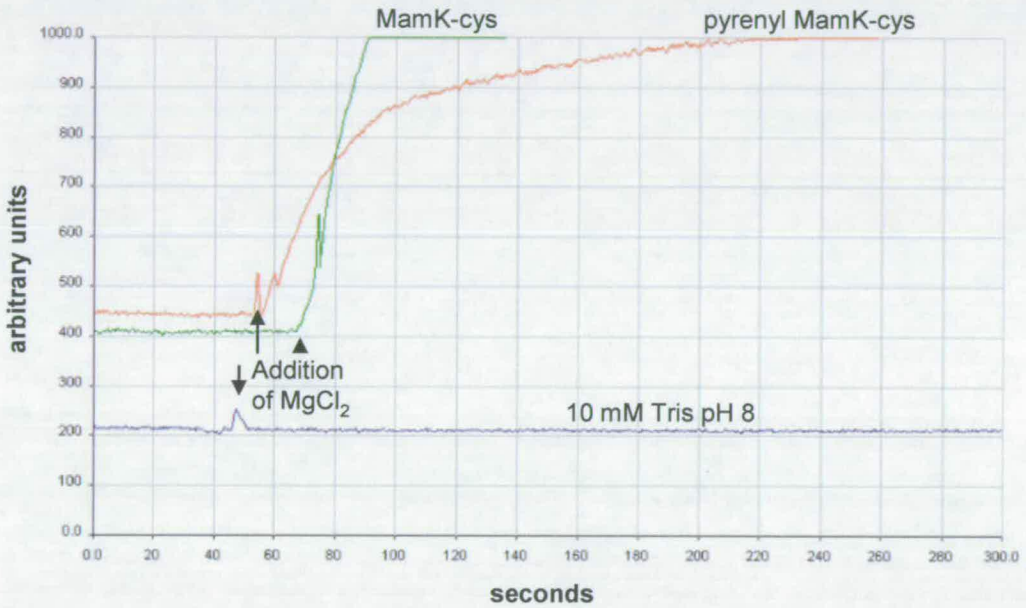

Figure 6.10 Light scattering readings of pyrenyl MamK-cys, MamK-cys control and a negative control (10 mM Tris pH 8.0) measured over 300 seconds before and after the addition of $MgCl_2$.

After the addition of $MgCl_2$ the fluorescence spectrum of the protein does not change yet the light scattering sees a marked increase which suggests that N-(1-pyrene)iodoacetamide may be unattached and therefore not contributing any data towards MamK-cys behaviour.

6.2.3.3 Result 3

In method 3 MamK-cys was purified by inclusion body preparation. N-(1-pyrene) iodoacetamide was added to the protein sample which was then dialysed against 10 mM Tris pH 8.0. It was hoped that this would achieve simultaneous folding of MamK-cys with binding of the pyrene compound to the terminal cysteine residue. After dialysis the sample was centrifuged at 9250 *x g* for 10 min to sediment N-(1-pyrene) iodoacetamide precipitate. The supernatant was removed and light scattering and fluoroscopy polymerisation experiments were conducted.

MamK-cys was dialysed with and without pyrene against 10 mM Tris pH 8.0. Fluorescent emission was recorded between 390 and 500 nm before and after the addition of $MgCl_2$ (Figure 6.11 a). Light scattering was measured over 500 seconds during which time 5 mM $MgCl_2$ was added (Figure 6.11 b).

Results were very similar for pyrenyl MamK-cys and the MamK-cys control. Light scattering increased after the addition of $MgCl_2$ but fluorescence results remained indistinguishable (Figure 6.11 a and b). As previously observed, fluorescence results yielded larger curves from the pyrenyl MamK-cys sample compared to the MamK-cys sample although neither curve increased on the addition of $MgCl_2$. MamK-cys has 9 cysteine residues and dialysing MamK-cys in the presence of N-(1-pyrene) iodoacetamide does not appear to have affected the folding of the protein as indicated by the increase of light scattering in Figure 6.11 b. If MamK were successfully labelled with pyrene, the fluorescence would be expected to be far greater than unlabelled MamK-cys. However, the fluorescence of pyrenyl MamK-cys is always slightly greater than that of MamK-cys.

The reason for the apparently higher signal for pyrenyl MamK-cys compared to MamK-cys may be that pyrene has attached to MamK-cys and for some reason there is no change in fluorescence or alternatively the pyrene is in solution giving higher fluorescence compared to the control or perhaps some pyrene has bound to MamK-cys and the background pyrene in solution is too high to notice any change in bound pyrene readings.

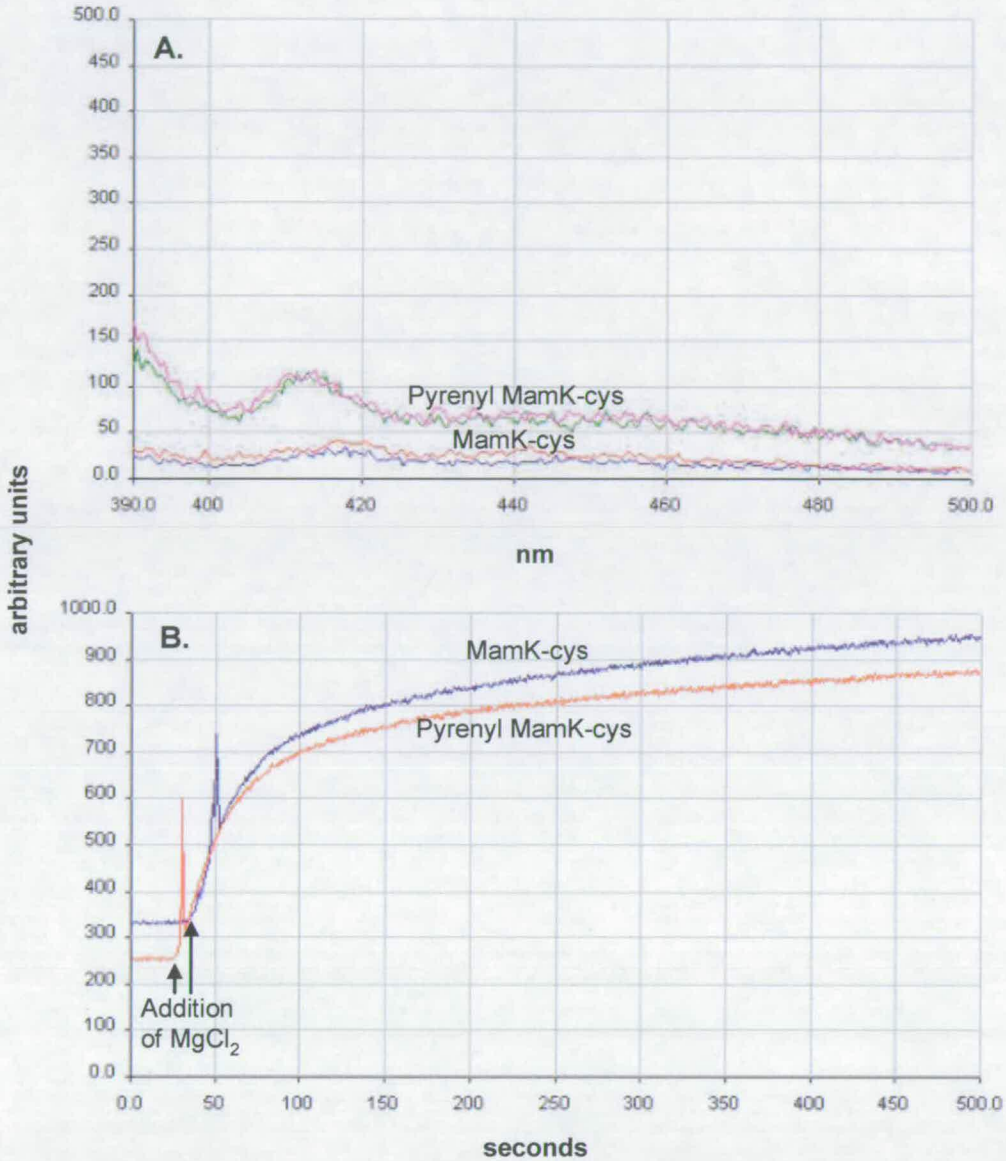

Figure 6.11 Fluorescence readings (A) and light scattering readings (B) of pyrenyl MamK-cys and non-pyrenyl MamK-cys before and after the addition of $MgCl_2$. Samples were dialysed against 10 mM Tris pH 8.0 and pyrene before dilution with 10 mM Tris pH and subsequent readings. Fluorescence readings were taken between 390 and 500 nm and light scattering was measured over a 500 second period.

6.2.3.4 Result 4

Pinder *et al.* (1995) found that high concentrations of Tris are effective in dissociating actin-containing complexes, such as the red cell membrane cytoskeleton. A preparative procedure for red cell actin is based on the dissociation of the membrane skeletal complex in a buffer containing 1 M Tris hydrochloride, followed by gel filtration chromatography in the same medium. The actin is recovered as the monomer and is fully native, as judged by its critical concentration of polymerisation, inhibition of DNase I, stimulation of myosin ATPase, and the appearance in the electron microscope of filaments, both bare and decorated with heavy meromyosin, and of magnesium ion-induced paracrystals. The Tris solution causes rapid depolymerisation of F-actin with no denaturation, and the solution of monomeric actin in this medium is stable for many weeks in the cold; concentrated Tris is more reliable than guanidinium hydrochloride for the depolymerisation of F-actin in the estimation of total actin concentration by the DNase I inhibition assay.

It was noticed that there was a depletion of soluble MamK-cys during dialysis from 8 M urea to 10 mM Tris pH 8.0 in previous methods. In method 4 MamK-cys was purified by inclusion body preparation and dialysed overnight from 8 M urea directly into 1 M Tris pH 8.0 and the supernatant was examined by SDS-PAGE (Figure 6.12). Judging by the strength of the bands presented in Figure 6.11 dialysis against 1 M Tris appears to inhibit self-polymerisation of MamK-cys compared to dialysis against 10 mM Tris pH 8.0.

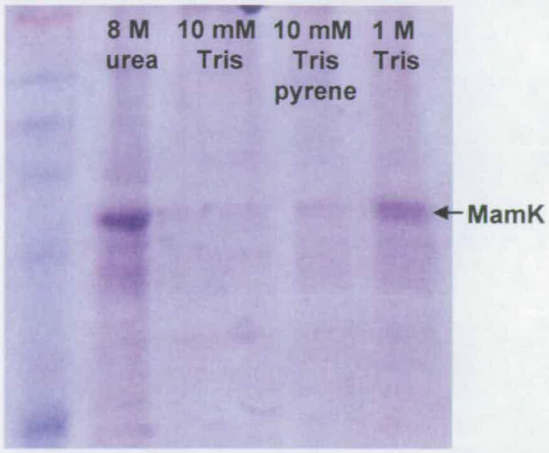

Figure 6.12 SDS-PAGE gel showing intensity of MamK-cys protein samples in 8 M urea, 1 mM Tris, 10 mM Tris with pyrene, 1 M Tris.

MamK-cys was dialysed against 1 M Tris pH 8.0 and then incubated in the presence or absence of N-(1-pyrene) iodoacetamide at room temperature for 3 hr. The sample was centrifuged at 9250 *x g* for 10 min to sediment N-(1-pyrene) iodoacetamide precipitate. Fluorescent emission between 390 and 500 nm was recorded before and after the addition of $MgCl_2$ (Figure 6.12 a). Light scattering was measured over 500 seconds during which time 5 mM $MgCl_2$ was added (Figure 6.12 b). Once again $MgCl_2$ caused an immediate increase in light scattering but fluorescence remained the same. As observed before, fluorescence results yielded larger curves from the pyrenyl MamK-cys sample compared to the MamK-cys control although neither curve changed on the addition of $MgCl_2$.

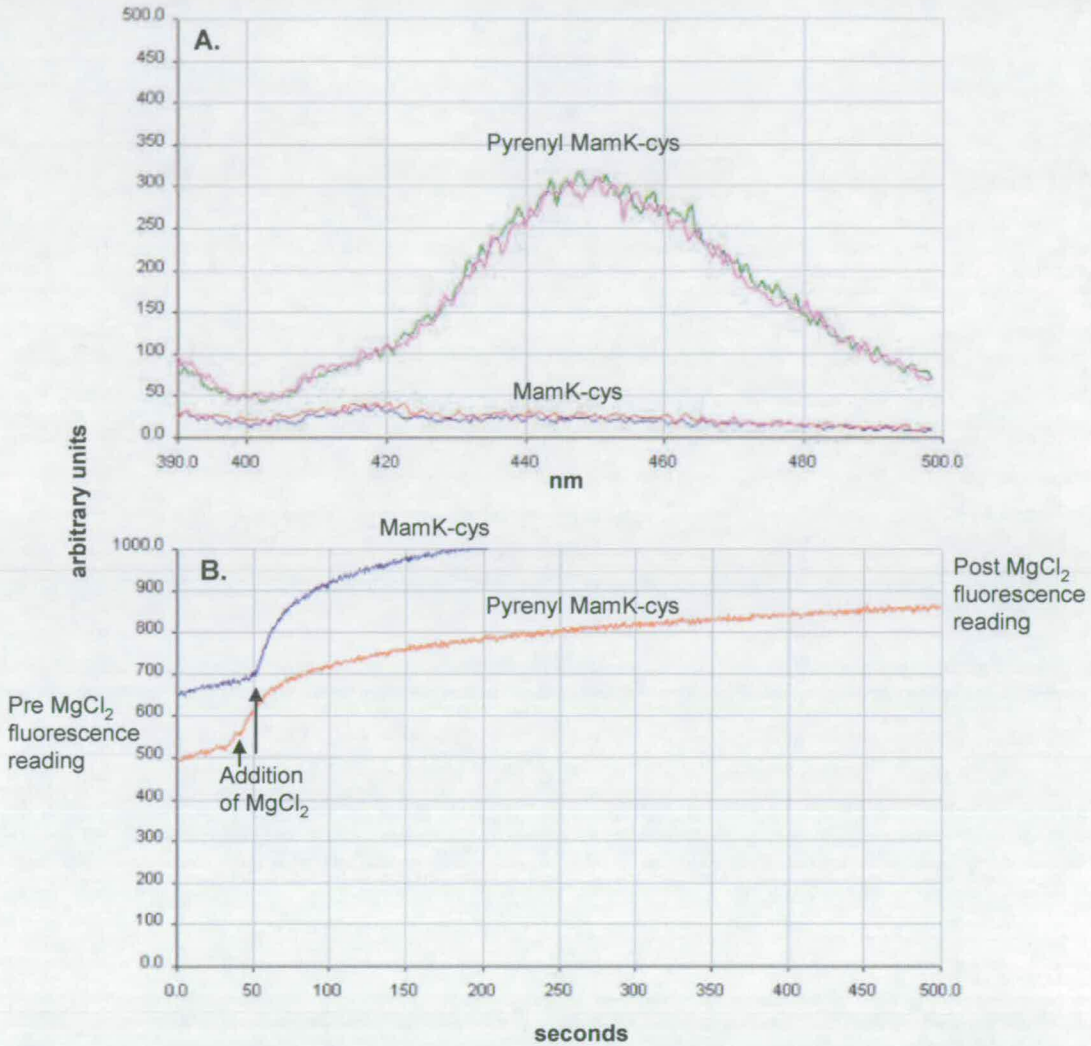

Figure 6.13 Fluorescence readings (A) taken before and after light scattering readings (B) and the addition of $MgCl_2$ taken from a pyrenyl MamK-cys sample and MamK-cys control. Samples were dialysed against 1 M Tris pH 8.0 and incubated with pyrene before dilution with 10 mM Tris pH and subsequent readings. Fluorescence readings were taken between 390 and 500 nm and light scattering was measured over a 500 second period before and after the addition of $MgCl_2$.

One observed difference was an increase in light scattering on dilution from 1 M Tris to 10 mM Tris from 0 – 50 sec prior to the addition of $MgCl_2$ (Figure 6.13 b). This was repeated without the addition of $MgCl_2$ and showed an increase in light scattering for both MamK-cys and pyrenyl MamK-cys (Figure 6.14). The significance of this is unclear but may be indicative of the spontaneous polymerisation or aggregation of the protein which in turn would explain the depletion of MamK-cys in Method 1.

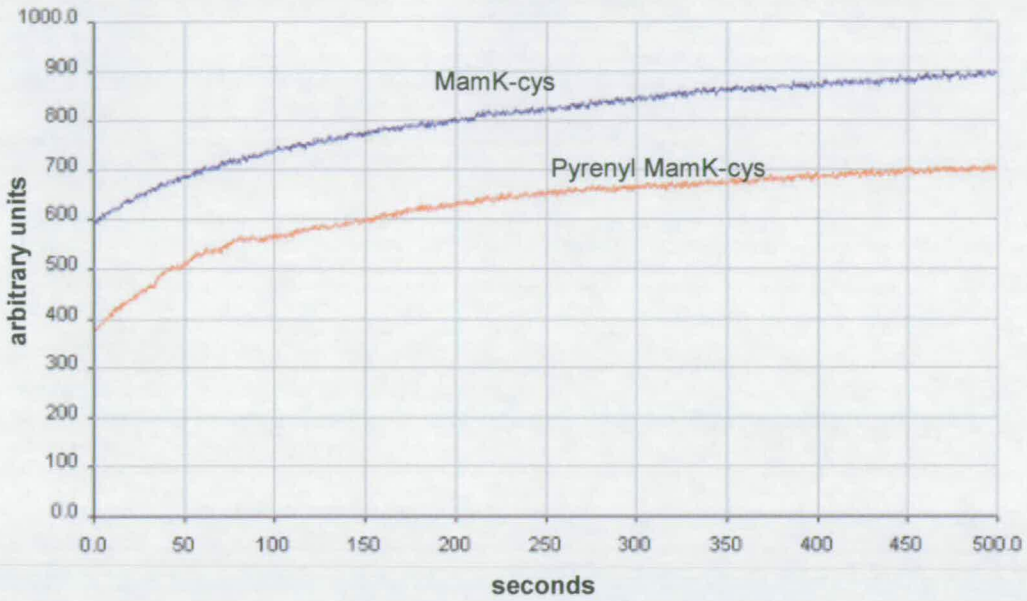

Figure 6.14 Light scattering readings taken from a pyrenyl MamK-cys sample and MamK-cys control. Samples were dialysed against 1 M Tris pH 8.0 and incubated with pyrene before dilution with 10 mM Tris pH and subsequent readings. Light scattering was measured over a 500 second period.

Following this (Figure 6.13) the samples were incubated for 2 hr at room temperature and further fluorescence readings were taken showing that fluorescence had not altered during incubation. The samples were centrifuged and further fluorescence readings of the supernatant were recorded. There was no marked decrease in fluorescence for MamK-cys (data not shown) but pyrenyl MamK-cys showed a decrease in fluorescence of approximately a fifth of the original reading (Figure 6.15). Observe the similarities in the curve of pyrenyl MamK-cys from Figure 6.12 compared to the pre-centrifugation results. This result could be due to sedimentation of polymerised pyrenyl MamK-cys from solution which would indicate pyrenyl MamK-cys does not contribute information to the behaviour of MamK-cys in the presence of $MgCl_2$. Alternatively, the decrease in fluorescence may be due to sedimentation of precipitated N-(1-pyrene)iodoacetamide that was not fully removed after the 25 minute centrifugation step.

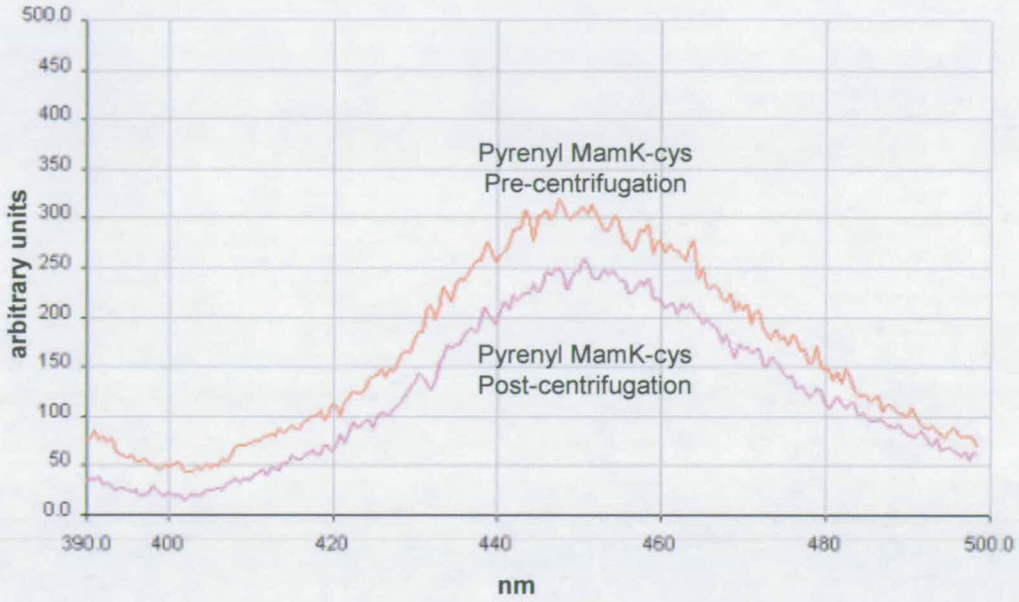

Figure 6.15 Fluorescence readings of pyrenyl MamK-cys before and after centrifugation. Fluorescence decreases approximately one fifth after centrifugation. Fluorescence readings were taken between 390 and 500 nm.

6.2.3.5 Result 5

In method 5 MamK-cys was purified by inclusion body preparation and dialysed overnight from 8 M urea directly into 1 M Tris pH 8.0. MamK-cys was incubated with N-(1-pyrene) iodoacetamide or tetramethyl rhodamine iodoacetamide at room temperature for 3 hr. The sample was centrifuged at 9250 *x g* for 10 min to sediment excess N-(1-pyrene) iodoacetamide or tetramethyl rhodamine iodoacetamide precipitate. After centrifugation at 9250 *x g* some of the sample was ultracentrifuged at 543,000 *x g* to remove all remaining compound precipitate and MamK-cys polymers/aggregates from the suspension to be left with soluble fluorescently labelled MamK-cys. Light scattering and fluorescence readings were taken from the supernatant (Figure 6.16 a) and the resuspended pellet (Figure 6.16 b) after ultracentrifugation. It appeared that all the protein had sedimented during ultracentrifugation so the resuspended pellet was diluted 20-fold in 10 mM Tris pH 8.0 to attain readings within the y-axis of the graph. There was an increase in light scattering for MamK-cys and pyrenyl MamK-cys pellets on addition of $MgCl_2$ although the increase was not as obviously marked by the addition of $MgCl_2$ as in

previous experiments. Lack of a significant increase in light scattering might have been due to the sedimentation of polymers and depletion of soluble protein below the critical concentration. Fluorescence readings were taken from MamK-cys and pyrenyl MamK-cys and as previously observed there was no change with $MgCl_2$. Fluorescence readings were not taken from rhodaminyl MamK-cys as there did not seem to be any protein present in the undiluted supernatant or pellet samples from light scattering. It is likely that the protein polymerised/precipitated during incubation in the presence of tetramethyl rhodamine iodoacetamide and sedimented out of the sample during initial centrifugation at 9250 *x g*.

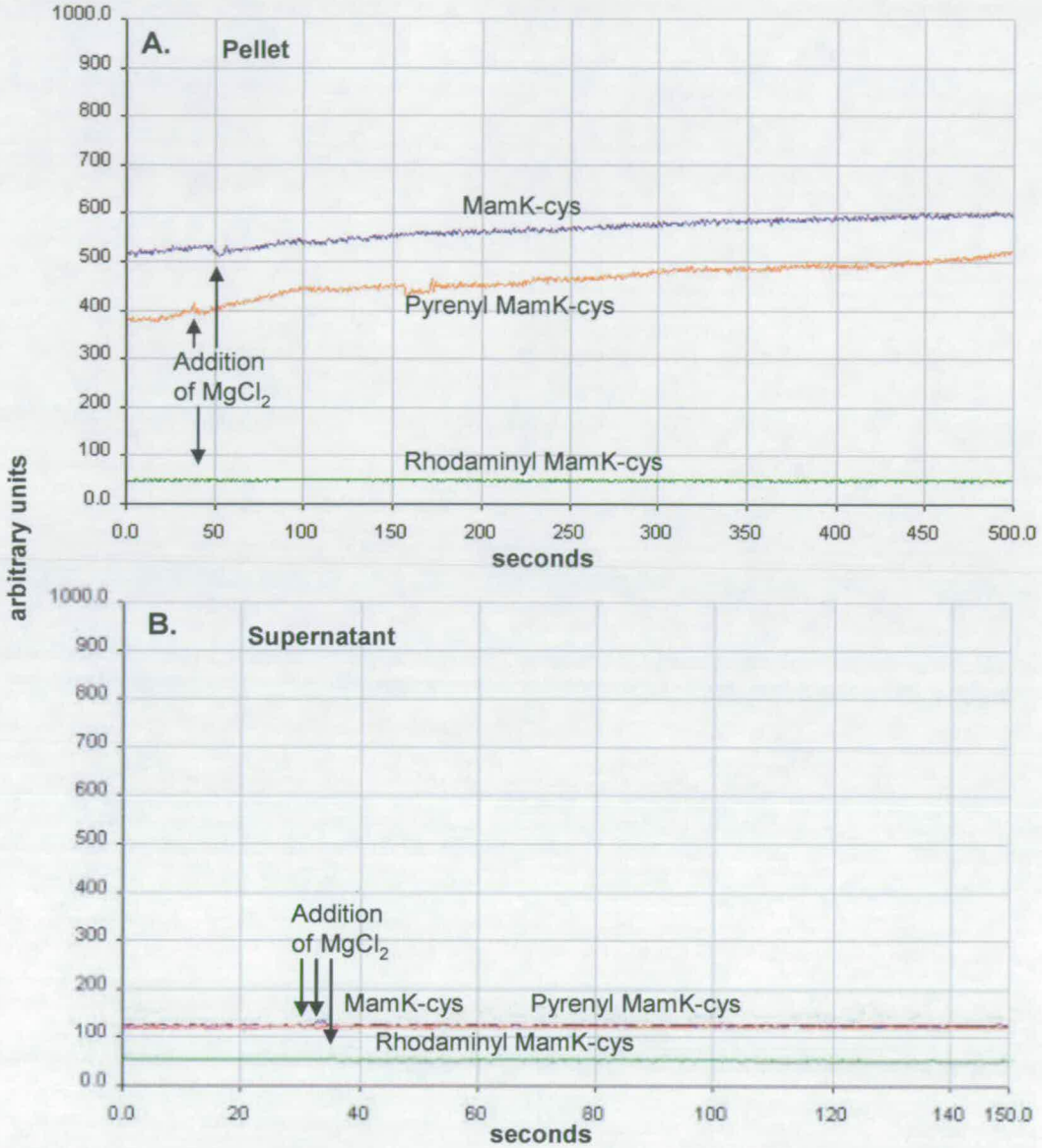

Figure 6.16 Light scattering readings of pellet (A) and supernatant (B) fractions of pyrenyl MamK-cys, rhodaminyl MamK-cys and a MamK-cys control after ultracentrifugation at 543,000 *x g*.

$MgCl_2$ was added to the pyrenyl MamK-cys and MamK-cys in 1 M Tris pH 8.0 stocks after the initial 9250 *x g* centrifugation step. These were incubated overnight and on their collection filamentous precipitate (up to 3 cm long) was observed in the suspension. The presence of $MgCl_2$ was enough to cause polymerisation/precipitation without having to dilute the Tris concentration in 10 mM Tris pH 8.0.

The samples were centrifuged to sediment the filamentous precipitate. The supernatant was removed and the pellet was washed three times and resuspended in 1 M Tris pH 8.0 with vortexing for 2 hr at room temperature in an attempt to disassociate the polymers/precipitate as observed for actin (Pinder *et al.*, 1995). If this was successful it might be possible to examine the effect of $MgCl_2$ addition on light scattering and fluorescence readings without a fluorescent background. The pellets did not disassociate. Regardless of the lack of resolubilisation of the samples light scattering (Figure 6.17) and fluorescence (Figure 6.17) readings were taken from samples during which time $MgCl_2$ was added.

There was an insignificant increase in light scattering recorded over a 150 second period (Figure 6.17).

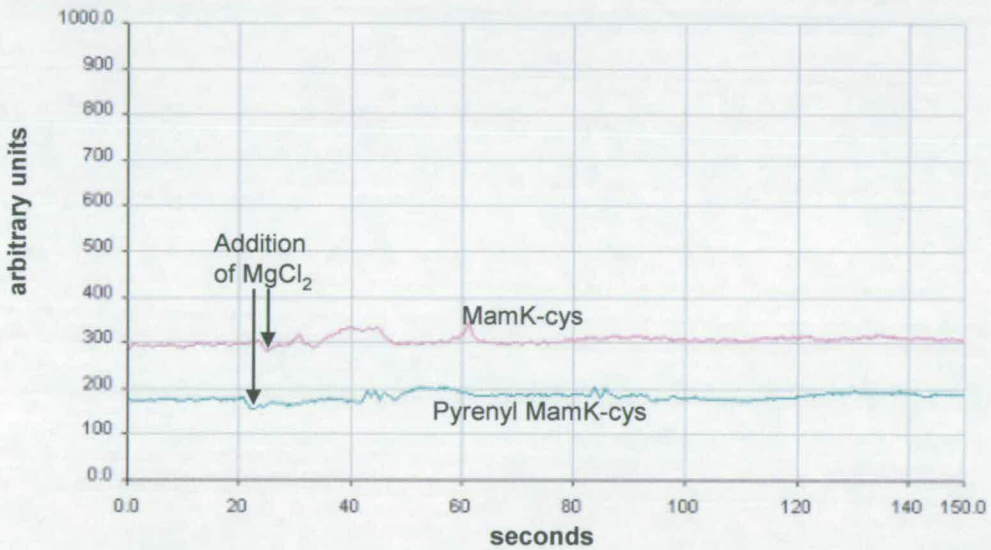

Figure 6.17 Light scattering readings of MamK-cys and pyrenyl MamK-cys after overnight incubation in 1 M Tris pH 8.0 with 15 mM $MgCl_2$, ultracentrifugation at 543,000 *x g*, washing of the pellet and resuspension by vortexing in 1 M Tris pH 8.0. Light scattering was measured over a 150 second period during which time $MgCl_2$ was added at a 5 mM concentration.

Fluorescence readings showed no distinct changes for pyrenyl MamK-cys or MamK-cys after the addition of $MgCl_2$ (Figure 6.17). The pyrenyl MamK-cys fluorescence readings are higher than the MamK-cys readings, consistent with previous experiments, perhaps indicating the presence of pyrene. The pyrenyl MamK-cys supernatant gave higher fluorescence readings compared to the washed pellet and the

peak of the supernatant curve has a distinctly different shape compared to that of the pyrenyl MamK-cys pellet. The shape of the peak of the supernatant in Figure 6.18 when compared to the shape of the peak of supernatant in Figure 6.15 shows a variation compared to previous curves from c. 390-450 nm although the significance of this is unclear it may indicate successful binding of the probe to the C-terminal cystein residue.

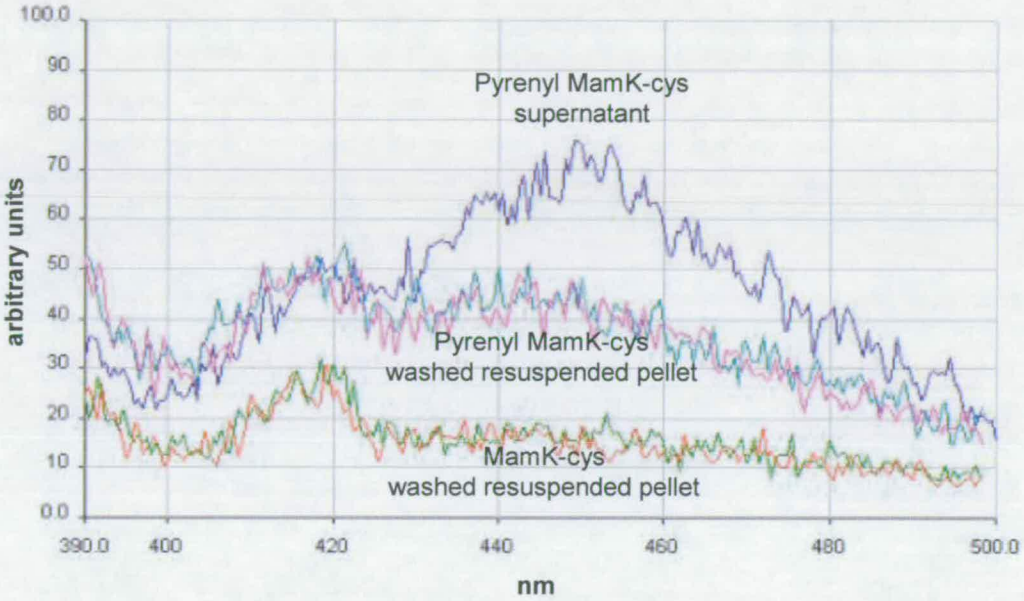

Figure 6.18 Fluorescence readings taken between 390 and 500 nm of pyrenyl MamK-cys supernatant after overnight incubation of the sample in 1 M Tris with 15 mM $MgCl_2$ and ultracentrifugation of the sample at 543,000 *x g*. Also washed resuspended pellet and MamK-cys washed resuspended pellet. Also, fluorescence emission readings of MamK-cys and pyrenyl MamK-cys after overnight incubation in 1 M Tris pH 8.0 with 15 mM $MgCl_2$, ultracentrifugation at 543,000 *x g*, washing of the pellet and resuspension by vortexing for 2 hr in 1 M Tris pH 8.0

6.2.4 Summary of fluorescence labelling results

Using method 1 MamK-cys appeared to be removed from solution. This may have been due to proteolysis of the protein or polymerisation/ aggregation and sedimentation out of solution during dialyses and centrifugation.

Speeding up the labelling process in method 2 kept enough protein in solution to record light scattering and fluorescence data. Light scattering increased on the

addition of $MgCl_2$ whilst fluorescence readings remained unchanged indicating that N-(1-pyrene) iodoacetamide had not bound to the cysteine residue.

Further method modification in method 3 involved refolding in the presence of N-(1-pyrene) iodoacetamide to speed up the method and encourage binding of the fluorescent label to the C-terminal cysteine residue. Either MamK-cys had bound to one of the 9 cysteine residues during dialysis and for some reason there was no change in fluorescence, or pyrene is in solution giving higher fluorescence compared to the control, or some pyrene had bound to MamK-cys and the background pyrene is too high to notice any change in bound pyrene readings.

Method 4 uses dialysis of MamK-cys from 8 M urea into 1 M Tris pH 8.0 to maintain as much protein in solution as possible in accordance with a similar method used on actin (Pinder *et al.*, 1995). SDS-PAGE shows lower intensity bands for samples dialysed against 10 mM Tris pH 8.0 compared to those dialysed against 1 M Tris pH 8.0 suggesting that 1 M Tris pH 8.0 helps maintain the protein solubility (Figure 6.12). Light scattering results suggest self polymerisation/aggregation on dilution from 1 M Tris pH 8.0 into 10 mM Tris pH 8.0 (Figure 6.14). $MgCl_2$ addition causes a marked increase in light scattering while fluorescence readings remain the same as before (Figure 6.12). Ultracentrifugation of pyrenyl MamK-cys at 543,000 *x g* gives a decrease in fluorescence of up to one fifth of the original reading suggesting removal either of precipitated N-(1-pyrene) iodoacetamide or polymerised/aggregated pyrenyl MamK-cys (Figure 6.15).

During method 5, ultracentrifugation was used to remove all insoluble material including MamK (Figure 6.16). The pellet was resuspended and $MgCl_2$ was added and yielded a lower response of MamK-cys compared to previous additions of $MgCl_2$ to soluble protein (Figure 6.17). Pre- and post- ultracentrifugation fluorescence readings reveal a difference in the curve shape between the supernatant and the pellet compared the fluorescence results of the supernatant in method 4 where ultracentrifugation was not used (Figure 6.18). Filamentous precipitate was observed in pyrenyl MamK-cys and MamK-cys 1 M Tris pH 8.0 stocks after the

initial 9250 *x g* centrifugation step to remove precipitate after overnight incubation with $MgCl_2$ but attempts to resolubilise the protein to attain convincing fluorescence results were unsuccessful.

6.2.5 Recombinant MamK interactions with proteins from *Magnetospirillum gryphiswaldense* MSR-1 crude cell extract

A brief attempt was made to couple MamK to CNBr-activated sepharose 4b using the method outlined in section 2.5.14. SDS-PAGE showed that MamK concentrations were too low to be visible. Silver staining of the same fractions also failed to show the presence of protein (not shown).

6.3 DISCUSSION

6.3.1 Visualisation of micro- and macro- structures of MamK

Remarkably, macroscopic observation of MamK self assembly were first noted when a Falcon tube containing pelleted *Escherichia coli* expressing MamK was left on the bench during an inclusion body preparation (Figure 6.1). The structures were identified as MamK by mass spectroscopy. The significance of this phenomenon, if any, is unclear and reports of this nature for similar proteins are undetectable in the available literature.

Microscopic structures were observed under phase contrast microscopy at 400 x magnification where sheets of MamK after incubation with 2 mM $MgCl_2$ were measured at approximately 2 µm to an immeasurable sise as the sheets extended on all sides out of the field of view. The depth of such sheets was measured in excess of 200 µm suggesting folding of the sheets or multiple lattices on top of one another. Rectangular sheets in actin that depart from complete regularity in that dislocation zones may be found as strips along their length have been discussed (Aebi *et al.*, 1981). Within these strips, one of the two lattices is sheared with respect to the corresponding lattices in the neighbouring zones while being continuous with them at the edge of the zone. Although each zone is of constant width along its length, different zones may have widths from 100 to several hundred nanometers. Reports of sheets of a higher scale of magnitude comparable to what was observed for MamK were undetected in the available literature.

Micrograph images of sheets formed by purified recombinant MamK after incubation with 2 mM $MgCl_2$ have been presented (Figures 6.3, 6.4, 6.5 and 6.6). A closer comparison of sheared actin lattices (Aebi *et al.,* 1981) to sheared MamK lattices from this work is presented in Figure 6.19.

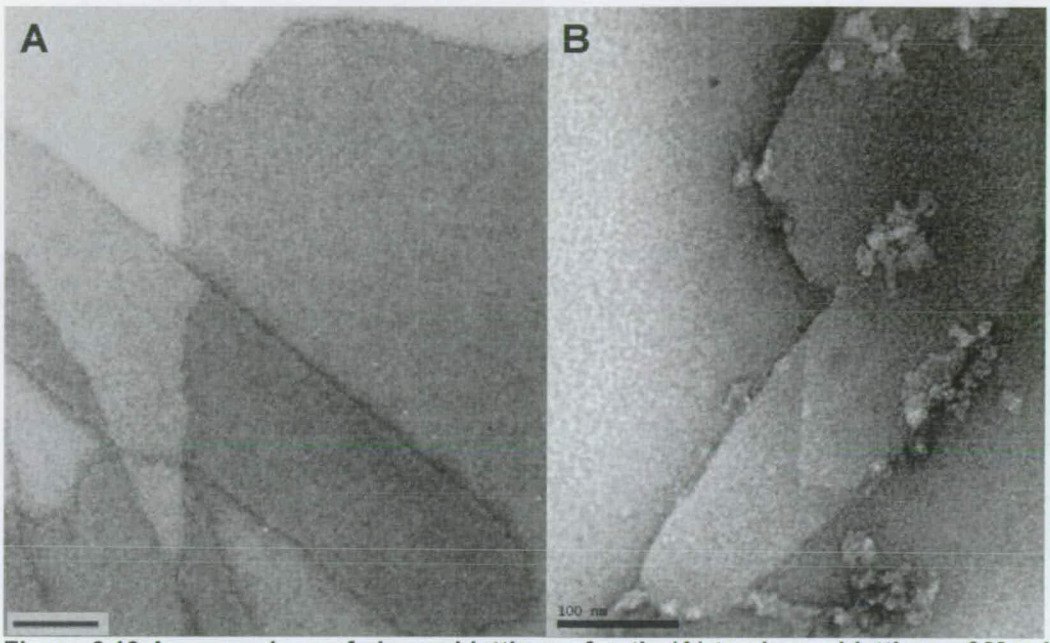

Figure 6.19 A comparison of sheared lattices of actin (A) to sheared lattices of MamK (B). The actin lattice image (A) is adapted from Aebi *et al.* (1981) whilst the MamK lattice image (B) is a reproduction of Figure 6.6. In both cases the bar represents 100 nm.

Rectangular crystalline sheets of actin showing two layers and their relative stagger are highlighted in Figure 6.20 (adapted from Aebi *et al.*, 1981) that compare well to observations of MamK sheets particularly those presented in Figure 6.4.

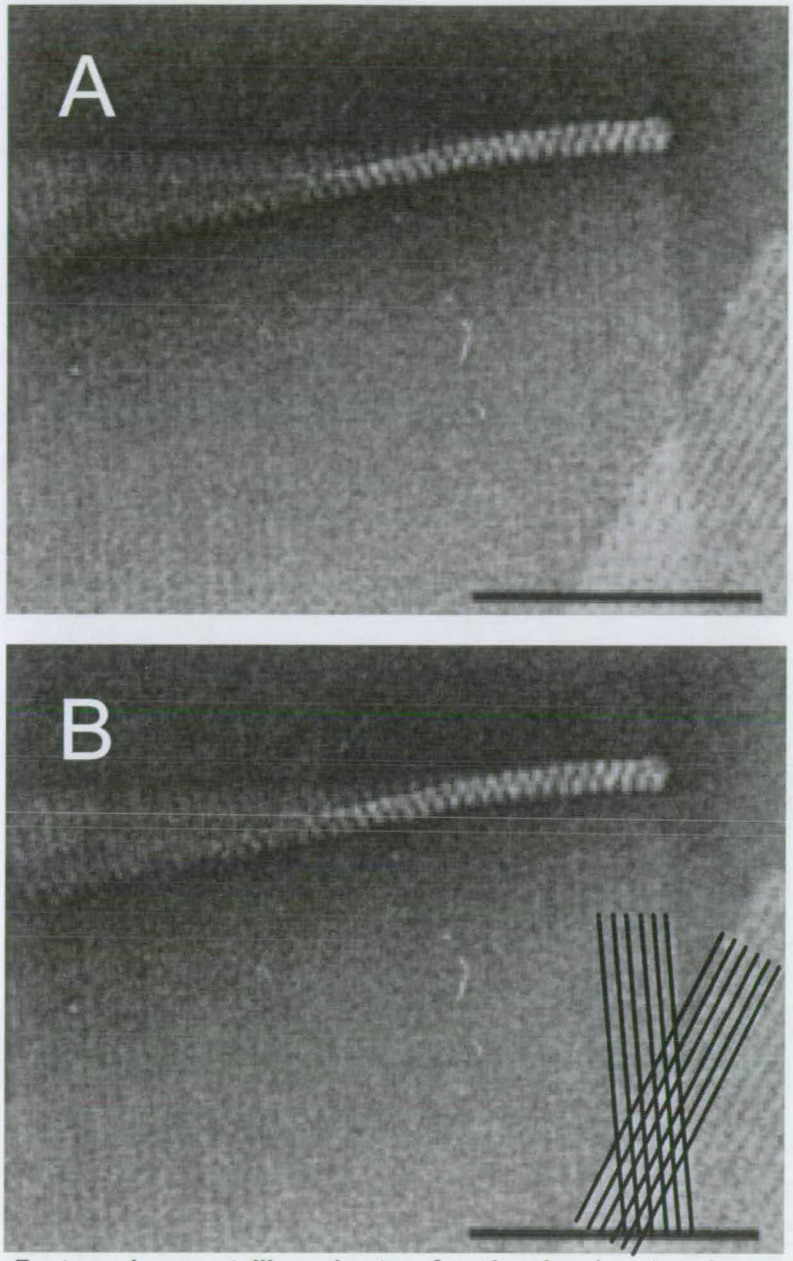

Figure 6.20 Rectangular crystalline sheets of actin showing two layers and their relative stagger (A), highlighted in (B) (bars = 100 nm) (Adapted from Aebi *et al.*, 1981).

Sheared lattices of actin were observed (Aebi *et al.*, 1981) in actin micrographs and there appears to be similar shearing of MamK lattices in the micrograph presented in Figures 6.3, 6.4 and 6.6. Gadolinium induced crystalline actin sheets from *Acanthamoeba* have been examined (Aebi *et al.*, 1981). These sheets exist in three different polymorphic forms, which show different striation patterns and surface topographies. They named these forms "*rectangular*", "*square*" and "*cylinder*" and showed that each is constructed from common "*basic*" lattices associated in different ways. *Acanthamoeba* actin sheets are stable for weeks in sheet buffer at 4 °C as long as the protein concentration is kept above 0.5 mg/ml but they do aggregate with time (Aebi *et al.*, 1981). Recombinant MamK sheets have been observed in samples after one year incubation in 2 mM $MgCl_2$ at 4 °C and similarly seem to aggregate over time. It is also possible to prepare recombinant MamK sheets from protein stored in 10 mM Tris pH 8.0, 2 mM DTT, 1 mM NaN_3 after one year by the addition of 2 mM $MgCl_2$.

Some of the features of a "*basic*" sheet are on a near-rectangular lattice with an average width of 6.55 nm which is in keeping with an estimate of 7 nm for MamK (Aebi *et al.*, 1981). ParM filaments were measured with a width of 7 nm (Møller-Jensen *et al.*, 2002) compared to F-actin (two protofilaments) with a width of 6.5 nm and MreB with a width of 3.9 nm (Steinmetz *et al.*, 1998; van den Ent *et al.*, 2001). A striking feature of the basic sheet from *Acanthamoeba* is the difference in the topographies of its two surfaces visualised on freeze dried and shadowed specimens where one surface of the basic sheet appears coarse and untextured with no apparent lattice, and the other appears smooth and textured with the same near-rectangular lattice as the negatively stained basic sheet. There are variations in sheet formation of actin from different species due to variations in amino acid sequences and the preparation of the sample, usually to do with salt concentration. Further work is required to define the structure of MamK sheets for more direct comparison to actin and other actin-like proteins.

His-tagged MamK was prepared for *in vitro* polymerisation in 100 mM Tris-HCl pH 7.0, 14 mM $MgCl_2$, 100 mM NaCl, centrifuged at 150,000 *x g* and polymerised by

the addition of 2 mM ATP or ATP-γ-S (a non hydrolysable ATP analogue) and when examined by TEM was shown to form what were described as "filamentous bundles" (Figure 6.21) (Taoka *et al.*, 2007). The results and discussion of the study vary from work towards this thesis as no light scattering data were shown and no comment on the role of Mg^{2+} or nucleotides in polymerisation was made. The subsequent TEM images clearly showed well developed bundles of MamK that measured 100 μm in length and 100 nm in width and smaller twisted bundles with total diameters of 8 to 18 nm composed of fine helical filaments of approximately 6 nm in width which is in keeping with our observations of MamK (Figure 6.4). The TEM representations of MamK from Taoka *et al.* (2007) in some ways look remarkably similar to the sheets observed of MamK in this work particularly when comparing Figure 6.21 a to the edges of sheets in Figure 6.3. Also, Figure 6.21 e and f (Taoka *et al.*, 2007) depicts parallel filaments of MamK which also suggest sheet formation. Taoka *et al.* (2007) may have misinterpreted MamK to form bundles of filaments when in fact MamK is forming foldable sheets of MamK.

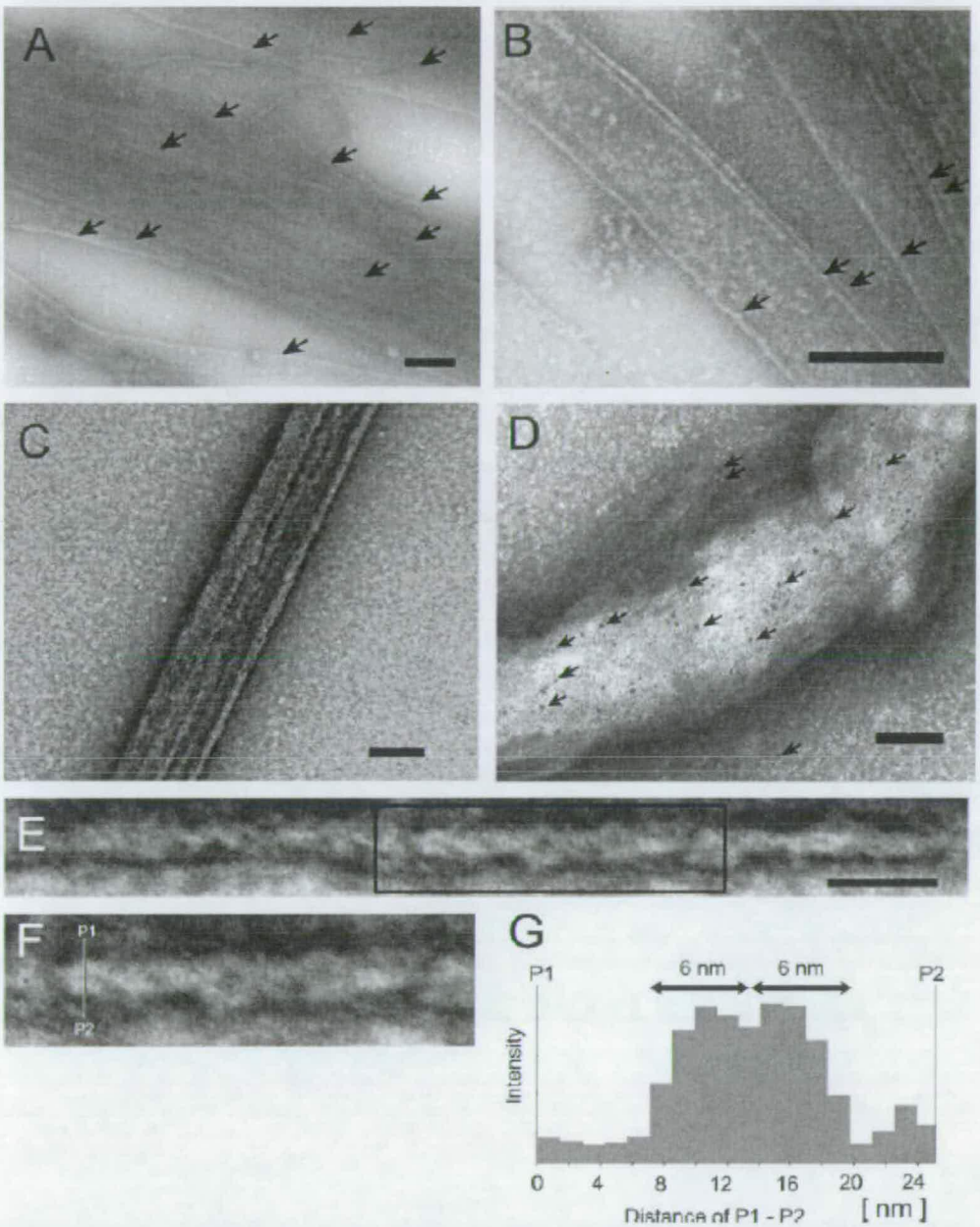

Figure 6.21 Micrographs of negatively stained MamK polymers. (A and B) Filamentous bundles of MamK. Arrows show the synthesised filamentous bundles of MamK. (C) The well-developed bundle of MamK. (D) Immunogold staining of the synthesised bundle using anti-MamK antibody. The arrows show the 5-nm gold particles. Many gold particles are attached to the bundle; in contrast, few gold particles are attached to the background. (E) The filamentous bundle ranged from 8 to 18 nm in width. (F) An enlargement of the box from panel E is shown. Each bundle consisted of fine helical filaments. (G) A line profile P1 to P2 of intensity from the enlarged bundle shown in panel F. Double-head arrows show the width of a single helical filament. The helical filament was about 6 nm in width. Panel A to C scale bars, 200 nm; panel D scale bar, 100 nm; panel E scale bar, 50 nm. (Figure and legend taken directly from Taoka *et al.*, 2007)

6.3.2 Light scattering and fluorescence experiments

6.3.2.1 Light scattering of recombinant MamK

Many light scattering and tryptophan fluorescence experiments were carried out to get an idea of the polymerisation properties of recombinant MamK. It was observed that during light scattering time course experiments recombinant MamK would polymerise after the addition of $MgCl_2$ in a buffer containing 10 mM Tris pH 8.0 and 2 mM DTT (Figure 6.8 b). Microscopic examination showed that the events observed under these conditions during light scattering were consistent with polymerisation of protein rather than aggregation of denatured material (Figure 6.2).

It is interesting that MamK does not require NTP for folding as sheets are formed on addition of $MgCl_2$ whether NTP is present or not. If anything ATP or GTP may keep MamK in a monomeric soluble form as during ion exchange chromatography MamK was easily eluted from the column when ATP or GTP was present and the fate of MamK was undetermined in the absence of NTP. It was also observed under phase contrast microscopy that the frequency of sheet formation appeared to be higher in samples without NTP compared to samples with ATP or GTP although this requires more stringent quantification. Reasons for this need further investigation.

For actin, it has been hypothesised that the sub-domains fold spontaneously so that the protein is in a quasi native conformation and in order to close the hinge of the two lobes, nucleotide is loaded into the interdomain cleft by a CCT (chaperonin containing t-complex polypeptide 1) (Egelman, 2003; Llorca *et al.*, 2000). It appears that the conformation of MamK has overcome this need or never required NTP to complete the folding process and bring the domains together. There are insertions in actin that seem to have a pivotal role in folding, polymerisation and allostery. For example, modification of the DNaseI binding loop (in actin residues 40-48, not present in MreB, undetermined in MamK) can change the properties of the C-terminus (in actin residues 353-357, not present in MreB, undetermined in MamK); modification of the 'hydrophobic plug' (in actin residues 262-274) alter properties of

the DNaseI binding loop and modification of the C terminus can also affect the hydrophobic loop (Crosbie *et al.*, 1994; Egelman, 2003; Orlova and Egelman, 2002).

EGTA was added to depolymerise MamK samples by scavenging Mg^{+}/Ca^{+} ions. The dilution of samples to approximately 1-2 μM suggests that the critical concentration of MamK is lower than that of F-actin whilst the addition of EGTA showed that the depolymerisation of MamK is reversible to some extent but does not appear to be readily achievable which is consistent with findings discussed in Section 5.2.7. Contrarily, *in vivo* studies indicated that MamK polymerisation in *Escherichia coli* is highly dynamic and a kinetically asymmetrical system undergoing continuous rearrangement (Pradel *et al.*, 2006) (Section 4.3.1). There may be undiscovered accessory proteins that contribute to the dynamic behaviour of MamK *in vivo* or these findings may have been due to an artefact produced by proteolysis while expressing MamK in *Escherichia coli* (Mornet and Ue, 1984; Carbonell and Villaverde, 2002). Additionally, comparison of the appearance of MamK as filaments or sheets under various purification methods (Figures 5.3, 5.4, 5.6, 5.7 and 6.2) suggests that there may be undiscovered conditions that contribute to a more dynamic behaviour of MamK *in vitro*.

For example, *in vitro* work on *Acanthamoeba* actin sheets shows they are stable for weeks in sheet buffer at 4°C as long as the protein concentration is kept above 0.5 mg/ml, but they do aggregate with time (Aebi *et al.*, 1981). However, when sheet preparations are dialysed against Gd-free buffer containing KCl, all sheets are converted to filamentous material in <5 h. Sheet preparations at a concentration of >0.5 mg/ml protein dialysed against Gd-free, salt-free buffer remain intact for 24 h, after which they slowly disintegrate. However, if after only 12 hr of dialysis against Gd-free, salt-free buffer the sheets are dialysed against F-actin buffer (2 mM $MgCl_2$, 50 mM KCl), the sheets are completely converted to F-actin.

6.3.2.2 Tryptophan fluorescence of recombinant MamK

Intrinsic tryptophan fluorescence of proteins offers an alternative to the use of extrinsic probes for monitoring local structural changes around labelled residues (Burstein *et al.*, 1973; Doyle *et al.*, 2001; Eftink and Ghiron, 1976, Eftink and

Ghiron, 1977). In actin, the intrinsic fluorescence of tryptophan has been used to monitor changes associated with divalent cation exchange and actin polymerisation (Selden *et al.*, 1994). These conformational changes result in changes in tryptophan fluorescence that can be used to map changes to specific sites on actin. Tryptophan fluorescence experiments conducted on recombinant MamK did not yield any information of local structural changes (Figures 6.7 a).

6.3.2.3 C-terminal cysteine mutation causes MamK-cys to self polymerise without a requirement for $MgCl_2$

Fluorescence labelling of MamK was conducted to overcome the lack of information from local structural changes using tryptophan fluorescence assays carried out on recombinant MamK (Figures 6.7 a). In fluorescence assays carried out on actin the pyrene label is bound to the penultimate cysteine residue (Cooper *et al.*, 1983; Pinder *et al.*, 1995). MamK does not have a penultimate cysteine residue so a mutation was engineered that added a cysteine residue to the C-terminal of recombinant MamK to be available for fluorescence labelling thus extending the MamK amino acid sequence by one amino acid, hence MamK-cys. The addition of the cysteine residue to the C-terminal of MamK appeared to result in the self polymerisation of the protein which had not been observed in any earlier light scattering experiments with MamK lacking the addition of the cysteine residue. MamK-cys seemed to polymerise from the moment it was dialysed into 10 mM Tris pH 8.0 suggested by the speed at which refolding and fluorescent probe attachment was required to maintain the protein in solution.

From early attempts to fluorescently label MamK-cys it was obvious that the protein sedimented out of solution during centrifugation and that a shorter preparation period was required to maintain a high enough protein concentration to make experiments worthwhile. After inclusion body preparations and dialysis from 8 M urea into 1 M Tris it appeared that 1 M Tris pH 8.0 assisted in keeping MamK-cys in solution compared to 10 mM Tris pH 8.0 as demonstrated by SDS-PAGE (Figure 6.12). Light scattering showed the tendency for MamK-cys to self polymerise on dilution in 10 mM Tris pH 8.0 from 1 M Tris pH 8.0 (Figures 6.12 and 6.13). It would be interesting to observe the effect that ATP might have on either maintaining the

solubility of MamK-cys as when ATP was present during ion exchange chromatography it seemed to promote the elution of soluble monomeric MamK from the column (Figure 5.8).

High concentrations of Tris have been found to be effective in dissociating actin-containing complexes, such as the red cell membrane cytoskeleton (Pinder *et al.*, 1995) as discussed in Section 6.2.3.4.

6.3.2.3.1 Differentiating between background and true fluorescence signals of recombinant MamK-cys by ultracentrifugation

Similar results to tryptophan fluorescence experiments conducted on recombinant MamK (Figures 6.7 a) were obtained for MamK-cys (Figures 6.10 a, 6.12 a). Changes in fluorescent signal were not observed after the addition of $MgCl_2$ but an immediate sharp increase in 90 ° light scattering that continued to increase over time was observed (Figures 6.10 b, 6.12 b). It appeared that the presence of pyrene was not affecting the ability of MamK-cys to fold and it was possible that levels of pyrene remaining in solution produced a background that might drown out any signal from fluorescently labelled MamK-cys (Figure 6.15). Labelling with rhodamine seemed to cause the protein to sediment completely out of solution during centrifugation Figure 6.16).

Centrifugation of pyrenyl MamK-cys at 543000 *x g* for 1 hr reduced the fluorescent signal of pyrenyl MamK-cys by a fifth of the pre-centrifuged sample (Figure 6.15). The fluorescent signals of the washed resuspended pellets of MamK-cys and pyrenyl MamK-cys, and pyrenyl MamK-cys supernatant after ultra-centrifugation at 543000 *x g* for 1 hr showed promising differences indicating the successful binding of pyrene to recombinant MamK-cys (Figure 6.18).

6.3.2.3.2 A MamK-cys dead end for understanding local structural changes in MamK

The addition of the cysteine residue to recombinant MamK induced self polymerisation of the protein (Figure 6.12 and 6.13). Ultracentrifugation shows that there is a likelihood that MamK-cys was labelled with pyrene but as this was

noticeable in the pelleted fraction indicating the protein had polymerised or denatured out of solution (Figure 6.16). It is difficult to depolymerise MamK (Figure 6.9; Section 6.2.3.5; Figure 6.17) and this presents difficulties in investigating the structural conformation of debris in the pelleted fraction to know whether or not the pyrene bound successfully. This question could be answered by TEM examination for the presence or absence of polymeric material but the purpose of labelling to read changes in fluorescent signal has been defeated unless there is an efficient way of depolymerising the protein without detaching the probe. The fluorescent signal given by the supernatant after ultracentrifugation remained at a level high enough to drown out the signal of pyrenyl MamK-cys after the addition of $MgCl_2$ (Figure 6.18).

6.3.3 Interactions of recombinant MamK with protein from *Magnetospirillum gryphiswaldense* MSR-1 crude cell extract

A preliminary attempt to get information regarding MamK interactions with proteins from *Magnetospirillum gryphiswaldense* MSR-1 was undertaken. A method was used to couple MamK to CNBr-activated Sepharose 4b to use as a matrix for binding proteins from *Magnetospirillum gryphiswaldense* MSR-1 crude cell extract to check for interactions with MamK. *Magnetospirillum gryphiswaldense* MSR-1 crude cell extract was loaded to the column of MamK coupled CNBr-activated beads and the protein was eluted with an ion gradient. Spectrophotometry readings and SDS-PAGE showed that protein concentrations were too low to be visible and silver staining also failed to show the presence of protein. Considering the volume of matrix used was so small (3.5 ml swollen gel) it is difficult to conclude what happened to the protein, whether the procedure to bind MamK to the sepharose was successful and if it was successful were there any protein-protein interactions that either bound irreversibly to the column or were at such low concentrations that they were not detected.

Protein-protein interactions are complex. Nearly one-third of all genes in various organisms encode membrane-associated proteins that participate in numerous protein-protein interactions important to the processes of life (Hooker *et al.*, 2007). MamK interaction with other *Magnetospirillum gryphiswaldense* MSR-1 proteins is an area that is ripe for further investigation. It is expected that due to the close

proximity of MamK to the magnetosome membrane and the role it plays in maintaining their linear position that it has interactions with membrane bound proteins *in vivo.* Membrane protein interactions pose significant challenges due to the need to solubilise membranes without disrupting protein–protein interactions (Hooker *et al.,* 2007). Traditionally, analysis of isolated protein complexes by high-resolution 2D gel electrophoresis has been the main method used to obtain an overall picture of proteome constituents and interactions. However, this method is time consuming, labour intensive, detects only abundant proteins and is limited with respect to the coverage required to elucidate large interaction networks. Hooker *et al.* (2007) review the application of various methods to elucidate interactions involving membrane proteins. The outlined techniques include methods for the direct isolation of single complexes or interactors as well as methods for characterisation of entire subcellular and cellular interactomes.

The interaction of MamK with MamJ was predicted to be the most likely of all interactions that MamK might have with associated magnetosome proteins. With further more detailed reference to work conducted on MamJ (Section 4.3.1), the construction of various truncated MamJ proteins enabling the mapping of essential regions of MamJ by assaying the potential of mutant proteins to restore magnetosome chain formation in a *mamJ* deletion strain was investigated (Scheffel and Schüler, 2007). During investigations evidence for physical interaction between MamJ and MamK were found and showed that the C- and N- terminal sequence regions of MamJ mediate interaction whereas the acidic repetitive domain of MamJ is dispensable for MamJ function under all tested conditions contrary to the model proposed earlier (Figure 4.5). Two-hybrid interaction analysis of MamJ and MamK were performed (Scheffel and Schüler, 2007) by means of a commercial version of a prokaryotic two-hybrid system developed by Dove *et al.* (1997). In this method one protein of the pair of interest is expressed as a C-terminal fusion with the bait *(mamJ)* fusion encoded on a plasmid while the other is fused to the C- terminus of a prey *(mamK)* fusion encoded on another plasmid. Recombinant bait and prey expression vectors are cotransformed into the *Escherichia coli* reporter strain for expression of the protein fusions. It is believed that C- and N- terminal sequence regions of MamJ

are essential for oligomerisation of MamK *in vivo* although this requires further clarification (Scheffel and Schüler, 2007).

7 CONCLUSION AND FURTHER INVESTIGATION

The aims of this thesis were to provide a comprehensive introduction to magnetic bacteria and bacterial cytoskeletal proteins, and to present novel results of *in vitro* behaviour of recombinant MamK from *Magnetospirillum gryphiswaldense* MSR-1 and to discuss the results in comparison to other work in the field.

MamK is highly conserved within magnetic bacteria (Chapter 3). MamK amino acid sequence groups into a clade that is evolutionarily distinct from other cytoskeletal proteins (Figures 3.1 and 3.2) yet analogously codes for active sites that are conserved in actin and MreB (Figure 3.4). Predictions of MamK amino acid sequence showed that it is closely comparable to predictions of actin and MreB (Figure 3.5) which was useful as methods used to characterise actin and MreB were found to be applicable to MamK.

During work contributing to this thesis MamK was purified to near homogeneity and preliminary *in vitro* biochemical characterisation using microscopy and light scattering was conducted. MamK was shown to refold in a monomeric form after dialysis with ATP, GTP or no NTP. This enabled studies of polymerisation and depolymerisation of MamK and comparisons with actin, other bacterial actin-like proteins, and *in vivo* observations of MamK (Komeilli *et al.*, 2006; Scheffel *et al.*, 2006; Scheffel and Schüler, 2007; Pradel *et al.*, 2006).

Light scattering increases were observed and found to be consistent with Mg^{2+}/Ca^{2+} dependent polymerisation. Partial depolymerisation was observed in the presence of EGTA but complete depolymerisation was not achieved under the conditions tested. Light scattering results suggest that the mechanism for polymerisation and depolymerisation of MamK differs from that of actin where the presence of NTP is required for polymerisation and the depolymerisation of actin is readily achievable on the addition of EGTA. Ion exchange chromatography suggested that the presence of ATP or GTP seemed to contribute to the maintenance of MamK in a soluble form, and under fluorescence and phase contrast microscopy ATP or GTP appeared to reduce the amount of sheet formation.

In vitro observations of MamK contrasted to *in vivo* observations in *Escherichia coli* (Pradel *et al.*, 2006) as MamK did not behave as dynamically under *in vitro* test conditions in this work. For example, once MamK polymerised and formed sheets the depolymerisation of MamK was not achieved using methods regularly used to depolymerise actin. In Section 6.3.2.1 it was suggested that there may be undiscovered accessory proteins that contribute to the dynamic behaviour of MamK *in vivo,* and that comparison of the appearance of MamK under various purification methods (Figures 5.3, 5.4, 5.6, 5.7 and 6.2) suggests that there may also be undiscovered conditions that contribute to a more dynamic behaviour of MamK *in vitro.* The dynamic behaviour of MamK filament formation in *Escherichia coli* (Pradel *et al.,* 2006) as a consequence of interference from proteolytic enzymes (Mornet and Ue, 1984; Carbonell and Villaverde, 2002) cannot be discounted either (Section 4.3.1). Discussion presented in Section 5.2.7 suggests that wild-type MamK does not easily depolymerise.

Through undertaking this work a number of ideas have arisen that are felt to be worth further investigation. The following paragraphs will make reference to the text in this thesis that gives a little background to these ideas in order to assist future development.

Magnetosome formation is an artefact of a greater benefit for iron sequestration in magnetic bacteria. The study of magnetosome formation has become a pursuit of the molecular biologist. As touched upon in sections 1.1.1 and 1.1.3 there is a lack of information in the available literature determining the ecological cues of magnetosome formation in magnetic bacteria *in situ.* Further work to examine the possibility that magnetosome formation is an artefact of a more meaningful reason to why bacteria invest so much in compartmentalising biomineralised iron within their cells would add novel information to the current literature regarding magnetosome formation. Further hypotheses for biomineralising iron may include storage in times of starvation, and compartmentalisation of toxic concentrations of iron (Section 1.1.4).

Repeat this work with MamK as expressed from the AMB-1 start site. MamK amino acid sequence comparison (Figure 3.3) indicates that the *Magnetospirillum magneticum* AMB-1 start site is the most likely for native MamK expression. Now that protocols have been set up to look at *Magnetospririllum gryphiswaldense* MSR-1 MamK as annotated it would be interesting to repeat the work with protein expressed from the AMB-1 start site.

Distinguish between the possibilities of one or two forms of MamK being expressed from pT7-7. During this work MamK was expressed from the MSR-1 start site meaning there is potential for protein to also be expressed from the AMB-1 start site, 13 codons downstream. If two forms of the protein have been expressed further work can be done to investigate whether one or other or both forms survived the purification process which may in turn strengthen or weaken the argument surrounding the correct start site of native MamK expression in *Magnetospirillum gryphiswaldense* MSR-1.

Structural characterisation of MamK. This work shows that MamK polymerises *in vitro* under certain conditions although the position of the subunits in these structures has not been solved (Sections 5.3.2 and 6.2.1). More work is required to understand the structure of MamK and its interaction with other subunits. Further work using TEM, crystallisation, light scattering and fluorescence techniques is required to elucidate the process of polymerisation of MamK in more molecular detail.

Direct experimental comparison of MamK to actin and MreB. MamK is a bacterial actin-like protein (or "bactin" as coined by Dr. Chris French) so it is expected that it has similar features to other proteins in the same family. Cooper *et al.* (1983) have described how the properties of actin have been characterised under various conditions using criteria such as (1) time course of polymerisation; (2) elongation rate constants; (3) intrinsic viscosity; and (4) critical concentration. This work is at the beginning of understanding MamK under these criteria (Section 6.2.2.1). Direct experimental comparison of MamK to actin and MreB was considered throughout this work and was set aside until the biochemistry of MamK was better understood.

There is much work to be done to understand the biochemistry of MamK, which may then be compared and contribute information to the understanding of actin and other bacterial actin-like proteins.

MamK interacts with accessory proteins to polymerise *in vivo*. Scheffel and Schüler (2007) give preliminary results showing interactions between MamK and MamJ (Section 4.3.1). *In vivo* results show that MamK is expressed separate to the magnetosome membrane and is eventually drawn closer to the magnetosome membrane where it interacts with MamJ to keep the magnetosomes in alignment. The interaction of MamK with accessory proteins other than MamJ has not been discounted. It has been shown here that MamK polymerises into filaments (Figures 5.3, 5.4, 5.7 and 6.1) and large sheets (Figures 5.7, 6.2, 6.3, 6.4, 6.5 and 6.6), whilst MamK has been shown to polymerise into filaments *in vivo* (Figure 4.2 and Komeilli *et al.,* 2006; Pradel *et al.,* 2006). Actin interacts with accessory proteins that help determine its form and role *in vivo* (Section 1.3.1). It may be that MamK also interacts with accessory proteins to assist in guiding the form and the role that the polymers take. MamK has a homologue in the *Deltaproteobacterium* MLMS-1 that may undertake a different role depending on accessory proteins present in the cell (Section 3.2.1). MamK may have concentration limited accessory proteins required to restrict polymerisation.

In conclusion this work presents strong evidence supporting the characterisation of MamK as a novel bacterial cytoskeletal protein and in so doing complements the contemporary understanding of the *in vivo* function of MamK in magnetic bacteria.

8 REFERENCES

Aebi, U., Walter, E. F., Isenberg, G., Pollard, T. D., and Smith, P. R., 1981. Crystalline actin sheets: their structure and polymorphism, *The Journal of Cell Biology*, **91:** 340-351.

Alberts, B., Bray, D., Lewis, J., Raff, M., Roberts, K., and Watson, J.D., 1999. Molecular biology of the cell (Third Edition), *Garland Publishing New York*, pp 916-917.

Aleem, A., Isar, J., and Malik, A., 2003. Impact of long-term application of industrial wastewater on the emergence of resistance traits in *Azotobacter chroococcum* isolated from rhizospheric soil, *Bioresource Technology,* **86:** 7– 13.

Altschul, S.F., Gish, W., Miller, W., Myers, E.W., and Lipman, D.J., 1990. Basic local alignment search tool, *Journal of Molecular Biology*, **215:** 403-410.

Arakaki, A., Webb, J., and Matsunaga, T., 2003. A novel protein tightly bound to bacterial magnetic particles in *Magnetospirillum magneticum* strain AMB-1, *Journal of Bacteriology*, **278:** 8745-8750.

Bagg, A., and Neilands, J.B., 1987. Molecular mechanism of regulation of siderophore-mediated iron assimilation, *Microbiological Reviews*, **51:** 509-518.

Balkwill, D. L., Maratea, D., and Blakemore, R. P., 1980. Ultrastructure of a magnetotactic spirillum, *Journal of Bacteriology*, **141:** 1399-1408.

Bauer, G.B., Fuller, M., Perry, A., Dunn, J. R., and Zoeger, J. 1985. Magnetoreception and biomineralisation of magnetite in Cetaceans, *In: Kirschvink, J.L., Jones, D.S., MacFadden, B.J. Eds., Magnetite biomineralisation and magnetoreception in organisms, Plenum Press, New York*, pp 489-507.

Bazylinski, D. A., 1999. Synthesis of the bacterial magnetosome: the making of a magnetic personality, *International Microbiology*, **2:** 71-80.

Bazylinski, D. A., and Blakemore, R. P., 1983. Denitrification and assimilatory nitrate reduction in *Aquaspirillum magnetotacticum, Applied Environmental Microbiology*, **46** (5): 1118-1124.

Bazylinski, D. A., and Frankel, R. B., 2004. Magnetosome formation in prokaryotes, *Nature Reviews Microbiology*, **2:** 217-230.

Bazylinski, D. A., Frankel, R. B., and Jannasch, H.W., 1998. Anaerobic magnetite production by a marine magnetotactic bacterium, *Nature*, **334:** 518-519.

Bazylinski, D. A., Frankel, R. B., Heywood, B. R., Mann, S., King, J. W., Donaghay, P. L., and Hanson, A. K., 1995. Controlled biomineralisation of magnetite (Fe_3O_4) and greigite (Fe_3S_4) in a magnetotactic bacterium, *Applied Environmental Microbiology*, **61** (9): 3232–3239.

Bazylinski, D. A., Schlesinger, D. R., Howes, B. H., Frankel, R. B., and Epstein, S. S., 2000. Occurrence and distribution of diverse populations of magnetic protests in a chemically stratified coastal salt pond, *Chemical geology*, **169** (3-4): 319-328.

Begg, K., Nikolaichik, Y., Crossland, N., and Donachie, W. D., 1998. Roles of FtsA and FtsZ in activation of division sites, *Journal of Bacteriology*, **180** (4): 881–884.

Bell, P. E., Mills, A. E., and Herman, S. J., 1987. Biogeochemical conditions favoring magnetite formation during anaerobic iron reduction, Applied Environmental Microbiology, **53:** 2610-2616.

Berquo, T. S., Thompson, R., and Partiti, C. S. M., 2004. Magnetic study of Brazilian peats from Sao Paulo state, Geoderma, **118:** 223-243.

Bertani, L. E., Huang, J. S., Weir, B. A., and Kirschvink, J. L., 1997. Evidence for two types of subunits in the bacterioferritin of Magnetospirillum magnetotacticum, Gene, **201:** 31-36.

Bertani, L. E., Weko, J., Phillips, K. V., Gray, R. F., and Kirschvink, J. L., 2001. Physical and genetic characterisation of the genome of *Magnetospirillum magnetotacticum*, strain, MS-1, *Gene*, **264:** 257-263.

Bi, E., and Lutkenhaus, J., 1992. Genetics of bacterial cell division, *In: S. Mohan, C. Dow, and J. A. Cole (ed.), Bacterial structure and function: a new perspective, Cambridge University Press, Cambridge*, pp 123–152.

Bisio, G., Rubatto, G., and Schiapparelli, P., 1999. Magnetic systems depending on three or two variables; thermodynamic analysis and some existing and possible applications, *Energy Conversion and Management*, **40** (12): 1267-1286.

Blakemore, R. P., 1975. Magnetotactic bacteria, *Science*, **190:** 377-385.

Blakemore, R. P., Frankel, R. B., and Kalmijn, Ad. J., 1980. South-seeking magnetotactic bacteria in the Southern Hemisphere, *Nature*, **286:** 384 – 385.

Blakemore, R. P., Short, K. A., Bazylinski, D. A., Rosenblatt, C., and Frankel, R. B., 1985. Microaerobic conditions are required for magnetite formation within *Aquaspirillum magnetotacticum, Geomicrobiology Journal,* **4:** 53–71.

Blatch, G. L., and Lässle, M., 1999. The tetracopeptide repeat: a structural motif mediating protein-protein interactions, *BioEssays*, **21:** 932-939.

Bork, P., Sander, C., and Valencia, A., 1992. An ATPase domain common to bacterial cell cycle proteins sugar kinases, actin and hsp70 heat shock proteins. *Proceeding of the National Academy of Science*, **89:** 7290-7294.

Bramhill, D., and Thompson, C. M., 1994. GTP-dependent polymerisation of *Escherichia coli* FtsZ protein to form tubules, *Proceedings of the National Academy of Science USA*, **91:** 5813-5817.

Buehler, E. R., and Wasilewski, P. J., 1985. Magnetic remanence in bats, *In: Kirschvink, J.L., Jones, D.S., MacFadden, B.J. Eds., Magnetite biomineralisation and magnetoreception in organisms, Plenum Press, New York,* pp 483-488.

Burgess, J. G., Kawaguchi, R., Sakaguchi, T., Thornhill, R. H., and Matsunaga, T., 1993. Evolutionary relationships among *Magnetospirillum* strains inferred from phylogenetic analysis of 16S rDNA sequences, *Journal of Bacteriology*, **175:** 6689-6694.

Burstein, E. A., Vedenkina, N. S., and Ivkova, M. N., 1973. Fluorescence and the location of tryptophan residues in protein molecules, *Photochemistry and Photobiology*, **18:** 263-279.

Buseck, P. R., Dunin-Borkowski, R. E., Devouard, B., Frankel, R. B., McCartney, M. R., Midgley, P. A., Posfai, M., and Weyland, M., 2001. Magnetite morphology and life on Mars, *Proceedings of the National Academy of Sciences of the United States of America,* **98** (24)**:** 13490 – 13495.

Buskirk, R. E., and O'Brien Jr., W. P., 1985. Magnetic remanence response to magnetic fields in Crustacea, *In: Kirschvink, J.L., Jones, D.S., MacFadden, B.J. Eds., Magnetite biomineralisation and magnetoreception in organisms, Plenum Press, New York*, pp 365-384.

Calugay, R. J., Miyashita, H., Okamura, Y., and Matsunaga, T., 2003. Siderophore production by the magnetic bacterium *Magnetospirillum magneticum* AMB-1, *FEMS Microbiology Letters,* **218:** 371-375.

Carbonell, X., and Villaverde, A., 2002. Protein aggregated into bacterial inclusion bodies does not result in protection from proteolytic digestion, *Biotechnology Letters*, **24:** 1939-1944.

Casella, J. F., Maack, D. J. and Lin, S., 1986. Purification and initial characterisation of a protein from skeletal muscle that caps the barbed ends of actin polymers, *Journal of Biological Chemistry,* **261:** 10915-10921.

Chalfie, M., Tu, Y., Euskirchen, G., Ward, W. W., and Prasher, D. C., 1994. Green fluorescent protein as a marker for gene expression, *Science,* **263:** 802-805.

Chang, S. B. R., Kirschvink, J. L., and Stolz, J. F., 1987. Biogenic magnetite as a primary remanence carrier in limestone deposits, *Earth and Planetary Science Letters,* **46** (1-3): 289-303.

Chang, S-B. R., and Kirschvink, J. L., 1989. Magnetofossils, the magnetisation of sediments, and the evolution of magnetite biomineralisation, *Annual Review of Earth and Planetary Sciences*, **17:** 169-95.

Chang, S-B. R., and Kirschvink, J.L., 1989. Magnetofossils, the magnetisation of sediments, and the evolution of magnetite biomineralisation, *Annual Review of Earth and Planetary Sciences*, **17:** 169-95.

Chenna, R., Sugawara, H., Koike, T., Lopez, R., Gibson, T. J., Higgins, D. G., and Thompson, J. D, 2003. Multiple sequence alignment with the Clustal series of programs, *Nucleic Acids Research*, **31** (13): 3497-500.

Cooper, J. A., Walker, S., and Pollard, T., 1983. Pyrene actin: documentation of the validity of a sensitive assay for actin polymerisation, *Journal of Muscle Research and Cell Motility*, **4:** 253-262.

Cornell, R. M., and Schwertmann, U., 2003. The iron oxides: Structure, properties, reactions, occurrences and uses, 2nd Edition, Wiley, Weinheim, Germany

Crosbie, R. H., Miller, C., Cheung, P., Goodnight, T., Muhlrad, A., and Reisler, E., 1994. Structural connectivity in actin: effect of C-terminal modifications on the properties of actin, *Biophysical Journal*, **67:** 1957-1964.

Daniel, R. A., and Errington, J., 2003. Control of cell morphogenesis in bacteria: Two distinct ways to make a rod-shaped cell, *Cell*, **113** (6): 767-776.

Davanloo, P., Rosenberg, A. H., Dunn, J. J., and Studier, F. W., 1984. Cloning and expression of the gene for bacteriophage T7 RNA polymerase, *Proceedings of the National Academy of Sciences of the United States of America,* **81:** 2035–2039.

Davis, W. L., and McKay, C.P., 1996. Origins of life: a comparison of theories and application to Mars, *Origins of Life and Evolution of the Biosphere,* **26:** 61-73.

de Boer, P. A. J., Cook, W. R., and Rothfield, L. I., 1990. Bacterial cell division, *Annual Review of Genetics*, **24:** 249–274.

De Long, E. F., Frankel, R. B., and Bazylinski, D. A., 1993. Multiple evolutionary origins of magnetotaxis in bacteria, *Science*, **259:** 803-806.

Dean, A. J., and Bazylinski, D. A, 1999. Genome analysis of several marine magnetic bacterial strains by pulsed-filed gel electrophoresis, *Current Opinion in Microbiology*, **39:** 219-225.

Dewar, S. J., Begg, K. J., and Donachie, W. D., 1992. Inhibition of cell division initiation by an imbalance in the ratio of FtsA to FtsZ, *Journal of Bacteriology*, **174:** 6314–6316.

Doi, M., Wachi, M., Ishino, F., Tomioka, S., Ito, M., Sakagami, Y., Suzuki, A., and Matsuhashi, M., 1988. Determinations of the DNA sequence of the *mreB* gene and of the gene products of the *mre* region that function in formation of the rod shape of *Escherichia coli* cells, *Journal of Bacteriology*, **170:** 4619–4624.

Dove, S. L., Joung, J. K., and Hochschild, A., 1997. Activation of prokaryotic transcription through arbitrary protein-protein contacts, *Nature*, **386:** 627-630.

Doyle, T. C., Hansen, J. E., and Reisler, E., 2001. Tryptophan fluorescence of yeast actin resolved via conserved mutations, *Biophysics Journal*, **80 (1):** 427-434.

Dubbels, B. L., DiSpirito, A. A., Morton, J. D., Semrau, J. D., Neto1, J. N. E., and Bazylinski, D. A., 2004. Evidence for a copper-dependent iron transport system in the marine, magnetotactic bacterium strain MV-1, *Microbiology*, **150**, 2931-2945.

Eftink, M. R., and Ghiron, C. A., 1976. Exposure of tryptophanyl residues in proteins. Quantitative determination by fluorescence quenching studies, *Biochemistry*, **15:** 672-680.

Eftink, M. R., and Ghiron, C. A., 1977. Exposure of tryptophanyl residues and protein dynamics, *Biochemistry*, **16:** 5546-5551.

Egelman, E. H., 2003. Actin's bacterial homologues , *Current Opinion in Structural Biology,* **13:** 244-248.

Egelman, E. H., Francis, N., and DeRosier, D. J., 1982. F-actin is a helix with a random variable twist, *Nature*, **298:** 131-135.

Esue, O., Cordero, M., Wirtz, D., and Tseng, Y., 2005. The assembly of MreB, a bacterial homologue of actin, *The Journal of Biological Chemistry*, **280:** 2628-2635.

Farina, M., Esquivel, D. M. S., and Lins de Barros, H. G. P., 1990. Magnetic iron-sulphur crystals from a magnetotactic microorganism, *Nature*, **343:** 256-258.

Feucht, A., Lucet, I., Yudkin, M. D., and Errington, J., 2001. Cytological and biochemical characterisation of the FtsA cell division protein of *Bacillus subtilis, Molecular Microbiology,* **40** (1): 115-125.

Flatman, P. W., 1984. Magnesium transport across cell membranes, *Journal of Membrane Biology*, **80:** 1-14.

Frankel, R. B., and Bazylinski, D.A., 2001. Magnetotaxis: microbial. *In: Electronic Encyclopaedia of the Life Sciences, Nature Publishing Group, London, www.els.net.*

Frankel, R.B., Papaefthymiou, G. G., Blakemore, R. P., O'Brien, W., 1983. Fe_3O_4 precipitation in magnetotactic bacteria, *Biochimica Biophysica Acta*, **763:** 147-159.

Funaki, M., Sakai, H., and Matsunaga, T., 1989. Identification of the magnetic poles on strong magnetic grains from meteorites using magnetotactic bacteria, *Journal of Geomagnetism and Geoelectricity,* **41** (1): 77-87.

Gorby, Y. A., Beveridge, T. J., and Blakemore, R. P., 1988. Characterisation of the bacterial magnetosome membrane, *Journal of Bacteriology*, **170:** 834-841.

Gould, J. L., Kirschvink, J. L., Deffeyes, K. S. 1978. Bees have magnetic remanence, *Science,* **201:** 1026-1028.

Graceffa, P., and Dominguez, R., 2003. Crystal Structure of Monomeric Actin in the ATP State: Structural basis of nucleotide-dependent actin dynamics, *Journal of Biological Chemistry*, **278** (36): 34172-34180.

Grossman, M. J., Hinton, S. M., Minak-Bernero, V., Slaughter, C., and Stiefel, E. I., 1992. Unification of the ferritin family of proteins, *Proceedings of the National Academy of Sciences*, **89:** 2419-2423.

Grünberg, K., Müller, E.-C., Otto, A., Reszka, R., Linder, D., Kube, M., Reinhardt, R., and Dirk Schüler, D., 2004. Biochemical and proteomic analysis of the magnetosome membrane in *Magnetospirillum gryphiswaldense*, *Applied and Environmental Microbiology*, **70** (2): 1040-1050.

Grünberg, K., Wawer, C., Tebo, B.M., Schüler, D., 2001. A large gene cluster encoding several magnetosome proteins is conserved in different species of magnetotactic bacteria, *Applied and Environmental Microbiology*, **67** (10): 4573-4582.

Gudmundsson, G. A., and Sandberg, R., 2000. Sanderlings (*Calidris alba*) have a magnetic compass: Orientation experiments during spring migration in Iceland, *Journal of Experimental Biology* [print], **203** (20): 3137-3144.

Guerinot, M. L., 1994. Microbial iron transport, *Annual Review of Microbiology*, **48:** 743-72.

Haas, J., Park, E. -C., and Seed, B., 1996. Codon usage limitation in the expression of HIV-1 envelope glycoprotein, *Current Biology,* **6:** 315-324.

Halliburton, W. D., 1887. On muscle plasma, *Journal of Physiology*, **8:** 133.

Handrick, R., Reinhardt, S., Schultheiss, D., Reichart, T., Schuler, D., Jendrossek, V., Jendrossek, D., 2004 a. Unraveling the function of the *Rhodospirillum rubrum* activator of polyhydroxybutyrate (PHB) degradation: the activator is a PHB-granule-bound protein (phasin), *Journal of Bacteriology,* **186** (8): 2466-2475.

Handrick, R., Technow, U., Reichart, T., Reinhardt, S., Sander, T., Jendrossek, D., 2004 b. The activator of the *Rhodospirillum rubrum* PHB depolymerase is a polypeptide that is extremely resistant to high temperature (121C) and other physical or chemical stresses, *FEMS Microbiology Letters,* **230:** 265-274.

Hartmann, A., and Braun, V., 1981. Iron uptake and iron limited growth of *Escherichia coli* K-12, *Archives of Microbiology*, **130:** 353-356.

Higgins D., Thompson J., Gibson T., Thompson, J. D., Higgins, D. G., and Gibson, T. J., 1994. CLUSTAL W: improving the sensitivity of progressive multiple sequence alignment through sequence weighting, position-specific gap penalties and weight matrix choice, *Nucleic Acids Research*, **22:** 4673-4680.

Hoeft, S. E., Kulp, T. R., Stolz, J. F., Hollibaugh, J. T., Oremland, R. S., 2004. Dissimilatory arsenate reduction with sulfide as electron donor: Experiments with Mono Lake water and isolation of strain MLMS-1, a chemoautotrophic arsenate-respirer, *Applied and Environmental Microbiology,* **70:** 2741-2747.

Holmes, K. C., Popp, D., Gebhard, W., Kabsch, W., 1990. Atomic model of the actin filament, *Nature*, **347:** 44–49.

Hooker, B. S., Bigelow, D. J., Lin, C.-T., 2007. Methods for mapping of interaction networks involving membrane proteins, *Biochemical and Biophysical Research Communications*, **363:** 457–461.

Hrabak, E.M., and Willis, D.K., 1992. The *lemA* gene required fro pathogenicity of *Pseudomonas syringae* pv. syringae on bean is a member of a family of two-component regulators, *Journal of Bacteriology*, **174** (9): 3011-3020.

Yijun Huang, Y., Zhang, W., Jiang, W., Rong, C., and Li, Y., 2007. Disruption of a *fur* -like gene inhibits magnetosome formation in *Magnetospirillum gryphiswaldense* MSR-1, *Biochemistry (Moscow)*, **72** (11): 1532-1539.

Inouye, S., and Tsuji, F. I., 1994. *Aequorea* green fluorescent protein: Expression of the gene and fluorescent characteristics of the recombinant protein, *FEBS Letters* **341:** 277-280.

Jeon, K. W., 1987. Change of Cellular "Pathogens" into Required Cell Components, *Annals of the New York Academy of Sciences,* **503** (1): 359–371.

Jeon, K. W., 2000. Bacterial endosymbiosis in bacteria, *Trends in Cell Biology,* **5** (3): 137-140.

Jensen, R. B., and Gerdes, K., 1997. Partitioning of plasmid R1. The ParM protein exhibits ATPase activity and interacts with the centromere-like ParR-*parC* complex, *Journal of Molecular Biology*, **269** (4): 505-513.

Jones, L. J. F., Carballido-Lopez, R., Errington, J., 2001. Control of cell shape in bacteria: helical, actin-like polymers in *Bacillus subtilis*, *Cell*, **104:** 913-922.

Jumas-Bilak, E., Michaux-Charachon, S., Bourg, G., Ramuz, M., and Allardet-Servent, A., 1998. Unconventional genomic organisation in the alpha subgroup of the Proteobacteria, *Journal of Bacteriology*, **180** (10): 2749-2755.

Junge, K., Lang, C., and Schüler, D., 2006. MamM and MamB are magnetosome-associated CDF proteins involved in magnetosome-directed iron transport, *American Society for Microbiology 106th general meeting, May 21st – 25th 2006, Orlando, Florida, USA, http://ieg.ou.edu/ASM2006/data/papers/K_065.htm.*

Kabsch, W., and Holmes, K. C., 1995. Protein motifs 2. The actin fold. *The Federation of American Societies for Experimental Biology Journal,* **9:** 167–174.

Kimchi, E., and Terkel, J., 2001. Magnetic compass orientation in the blind mole rat *Spalax ehrenbergi*, *Journal of Experimental Biology* [print], **204** (4): 751-758.

Kirschivnk, J. L., Walker, M. M., and Diebel, C. E., 2001. Magnetite based magnetoreception, *Current Opinion in Neurobiology,* **11:** 462-467.

Kirschvink J. L., Jones, D. S., and MacFadden, B. J., 1985 a. Magnetite biomineralisation and magnetoreception in organisms: a new biomagnetism, *Kirschvink J. L., Jones, D. S., and MacFadden, B. J., eds. New York, Plenum, pp 682.*

Kirschvink, J. L., 1981. Ferromagnetic crystals (magnetite?) in human tissue. *Journal of Experimental Biology*, **92:** 333-335.

Kirschvink, J. L., 1982. Paleomagnetic evidence for fossil biogenic magnetite in western Crete, *Earth and Planetary Sciences Letters*, **59** (2): 388-392.

Kirschvink, J. L., 1997. Magnetoreception: Homing in on vertebrates, Nature, **390:** 339-340.

Kirschvink, J. L., and Chang, S. B. R., 1984. Ultrafine-grained magnetite in deep-sea sediments - possible bacterial magnetofossils, *Geology*, **12** (9): 559-562.

Kirschvink, J. L., and Gould, J. L., 1981. Biogenic magnetite as a basis for magnetic direction in animals, *Biosystems,* **13:** 181-201.

Kirschvink, J. L., and Walker, M. M., 1986. Biogenic magnetite in higher organisms and the current state of the hypothesis of ferromagnetic magnetoreception, In: *Biophysical effects of steady magnetic fields workshop; Springer Proceedings in Physics,* 180-188.

Kirschvink, J. L., and Weiss, B. P., 2002. Mars, panspermia, and the origin of life: Where did it all begin? *Palaeolontogia Electronica,* **4** (2): 8-15.

Kirschvink, J. L., Dizon, A. E., and Westphal, J. A., 1985 b. Evidence from strandings for geomagnetic sensitivity in cetaceans, *Journal of Experimental Biology*, **120:** 1-24.

Kirschvink, J. L., Walker, M. M., Chang, S. B., Daizon, A. E., and Peterson, K. A., 1985 c. Chains of single-domain magnetite particles in chinook salmon, *Oncorhynchus tshawytscha, Journal of Comparative Physiology A: Neuroethology, Sensory, Neural, and Behavioral Physiology,* **157** (3): 375-381.

Kirschvink, J.L., Kobayashi-Kirschvink, A., and Woodford, B. J., 1992. Magnetite biomineralisation in the human brain, *Proceedings of the National Academy of Science* of the United States of America, **89:** 7683-7687.

Komeili, A., Vali, H., Beveridge, T. J., and Newman, D. K., 2004. Magnetosome vesicles are present before magnetite formation, and MamA is required for their activation, *Proceedings of the National Academy of Sciences of the United States of America*, **101** (11): 3839-3844.

Komeili, A., Zhuo L., Newman, D. K., Jensen, G. J., 2006. Magnetosomes are cell membrane invaginations organised by the actin-like protein MamK, *Science*, **311** (5758): 242 – 245.

Korn, E. D., Carlier, M.-F., and Pantaloni, D., 1987. Actin polymerisation and ATP hydrolysis, *Science*, **238:** 638–644.

Kovach, M. E., Elzer, P. H., Hill, D. S., Robertson, G. T., Farris, M. A., Roop II, R. M., and Peterson, K. M., 1995. Four new derivatives of the broad-host-range cloning vector pBBR1MCS, carrying different antibiotic-resistance cassettes, *Gene,* **166:** 175-176.

Lankford, C. E., 1973. Bacterial assimilation of iron, *Critical Reviews in Microbiology*, **2:** 273-331.

Lara, B., Rico, A. I., Petruzzelli, S., Santona, A., Jacques Dumas, J., Biton, J., Vicente, M., Mingorance, J., and Massidda, O., 2005. Cell division in cocci: localisation and properties of the *Streptococcus pneumoniae* FtsA protein, *Molecular Microbiology*, **55** (3): 699-711.

Leavitt, J., 2005. Actin – An ageless protein with an intelligent design, *Online in: http://blog.nerac.com/2005/08/25/actin-%E2%80%93%-an-ageless-protein-with-an-intelligent-design/*

Li, W., Yu, L., Zhou, P., and Zhu, M., 2007. A Magnetospirillum strain WM-1 from a freshwater sediment with intracellular magnetosomes, *World Journal of Microbiology and Biotechnology,* **23** (10): 1489-1492.

Lins, U., and Farina, M., 1999. Organisation of cells in magnetotactic multicellular aggregates, *Microbiological Research*, **154** (1): 9-13.

Liu, S. V., Zhou, J., Zhang, C., Cole, D. R., Gajdarziska-Josifovska, M., and Phelps, T. J., 1997. Thermophilic Fe(III)-Reducing Bacteria from the Deep Subsurface: The Evolutionary Implications, *Science*, **277** (5329): 1106 – 1109.

Llamas, I., Argandon˜a, M., Quesada, E., and del Moral, A., 2000. Transposon mutagenesis in *Halomonas eurihalina. Research in Microbiology.* **151:** 13– 18.

Llorca, O., Martin-Benito, J., Ritco-Vonsocici, M., Grantham, J., Hynes, G. M., Willison, K. R., Carrascosa, J. L., and Valpuesta., J. M., 2000. Eukaryotic chaperonin CCT stabilises actin and tubulin folding intermediates in open quasi-native conformations, *The European Molecular Biology Organisation (EMBO) Journal*, **19:** 5971-5979.

Lohman, K. J., and Johnsen, S., 2000. The neurobiology of magnetoreception in vertebrate animals, *Trends in Neurosciences*, **23** (4): 153-159.

Lovlie, R., and Larsen, E., 1981. Paleomagnetism and magnetomineralogy of a holocene lake sediment from Vagsoy, western Norway, *Physics of the Earth and Planetary Interiors,* **27** (2): 143-150.

Lovley, D. R., Stolz, J. F., Nord, G. L. Jr., Phillips, E. J. P. 1987. Anaerobic Production of Magnetite by a Dissimilatory Iron-Reducing Microorganism, *Nature,* **330** (6145): 252-254.

MacFadden, B. J., and Jones, D. S., 1985. Magnetic butterflies: a case study of the Monarch (*Lepidoptera, Danaidae*).*In: Kirschvink, J.L., Jones, D.S., MacFadden, B.J. Eds., Magnetite biomineralisation and magnetoreception in organisms. Plenum Press, New York, pp 407-416.*

Mann, S., and Frankel, R. B., 1989. In: *Biomineralisation: Chemical and Biochemical Perspectives*, eds. Mann, S., Webb, J., And Williams, R. J. P., pp 389-426, VCH Publishers, New York.

Mann, S., Sparks, N. H. C., Frankel, R. B., Bazylinski, D. A., and Jannasch, H. W., 1990. Biomineralisation of ferrimagnetic greigite (Fe_3S_4) and iron pyrite (FeS_2) in a magnetotactic bacterium, *Nature*, **343:** 258-261.

Mann, S., Sparks, N. H. C., Walker, M. M., and Kirschvink, J. L., 1988. Ultrastructure and characterisation of anisotropic magnetic inclusions in

magnetotactic bacteria. *Proceedings of the Royal Society of London Series B,* **231:** 477-487.

Margulis, L., and Sagan, D., 1997. Microcosmos. *University of California Press, Ltd. Berkeley, Los Angeles and London, pp. 103-104, 121-123*

Martin, A. C., Welch, M. D., and Drubin, D. G., 2006. Arp2/3 ATP hydrolysis-catalysed branch dissociation is critical for endocytic force generation, *Nature Cell Biology*, **8:** 826-833.

Mather, J. G., 1985. Magnetoreception and the search for magnetic material in rodents, *In: Kirschvink, J.L., Jones, D.S., MacFadden, B.J. Eds., Magnetite biomineralisation and magnetoreception in organisms. Plenum Press, New York, pp 509-536.*

Matsunaga, T., and Okamura, Y., 2003. Genes and proteins involved in bacterial magnetic particle formation, *Trends in Microbiology*, **11:** 536-541.

Matsunaga, T., and Tsujimura, N., 1993, Respiratory inhibitors of a magnetic bacterium *Magnetospirillum* sp. AMB-1 capable of growing aerobically, *Applied Microbiology and Biotechnology,* **39:** 368–371.

Matsunaga, T., Nakamura, C., Burgess, J. G., and Sode, K., 1992. Gene transfer in magnetic bacteria: transposon mutagenesis and cloning of genomic DNA fragments required for magnetosome synthesis, *Journal of Bacteriology,* **174** (9)**:** 2748-2753.

Matsunaga, T., Sakaguchi, T., and Tadokoro, F., 1991. Magnetite formation by a magnetic bacterium capable of growing aerobically, *Applied Microbiology and Biotechnology,* **35:** 651-655.

Matsunaga, T., Suzukia, T., Tanakaa, M., Arakakia, A., 2007. Molecular analysis of magnetotactic bacteria and development of functional bacterial magnetic particles for nano-biotechnology, *Trends in Biotechnology*, **25** (4)**:** 182-188.

Matsunaga, T., Tsujimura, N., and Kamiya.S., 1997. Genetic analysis of biomagnetic crystal formation, *Journal Physique IV*, **7:** 651-654.

Matsunaga, T., Tsujimura, N., Okamura, Y., and Takeyama, H., 2000. Cloning and characterisation of a gene, *mpsA*, encoding a protein associated with intracellular magnetic particles from *Magnetospirillum* sp. Strain AMB-1, *Biochemical and Biophysical Research Communications,* **268** (3)**:** 932-937.

McCrea, W. H., 1981. Long time-scale fluctuations in the evolution of the earth, *Proceedings of the Royal Society of London Mathematics,* **375** (1760): 1-41.

McLaughlin, P. J., Gooch, J. T., Mannherz, H. G., and Weeds, A. G., 1993. Structure of gelsolin segment-1-actin complex and the mechanism of filament severing, *Nature*, **364:** 685-692.

Meldrum, F. C., Mann, S., Heywood, B. R., Frankel, R. B., and Bazylinski, D. A., 1993. Electron microscopy study of magnetosomes in two cultured vibrioid magnetotactic bacteria, *Proceedings of the Royal Society of London Series B,* **251:** 237-242.

Meldrum, Fiona C., Stephen Mann, Brigid R. Heywood, Richard B. Frankel, Dennis A. Bazylinski, 1993. Electron microscopy study of magnetosomes in two cultured coccoid magnetotactic bacteria, *Proceedings of the Royal Society of London Series B,* **251:** 231-236.

Moench, T.T., 1988. *Bilophococcus magnetotacticus* gen. nov. Sp. nov., a motile, magnetic coccus, *Antonie van Leeuwenhoek,* **54** (6): 483-496.

Mogensen, J., Klausen, I. C., Pedersen, A. K., Egeblad, H., Bross, P., Kruse, T. A., Gregersen, N., Hansen, P. S., Baandrup, U., and Børglum, A. D., 1999. α-cardiac actin is a novel disease gene in familial hypertrophic cardiomyopathy, *The Journal of Clinical Investigation,* **103** (10): 39–43.

Møller-Jensen, J., Jensen, R. B., Löwe, J., Gerdes, K., 2002. Bacterial DNA segregation by an actin-like filament, *The European Molecular Biology Organisation Journal,* **21** (12): 3119-3127.

Mora, C. V., Davison, M., Wild, J. M., and Walker, M. M., 2004. Magnetoreception and its trigeminal mediation in the homing pigeon, *Nature*, **432:** 508-511.

Mornet, D., and Ue., K., 1984. Proteolysis and structure of skeletal muscle actin, *Proceedings of the National Academy of Sciences, USA,* **81:** 3680-3684.

Mukherjee, A., and Lutkenhaus, J., 1994. Guanine nucleotide-dependent assembly of FtsZ into polymers, *Journal of Bacteriology*, **176:** 2754-2758.

Nakamura, C., Burgess, J. G., Sode, K., and Matsunaga, T., 1995a. An iron-regulated gene, *magA*, encoding an iron transport protein of *Magnetospirillum* sp. strain AMB-1, *Journal of Biological Chemistry*, **270** (47): 28392-28396.

Nakamura, C., Kikuchi, T., Burgess, J. G., and Matsunaga, T., 1995b. Iron-regulated expression and membrane localisation of the MagA protein in *Magnetospirillum* sp. Strain AMB-1, *Journal of Biochemistry*, **118** (1): 23-27.

Nakamura, C., Sakaguchi, T., Kudo, S., Burgess, J. G., Sode, K., and Matsunaga, T., 1993. Characterisation of iron uptake in the magnetic bacterium *Aquaspirillum* sp. AMB-1, *Applied Biochemistry and Biotechnology,* **39/40:** 169-176.

Nakamura, N., and Matsunaga, T., 1993. Highly sensitive detection of allergen using bacterial magnetic particles, *Analytica Chimica Acta,* **281:** 585-589.

Nakamura, N., Hashimoto, K., and Matsunaga, T., 1991. Immunoassay method for the determination of immunoglobulin G using bacterial magnetic particles, *Analytical Chemistry,* **63:** 268-272.

Nielands, J. B., 1984. Methodology of siderophores, Structural Bonding, **58:** 1-24.

Noguchi, Y., Fujiwara, T., Yoshimatsu, K. and Fukumori, Y., 1999. Iron reductase for magnetite synthesis in the magnetotactic bacterium *Magnetospirillum magnetotacticum, Journal of Bacteriology,* **181:** 2142-2147.

Norris, V., Grant, S., Freestone, P., Canvin, J., Sheikh, F. N., Toth, I., Trinei, M., Modha, K., and Norman, R. I., 1996. Calcium signalling in bacteria, *Journal of Bacteriology,* **178** (13): 3677-3682.

Ochman, H., Lawrence, J. G., and Grossman, E. A., 2000. Lateral gene transfer and the nature of bacterial innovation, *Nature,* **405:** 299-304.

Okamura, Y., Takeyama, H., and Matsunaga, T., 2001. A magnetosome specific GTPase from the magnetic bacterium *Magnetospirillum magneticum* AMB-1, *Journal of Biological Chemistry,* **276:** 48183-48188.

Okuda, Y., and Fukamori, Y., 2001. Expression and characterisation of a magnetosome-associated protein, TPR-containing MAM22, in *Escherichia coli, FEBS Letters,* **491:** 169-173.

Okuda, Y., Denda, K. and Fukumori, Y., 1996. Cloning and sequencing of a gene encoding a new member of the tetratricopeptide protein family from magnetosomes of *Magnetospirillum magneticum, Gene,* **171** (1): 99-102.

Orlova, A., and Egelman, E. H., 2002. Structural dynamics of F-actin. I. Changes in the C-terminus, *Journal of Molecular Biology,* **245:** 582-597.

Otterbein, L. R., Graceffa, P., and Dominguez, R., 2001. The crystal structure of uncomplexed actin in the ADP state, *Science,* **293:** 708-711.

Nolen, B. J., and Pollard, T. D. 2007. Insights into the influence of nucleotides on actin family proteins from seven new structures of Arp2/3 complex, *Molecular Cell*, **26** (3): 449-457.

Paoletti, L. C. and Blakemore, R. P., 1986. Hydroxamate production by *Aquaspirillum magnetotacticum*, *Journal of Bacteriology*, **167:** 73-76.

Panina, E. M., Mironov, A. A., and Gelfand, M. S., 2001. Comparative analysis of Fur regulons in gamma-proteobacteria, *Nucleic Acids Research*, **29** (24): 5195-5206.

Peck, J. A., and King, J. W., 1996. Magnetofossils in the sediment of Lake Baikal, Siberia, *Earth and Planetary Science Letters*, **140** (1-4): 159-172.

Perry, A., Bauer, G. B., and Dizon, A.E., 1985. Magnetoreception and biomineralisation of magnetite in amphibians and reptiles. *In: Kirschvink, J.L., Jones, D.S., MacFadden, B.J. Eds., Magnetite biomineralisation and magnetoreception in organisms. Plenum Press, New York, pp 439-453.*

Phillips, J. B., Deutchlander, M. E., Freake, M. J., and Borland, S. C., 2001. The role of extraocular photoreceptors in newt magnetic compass orientation: parallels between light-dependent magnetoreception and polarised light detection in vertebrates, *Journal of Experimental Biology*, **204:** 2543-2552.

Pinder, J. C., Sleep, A., Bennett, P. M., and Gratzer, W. B., 1995. Concentrated Tris solutions for the preparation, depolymerisation, and assay of actin: Application to erythroid actin, Analytical *Biochemistry*, **225:** 291-295.

Posfai, M., Buseck, P.R., Bazylinski, D.A., and Frankel, R.B., 1998. Reaction sequence of iron sulphide minerals in bacteria and their use as biomarkers, *Science*, **280:** 880-883.

Pradel, N., Santini, C.-L., Bernadac, A., Fukumori, Y., and Wu, L.-F., 2006. Biogenesis of actin-like bacterial cytoskeletal polymers destined for positioning bacterial magnetic organelles, *Proceedings of the National Academy of Sciences*, **103** (46): 17485-17489.

Prasher, D. C., Eckenrode, V. K., Ward, W. W., Prendergast, F. G., and Cormier, M.J., 1992. Primary structure of the *Aequorea victoria* green fluorescent protein, *Gene*, **111:** 229-233.

Pümpel, T., Pernfuß, B., Pigher, B., Diels, L., and Schinner, F., 1995. A rapid screening method for the isolation of metal accumulating microorganisms, *Journal of Industrial Microbiology and Biotechnology,* **14:** 213– 217.

Raulin-Cerceau, F., Maurel, M.-C., and Schneider, J., 1998. From panspermia to bioastronomy, the evolution of the hypothesis of universal life, *Origins of Life and Evolution of the Biosphere*, **28:** 597-612.

Robinson, S. G., 1986. The late Pleistocene paleoclimatic record of north-Atlantic deep-sea sediments revealed by mineral-magnetic measurements, *Physics of the Earth and Planetary Interiors*, **42** (1-2): 22-47.

Rodgers, F. G., Blakemore, R. P., Blakemore, R. A., Frankel, R. B., Bazylinski, D. A., Maratea, D., and Rodgers, C., 1990. Intercellular structure in a many celled magnetotactic prokaryote, *Archives of Microbiology*, **154** (1): 18-22.

Rould, M. A., Wan, Q., Joel, P. B., Lowey, S., and Trybus, K. M., 2006. Crystal structures of expressed non-polymerizable monomeric actin in the ADP and ATP states, *Journal of Biological Chemistry,* **281** (42): 31909-31919.

Sakaguchi, T., Arakaki, A., and Matsunaga, T., 2002. *Desulfovibrio magneticus* sp. nov., a novel sulfate-reducing bacterium that produces intracellular single-domain-sised magnetite particles. *International Journal of Systematic and Evolutionary Microbiology,* **52:** 215-221.

Sakaguchi, T., Burgess, J. G., and Matsunaga, T., 1993. Magnetite formation by a sulphate-reducing bacterium, *Nature,* **365:** 47-49.

Sakaguchi, T., Tsujimura, N., and Matsunaga, T., 1996. A novel method for isolation of magnetic bacteria without magnetic collection using magnetotaxis, *Journal of Microbial Methods*, **26:** 139-145.

Scheffel, A., and Schüler, D., 2007. The acidic repetitive domain of the *Magnetospirillum gryphiswaldense* MamJ protein displays hypervariability but is not required for magnetosome chain assembly, *Journal of Bacteriology*, **189** (17): 6437-6446.

Scheffel, A., Gärdes, A., Grünberg, K., Wanner, G., and Schüler, D., 2008. The major magnetosome proteins MamGFDC are not essential for magnetite biomineralisation in *Magnetospirillum gryphiswaldense* but regulate the sise of magnetosome crystals, *Journal of Bacteriology*, **190** (1): 377–386.

Scheffel, A., Gruska, M., Faivre, D., Linaroudis, A., Plitzko, J. M., and Schüler, D., 2006. An acidic protein alignes magnetosomes along a filamentous structure in magnetotactic bacteria, *Nature*, **440:** 110-114.

Schleifer, K., D., Schüler, D., Spring, S., Weisenegger, M., Amann, R., Ludwig, W., and Kőhler, M., 1991. The genus *Magnetospirillum* gen. nov., description of *Magnetospirillum gryphiswaldense* sp. nov. and transfer of *Aquaspirillum magnetotacticum* to *Magnetospirillum magnetotacticum* comb. nov., *Systematic and Applied Microbiology*, **14:** 379-385.

Schmidt, A., and Hall, M.N., 1998. Signalling to the actin cytoskeleton. *Annual Review of Cell Developmental Biology*, **14:** 305–338.

Schübbe, S., Kube, M., Scheffel, A. Wawer, C., Heyen, U., Meyerdierks, A, Madkour, M. H., Mayer, F. Reinhardt, R., and Schüler, D., 2003. Characterisation of a spontaneous nonmagnetic mutant of *Magnetospirillum gryphiswaldense* reveals a large deletion comprising a putative magnetosome island, *Journal of Bacteriology*, **185** (19): 5779-5790.

Schubert, S., Rakin, A., and Heesemann, J., 2004. The Yersinia high-pathogenicity island (HPI): evolutionary and functional aspects, *International journal of medical microbiology,* **294** (2-3): 83-94.

Schüler, D., 1999. Formation of magnetosomes in magnetotactic bacteria, *Journal of Molecular Microbiology and Biotechnology* [print], **1** (1): 79-86.

Schüler, D., 2002. The biomineralisation of magnetosomes in *Magnetospirillum gryphiswaldense*, *International Microbiology*, **5:** 209-214.

Schüler, D., 2004. Molecular analysis of a subcellular compartment: the magnetosome membrane in *Magnetospirillum gryphiswaldense*, *Archives of Microbiology*, **181:** 1–7.

Schüler, D., and Baeuerlein, E., 1996. Iron-limited growth and kinetics of iron uptake in *Magnetospirillum, Archives of Microbiology,* **166** (5): 301-307.

Schultheiss, D., and Schüler, D., 2003. Development of a genetic system for *Magnetospirillum gryphiswaldense*, *Archives of Microbiology*, **179:** 89-94.

Schultheiss, D., Handrick, R., Jendrossek, D., Hanzlick, M., and Schüler, D., 2005. The presumptive magnetosome protein Mms16 is a poly(3-hydroxybutyrate) granule-bound protein (phasin) in *Magnetospirillum gryphiswaldense*, *Journal of Bacteriology,* **187** (7): 2416-2425.

Schultheiss, D., Kube, M., and Schüler, D., 2004. Inactivation of the flagellin gene *flaA* in *Magnetospirillum gryphiswaldense* results in nonmagnetotactic mutants

lacking flagellar filaments, *Applied and Environmental Microbiology,* **70** (6): 3624-3631.

Selden, L. A., Kinosian, H. J., Estes, J. E., and Gershman L. C., 1994. Influence of the high affinity divalent cation on actin tryptophan fluorescence, *Advanced Experimental Medical Biology*, **358:** 51-57.

Shetterline, P., and Sparrow, J. C., 1994. Biological characteristics of actin, *Protein Profile*, **1:** 1-12.

Simmons, S. L. Sievert, S. M., Frankel, R. B., Bazylinski, D. A., and Edwards, K. J., 2004. Spatiotemporal distribution of marine magnetotactic bacteria in a seasonally stratified coastal salt pond, *Applied and Environmental Microbiology*, **70** (10): 6230-6239.

Simmons, S.L., Bazylinski, D.A., and Edwards, K.J., 2006. South-seeking magnetotactic bacteria in the Northern Hemisphere, *Science*, **311** (5759): 371 – 374.

Singh, S., M., and Panda, A., K., 2005. Solubilisation and refolding of bacterial inclusion body proteins, *Journal of Bioscience and Bioengineering*, **99** (4): 303-310.

Snowball, I., Zillén, L., and Sandgren, P., 2002. Bacterial magnetite in Swedish varved lake-sediments; a potential bio-marker of environmental change, *Quartenary International*, **88** (1): 13-19.

Sode, K., Kudo, S., Sakaguchi, T., Nakamura, N., and Matsunaga, T., 1993. Application of bacterial magnetic particles for highly selective mRNA recovery system, *Biotechnology Techniques*, **7:** 688-694.

Spring, S, Amann, R., Ludwig, W., Schleifer, K., van Gemerden, H., and Petersen, N., 1993. Dominating role of an unusual magnetotactic bacterium in the microaerobic zone of a freshwater sediment, *Applied and Environvironmental Microbiology,* **59** (8): 2397-2403.

Spring, S., and Bazylinski, D., 2000, Magnetotactic bacteria. *In M. Dworkin (ed.), The prokaryotes: an evolving electronic resource for the microbiological community, release 3.4. [Online.] Springer Verlag, New York, N.Y. http://link.springer-ny.com/link/service/books/10125/.*

Steinmetz, M. O., Hoenger, A., Tittmann, P., Fuchs, K. H., Gross, H., and Aebi, U., 1998. An atomic model of crystalline actin tubes: combining electron microscopy with X-ray crystallography, *Journal of Molecular Biology,* **278** (4): 703-711.

Stolz, J. F., 1993. Magnetosomes, *Journal of General Microbiology,* **139** (8): 1663-1670.

Straub F. B., 1942. Actin. *In: Studies from the Institute of Medical Chemistry University Szeged, vol. II (Szent-Gyi, A. ed.) Krager, Basel-New-York: S. Krager. pp. 1-15, S.*

Studier, F. W. and Moffatt, B. A., 1986. Use of bacteriophage T7 RNA polymerase to direct selective high-level expression of cloned genes, *Journal of Molecular Biology,* **189:** 113–130.

Tabor S., and Richardson C. C., 1985. A bacteriophage T7 RNA polymerase/promoter system for controlled exclusive expression of specific genes. *Proceedings of the National Academy of Sciences of the United States of America,* **82:** 1074-1078.

Takeyama, H., Yamazawa, A., Nakamura, C., and Matsunaga, T., 1995. Application of bacterial magnetic particles as novel DNA carriers for ballistic transformation of a marine cyanobacterium, *Biotechnology Techniques,* **9:** 355-360.

Tamegai, H., and Fukamori, Y., 1994. Purification and some molecular and enzymatic features of a novel ccb-type cytochrome c oxidase from a microaerobic denitrifier, *Magnetospirillum magnetotacticum, FEBS Letters,* **347** (1): 22-26.

Taoka, A., Asada, R., Sasaki, H., Anzawa, K., Wu, L.-F., and Fukumori, Y., 2006. Spatial localisations of Mam22 and Mam12 in the magnetosomes of *Magnetospirillum magnetotacticum, Journal of Bacteriology,* **188** (11): 3805-3812.

Taoka, A., Asada, R.,Wu, L.-F., and Fukumori, Y., 2007. The polymerisation of actin-like protein MamK associated with magnetosomes, *Journal of Bacteriology,* **189** (23), 8737-8740.

Torres de Araujo, F. F., Pires, M. A., Frankel, R. B., and Bicudo, C. E. M., 1986. Magnetite and magnetotaxis in algae, *Biophysics Journal,* **50:** 375-378.

Urban, J. E., 1998. Microgravity effects on magnetotactic bacteria, In: *Space technology and applications forum – 1998, American Institute of Physics Conference Proceedings, Albuquerque,* **420:** 761-764.

Vali, H., Froster, O., Amarantidis, G., and Petersen, N., 1987. Magnetotactic bacteria and their magnetofossils in sediments, *Earth and Planetary Science Letters,* **86:** 389-400.

Van den Ent, F., Amos, L. A., and Löwe, J., 2001. Bacterial origin of the actin cytoskeleton, *Nature,* **413:** 39-44.

van den Ent, F., and Löwe, J., 2000. Crystal structure of the cell division protein FtsA from *Thermotoga maritima, The European Molecular Biology Organisation Journal*, **19:** 5300–5307.

Venter, J. C., Remington, K., Heidelberg, J. F., Halpern, A. L., Rusch, D., Eisen, J. A., Wu, D., Paulsen, I., Nelson, K. E., Nelson, W., Fouts, D. E., Levy, S., Knap, A. H., Lomas, M. W., Nealson, K., White, O., Paterson, J., Hoffman, J., Parsons, R., Baden-Tillson, H., Pfannkoch, C., Rogers, Y.-H., and Smith, H. O., 2004. Environmental Genome Shotgun Sequencing of the Sargasso Sea, *Science*, **304:** 66-74.

Vorbiev, S., Strokopytov, B., Drubin, D.G., Frieden, C., Ono, S., Condeelis, J., Rubenstein, P. A., and Almo, S. C., 2003. The structure of nonvertebrate actin: implications for the ATP hydrolytic mechanism, Proceedings of the National Academy of Sciences USA, **100:** 5760-5765.

Walcott, C., Gould, J. L., and Kirschvink, J. L., 1979. Pigeons have magnets, *Science,* **205:** 1027-1029.

Walker , M. M., Quinn, T. P., Kirschvink, J. L. Groot, C., 1988. Production of single-domain magnetite throughout life by sockeye salmon, *Oncorhynchus nerka, Journal of Experimental Biology,* **140:** 51-63.

Walker, M. M., Kirschvink, J. L., Chang, S. -B., 1984. A candidate mangnetic sense organ in the yellow fin tuna, *Thunnus albacares, Science*, **224:** 751-753.

Weber, K., Lazarides, E., Goldman, R. D., Vogel, A., and Pollack, R., 1975. Localisation and distribution of actin fibers in normal transformed and revertant cells, *Cold Spring Harbor Symposium on Quantitative Biology.* **39** (1): 363–369.

Williams, M. L., and Jercinovic, M. J., 2002. Microprobe monazite geochronology: Putting absolute time into microstructural analysis, *Journal of Structural Geology,* **24** (6-7): 1013-1028.

Wiltschko, R., and Wiltschko, W., 1995. Magnetic orientation in animals, Vol. 33, Springer, Berlin.

Wisniowiecki, M. J., Vandervoo, R., and McCabe, C., 1983. A Pennsylvanian paleomagnetic pole from the mineralised late Cambrian bonneterre formation, southeast Missouri, *Journal of Geophysical Research,* **88** (8): 6540-6548.

Yamazaki, T., Oyanagi, H., Fujiwara, T., and Fukumori, Y., 1995. Nitrite reductase from the magnetotactic bacterium *Magnetospirillum magnetotacticum*; a novel cytochrome cd_1 with Fe (II):nitrite oxidoreductase activity, *European Journal of Biochemistry*, **233:** 665-671.

Yang, F., Moss, L., and Phillips, G. 1996. The molecular structure of green fluorescent protein. *Nature Biotechnology,* **14** (10): 1246–51.

Yanisch-Perron, C., Vieira, J., and Messing, J., 1985. Improved M13 phage cloning vectors and host strains: nucleotide sequences of the M13mp18 and pUC19 vectors. *Gene*, **33:** 103–119.

Zhang, C., Vali, H., Romanek, C. S., Phelps, T. J., and Liu, S. V., 1998. Formation of single-domain magnetite by a thermophilic bacterium, *American Mineralogist*, **83:** 1409-1418.